METHODOLOGIES FOR THE DESIGN OF HYBRID VEHICLE POWER PLANTS

A Dissertation

by

THOMAS W. IVES

Submitted to the Office of Graduate Studies of
Texas A&M University
in partial fulfillment of the requirements for the degree of

DOCTER OF PHILOSOPHY

August 1997

Major Subject: Mechanical Engineering

METHODOLOGIES FOR THE DESIGN OF HYBRID VEHICLE POWER PLANTS

A Dissertation

by

THOMAS WAYNE IVES

Submitted to Texas A&M University
in Partial fulfillment of the requirements
for the degree of

DOCTOR OF PHILOSOPHY

Approved as to style and content by:

T. R. Lalk (Chair of Committee)	M. McDermott, Jr. (Member)
K. Butler (Member)	M. Ehsani (Member)
R. Abrams (Graduate College Representative)	J. A. Caton (Head of Department)

August 1997

Major Subject: Mechanical Engineering

DEDICATION

Primarily to God

and secondarily to my partners during life on earth

Sue, Gabriel, Anna, and those that will hopefully follow

ACKNOWLEDGMENTS

What graduate student could fail to mention his wife after going through the “ordeal” of graduate school. Her encouragement to finish, and her pride in me, allowed me to finish. Thanks for this great gift Sue.

I am grateful to Dr. Lalk for his sound high level advice and guidance and for trusting me to attain the maturity and level of growth necessary to accomplish this work. Dr. Lalk is a philosopher worthy of being emulated in many ways, and I hope to do so.

Although not on my committee, I cannot fail to mention Dr. Redfield who is now teaching at the U.S. Air Force Academy. He aided my continued growth in, and love for, the use and appreciation of the generalized approach which has served to perpetually deepen my love for, and understanding of, the fields of engineering and science.

I also wish to thank my office mate, Michael Wienen, for his friendship. Our conversations and his company greatly fostered my personal growth in many ways.

ABSTRACT

Methodologies for the Design of Hybrid Vehicle Power Plants. (August 1997)

Thomas W. Ives, M.S. Texas A&M University; B.S., The University of Texas at Austin

Chair of Advisory Committee: Dr. T. R. Lalk

Design and modeling methodologies for hybrid vehicle power plants are demonstrated by using them to develop models that can help identify critical design parameters. The design methodology develops the important interrelations of general hybrid vehicle power plant design functions. The modeling methodology consists of three major aspects: approach, level of detail and modularity. The modeling is approached by using a common method and convention (i.e. language, spoken and/or written) for all disciplines so that multi-disciplined hybrid vehicle power plant design teams can work better together. The modeling is done at a level of detail that yields realistic performance predictions and that gives an adequate amount of information to give direction for design improvements. Modularity was achieved with the models, because designers need to consider several concepts and architectures when trying to find the best ways to improve predicted power plant performance. The developed models exhibited realistic performance predictions and dynamic behavior. They were used to identify critical design parameters, they were easy to reconfigure, and they proved to be useful design tools.

EXECUTIVE SUMMARY

1Overview of Work

1.1The Interest in Hybrid Vehicle Power Plants

The independent spirit of our culture dictates that advancements in U.S. transportation will be heavily focused on automotive engineering. Automotive designers are investigating electric vehicles (EV's) in an effort to address the multi-faceted challenges facing the modern automobile. However, the restrictive tradeoffs of EV's have led many automotive engineers to consider hybrid vehicle power plants (HVPP's).

The main objective of HVPP design is to combine two or more energy storage and transformation devices to achieve improved efficiency and performance. But, hybrid power plant advocates are at odds over which methods are best to achieve these objectives. Until there is agreement on the specific criteria and objectives leading HVPP research, engineers will continue to investigate HVPP's that satisfy their individual convictions.

The author foresees three major steps that must be completed before a consensus can be reached on which hybrid vehicle power plant concepts should be mass produced:

Step 1: Establish design and modeling methodologies that give adequately accurate predictions of the performance and realistic characteristics of various HVPP concepts.

Step 2: Use the design and modeling methodologies to identify the most promising HVPP concepts.

Step 3: Construct prototypes of the HVPP concepts identified in Step 2 and thoroughly test them.

Step 4: Manufacture the best concepts from step 3.

Designers need flexible design tools that make accurate performance predictions, and display realistic dynamics, of proposed designs. Such tools can help eliminate, or at least indicate, many of the difficulties designers may face in the development of prototypes which will help save time and money.

Most models currently used in HVPP studies are empirically generated performance maps. Such models cannot show how changes in design parameters will affect the performance of the plant. Thus, these models are not flexible design tools. The author has identified no existing design tools or methods for hybrid vehicles.

1.2Objectives of this Work

This work has sought to make a contribution to step 1. Design and modeling methodologies were developed and demonstrated in this work that can be used to identify critical design parameters of hybrid vehicle power plants. Models developed from this methodology proved to be flexible design tools that indicate sensitivities resulting from various interfaces among the sub-components. The models also show the relationships and sensitivities among the design, operating and performance parameters.

1.3The Design Methodology

A function structure that includes the essential functions required of any HVPP was developed. These essential functions were used to form a unique tool, a function system diagram, for pre-conceptual abstract analysis of HVPP's. The function system diagram is a high level, or macroscopic, tool that provides a skeletal frame for the genesis of concepts. It serves as a mental table for the group as they layout ideas before one another and jointly refine, accept or reject their trial concepts. Differences in energy management between various concepts are clearly demonstrated in a standardized manner.

The value of such a tool was experienced in previous design team work. The design team found the function system diagram to be a valuable tool in the following ways:

1) It allows design group members to visually communicate their thoughts to one another within a standardized convention.

2) It visually relates the energy and information transfer between the devices that will be designed to fulfill the functions of the function structure without actually showing concepts that might bias or hinder the creativity of the design team.

3) It shows the functions the design must fulfill without regard to physical limitations and yet reminds the group of basic physical limitations that exist such as the existence of uni-directional energy transmission and transformation devices.

4) Once actual concepts replace the functions, the new system diagram provides a concise, clear, and visual convention for recording the history of concepts that were compared, rejected and refined by the group.

1.4The Modeling Methodology

There are three important aspects to the modeling methodology of this work: approach, level of detail and modularity. Modeling approach is important, because a HVPP is a multi-disciplined design that requires a careful coordination of the contributing disciplines. Designers should adopt a common convention and modeling methodology to minimize the difficulties of working within a multi-disciplined team. Therefore, the generalized modeling approach was applied and communicated using bond graphs. The level of modeling was the most important aspect to the success of the modeling methodology. Component level modeling was chosen, because it is detailed enough to accurately predict performance, but not so detailed that simulations are slowed to impractical speeds. Modularity is important, because designers need to be able to study many variations in configuration. There are a variety of possible HVPP configurations that need to be tested. There is also a variety of components that can be used in a HVPP. Furthermore, there is sometimes a large variety of configurations that can be proposed for one of the power supplies in a HVPP.

1.4.1Drive Train Modeling

The first important area of the modeling was the drive train. A special drive train modeling scheme called the MRD scheme was devised that allows sub-systems with their own inertias to be rigidly connected to many other sub-systems with their own inertias in a flexible modular scheme. It also properly models the relations of two or more modular rigid systems when they connect to, and disconnect from, other modular rigid systems. The key to this method was the passing of generalized momentums and inertias through the drive train and through any devices that cause discontinuities. Speed calculations could be performed at any point in the drive train system. There was direct correspondence between all velocities in the systems when the systems were fully connected, and the scheme allowed the separate systems to operate properly when they were disconnected from one another. Momentum was passed through the disconnection points in proportion to the degree of connection. This scheme works in systems with or without breakable connections (e.g. with or without clutches). Special treatment of standard integration routines had to be made to reset state variables at appropriate times in the simulation.

1.4.2ICE Modeling

The engine models were comprised of several, simple and accurate, design parameter based sub-component models. This allowed the engine modeling to be modular so that different engine configurations could be studied. The complete ICE models exhibited sensitivities comparable to those of real engines. The complete ICE models also exhibited very good accuracy. When ICE configuration and parameter values, and vehicle parameter values, comparable to a Honda Ascot were used to simulate a motorcycle, the vehicle simulation results accurately predicted the acceleration performance of the Honda Ascot.

1.4.3Electric Machine Modeling

DC Machine models do not require validation, because they are always very accurate when compared to experimental results. An IM model that could meet the modeling objectives was developed using modeling methodology. The electrical, magnetic, and mechanical processes in the machine were modeled as separate, discrete regions or processes. The model proved to be adequately accurate for the purposes of this work and to reproduce realistic performance characteristics. This model requires more computation time than any of the other models in this work, but the speed was found to be tolerable. Ten seconds of dynamic simulation required 3 hours to run on a Digital VAX Alpha computer.

Design parameter values for an existing production IM used in vehicle applications were estimated to validate the IM model as demonstrated in section 3.4 and 4.2. Simulation predictions using the model and the estimated design parameters were good. The simulated characteristics of the modeled machine exhibited characteristics one would expect to measure from a real machine, and the modeled IM exhibited sensitivities to design changes that would be experienced in experimentation. When used in a variable speed application, the IM model also exhibited realistic sensitivities to control and design parameter value changes and gave accurate predictions. It proved to be very valuable in the process of developing variable speed IM controls. When IM ratings and vehicle parameter values comparable to a GM impact were used to simulate an EV, the vehicle simulation results predicted the same acceleration performance of the GM Impact.

1.4.4Battery Modeling

The battery model is accurate and is based on simple first principles. Adequate simulation accuracy can be achieved by making small adjustments to the published functions for nonlinear resistances and nonlinear battery capacitance based on knowledge of a given battery's energy storage capacity and power density. More accurate results can be achieved by experimentally identifying the nonlinear parameters. This model proved to be extremely valuable to the objectives of this work. The most influential interface sensitivities encountered were due to the batteries. Their dynamics influenced the design of the plant more than any other component.

1.5Application of the Methodologies

The design and modeling methods were illustrated by applying them to three non-hybrid power plants and to four different HVPP's. Bond graph models were formed from the concept system diagrams that were developed from the general function system diagram's structure. The bond graphs were used to inspect the causality and dependencies of the overall numerical models for the HVPP's. In each case, the MRD scheme allowed simplifications to the bond graphs where numerical dependencies would have normally resulted. The bond graph models were then used as guides in the formation of the ACSL graphic models. The graphic models were formed from the MRD drive train components, the modules for the detailed models, and user defined controllers. The graphic models were simulated and used to briefly illustrate how a designer might use them when investigating ways to improve the performance of new HVPP concepts.

It was found that regenerative braking was not very practical when using batteries to store the vehicle's kinetic energy. In order for batteries to be practical in regenerative braking, they must be able to handle high charging currents. Furthermore, the high battery voltages that exist during high power battery charging require excessive operating ranges for the electric machines, which results in unreasonable electric machine designs. Regenerative braking is desirable. Therefore, devices with much lower power densities, capable of delivering and receiving high power during severe vehicle transients, will be studied in the future.

1.6Summary of Findings

The above findings are reviewed and categorized. There are three general findings regarding the utility of the modeling methodology used in this work. Models developed using the modeling methodologies for the studies in this work

1) were useful in identifying critical design parameters
2) proved to be flexible design tools
3) showed relationships and sensitivities among the design, operating and control parameters
4) were useful in finding ways to improve performance.

There are two important findings regarding the level of detail that was chosen for the modeling in this work. Component level modeling of the vehicle power plant sub-component models in this work

1) yielded accurate performance predictions
2) exhibited realistic dynamic responses.

The modular-rigid-discontinuous (MRD) drive train modeling scheme was very important in meeting the objectives of this work. For the plants studied in this work, the MRD scheme

1) made it possible to modularize the vehicle power plants
2) automatically handled dependencies that arise when sub-systems with their own inertias are rigidly connected and thus simplified the vehicle power plant models
3) properly modeled the relations between systems that connect and disconnect during operation.

The most sensitive component in the plants studied were the batteries. Therefore, in these studies

1) electric machine control logic affected plant performance more than any other design factor
2) regenerative braking was not very practical due to battery limitations and due to the excessive operating ranges that regenerative braking requires.

2Conclusions

2.1Discussions

The author has found no existing design tools or methods for hybrid vehicles. This is unfortunate. If none are ever composed and revised, the community of HVPP designers will never approach a common set of functions upon which we can jointly focus. The design methods can benefit those who are open to using them. Those who use them will be useful to the HVPP design community if they refine, improve and/or add to them. And, the HVPP design community can progress more rapidly if they share their refinements and additions to the design methods with others. Competition may prevent this in industry, and it is understandable that even academic design teams will want to keep their specific design concepts secret. But, competition should not prevent the community from sharing design methodologies in industry or academia.

The models in this work do run slowly, and associates have expressed a high degree of frustration to the author on this point. However, one must consider the purpose of any modeling effort. The objective for the modeling in this work was to develop a methodology that would reveal critical design parameters in any conceivable HVPP. Furthermore, the models should properly indicate sensitivities in component interfaces, and relations between design, performance and control parameters. The modeling methodology is meeting this objective, primarily because the level of modeling chosen provided the best balance between speed and accuracy in light of current computational capabilities. And, even though the models are slow, they are not prohibitively slow. The predictive capabilities of models developed using the methodology make them attractive for analyzing and refining designs.

The best thing for this work is to have other disciplines apply the modeling methodology to components within their specific realms of expertise. Recall step 1 in moving toward the mass production of HVPP’s. One person, or even several engineers from one discipline, cannot do justice to fulfilling this step. For this work to be a contribution, HVPP designers from other disciplines must get involved and develop component models in accordance with these methodologies, or even refined versions of these methodologies. As the library of virtual sub-component models builds, and as the design methods improve, the potential of the HVPP community to determine the best configurations will increase.

Electric machine control logic is not too difficult to develop when working with a near constant voltage source. But, any voltage source on an EV, or on a HVPP, is most likely going to experience some significant fluctuations. This makes the development of electric machine control logic much more challenging. The studies in this work indicate that electric machine control logic is the single most important design factor affecting the performance of the configurations that were studied in this work. Thus, it is highly desirable to involve electric machine control experts in applying and using the methodologies of this work to develop more flexible and robust electric machine controls.

2.2Future Works and Directions

Power electronics modeling is directly related to electric machine control. Power electronic components were not modeled in this work, but they need to be. They control the interface between the electric storage devices (usually batteries at this point in history) and the electric machines, and they have their own unique dynamics that influence the performance of the plant.

The development of low power density devices that would be used to deliver and store energies in high power transients could greatly improve the performance of HVPP's and EV's. In some power plant configurations, the batteries could be replaced by these devices. If used in EV's, they could handle the high power transients while the batteries operated in ranges of higher efficiency. The design of devices that show the greatest potentials for this purpose are multi-disciplined devices too. If these devices do become practical for EV and HVPP design, they will still most likely have higher energy densities than batteries. Thus, battery designers will continue to consider methods of improving the efficiency, energy densities and power densities of batteries.

Considering the current state of battery modeling and design, the battery modeling used in this work is accurate and acceptable. It gives good insight into dynamic battery phenomena when used in the power plant models. However, it would be best to have models that were based on the actual physical measurements of the battery components. Models that currently do this are finite element based, and they would not be practical for vehicle performance predictions. Thus, HVPP designers can only hope for a faster means of computation in the future, so that finite element models can be used when necessary.

Improving the speed of the models is still a major concern, but it is also important to maintain, and even improve upon, their accuracy and usefulness in the design process. We must be looking to the future when we think about how we want to model. Microprocessor speed has improved exponentially over the last ten years. Projections in speed improvements made by major microprocessor companies one year ago appear to be well on track, and their speed projections for the next 4 years will enable the detailed models of this work to run significantly faster. It is highly likely that the microprocessors used by design engineers ten to twenty years from now will enable designers to use finite-element based models to make vehicle performance predictions and to meet objectives far more extensive than those in this work. When this occurs, the models like the ones in this work, which are considered “so slow,” will be considered simple models, and they will be used to identify initial design parameter values. Those who want to anticipate this future should learn how to use finite element methods to model dynamic systems, because it is inevitable that models will become more detailed and more valuable in design as microprocessor speeds increase.

2.3Summary of Conclusions

The findings in this work have led the author to make the following major conclusions. Models developed using the modeling methodology

1) can be used to identify critical design parameters
2) are modular and flexible design tools
3) show relationships and sensitivities among the design, operating and control parameters
4) can help find ways to improve the performance of multi-component dynamic systems
5) will yield accurate performance predictions
6) will exhibit realistic dynamic responses.

The modular-rigid-discontinuous (MRD) drive train modeling scheme

1) makes it possible to modularize rigidly connected dynamic systems
2) will handle dependencies when sub-systems with their own inertias are rigidly connected
3) simplifies the modeling and study of rigidly connected dynamic systems
4) properly models interactions of dynamic systems connecting and disconnecting.

Conclusions drawn from specific experiences with the batteries in this work indicate that

1) it is necessary to have designers of electric machine controllers contribute controller and power electronic model modules to the model component library using the methodologies

2) regenerative braking was not very practical due to

- battery limitations
- the excessive electric machine operating ranges that regenerative braking requires

1) low power density devices should be investigated and developed so that

- battery usage can be more efficient in EV's
- batteries can be replaced in some hybrid vehicle power plants to lower weight and improve performance

TABLE OF CONTENTS

Page

1. INTRODUCTION....1

1.1 Background of Hybrid Vehicle Power Plants....1
1.2 Early Background to this Work....3
1.3 Research Objectives....4
1.4 Design Methodology for Multi-Disciplined Systems....5
1.5 Modeling Methodology....5
1.6 Overview of Dissertation....11

2. DESIGN METHODOLOGY FOR HYBRID VEHICLE POWER PLANT....12

2.1 Abstract Design Tools....12
2.2 Application of Abstract Design Tools....17
2.3 Summary....17
2.4 Conclusions....17

3. DEVELOPMENT OF HYBRID VEHICLE POWER PLANT SUB-COMPONENT MODELS....18

3.1 Drive Train Modeling....19
3.2 Modeling of ICE's and their Sub-Components....29
3.3 Electric Machine Modeling....50
3.4 Battery Modeling....78

4. VALIDATION OF THE MODELING METHODOLOGY USING SIMULATIONS OF NON-HYBRID POWER PLANT VEHICLES....84

4.1 Conventional Vehicle....85
4.2 Electric Vehicles....101

5. HYBRID VEHICLE POWER PLANT MODELS AND SIMULATIONS....134

5.1 Design - Function System Diagrams....136
5.2 Bond Graph Models....142
5.3 Initial Design Analysis - Initial Parameter Value Estimates....145
5.4 Graphic Model Synthesis of HVPP Components....151
5.5 Design of the Hybrid Vehicle's Power Supply Components....154
5.6 Simulations....156
5.7 Summary....188

6. SUMMARY....189

6.1 The Interest in Hybrid Vehicle Power Plants....189
6.2 Objectives of this Work....189
6.3 The Design Methodology....190
6.4 The Modeling Methodology....191

Page

6.5 Application of the Methodologies....193
6.6 Summary of Findings....194

7. CONCLUSIONS....196

7.1 Specific Conclusions....196
7.2 Discussions....198
7.3 Summary of Conclusions....199
7.4 Future Work and Directions....200

REFERENCES....202

APPENDIX A....204

APPENDIX B....211

APPENDIX C....216

APPENDIX D....223

APPENDIX E....226

APPENDIX F....236

APPENDIX G....240

APPENDIX H....246

APPENDIX I....255

APPENDIX J....257

VITA....262

LIST OF FIGURES

Page

Figure 2.1.1: Essential Function Structure for any Hybrid Vehicle Power Plant Design. 13

Figure 2.1.2: Function System Diagram...14

Figure 3.1.1: Electric Vehicle Drive Train..20

Figure 3.1.2: Value Passing Scheme for Modularization of Rigidly Connected Systems.........................20

Figure 3.1.3: Conventional Vehicle Drive Train...22

Figure3.1.4: Parallel Hybrid Vehicle Drive Train...22

Figure 3.1.5: Illustration of MRD Interface Block Calculations for Power Supplies and Loads...............24

Figure 3.1.6: Illustration of MRD Clutch Block Calculations...25

Figure 3.1.7: Illustration of MRD Ratio Block Calculations...26

Figure 3.1.8: Illustration of MRD Block for Specific Load Calculations..26

Figure 3.1.9: Illustration of MRD Coupling Block Calculations...27

Figure 3.2.1: Simple Four Stroke ICE Drawing..29

Figure 3.2.2: Pseudo Power Bonds Used in Thermal Fluid Systems...30

Figure 3.2.3: Bond Graphs of Thermal Fluid System Constant, and Variable, Area Resistors.................31

Figure 3.2.4: Bond Graphs of Thermal Fluid System Capacitors...32

Figure 3.2.5: Thermal Fluid Section of a Four Stroke ICE..38

Figure 3.2.6: Bond Graph of Thermal Fluid Portions of a Four Stroke ICE..38

Figure 3.2.7: ICE Bond Graph of Figure 3.2.6 with the Additions of Translational and Rotational Mechanics...39

Figure 3.2.8: Drawing of a Simple Two Stroke Engine...40

Figure 3.2.9: Bond Graph of a Simple Two Stroke Engine..41

Figure 3.2.10: Illustration of Ascot Configuration...42

Figure 3.2.11: Ascot Configuration Showing One of Two Thermal Fluid Paths and Connections to the Other Thermal Fluid Path...43

Page

Figure 3.2.12: ACSL Power Blocks for One Thermal Fluid Path and its Associated Mechanics............44

Figure 3.2.13: Complete Ascot Engine Model in the ACSL Graphic Modeller.......................................45

Figure 3.2.14: Grouped Ascot Engine Connected to an Engine Interface for the Rigid-Modular-Discontinuous Connection Scheme...46

Figure 3.2.15: Grouped version of Figure 3.2.14...47

Figure 3.2.16: Pressure (Pa) verses Volume (m^3) Curve for the Honda Ascot Motorcycle Engine Model Operating at 742 rad/sec...47

Figure 3.2.17: Torque Speed Curve for the Ascot Engine Model Operating between 100 and 1000 rad/sec..48

Figure 3.3.1: Bond Graph Model of a Separately Excited DC Machine..52

Figure 3.3.2: Bond Graph Model of an Ideal Transformer with Air Gaps and a Secondary Resistance...54

Figure 3.3.3: Transformer with Flux Leakage and its Bond Graph..55

Figure 3.3.4: Delta Wound Stator Configuration for an Induction Machine...57

Figure 3.3.5: Bond Graph for a Three Phase Delta Wound Stator..58

Figure 3.3.6: Simplification of Figure 3.3.5’s Bond Graph to use Phase Voltages as the Sources of Effort. 58

Figure 3.3.7: Simple Squirrel Cage Rotor Used to Explain Induction Motor Model Development.........60

Figure 3.3.8: Bond Graph Model without Causal Strokes for the Squirrel Cage Rotor in Figure 3.3.7.. .60

Figure 3.3.9: Illustration of Steps to Simplify the Bond Graph Shown in Figure 3.3.8............................61

Figure 3.3.10: Induction Motor Bond Graph...62

Figure 3.3.11: Torque (Nm) verses Rotor Speed (rad/sec) Predictions Using the Ideal IM Model for a 18 kW Nominal Power IM Powered From a Simulated Battery Bank of 39 Sears Batteries................67

Figure 3.3.12: Torque (Nm) verses Rotor Speed (rad/sec) in a Free Acceleration of a 18 kW Nominal Power IM without End Ring Adjustment to the Rotor Bar Resistance..68

Figure 3.3.13: Electrical Power (watts, solid line) and Torque (Nm, dotted line) verses Rotor Speed (rad/sec) in a Free Acceleration of a 18 kW Nominal IM...69

Figure 3.3.14: Mechanical Power (watts, solid line) and Electrical Power (watts, dotted line) verses Rotor Speed (rad/sec) in a Free Acceleration of a 18 kW Nominal IM...70

Page

Figure 3.3.15: Terminal Current (amps, solid line) and Electrical Power (watts, dotted line) verses Rotor Speed (rad/sec) in a Free Acceleration of a 18 kW Nominal IM..71

Figure 3.3.16: Volt Amperes (watts, solid line) and Terminal Current (amps, dotted line) verses Rotor Speed (rad/sec) in a Free Acceleration of a 18 kW Nominal Power IM..72

Figure 3.3.17: Phase Voltage (volts, solid line) and Phase Current (amps, dotted line) verses Time (seconds) for a 18 kW Nominal Power IM at idle...73

Figure 3.3.18: IM Torque (Nm) verses Rotor Speed (rad/sec) for the Free Acceleration of a 18 kW Nominal IM with the End Ring Resistance Adjustment Made to the Rotor Bars..............................74

Figure 3.3.19: Torque (Nm) verses Rotor Speed (rad/sec) for a 18 kW Nominal IM Powered by 26 Lead Acid Sears Batteries..75

Figure 3.3.20: Torque (Nm) verses Rotor Speed (rad/sec) for a 18 kW Nominal IM Powered by 26 Lead Acid Sears Batteries..76

Figure 3.4.1: (a) Battery Schematic Model, (b) Single Battery Bond Graph Model, (c) Battery Bank Bond Graph Model..80

Figure 3.4.2: Battery Bank Power Blocks...81

Figure 3.4.3: Battery Model Voltage Response (volts, solid line) and Input Current (amps, dotted line) verses Time (hours) for the Battery Model and Specifications Used in this Work............................82

Figure 4.1.1: Conventional Vehicle Concept Applied to the Function System Diagram...........................86

Figure 4.1.2: Conventional Vehicle Bond Graph..87

Figure 4.1.3: Velocity verses Time for Ascot Motorcycle Simple Simulation...89

Figure 4.1.4: Velocity verses Time for Taurus SHO Simple Simulation...90

Figure 4.1.5: Virtual Ascot Motorcycle Test Bed for ICE Power Plant Performance Evaluations...........91

Figure 4.1.6: Velocity (m/sec, solid line) and Driver's Desired Velocity (m/sec, dotted line) verses Time (sec) from Simulation of the Ascot Motorcycle on the Short Drive Cycle...92

Figure 4.1.7: Engine RPM (solid line) and Vehicle Velocity (m/sec, dotted line) verses Time (sec) from Simulation of the Ascot Motorcycle on the Short Drive Cycle...93

Figure 4.1.8: Gear Number (solid line) and Engine RPM (dotted line) verses Time (sec) from Simulation of the Ascot Motorcycle on the Short Drive Cycle...94

Figure 4.1.9: Clutch (solid line) and Engine RPM (dotted line) verses Time (sec) from Simulation of the Ascot Motorcycle on the Short Drive Cycle..95

Page

Figure 4.1.10: Velocity (mph) verses Time (sec) from Simulation of the Ascot Motorcycle on a Maximum Acceleration....96

Figure 4.1.11: Engine RPM (solid line) and Velocity (mph, dotted line) verses Time (sec) from Simulation of the Ascot Motorcycle on a Maximum Acceleration....97

Figure 4.1.12: Gear Number (solid line) and Engine RPM (dotted line) verses Time (sec) from Simulation of the Ascot Motorcycle on a Maximum Acceleration....98

Figure 4.1.13: Throttle Actuation (solid line) and Engine RPM (dotted line) verses Time (sec) from Simulation of the Ascot Motorcycle on a Maximum Acceleration....99

Figure 4.1.14: Clutch Actuation (solid line) and Engine RPM (dotted line) verses Time (sec) from Simulation of the Ascot Motorcycle on a Maximum Acceleration....100

Figure 4.2.1: Electric Vehicle Concept Applied to a Function System Diagram....102

Figure 4.2.2: Bond Graph of an Electric Vehicle....103

Figure 4.2.3: Velocity verses Time for Simple Simulation of the DC Motor Powered EV....105

Figure 4.2.4: ACSL Graphic Model of DC Motor Powered EV....107

Figure 4.2.5: Velocity (m/sec) verses Time (sec) for the DC Motor Powered EV during Maximum Acceleration....108

Figure 4.2.6: DC Motor Controller Output Voltage (volts) verses DC Motor Rotational Velocity (rad/sec) for the DC Motor Powered EV during Maximum Acceleration....109

Figure 4.2.7: Battery Voltage (volts, solid line) and DC Motor Controller Output Voltage (volts, dotted line) verses DC Motor Rotational Velocity (rad/sec) for the DC Motor Powered EV during Maximum Acceleration....110

Figure 4.2.8: Power Drawn from Batteries (watts) verses DC Motor Rotational Velocity (rad/sec) for the DC Motor Powered EV during Maximum Acceleration....111

Figure 4.2.9: Torque (Nm, solid line) and Motor flux (dotted line) verses DC Motor Rotational Velocity (rad/sec) for the DC Motor Powered EV during Maximum Acceleration....112

Figure 4.2.10: Car Velocity (m/sec, solid line) and Driver's Desired Velocity (m/sec, dotted line) verses Time (sec) for the DC Motor Powered EV during the Simple Drive Cycle....113

Figure 4.2.11: DC Motor Controller Output Voltage (volts) verses DC Motor Rotational Velocity (rad/sec) for the DC Motor Powered EV during the Simple Drive Cycle....114

Figure 4.2.12: Battery Bank Voltage (volts, solid line) and Controller Voltage (volts, dotted line) verses DC Motor Rotational Velocity (rad/sec) for the DC Motor Powered EV during the Simple Drive Cycle....115

Page

Figure 4.2.13: Power Drawn from Batteries (watts) verses DC Motor Rotational Velocity (rad/sec) for the DC Motor Powered EV during the Simple Drive Cycle..116

Figure 4.2.14: DC Motor Torque (Nm, solid line) and Motor Flux Value (dotted line) verses DC Motor Rotational Velocity for the DC Motor Powered EV during the Simple Drive Cycle......................117

Figure 4.2.15: Velocity verses Time for the IM Powered EV Simple Simulation...................................119

Figure 4.2.16: ACSL Graphic Model of DC Motor Powered EV...120

Figure 4.2.17: Exploded View of Compound Power Block for Induction Machines, their Inverter, and the Power Supply MRD Interface...120

Figure 4.2.18: Car Velocity (m/sec) verses Time (sec) for the Induction Motor Powered Vehicle with No Natural Mode Adjustments...122

Figure 4.2.19: Slip Speed (rad/sec) verses Time (sec) for IM Powered EV Before the Natural Mode Region of the IM Was Reached..123

Figure 4.2.20: Velocity (m/s) verses Time (sec) during Maximum Acceleration of IM powered EV through the Three Regions of IM Variable Speed Operation and No Control of Maximum Speed. 124

Figure 4.2.21: Electrical Power Drawn (watts) verses Time (sec) from One IM during Maximum Acceleration of IM powered EV through the Three Regions of IM Variable Speed Operation and No Control of Maximum Speed...125

Figure 4.2.22: IM Current (amps) verses Rotor Speed (rad/sec) during Maximum Acceleration of IM powered EV through the Three Regions of IM Variable Speed Operation and No Control of Maximum Speed..126

Figure 4.2.23: IM Slip (rad/sec) verses Rotor Speed (rad/sec) during Maximum Acceleration of IM powered EV through the Three Regions of IM Variable Speed Operation and No Control of Maximum Speed..127

Figure 4.2.24: Car Velocity (m/sec) verses Time (sec) during Maximum Acceleration of IM powered EV through the Three Regions of IM Variable Speed Operation and Control of Maximum Speed.….128

Figure 4.2.25: Slip Speed (rad/sec) verses Rotor Speed (rad/sec) during Maximum Acceleration of IM powered EV through the Three Regions of IM Variable Speed Operation and Control of Maximum Speed...129

Figure 4.2.26: Velocity (m/sec) verses Time (sec) during Maximum Acceleration to a Cruising Speed for the IM powered EV with Final Improvements to the IM Controller...130

Figure 4.2.27: IM Slip Speed (rad/sec, solid line) and Car Velocity (m/sec, dotted line) verses Time (sec) during Maximum Acceleration to a Cruising Speed for the IM powered EV with Final Improvements to the IM Controller...131

Page

Figure 4.2.28: IM Controller Voltage (volts, lower line) and Battery Bank Voltage (volts, higher line) verses Time (sec) during Maximum Acceleration to a Cruising Speed for the IM powered EV with Final Improvements to the IM Controller..132

Figure 5.1.1: Application of the Parallel Hybrid Concept to the Function System Diagram..................137

Figure 5.1.2: Application of the Series Hybrid Concept to the Function System Diagram.....................138

Figure 5.1.3: EV Concept Applied to Function System Diagram with Potential Future Concepts Added. 141

Figure 5.1.4: Parallel HVPP Concept Applied to Function System Diagram with Potential Future Concepts Added...142

Figure 5.2.1: Parallel Hybrid Vehicle Bond Graph..144

Figure 5.2.2: Series Hybrid Vehicle Bond Graph...145

Figure 5.3.1: Predicted Acceleration Performance of a Parallel Hybrid Vehicle Using Parameter Values from Table 5.3.1...148

Figure 5.3.2: Predicted Acceleration Performance of an Electrical Parallel / Series Hybrid Vehicle Using Parameter Values from Table 5.3.2...150

Figure 5.4.1: ACSL Graphic Model for a Parallel Hybrid Vehicle Power Plant that Uses a DC Traction Motor...152

Figure 5.4.2: ACSL Graphic Model for a Parallel Hybrid Vehicle Power Plant that Uses an Induction Traction Motor..152

Figure 5.4.3: ACSL Graphic Model for an Electrical Parallel / Series Hybrid Vehicle Power Plant that Uses a DC Traction Motor...153

Figure 5.4.4: ACSL Graphic Model for an Electrical Parallel / Series Hybrid Vehicle Power Plant that Uses an Induction Traction Motor...154

Figure 5.5.1: ACSL Graphic Model for the Engine Used in the HVPP Models.....................................155

Figure 5.5.2: Predicted Torque Speed Characteristics for the Engine Used in the HVPP Models..........156

Figure 5.6.1: Velocity (m/sec) verses Time (sec) for Maximum Acceleration of the Parallel HVPP / DC Motor Design..158

Figure 5.6.2: Motor Controller Voltage (solid line) and Battery Bank Voltage (dotted line) verses Time (sec) for Maximum Acceleration of the Parallel HVPP / DC Motor Design..................................159

Figure 5.6.3: Engine RPM (solid line) and Vehicle Velocity (m/sec, dotted line) verses Time (sec) for Maximum Acceleration of the Parallel HVPP / DC Motor Design...160

Page

Figure 5.6.4: Engine Speed (RPM, solid line) and Clutch Actuation (dotted line) verses Time (sec) During Maximum Acceleration of the Parallel HVPP / DC Motor Design......................................161

Figure 5.6.5: New Design for the Parallel HVPP / DC Motor..162

Figure 5.6.6: Velocity (m/sec) verses Time (sec) during Maximum Acceleration of the New Design for the Parallel HVPP with the DC Motor Off during Shifting...163

Figure 5.6.7: Velocity (m/sec) verses Time (sec) during Maximum Acceleration of the New Design for the Parallel HVPP with the DC Motor On during Shifting and with Faster Driver Shifting...........164

Figure 5.6.8: Motor Controller Voltage (solid line) and Battery Bank Voltage (dotted line) verses Time (sec) for Maximum Acceleration of the Parallel HVPP / DC Motor Design that Uses Gear Shifting for the ICE..165

Figure 5.6.9: Velocity (m/sec) verses Time (sec) during a Maximum Acceleration of the Parallel HVPP with IM Design...166

Figure 5.6.10: Slip Speed (rad/sec) verses Time (sec) for Maximum Acceleration of the Parallel HVPP / IM Design..167

Figure 5.6.11: IM Controller Voltage (lower line) and Battery Bank Voltage (upper line) verses Time (sec) for a Maximum Acceleration of the Parallel HVPP with IM Design.......................................168

Figure 5.6.12: Engine RPM verses Time (sec) for Maximum Acceleration of the Parallel HVPP / IM Design...169

Figure 5.6.13: Velocity (m/sec) verses Time (sec) during Maximum Acceleration of the Parallel HVPP / IM Design after Controller, Battery Bank and Gear Ratio Changes...170

Figure 5.6.14: IM Controller Voltage (lower line) and Battery Bank Voltage (upper line) verses Time (sec) during Maximum Acceleration of the Parallel HVPP / IM Design after IM Controller, Battery Bank, and Gear Ratio Changes...171

Figure 5.6.15: Engine RPM verses Time (sec) during Maximum Acceleration of the Parallel HVPP / IM Design after IM Controller, Battery Bank, and Gear Ratio Changes..172

Figure 5.6.16: Velocity (m/sec) verses Time (sec) during Maximum Acceleration of the EP HVPP / DC Traction Motor Design...173

Figure 5.6.17: Motor Controller Voltage (solid line) and ICE / Generator Speed (rad/sec, dotted line) verses Time (sec) during Maximum Acceleration of the EP HVPP / DC Traction Motor Design. 174

Figure 5.6.18: DC Motor Armature Current (amps, solid line) and Vehicle Velocity (m/sec, dotted line) verses Time (sec) during Maximum Acceleration of the EP HVPP / DC Traction Motor Design. 175

Figure 5.6.19: DC Motor Torque (Nm, solid line) and DC Motor Field (dotted line) verses Time (sec) during Maximum Acceleration of the EP HVPP / DC Traction Motor Design...............................176

Page

Figure 5.6.20: Battery Bank Current (amps, solid line) and DC Generator Armature Current (amps, dotted line) verses Time (sec) during Maximum Acceleration of the EP HVPP / DC Traction Motor Design...177

Figure 5.6.21: Vehicle Velocity (m/sec) verses Time (sec) during Maximum Acceleration of the EP HVPP / DC Traction Motor Design with the Improved ICE Control..178

Figure 5.6.22: Motor Controller Voltage verses DC Motor Speed (rad/sec) during Maximum Acceleration of the EP HVPP / DC Traction Motor Design with the Improved ICE Control.........179

Figure 5.6.23: Engine RPM verses DC Motor Speed (rad/sec) during Maximum Acceleration of the EP HVPP / DC Traction Motor Design with the Improved ICE Control..180

Figure 5.6.24: Generator Armature Current (amps, solid line) and Battery Bank Current (amps, dotted line) verses DC Motor Speed (rad/sec) during Maximum Acceleration of the EP HVPP / DC Traction Motor Design with the Improved ICE Control...181

Figure 5.6.25: Generator Output Power (watts) verses Time (sec) during Maximum Acceleration of the EP HVPP / DC Traction Motor Design with the Improved ICE Control...182

Figure 5.6.26: Vehicle Velocity (m/sec) verses Time (sec) during Maximum Acceleration of the EP HVPP / DC Traction Motor Design with the Improved Generator Control.....................................183

Figure 5.6.27: Generator Armature Current (amps solid line) and Battery Bank Current (amps, dotted line) verses DC Motor Speed (rad/sec) during Maximum Acceleration of the EP HVPP / DC Traction Motor Design with the Improved Generator Control...184

Figure 5.6.28: DC Generator Output Power (watts) verses Time (sec) during Maximum Acceleration of the EP HVPP / DC Traction Motor Design with the Improved Generator Control..........................185

Figure 5.6.29: Vehicle Velocity (m/sec) verses Time (sec) for the EP HVPP / IM Design during Maximum Acceleration...186

Figure 5.6.30: IM Slip Speed (rad/sec) verses Time (sec) for the EP HVPP / IM Design during maximum acceleration..187

LIST OF TABLES

Page

Table 3.2.1: Specific Heat and Ratio of Specific Heats Parameters for Equation 3.2.6............................35

Table 3.3.1: Equations for Dynamic Simulation of the Ideal Transformer in Figure 3.3.2.......................55

Table 3.3.2: Equations from the Transformer with Flux Leakage Bond Graph in Figure 3.3.3...............56

Table 3.3.3: Equations from Bond Graph in Figure 3.3.10..64

Table 4.1.1: Ascot Motorcycle Settings for Simple Simulation..88

Table 4.1.2: Taurus SHO Settings for Simple Simulation...89

Table 4.1.3: Simulated verses Actual Times to Speed for the Ascot Motorcycle Model..........................96

Table 4.2.1: DC Powered EV Settings for Simple Simulation..105

Table 4.2.2: IM Powered EV Settings for Simple Simulation...118

Table 5.1.1: Power Densities of Common Components found in HVPP's..140

Table 5.3.1: Parameter Values for a Simple Simulation of a Parallel Hybrid Vehicle Power Plant.......147

Table 5.3.2: Parameter Values for a Simple Simulation of a Electrical Parallel / Series Hybrid Vehicle Power Plant...150

Table 6.5.1: Overview of Models Built in this Work...194

1INTRODUCTION

1.1Background of Hybrid Vehicle Power Plants

Engineers involved in transportation are facing the problems of fuel availability, fuel costs and mandates on emissions reduction. It would seem logical to make improvements to, and expansions of, mass transit systems, but the independence of our culture is a hard thing to tame. People do not appear willing to give up their cars. Thus, the focus for solving these problems remains in the more challenging field of automotive engineering.

The interests of the market result in automotive designers competing to design quicker and faster cars at a reduced cost with greater efficiency. But they also deal with the added pressure from governments to reduce emissions. Engineers of all disciplines, being part of this automotive culture, have been faithfully working to address the challenges facing the automobile.

The spark ignition internal combustion engine (SI ICE) has made large improvements in fuel efficiency and emissions reduction during its years of operation. However, increasingly demanding mandates from governments on emissions limits and the constant dependence on foreign oil are causing many automotive engineers to investigate electric vehicles (EV's).

However, there are some restrictive tradeoffs involved in the fundamental design of EV's. The major advantage of EV's is that electric motors have much better torque speed characteristics than ICE's. Their major disadvantage is that it takes a significantly larger mass and volume of batteries than gasoline to propel a vehicle a given distance. This is the main reason the roads are not filled with EV's. Battery charging time and energy requirements to run accessory loads such as air conditioning are other major obstacles for EV's.

In spite of these obstacles, EV advocates have convincing arguments. The most common argument is emissions reduction. The opposition would say that EV's emissions come from a different source - power plants. EV advocates argue that emissions from power plants can be more effectively reduced than emissions from millions of cars. The mass of batteries needed to store energy for typical daily driving distances is reasonable, and battery energy density is improving rapidly. EV battery recharging is usually convenient, because most dwellings in the country have electric outlets, and modern battery recharge time is impressive. Also, EV's are simple and durable [1].

The style and format of this thesis document follow that modeled by *IEEE Transactions on Robotics and Automation.*

But, there is one remaining issue. Many households still need a car with long range capabilities. It is risky to alter the automobile market to deliver two types of automobiles. Auto manufacturers would rather produce a single car that exceeds the specifications of conventional cars and that produces emissions well below the legal limits.

Both the electric and ICE automobiles store energy and transform this energy to provide mechanical power. A large group of engineers believe it is possible to combine these two means of storage and transformation to develop a power plant that has better performance (acceleration, range, efficiency and speed), than either of the previous alternatives. This power plant could also have extremely low emissions. Such a power plant is called a hybrid vehicle power plant.

Hybrid vehicles are not limited to gasoline and electric energy, although these are the most commonly used energy sources. A hybrid vehicle can include many combinations of energy storage and transformation devices. In consideration of the weaknesses and strengths described above, the torque speed characteristics of the hybrid vehicle's power plant is improved over the ICE car by the electric motor, and the range capability is improved over the EV by the presence of the stored energy in gasoline. The efficiency and range is improved through the controlled mating of the two devices. The engineering challenge is to produce the desired results of improved efficiency and performance through a balance of power plant architecture, design and operational control.

Hybrid power plant advocates are at odds over which methods are best to achieve the objectives. Advocates of parallel plant architectures believe that adding torques from the devices is the best way, and series advocates believe that balancing power flows is the best. Both groups have good reasons for their approach. However, there is even disagreement within each group about the objectives, the criteria, and the means by which to achieve them [2] [3]. Until there is agreement on the actual criteria and objectives leading the overall research, engineers will continue to investigate the hybrid power plants that satisfy their individual convictions.

In light of this situation, there remains an academic challenge to make sure that the methods used to design and model hybrid power plant prototypes are optimal in utility, so that engineers can adequately test their proposed designs without immediately involving themselves in the timely and expensive process of power plant development. The author foresees three major steps that must be completed before a consensus can be reached on which hybrid vehicle power plant concepts should be mass produced:

Step 1: Establish design and modeling methodologies that give adequately accurate and realistic predictions of the performance characteristics of various hybrid vehicle power plant concepts.

Step 2: Use the design and modeling methodologies to identify the most promising HVPP concepts.

Step 3: Construct prototypes of the HVPP concepts identified in Step 2 and thoroughly test them.

Step 4: Manufacture the best concepts from step 3.

The goal of this work was to make a significant contribution to step 1. Designers need models that will serve as flexible design tools. The models should allow designers to make performance predictions of proposed designs, and they should show them the difficulties that they may face in the construction and design of prototypes.

Currently, all but perhaps a few of these models are comprised of empirically generated performance maps for each of the power plant devices [4] [5]. This was a good approach for the initial stages of hybrid power plant design. The concepts and performance of the various proposed architectures needed to be verified. Off the shelf components were used for these initial plants, and their performance data was readily attainable. Furthermore, empirical models are computationally fast. However, the designer using such models cannot see how changes in specific design parameters will affect the performance of the plant. Scaling these models gives a gross indication of performance changes, but the designer cannot have much confidence in scaled results, because these models are developed to predict the performance of a device whose design parameters are fixed. Thus, these models are not flexible design tools.

1.2Early Background to this Work

The author's first exposure to HVPP's was received in a graduate level design course. The design group spent a large portion of time concentrating on the abstract design aspects of HVPP's. The abstract design viewpoint considers only what a design must do rather than how it will do it. This group developed initial versions of abstract design tools, and the author developed an initial version of a new abstract design tool while in this group. The latest version of this new abstract design tool is presented in section 2. The new tool provided many useful benefits for group design, but the group was only able to perform simple model simulations to validate proposed design concepts.

As a result of this graduate design course work, the author joined an interdisciplinary design group that was working on a specific HVPP design. This design incorporated a specific architecture and a specific operational scheme. It was named the "Electrically Peaking Hybrid" or ELPH for short. This group was primarily comprised of members from the Texas A&M University Electrical Engineering Department. The previously developed abstract design tools were not applied, because the group had already established a specific design concept. Among other things, the author contributed a modular and detailed ICE model written in Matlab/Simulink to this group. He also contributed a scheme for passing component model values between the model's sub-components. This was implemented by another group member. This scheme allowed the ELPH model to be modular, but the ELPH clutch model resulted in disparity between the velocities on each side of the clutch. Furthermore, the ELPH clutch model did not predict proper loading of the engine during clutch engagement. A good clutch model is essential for correct modeling of the connection dynamics between the engine and the drive train.

The author's experiences with both groups were valuable, and they pointed out some important aspects of HVPP design and modeling. First, there was no common basis for communication and interaction among the members of the groups. The first and second generation ELPH models employed an empirical performance map ICE model. There could little confidence in the performance predictions of this model, since it had been developed for a particular engine and, therefore, had to be scaled for the ELPH model which used a much smaller engine. The modeling effort for ELPH was not initiated from an identification of the fundamental functions that must be provided by any hybrid vehicle power plant (i.e. there was no system design approach). The component models were developed by individuals with expertise in various fields, and then connected in a manner that did not properly accommodate the discontinuities in the drive train caused by the clutch. The clutch model actually hide important interface sensitivities such as the sudden loading of the engine which could result in stalling. This prevented a comprehensive identification of critical design parameters.

Based on these experiences, and the current needs in the field of HVPP design that were stated in section 1.1, the author hoped to extend the field of HVPP design by establishing universal design and modeling methodologies that could assist HVPP designers originate and study a wide variety of HVPP architectures and operational schemes. The design methodology should use a systems design approach to develop abstract design tools, so that all functions and interfaces essential to the overall system are identified and none are overlooked. The modeling methodologies should: use a common approach, so that design group members have a common basis for communication and interaction; use a common level of modeling detail for all of the component models that will be used in HVPP models, so that the overall system will possess a level of detail that can facilitate intelligent design choices; be modular to the point where the models can properly accommodate dependencies and discontinuities.

1.3Research Objectives

Based on the above, the objective of the proposed work is to develop and demonstrate design and modeling methodologies that can be used to identify the critical design parameters of hybrid vehicle power plants. Models developed from such a methodology will be flexible design tools that accurately represent the relationships and sensitivities among the design, operating and performance parameters. They can also be used to identify sensitivities resulting from various interfaces. These items will be discussed in detail below.

In order to best achieve this objective, the following philosophies will be followed. The design of hybrid vehicle power plants should be derived from a thorough system design approach. The modeling methods should be based on first principles (i.e. based on the laws of physics rather than empirical models based on analysis of data) as often as possible. The models should be modular, so that the designers can rapidly change the architecture of the power plant and, when possible, rapidly change the configurations of the individual devices. Some empirical relations will be necessary. However, strong efforts should be made to use sub-component empirical relations that incorporate design parameters. The models, and methodology of developing them, should serve to improve the designers' understanding of the physics and the engineering tradeoffs involved in the design. Since engineers from the various disciplines will be working together, the modeling methodology should be generalized and visual, so that it is easily understood by members from each discipline.

Once completed and used in simulation studies, models developed with this methodology will be easily modifiable. Furthermore, these models will call attention to many of the difficult design issues before the physical development of the design rather during the development. The following sub-sections will further describe the system design approach and the modeling methodology.

1.4Design Methodology for Multi-Disciplined Systems

A system design approach will be followed and reviewed as necessary for each new hybrid vehicle power plant (HVPP) configuration that is studied and modeled in this work to make sure that the objectives of this work are properly directed and are derived from a thorough consideration of each power plant's required design functions. This approach provides safeguards against poor designs and assistance in design development by setting forth proven and successful design methods. Use of this proven design methodology also provides excellent guidelines for identifying improved concepts in the design of HVPP's [6]. Such methods are especially necessary in the design of a multi-disciplined system such as a HVPP, because there are many interactions and dependencies to consider. Following a careful design methodology will provide extra assurance that no important concerns are overlooked and will increase the likelihood of approaching the best possible design.

1.5Modeling Methodology

There are three important aspects to the modeling methodology in this work. The three aspects are approach, level of detail, and modularity. Each aspect should be followed in a common manner by the contributing disciplines to provide consistency. The consistency should facilitate improved group interaction and improved cross-disciplined understanding.

1.5.1Modeling Approach

The modeling of HVPP's presents unique challenges to the modellers of the individual components in the HVPP. Changes in the design parameters of the HVPP sub-components will affect their individual performances, the overall performance of the HVPP, and the performance of other sub-components. Therefore, the sub-component modellers of a HVPP modeling team must thoroughly understand: 1) the physics of the devices that they are modeling; 2) how their devices can affect other power plant components; 3) how their devices can be affected by other power plant components; and 4) how design parameter changes in their devices will affect the overall performance of the HVPP. In order to understand items 2) and 3), the sub-component modellers must also understand the physics of the other sub-component models.

Understanding the physics of components outside one's field of expertise can be a formidable challenge. Although the mathematics that describe the physics across different fields of engineering are similar, the approach to theory and model development across fields can be quite different. Learning new approaches to theory and model development seems time consuming and impractical to most engineers who have spent a long time gaining a detailed knowledge of their own specific areas within their specific fields. Language idioms that exist in each field of engineering further complicate cross-disciplined learning.

Adoption of a cross-disciplined "trade language" and methodology could lower these barriers significantly when engineers from different fields must work together on a common project. Learning this "trade language" and methodology can be an easy task if analogies between the specific and general fields are provided. This cross-disciplined "trade language" and methodology is called the generalized approach, and it will be used in an attempt to lower the cross-disciplined barriers that exist.

The synthesis and productivity of a design group will obviously improve if the engineers from different disciplines within the group use any good and common approach in a multi-disciplined design project, and this can make the design process more rapid. A generalized approach also has the potential to improve the perceptions of the group members into possible design improvements, because they are now looking at the system in a new and generalized way.

The generalized approach uses a common mathematical description for different physical systems. All systems store and dissipate energy. When the systems are linear, the relations are completely analogous among various types of systems. For example, stored kinetic energy due to a mass in motion is mathematically identical to stored magnetic energy in an inductor. Therefore, the magnetic energy can be thought of as a generalized kinetic energy. Furthermore, constitutive relations for the differential equations describing system dynamics can be derived from these energy relations even when the system components are nonlinear.

Even though the differential equations of nonlinear systems are different from one realm to another (e.g. mechanical and electrical) their development is similar and starts from energy considerations. If a relation for energy is derived for any system, the designer need only understand whether this energy is a type of generalized kinetic or potential energy. Once this is known, the necessary partial derivatives and/or derivatives can be taken to determine the proper non-linear constitutive relation. The state variable can then be factored from the resulting constitutive relation to determine the function for the nonlinear energy storage element.

If the modeling of components is broken up into the generalized sub-components, engineers from any discipline can gain adequate insight and detail about the individually modeled components. Such an approach can improve a designer's understanding of a system's operation. Model development using the generalized approach can make the development process more intuitive for all disciplines involved. Starting from system drawings of the HVPP components, each sub-component is labeled according to the generalized way in which it manipulates energy. Once this is done, the constitutive relations can be obtained from energy considerations, theories from basic first principles, Newtonian mechanics, and/or bond graph modeling techniques.

1.5.2Level of Modeling

For the generalized approach to have its greatest utility as a design tool, all models should be based directly on design parameters to the greatest extent possible, and all physical state variables for any time in the simulation should be available for study.

This statement of modeling criteria requires some explanation. Consider the phrase, "…based directly on design parameters…." Obviously, empirical models developed directly from experimental data in the form of input parameters verses output performance parameters would not meet this modeling criteria. The only time one can have confidence in this type of model is when it is being used to predict the performance of the actual device for which it was developed. If a HVPP designer was using such a model for an engine, he could not study the predicted performance changes due to changes in design parameters such as bore to stroke ratio, exhaust duct length, etc. Sometimes it is necessary to use such empirical models, because the knowledge of certain physics has not attained a sufficient level. For example, battery modeling is not yet at a stage where physicists and engineers can develop accurate constitutive relations directly related to physical design parameters. There are other important reasons that the modeller will occasionally need to use empirical models. These reasons will be discussed below. However, even when an empirical relation becomes necessary, an empirical relation based on design parameters should be used whenever possible. Therefore, the modeling methods should be based on design parameters, not just operational and control parameters, and first principles relations should be used as often as possible.

Now, consider the statement, "…all state variables for any time in the simulation should be available for study." In some disciplines, a set of sub-components is grouped together to form one equivalent sub-model. Sometimes this is necessary due to the physical dependencies that exist. Other times it is done to reduce the amount of calculations or to avoid implicit solutions. For example, equivalent circuit models are developed for AC electrical machinery. This practice is beneficial, because it reduces the amount of required calculations. The modeller can set up his simulation code to automatically calculate the changes in the equivalent circuit parameters resulting from physical changes in the electrical machine design. However, consider what remains hidden to the designer when this practice is employed on an AC induction motor. The dynamics of current and voltage in the individual rotor bars and end ring segments are hidden. It may be true at times that there is no benefit to being able to see all of the state variables in a modeled device when studying the contribution it makes to the performance of a vehicle. No judgments will be made regarding when this is true or not true, because there is at least an academic benefit in being able to study all the state variables. Therefore, the models will be developed with significant detail so that the state variables of separate discrete devices can be seen for all times during a simulation.

Consider another example where a group of individual components in an ICE can be grouped into an equivalent sub-model. The air flowing into the cylinder will flow through several resistances in route to the cylinder. It will, at the least, flow through a throttle valve, intake port, and intake valve. An equivalent resistance could be determined by considering which resistance is the most restrictive at any time. This could significantly reduce the amount of integrations in the simulation and speed the runtime of the model, but important details would be lost. The dynamics of how each air passage fills and empties, and the effect of these dynamics on the air entering the cylinder, would be hidden.

By retaining the physical details of the model, the designer will be able to see the dynamics of all the state variables that actually exist in the devices. This will serve to improve his understanding of the device. It will also help him to see the detailed relations of the state variables to various parameters.

Levels of dynamic modeling are defined in the different fields of engineering, but they do not necessarily cross correlate to other fields very well. In order to avoid any potential confusion, six different levels of modeling will be briefly described and named according to their descriptions. Modeling level will be regarded by the level of system decomposition. The more components a given system is decomposed into, the higher the level of modeling.

The first, and lowest, level of modeling will be termed “black box” modeling. This level of modeling is essentially a curve fit of output data verses input data. The curve fit is performed by identifying parameters in mathematical functions that will result in the correct output for any given input within a given range of input data. The input/output data is obtained from experiments. The mathematical functions used for the curve fit provide no description of the actual physical processes, and they do not contain any system design parameters. The output of the model is only affected by the input parameters. Models of this type are very fast in simulations, but, since the model contains no design parameters, it cannot be scaled with confidence. They can only be used for the devices close in design to the device used to determine them. Furthermore, one can only have confidence in black box models when they are simulated using the original range of input parameters. This type of modeling is sometimes called empirical modeling. However, this name will be reserved for the next level of modeling which is significantly different.

The second level of modeling will be termed empirical modeling. This level of modeling takes black box modeling to the next step by curve fitting output parameters verses changes in input parameters and changes in design parameters. Empirical modeling is much more experimentally intensive than black box modeling, but once a good empirical model has been developed, it is very valuable.

The first two modeling levels are obviously not decomposed into sub-components. The given systems or processes modeled by these methods are treated as a whole. The next three levels of modeling deal with various levels of decomposition. In each of these higher levels of modeling, first principles are used as frequently as possible (e.g. Newtonian physics, conservation principles, etc.).

Lumped parameter modeling is the name given to the third level, and it is best illustrated to most readers by a simple example of an equivalent electrical circuit. While it is possible to determine the currents through two resistors in parallel, it may be desirable to simply replace the two resistors with one equivalent resistance. Once this is done, the currents through the individual resistances are hidden. Only their sum is considered. Sometimes, due to dependencies, it is necessary to lump physical parameters. An example of this will be seen in the actual ICE modeling.

The fourth level of modeling, called component modeling, is system decomposition into discrete physical parts, or into the obvious regions of physical change, in the system. Using the simple electrical circuit analogy again, one would not lump any of the discrete electrical components of a circuit into a single component unless dependencies require it. Choice of this level of modeling is used when adequate accuracy can be achieved by considering the discrete parts of the system as whole entities. For example, the voltage of a capacitor is considered to be modeled accurately by dividing the time integral of the current by the capacitance without having to divide the surfaces of the capacitor plates into various finite elements to determine the geometrical charge distribution.

However, certain system components do require a certain level of finite element decomposition (the name given to the fifth level of modeling) in order to achieve reasonably accurate predictions from models. Finite element modeling is also used to study how geometrical changes will tend to improve specific physical characteristics of the modeled system component. Examples of how this type of modeling are used would be: the modeling of induction motor rotors to balance flux leakage and rotor bar resistance for desired torque-speed characteristics; modeling of machine components to determine the geometrical shape that uses the least amount of material while providing the greatest possible strength; fluid dynamic flow passage shapes that result in the desired flow characteristics.

The finest detail of modeling actually involves no decomposition at all. This would be continuum modeling. However, this is usually prohibitively difficult, and is only done when possible, practical and useful.

The level of modeling chosen for this work is component modeling. This level of modeling has proven to be detailed enough to predict the actual physics of the components and accurately predict performance, but not so detailed that simulations are slowed to impractical speeds. It would be preferable to use finite element based models, because of their ability to predict how any geometrical change to a part can affect the performance of the system to which it belongs, but they would be prohibitively slow for vehicle performance simulations over a 10 to 1500 second drive cycle.

1.5.3 Modularity

As explained previously, the community of engineers designing HVPP's have not reached a consensus on the best HVPP architecture for automobiles. There are a variety of possible HVPP configurations that need to be tested. There is also a variety of components that can be used in a HVPP. Furthermore, there is sometimes a large variety of configurations that can be proposed for one of the components in the HVPP (e.g. the ICE). Therefore, in considering these possible variations, it is imperative that the modeling methodology be modular (i.e. the final models should be built from smaller component model modules), so that designers can easily change the power plant architecture and the configurations of individual devices. Modularity is essential to designers working through these conceptual design stages. Even if the ideal architecture and configurations were known, modularity would still be important, because engineers will always need to simulate new variations of HVPP's as new components are developed.

1.5.4 Bond Graphs

Bond graphs [7] are a powerful visual modeling technique that can fulfill the criteria for the generalized modeling approach stated previously. They can usually be derived, or followed, by looking at drawings or block diagrams of the systems being modeled. They visually indicate the flow of energy from one element to another within a system. They also visually define the differential equations of a system [7]. Fully labeled bond graphs can be entered directly into simulation routines that utilize differential equations. Pieces of code representing portions of the bond graph or system drawing can be easily catalogued into separate modules. When designers want to look at a new plant configuration, the catalogued sub-models derived from the labeled bond graphs can be pasted into the code with the required connections. Thus, the designer has a visual simulation design tool that provides rapid reconfiguration of the plant and its sub-components. By deriving and representing the models with this visual and graphical modeling method, it will be easier for the multi-disciplined design team to work together.

Bond graphs are popular, but they are still somewhat new. A short tutorial on bond graphs is supplied in Appendix A. This is only meant to serve as a qualitative overview of the utility of bond graph modeling to help those reading this work. For more detailed instruction in the multiple uses of bond graphs, see [7].

1.6Overview of Dissertation

Section 2 gives an overview of the abstract design methodology. Section 3 demonstrates the modeling methodology. Four important types of sub-component modeling are covered in the four subsections of section 3. The abstract design methods and the sub-component models are applied to specific concepts in sections 4 and 5 that deal with single power plant and HVPP designs, respectively. For each vehicle power plant, the design methods are first applied for each power plant concept. Then, simple models are studied to identify high level parameter values such as power densities, desired acceleration, power requirements, gear ratios and vehicle mass. Parameter values obtained using these initial models are used to determine parameter values for the more detailed models. Once the detailed models are developed, small changes to design, operation and control parameter values are made to improve performance of the models. If the models give realistic performance predictions, they will give good direction for choosing parameter values in the construction of prototypes. Each section has an overview at the beginning of the section, and most sections, and some sub-sections, have their own summarys and conclusions. The work and findings are summarized in section 6, and the conclusions are given in section 7.

2DESIGN METHODOLOGY FOR HYBRID VEHICLE POWER PLANT

2.1Abstract Design Tools

The essence of the system design approach to HVPP design is to abstract the physics of HVPP's. The abstraction of HVPP's includes the following: defining the need for HVPP's; defining the functions required of HVPP's and their structural hierarchy; defining the objectives of given HVPP's; and defining the possible relations between the functions allowed within the current knowledge of physics.

Different configurations and concepts exist for HVPP’s, because designers have weighted the essential objectives differently for their individual designs. However, the essential objectives of HVPP design are the same. It is not the goal of this section to argue about the best weighting for the essential objectives. Rather, it is hoped that the abstractions provided in this section will provide a common focus among HVPP engineers, and that the abstractions will provide a start in developing improved HVPP design guidelines. Therefore, this section will:

1) present an analysis of the need for, and the essential functions of, any conceivable HVPP design.
2) introduce a simple graphical tool that clearly illustrates the relations between the HVPP design functions of any conceivable HVPP design.
3) explain how to use the graphical tool to clearly demonstrate the energy management techniques of various HVPP concepts and configurations.

The proposed need statement for HVPP's is as follows:

A hybrid vehicle power plant that compares to conventional vehicle power plants as follows:

1) greatly improved fuel efficiency;
2) greatly reduced emissions;
3) approximately equal or better acceleration, speed, range, and cost.

Interest in HVPP's rose from the societal constraints are addressed by the three sections of the need statement.

A function structure that includes the essential functions required of any HVPP is shown in figure 2.1.1. The primary function of a HVPP design is to provide energy pathways. The energy source of the vehicle is transmitted and transformed one or more times until it propels the vehicle. Each transmission and transformation is considered an energy path.

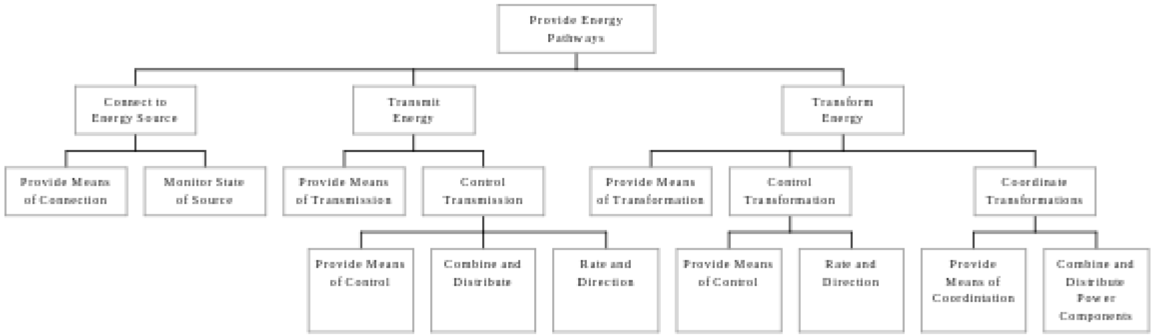

Figure 2.1.1: Essential Function Structure for any Hybrid Vehicle Power Plant Design.

Consider the example of a conventional automobile. A source of energy would be the gasoline in the gas tank. The gasoline is transmitted through gas lines to the fuel injectors. It is then transformed to both thermal and fluid mechanical energy in the cylinders of the ICE. The fluid mechanical energy is then transformed to translational mechanical energy with the piston and then to rotational mechanical energy using the ICE crank shaft. The rotational energy is transmitted through various shafts, and the torque and speed associated with the rotational energy are transformed via the vehicles transmission, until the energy arrives at the wheels. Finally, the rotational mechanical energy is transformed back to translational mechanical energy using the wheels of the vehicle, and the car is propelled. Therefore, three sub-functions logically fall from the main function of providing energy paths. The HVPP must connect to an energy source, transmit energy, and transform energy. Two sub-functions must be performed for the energy source connection. A means of connecting to the energy source must be provided, and the state of the source must be monitored. Three sub-functions must also be performed for the energy transformations. A means of energy transformation must be provided, the transformation must be controlled, and the various transformations must be coordinated. Two sub-functions exist for the energy transmission function. There must be a means of transmitting the energy, and there must be a means of controlling the transmission. The remaining layers of sub-functions are easily understood along these lines of thought and are shown in figure 2.1.1.

In any theoretical HVPP, there are sources of energy, there are devices that transform energy from one form to another, and there are devices that transform energy from one location to another. Figure 2.1.2 is used to illustrate the functional relationship of these devices within the HVPP concept. A theoretical HVPP can have any conceivable combination of energy sources, devices that transmit energy and devices that transform energy. All of these must be coordinated properly to yield the desired, or optimal, performance.

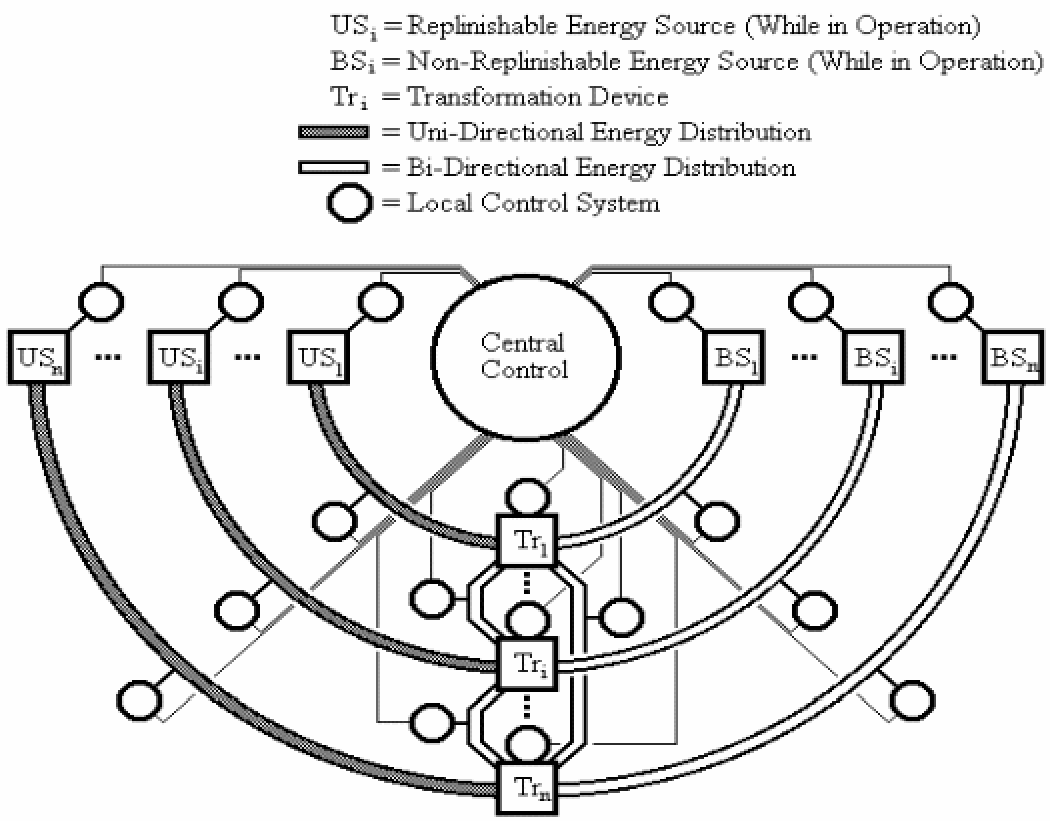

Figure 2.1.2: Function System Diagram

Normally, in abstract design stages, designers will only consider the functions the design must perform. In other words, they only catalog "what" the design must do. In order to do a thorough mental analysis in this stage of design, they will avoid immediate considerations of, or conclusions on, "how" to achieve the functions of the design. The stage of design where designers consider "how" to achieve the functions for the design is called the "conceptual design" stage. Therefore, some readers may note that the function system diagram, which is being called an "abstract" design tool, is introducing "concept" by giving a set structure for the functions. This is easily answered. This current discussion regarding HVPP design was born from a concept. In other words, the first words of the need statement for this design enforce the HVPP "concept." The function system diagram merely serves to show the relationships of the functions within this HVPP concept in the most abstract fashion possible. We should also remember that HVPP’s are actually a conceptual refinement within an existing design project that has spanned more than a century. This ongoing and lengthy design project is the automobile.

The use of the word devices in this discussion is used to represent a pre-conceived (but unknown device) that will fulfill the represented function(s). No other concepts should be considered at this point (i.e. resist any immediate conclusions about what devices should be used and how they should be configured). Therefore, figure 2.1.2 is comprised of the following functional devices: uni-directional and bi-directional energy transmission devices and their local control systems; energy transformation devices and their local control systems; energy sources that can be replenished while driving and their local control systems; energy sources that cannot be replenished while driving and their local control systems; and a central control system. The creation and discussion of this diagram is an attempt to fully exploit the pre-conceptual development (i.e. the abstract development) of the HVPP design concept. Furthermore, since no actual devices have yet been named, figure 2.1.2 shows the functions without regard to physical limitations or design choices. For example, some transformation devices might not be able to connect to both types of energy sources, but it is best not to assume that this is always the case. Taking such an approach will lay the strongest and broadest foundation possible for creativity among designers and improved concepts in the design of HVPP's. Figure 2.1.2 will be referred to as the function system diagram.

The central circle is the control center that executes the hybrid scheme. The central control takes control inputs from the driver and routes controls as necessary to the local control systems for the transformers, sources, and transmission devices. Central control is needed to coordinate the operation of the HVPP components. Any required feedback information from the local controllers of these HVPP devices is transmitted back to the central control.

The local control of the devices may be achieved in a passive manner by design. However, since this is a system diagram at the functional level for general HVPP design, and a "means of control" for each of these sub-functions must be provided by the design, controllers are included for each device that fulfills a function.

Energy sources supply energy to the system. Energy sources that can be replenished while driving will usually be storage devices, but they should not be limited in thought to this assumption. An example of an energy source that is typically not replenished while driving is the octane in a gas tank.

The transmission devices transmit energy to and from the energy sources and energy transformation devices. During the conceptual design phase, the designer may decide to use some uni-directional transmission and transformation devices in place of bi-directional devices. The transmission devices are controlled passively by design, or actively during operation.

Herein, a transformation device is considered to be any device that is designed to either: transform one form of energy to another (e.g. mechanical to electrical in an electric motor); or alter the variables associated with energy transmission (e.g. torque and speed manipulation with gears, or voltage and current with electric transformers). The transformation devices include ICE's, electric machines (i.e. motors, transformers, and generators), transmissions (e.g. gears or sets of gears), wheels, and more. All of the transformation devices are shown connected to each other with transmission devices so that energy can be transmitted and transformed as necessary to optimize the energy management of the HVPP. Some transformation devices go through multiple stages of transformation between their points of connection to transmission devices. It is an unfortunate physical fact that some transformation devices are not "completely bi-directional." For example, a conventional automobile ICE converts chemical potential energy of octane to rotational energy, but it will not convert rotational energy to octane. However, an ICE can transform rotational mechanical energy to fluid mechanical energy. It may be worthwhile to recapture some energy from a transformation device that is not completely bi-directional.

Figure 2.1.2 is obviously a high level, or macroscopic, tool for the iterative process of system design. It provides a skeletal frame for the genesis of concepts. It is useful to demonstrate at a glance the differences in energy management between various concepts.

It is hard to prove the utility of such an abstract tool through examples in a report. Its value can only be experienced in a group design project. Initial versions of this function system diagram were developed during a group design, and the group found it to be a valuable tool in the following ways:

1) It allows design group members to visually communicate their thoughts to one another within a standardized convention.
2) It visually relates the energy and information transfer between the devices that will be designed to fulfill the functions of the function structure without actually showing concepts that might bias or hinder the creativity of the design team.
3) Provides traceability of requirements to the functions that must be provided by any HVPP design.
4) It shows the functions the design must fulfill without regard to physical limitations and yet reminds the group of basic physical limitations that exist such as the existence of uni-directional energy transmission and transformation devices.
5) Once actual concepts are devised to satisfy the functions, the new system diagram provides a concise, clear, and visual convention for recording the history of concepts that were compared, rejected and refined by the group.

2.2 Application of Abstract Design Tools

Theoretical verifications (modeling) must still be performed to quantify large scale parameters against criteria and constraints and to measure these quantities against current capabilities. However, figures 2.1.1 and 2.1.2 can aid the designer as he thinks through various concepts in the process of designing a HVPP. The use of figure 2.1.2 will be illustrated in later sections in the conceptual development of the virtual vehicles that were simulated and studied.

2.3 Summary

The author has found no abstract design tools for the design of hybrid vehicle power plants in the literature. Abstract design tools were developed in this section. A need statement and a function structure were developed, and they only include the essential needs and functions that are common to any HVPP design. A new abstract design tool, the function system diagram, displays the interrelationships of the functions in the function structure. This diagram, which actually sets forth a system architecture concept, was formed, because the abstract HVPP design process was started from a concept.

2.4 Conclusions

The HVPP concept is a phase in mankind’s century old design refinement of the automobile. It is the hope of the author that the use, and/or refinement, of these abstract tools will provide a universal holistic base of thought that will lead the community of HVPP designers to a broader range of concepts from which potentially better designs will emerge. These abstract design tools are the first unique contribution of this work to the field of HVPP design. It is impossible to make specific conclusions regarding these abstract tools, because the arguments presented for their utility are subjective, and they have only been evaluated by two design groups. However, the arguments used in their favor are consistent with well established system design methods [6].

3. DEVELOPMENT OF HYBRID VEHICLE POWER PLANT SUB-COMPONENT MODELS

The sub-component models were validated independently using available experimental data or manufacturer ratings. The model parameters were set to match the design parameters of the devices from which the experimental data was obtained, or were designed to meet the specified ratings. If the simulation data agrees acceptably with the experimental data, or the rated performance parameters, and the characteristics of the dynamics, the model was considered adequately validated. If the two sets of data are not in good agreement, the model should be modified until the degree of agreement is acceptable. The design from which the data was obtained may not have the same specs and dimensions of a device to be simulated in a given hybrid power plant. However, if the component models are developed using the proposed modeling methodology and have adequate accuracy, then one can have good confidence that changes in design parameters will not drastically affect the model accuracy (e.g. if a small two cylinder ICE model is accurate, a slightly larger three cylinder model should also be accurate).

The finalized sub-component models should be used in the single power plant vehicle models to gain familiarity with how design, operational and control parameters can affect the performance characteristics of these individual power plants, because a complete hybrid power plant model will have a large number of design, control and operating parameters that will be difficult to adjust without a knowledge of how each of the individual power plants perform in a vehicle. Each of the components modeled below has its own unique responses to key parameters. Fundamental references covering the theories of each of these components explain in significant detail which parameters have the greatest effects on performance parameters. Using this knowledge, the appropriate design, operational and control parameters of the single power plant models can be changed until the virtual vehicle has achieved the desired performance.

The code for all HVPP component models was written in the Advanced Continuous Simulation Language (ACSL) using both ACSL for Windows, and the ACSL Graphic Modeller [8] [9] [10]. ACSL was used because it is a fast, well developed simulation language. The ACSL Graphic Modeller provides a visual front end for ACSL that encourages modularity of coding. This allows separate graphical blocks to be stored and reused in several models. Once these graphical blocks have been formed with their respective code, the end user can retrieve these blocks from a digital library and connect them as necessary to form new models for study. The graphical blocks for the various HVPP sub-components will be henceforth referred to as power blocks. All code for the various power block components are contained in the Appendices along with other useful information concerning the development of the models.

This section will explain the development of four important modeling areas: drive train modeling, ICE modeling, electric machine modeling, and battery modeling. The drive train modeling required special considerations. Rigidly connected systems are not modular. But maintaining modularity was crucial to this work. Therefore, a method was devised that allowed modularization of rigidly connected systems. This method also had to properly handle discontinuities in the rigid connections (e.g. clutches) and changing inertias causes by transformations in the drive train (e.g. gear changes). ICE sub-component models were developed that allowed a designer to change design parameters and engine configuration. Thus modularity is extended to the engine modeling also. Electric machine modeling covered dc machines, transformers and induction machines. DC machine models are accurate and simple. The chosen level of modeling required a new type of induction machine model. The methods used to develop this model are first introduced using simple transformers. The very good equivalent circuit model for batteries was used in this work. The equivalent circuit is based on first principles. The circuit elements are non-linear sub-models derived from experimental measurements. Validations were performed on all of the models. Each exhibited realistic performance predictions and realistic dynamic characteristics.

3.1 Drive Train Modeling

Rigidly connected systems and modularity are not synonymous concepts. If a system has rigid connections between its inertias, the inertias must be lumped and treated as one equivalent inertia, because they do not act independently. If this traditional practice was carried out in this work, the modularity of the drive train and the power plant could not be achieved as desired. A simple method of passing generalized efforts and inertias was developed to overcome this challenge. However, this method cannot deal properly with the occasional discontinuities that are encountered in some vehicle power plant configurations when one portion of the power plant must be disconnected from another. These discontinuities cause a notable difficulty when using methods of continuous simulation. In order to meet the objectives of this research, which dictate that designers be able to easily test different HVPP architectures, the modularity of the models had to be maintained, and the discontinuities that can occur in the models had to be properly addressed. A method was devised that allows modularization of rigidly connected systems and that also allows discontinuities to occur in the system.

3.1.1 Modular Rigid Drive Train Modeling

Modularizing a rigidly connected system without discontinuities is not difficult. Key values are simply passed back and forth through the system’s modules. Each module uses the input values it receives to calculate its output values in accordance with its purpose in the overall system. A scheme such as this can be applied to the EV drive train shown in figure 3.1.1. The value passing scheme for this EV drive train is illustrated by figure 3.1.2 and is explained below. Shaft inertias have been neglected.

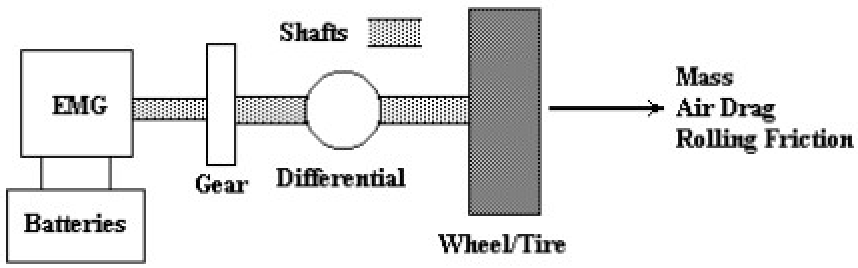

Figure 3.1.1: Electric Vehicle Drive Train.

$$\begin{matrix} T_{em} \\ J_{em} \end{matrix} \rightarrow \begin{matrix} T_{em} \cdot GR_g \\ J_{em} \cdot GR_g^2 + J_g \end{matrix} \rightarrow \begin{matrix} T_{em} \cdot GR_g \cdot GR_d \\ (J_{em} \cdot GR_g^2 + J_g) \cdot GR_d^2 + J_d \end{matrix} \rightarrow$$

$$\omega_{em} = GR_g \cdot GR_d \cdot V_{car} / R_t \leftarrow GR_g \cdot GR_d \cdot V_{car} / R_t \leftarrow GR_d \cdot V_{car} / R_t \leftarrow$$

$$\rightarrow \begin{matrix} T_{em} \cdot GR_g \cdot GR_d / R_t \\ ((J_{em} \cdot GR_g^2 + J_g) \cdot GR_d^2 + J_d) / R_t^2 \end{matrix} \rightarrow \begin{matrix} \sum e = T_{em} \cdot GR_g \cdot GR_d / R_t - F_{AD} - F_{RF} \\ \sum I = (J_{em} \cdot GR_g + J_g) \cdot GR_d / R_t + M_{car} \end{matrix}$$

$$\leftarrow V_{car} / R_t \leftarrow V_{car} = \int \sum e \cdot dt \Big/ \sum I$$

Figure 3.1.2: Value Passing Scheme for Modularization of Rigidly Connected Systems.

This drive train is powered by electric storage batteries through an electric motor/generator (EMG). The torque from the motor is transmitted through a shaft to a gear where the torque is transformed to a higher value. This increased torque is then transmitted through a differential which also has a gear ratio and transforms the torque to a still higher value. The torque out of the differential is transmitted to the drive wheels of the vehicle, and the wheels transform the torque to a force to propel the vehicle. The vehicle, which has mass, experiences road grads, air drag forces, and rolling friction [11]. Each transformation of effort (i.e. torque or force [7]) can be accomplished by one power block module. Each power block calculates the change in effort and passes the effort on to the next power block.

The velocity of the vehicle can be determined using Newton's third law of motion by integrating the sum of the forces on the vehicle mass to determine the momentum and then dividing the momentum by the mass [12]. The velocity of the vehicle determines the rotational velocity of the electric motor, and this rotational velocity must be known by the electric motor model so that its state variables can be calculated. Thus the velocity of the vehicle is passed back through the same power blocks and transformed by the same values (i.e. ratios) in each power block module which sends the right value of velocity back to the EMG power block.

One other consideration exists for the above scheme. The various components in the drive train other than the vehicle contain their own inertias which may not be negligible. The rotational inertias of the EMG can certainly not be ignored. By using conservation of energy methods and the ratios of the transformations [7], it is a simple matter to pass the equivalent inertias of the components through the power blocks and sum them until they reach a point where they are to be used to determine a velocity.

This scheme was not implemented exactly as described, because it could not properly deal with discontinuities that result when HVPP architectures, such as those shown in figures 3.1.3 and 3.1.4, include a clutch, or gear changing. Initially in this work, clutches were modeled as either energy conserving or effort transforming with a degree of connectivity that described the amount of engagement. This allowed one to use the scheme described above. However, these two methods caused a disparity between the velocities of the vehicle and the velocity of its power supplies when using the overall drive ratios between them for comparison. The energy conservation method caused a relatively small disparity when the clutch was operated quickly, but this actually hid the sensitive interactions that exist in fast clutch engagements, so neither of these schemes were used.

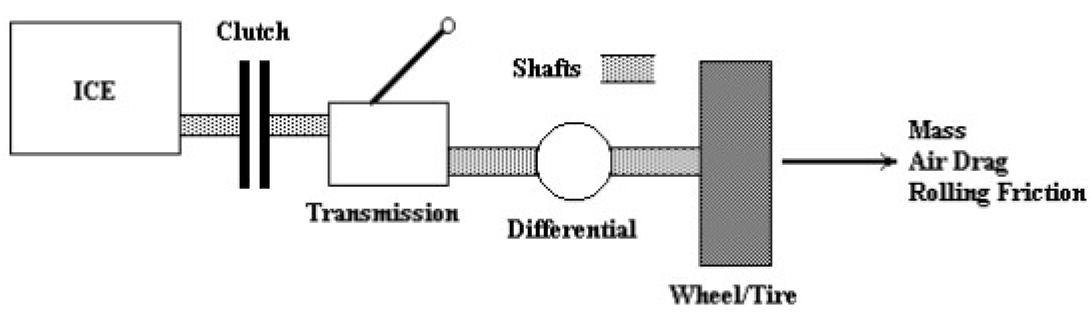

Figure 3.1.3: Conventional Vehicle Drive Train.

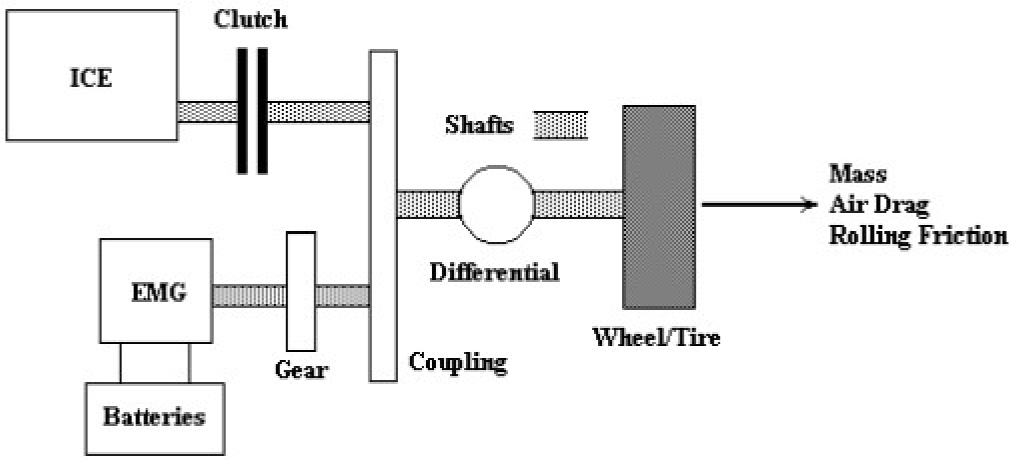

Figure3.1.4: Parallel Hybrid Vehicle Drive Train.

3.1.2 Modular-Rigid-Discontinuous Drive Train Modeling

A method that properly models the relations between systems connecting and disconnecting without hiding the sensitivities that exist in their interactions and that still allows modularity was devised. It will be referred to henceforth as the modular-rigid-discontinuous (MRD) drive train modeling scheme. The scheme will first be described in principle, and then explained in detail as it is applied to the drive trains in figures 3.1.3 and 3.1.4. The code for the MRD power blocks is contained in Appendix C.

This improved scheme is similar to the previously described scheme. However, generalized momentums (henceforth referred to as momentums) are passed through the drive train and through any devices that cause discontinuities (e.g. clutches) instead of efforts. In any power plant architecture, there are efforts that act as sources, and efforts that act as loads. Consider the sum of efforts in Newton's third law of motion equation. The efforts in this equation can be integrated separately to give separate momentums. These momentums are then passed through the power blocks of the virtual drive train, instead of the efforts, and are modified as required by drive train ratios, clutches, etc. When speed calculations are required, the current sum of momentums are divided by the equivalent inertia (which is also affected by changing gear ratios) at that point in the system.

Using momentums allows conservation of momentum to be applied to calculations across the clutch. This scheme resulted in a direct correspondence among all velocities in the system when the clutch was fully engaged and allowed the separate systems to operate properly when the clutch was disengaged. Any momentum being passed through the clutch is multiplied by the degree of connection. This scheme works in systems with or without the discontinuities caused by devices such as a clutch, and it properly models the energy lost in clutch connections and disconnections. However, a special treatment of standard integration routines had to be made.

Consider a scenario using this momentum transfer scheme in the simulation of the conventional plant shown in figure 3.1.3 with a standard integration routine. The clutch is initially disengaged, the engine is idling, and the vehicle is at rest. Since the engine is idling at a constant speed, the torques must sum to zero, and thus the momentum is constant based on previous conditions. The vehicle is at rest and therefore has no momentum. As the clutch engages, conservation of momentum dictates that the vehicle will begin to move, and the engine will slow down. The driver will increase throttle angle to get more torque from the engine as required to keep the engine from stalling and to accelerate the vehicle. At full engagement, the speeds will correspond exactly. During this time, the engine torque is being integrated with respect to time separately from the forces on the vehicle, and these momentums are being relayed to one another through the drive train power blocks. If the vehicle accelerates up to a constant cruising speed, the sum of the momentums in any power block will correspond to the cruising speed in accordance with the equivalent inertia and the ratio of that component to the vehicle speed. Thus, when efforts sum to zero (i.e. during constant speed), momentums do not sum to zero. The engine momentum determined from integrating the engine torque has been growing positive, and the vehicle momentum determined from load forces have been growing negative. This becomes a problem when the clutch starts to disengage, because they will no longer be able to offset one another. The engine and vehicle will appear to accelerate almost instantaneously as the clutch disengages but in opposite directions. There are two ways to deal with this problem. The best way would be to write a new integration algorithm that adds the current time step integration to the actual current momentum of the device rather than to the past time history of the integration. The second way, which works fine in ACSL [8], is to have the momentum state variable [7] reset to the actual momentum of the device at the beginning of any clutch disengagement. This way was chosen, because ACSL technical support cautioned the author on the difficulty in writing new integration algorithms that work with ACSL.

The full implementation of this scheme will now be applied to the conventional vehicle drive train of figure 3.1.3. The explanation will start at the ICE power block. Any sources or losses of mechanical power are not considered a part of the MRD drive train. They are connected to the MRD drive train through their own interface block that is part of the MRD drive train. The calculations for this interface block are illustrated in Figure 3.1.5.

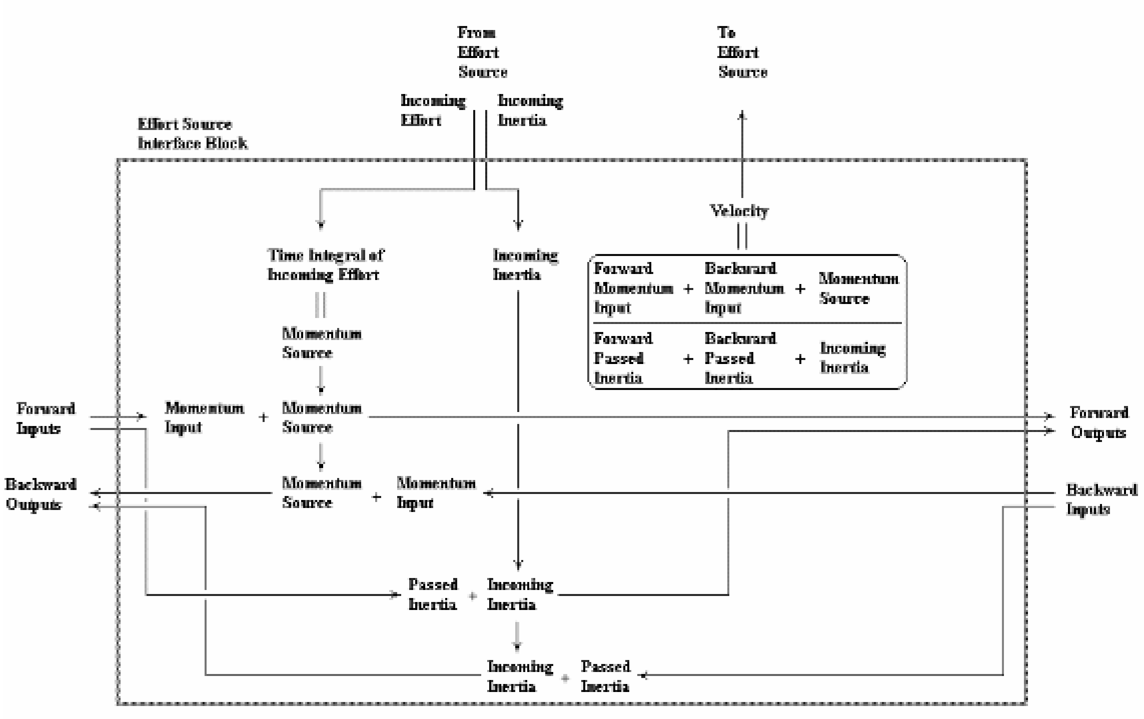

Figure 3.1.5: Illustration of MRD Interface Block Calculations for Power Supplies and Loads.

Note that there are inputs coming from the left and the right called forward and backward that also have respective outputs. The goal of this work was to design a flexible tool that allows designers to study many different model architectures. Mechanical power supplies often have shafts at both ends (e.g. ICE's and electric motors). Some designers may desire to study mechanical power supplies, or loads, that have connections to both ends of the shaft, so this feature was added.

A power supply or load is attached to the interface block. In the current example, the ICE power block is connected to this interface block. Its torque is integrated and added to the forward momentum input (which is zero for this drive train) before being passed to the forward output. Any inertia of the engine being considered in the modeling is then added to the forward passed inertia (which is also zero for this drive train) to be sent along the same power block connection line as the forward passed momentum. There is a backward passed momentum coming into this interface block which will be explained toward the end of this example.

The next component encountered in the drive train is the clutch. The calculations for its power block are illustrated in figure 3.1.6. The momentum and inertias being passed forward and backward through this power block are simply multiplied by the degree of clutch engagement which is from 0 to 1.

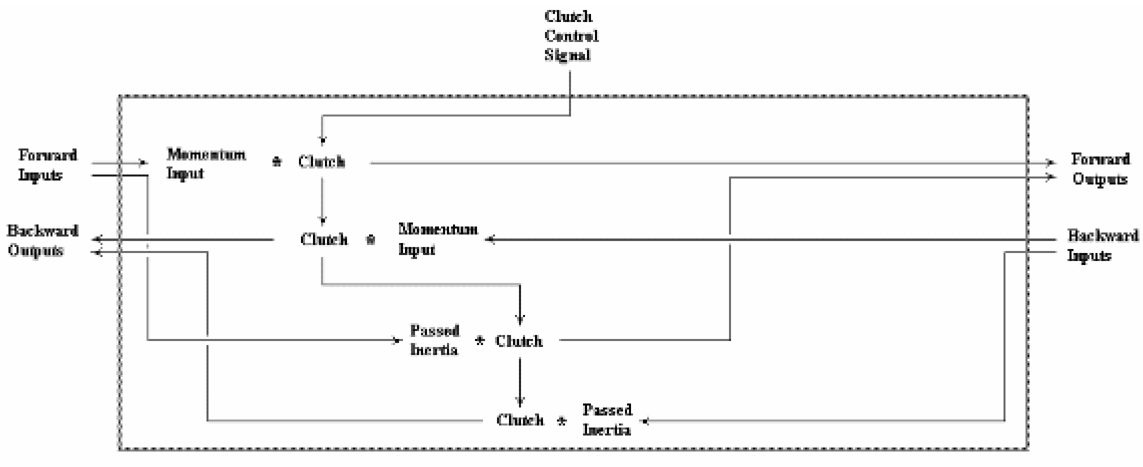

Figure 3.1.6: Illustration of MRD Clutch Block Calculations.

The next component encountered in the drive train is the transmission. The calculations for its power block are illustrated in figure 3.1.7. Note that this block can be set up to either receive a variable ratio to model discrete or continuous variations in gear ratio or to have a constant ratio. Thus, this same block can be used for gears, differentials, transmissions, wheels, etc. However, a separate power block was formed for wheels to avoid confusion in the use of the wheel radius as a ratio. The inertia is multiplied by the square of the ratio according to conservation of energy across the ratio [12]. If it is desirable to model losses in the gears, this can be done with a viscous load calculation attached to the MRD power supply and load interface block.

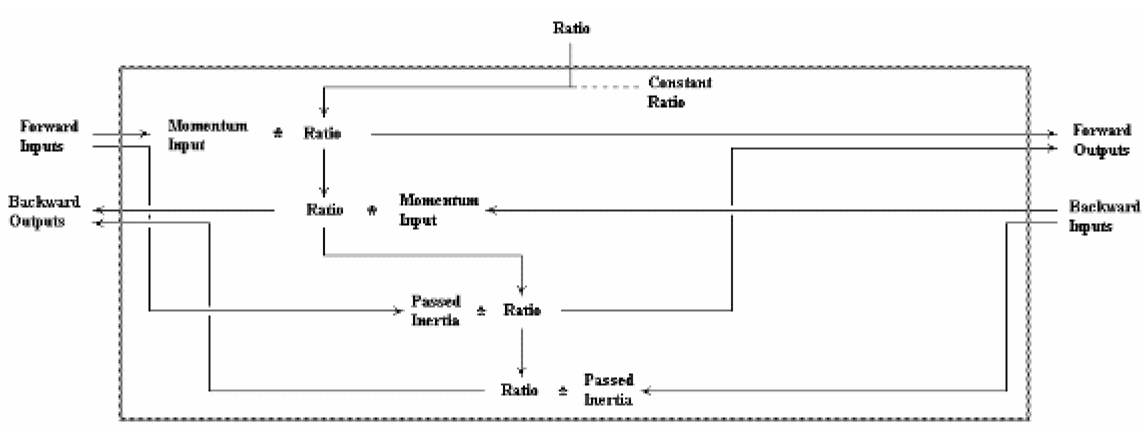

Figure 3.1.7: Illustration of MRD Ratio Block Calculations.

The only considerations remaining in this vehicle's drive train are the vehicle's loads as indicated in figure 3.1.3. The MRD power supply and load interface block shown in figure 3.1.5 can be used to process the load calculations and communicate their contributions to momentum through the MRD drive train model. However, a copy of the MRD power supply and load interface block was modified to be used primarily for typical vehicle loads, because there will always be vehicle loads in this work. They are typical and change only in value. The MRD vehicle power load block is shown in figure 3.1.8.

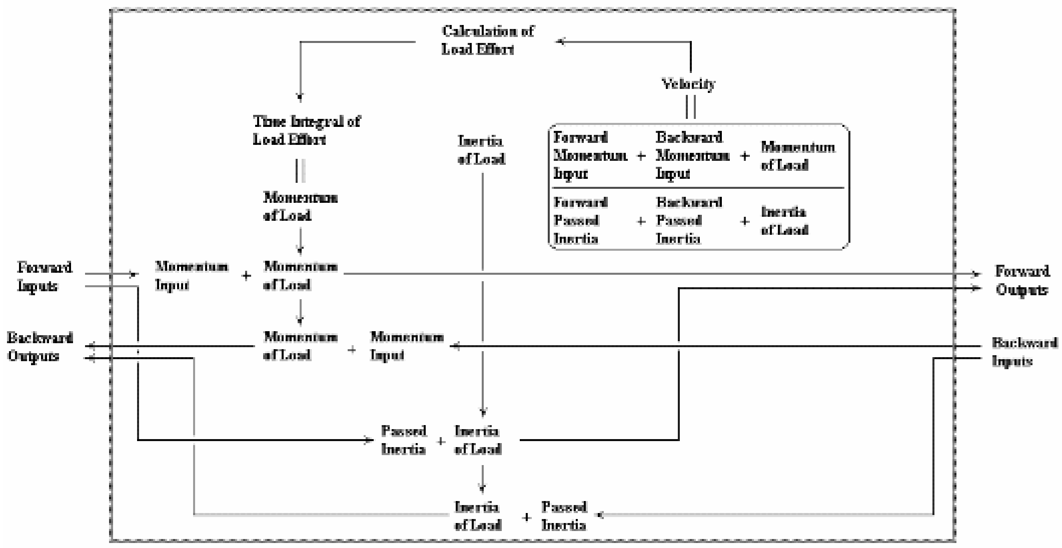

Figure 3.1.8: Illustration of MRD Block for Specific Load Calculations.

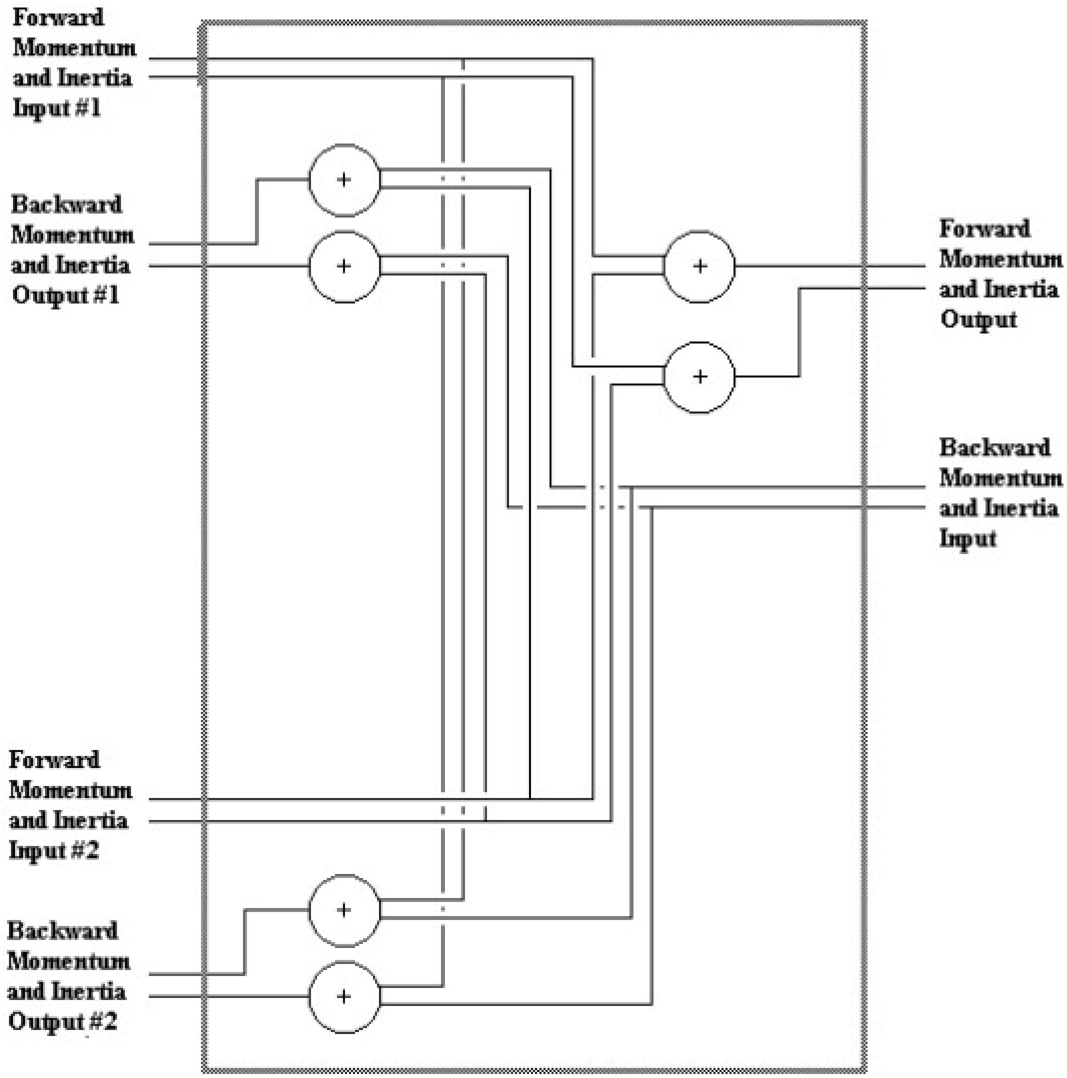

Figure 3.1.9: Illustration of MRD Coupling Block Calculations.

So far, only values being passed in the forward direction have been discussed. Although the block for the vehicle allows mechanical momentum to be passed further in the forward direction, the momentum is passed no further in the system being discussed. The values passed in the backward direction for the system shown in figure 3.1.3 would originate from the vehicle in this particular example, and would be passed (in like manner to the forward direction) back through the drive train to the engine. This allows the velocity of any component to be calculated in its respective block, as indicated in the figures for the MRD components, regardless of the state of the clutch.

One more important block to the MRD scheme needs to be introduced. Consider the coupling in the parallel HVPP shown in figure 3.1.4. Its calculations are illustrated in figure 3.1.9. The coupling adds the two forward momentum inputs from the two power supplies to determine the forward momentum output. But the backward momentum from the load to each power supply is reduced by the opposite power supply's forward momentum input. Inertias are passed such that each device senses the correct amount of inertia from the other devices.

3.1.3 Summary

A drive train modeling scheme, MRD, that allows modularity of rigidly connected systems and that properly models the relations of these modular rigid systems when connecting to, and disconnecting from, other modular rigid systems was devised. The key to this scheme is the passing of generalized momentums and inertias through the drive train and through any devices that cause discontinuities (e.g. clutches). These momentums and inertias are passed through the power blocks of the virtual drive train and modified by each block as necessary. When speed calculations are required, the current sum of momentums are divided by the equivalent inertia at that point in the system. This scheme resulted in a direct correspondence among all velocities in the system when the clutch was fully engaged and allowed the separate systems to operate properly when the clutch was disengaged. Any momentum being passed through the clutch is multiplied by the degree of connection. This scheme works in systems with or without the discontinuities caused by devices such as a clutch. Special treatment of standard integration routines had to be made to reset state variables at appropriate times in the simulation. The key blocks used in the MRD scheme are those shown in figures 3.1.5, 3.1.6, 3.1.7, and 3.1.9. Other special purpose blocks for this scheme can be formed by making simple modifications to these four blocks.

3.1.4 Conclusions

This MRD drive train modeling scheme is an important contribution to the development of HVPP modeling tools, because it easily accommodates dependencies and discontinuities that occur in drive train modeling. This allows designers to rapidly reconfigure drive trains for testing new architecture concepts without having to reconsider dependencies and discontinuities that can require major rewriting of codes. The development of an integration routine specifically designed for this scheme will be developed in the near future. This will eliminate the need for the end user to determine when, and which, state variables must be reset during the simulation. This is not a difficult task, but it would simplify the use of the virtual drive train components and the power supply models. The ability to include compliances is possible and is also planned for the continued development of this scheme.

3.2 Modeling of ICE’s and their Sub-Components

The engine models are comprised of several simple design parameter based sub-component models. This allows the engine modeling to be modular so that different engine configurations can be studied. The ICE models that have been built from the ICE sub-component models behave realistically and exhibit sensitivities comparable to those of real engines. They also exhibited very good accuracy.

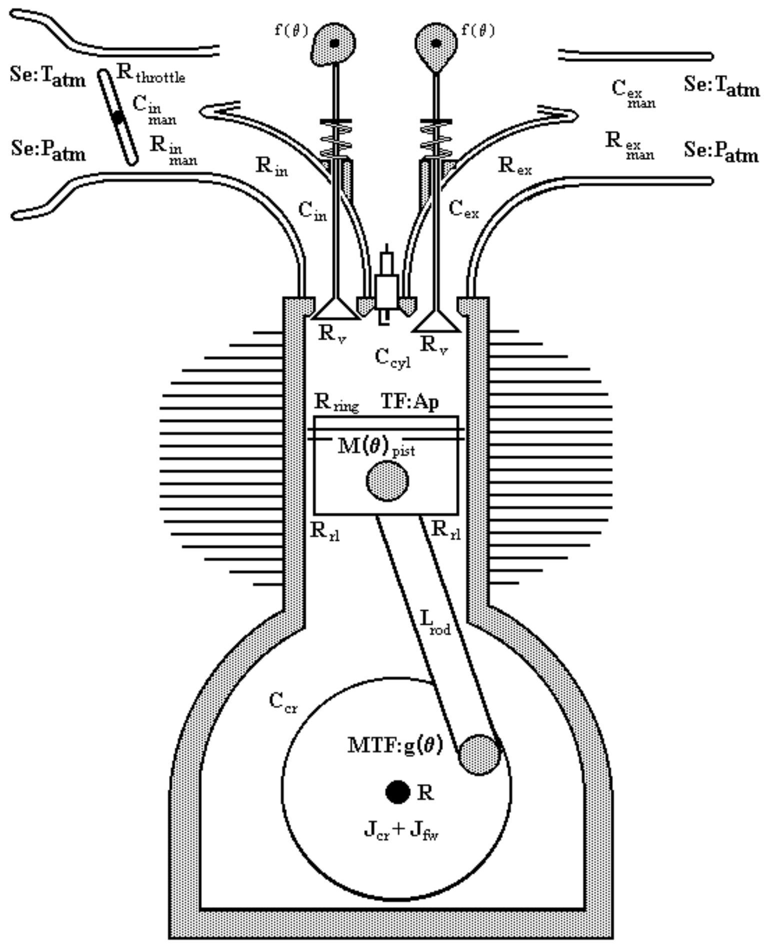

Figure 3.2.10: Simple Four Stroke ICE Drawing.

3.2.1 Generalized View and Decomposition of ICE’s

Using generalized principles, an ICE can be broken into several parts using the three generalized components (capacitances, inertias, and resistors), and other multi-port devices [7]. For example, the regions of the engine that direct fluids such as the intake and exhaust passages, can accumulate, and resist the flow of, mass and energy, so each passage is modeled as a capacitance and a resistor. The intake and exhaust valves of the engine obviously provide some resistance to fluid flow. The pistons, rods, and the crank have some inertia and are therefore treated as inertial elements. The piston acts as a transformer of pressure to force. Other elements are indicated in figure 3.2.1. Thermal fluid inertia is assumed negligible in this modeling when compared to other energy considerations throughout the engine.

3.2.2 Modeling of ICE Fluid Dynamics, and Thermodynamics

Bond graph bonds represent the true power transferred between a system's various multi-ports. For thermal systems, the effort variable is temperature, the flow variable is rate of entropy change, or rate of entropy flow, and the quantity variable is entropy. True power in thermal systems is the product of entropy flow and temperature. It is preferable to have thermal system variables in measurable forms such as temperature, pressure, mass and mass flow rate. It would also be valuable if traditional thermal fluid system constitutive relations could be used. To meet these two preferences, temperature and pressure are chosen for effort variables, and energy flow rate and mass flow rate are chosen as flow variables, and they are matched respectively. To represent these variable choices, two bonds are used as shown in figure 3.2.2. Since the products of these effort and flow variables do not result in true power, these bonds for thermal fluid systems are called pseudo bonds. The thermal fluid system elements' constitutive relations that relate these bond variables to one another will be explained below [7].

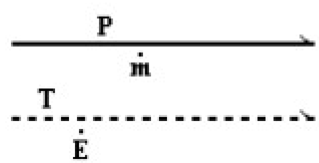

Figure 3.2.11: Pseudo Power Bonds Used in Thermal Fluid Systems

Consider the resistors first. A constant resistor such as a port is modeled using a constant area in equation 3.2.1. To model a valve or a throttle, the level of resistance to flow is changed according to a control signal. In this case, the resistance of the intake and exhaust valves would be changed by adjusting the height of the valves which affects the amount of cross sectional area for flow. Thus, the area term, A, in equation 3.2.1 would be changed according the valve control scheme, and the changing mass flow would affect the energy flow in equation 3.2.2. Thinner bonds with full arrow heads are used to depict control signals for changing the valve area such as the one shown in figure 3.2.3 for the intake valve. For a throttle valve, an input command from the driver would change the throttle angle and affect the area.

Constitutive Relations for Thermal Flow Resistors

$$\dot{m} = A\frac{P_u}{\sqrt{T_u}}\sqrt{\frac{2\gamma}{R(\gamma-1)}}\sqrt{P_r^{2/\gamma} - P_r^{(\gamma+1)/\gamma}}$$ **Equation 3.2.1**

$$P_{r_{crit}} = \left(\frac{2}{\gamma+1}\right)^{\gamma/(\gamma-1)} \qquad \begin{array}{l} \text{if } P_r > P_{r_{crit}} \text{ then } P_r = P_d/P_u \\ \text{if } P_r \le P_{r_{crit}} \text{ then } P_r = P_{r_{crit}} \end{array}$$

$$\dot{E}_u = C_p T_u \dot{m}$$ **Equation 3.2.2**

where m is mass, A is area, P is pressure, T is temperature, γ is the ratio of specific heats, C_p is constant pressure specific heat, R is the gas constant for air, E is energy, the subscript u is for upstream, the subscript d is for downstream, and the subscript crit is for critical pressure ratio [1].

Note the causality indicated by equations 3.2.1 and 3.2.2. For the pressure and mass flow bond, the pressure and γ (which is a function of temperature) result in a flow. Similarly, temperature and mass flow result in an energy flow. Therefore, the causality is set accordingly, and, since the resistance is a function of one or more bond variables, it is represented as a resistance field. Stated in general language, the efforts result in flows for all of the thermal fluid resistive elements in the engine as shown in figure 3.2.3.

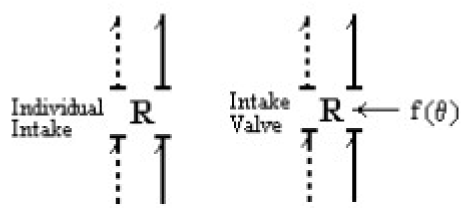

Figure 3.2.12: Bond Graphs of Thermal Fluid System Constant, and Variable, Area Resistors.

Now consider the capacitances, or accumulators, of the thermal fluid systems of the engine. Mass and energy can flow in and out of the accumulators. Net energy and mass flows are integrated to determine the accumulated mass and energy in the capacitances at any time. These quantities are then used to determine the efforts on the pseudo bonds, temperature and pressure, using equations 3.2.3 and 3.2.4. If the capacitance (accumulator volume) is constant as with a pipe or manifold, there is no work transferred across its boundary. In the case of a cylinder and piston, the accumulator volume varies with time. Energy in the form of work can be transferred to or from the accumulator by a change in its volume. The bond graphs for constant and variable accumulators are shown in figure 3.2.4.

Constitutive Relations for Capacitance / Accumulator

$$P = \frac{R}{C_v}\left(\frac{E}{V}\right)$$ **Equation 3.2.3**

$$T = \frac{1}{C_v}\left(\frac{E}{m}\right)$$ **Equation 3.2.4**

where Cv is constant volume specific heat and the other terms were described above.

The accumulator that has a variable volume has a true power bond (volume flow and pressure) connected to it. The product of volume flow and pressure result in a flow of energy out of the accumulator. This transfer of energy is regarded as a source of energy flow from the accumulator, and is also fed back to the junction that sums fluid energy flows with a control signal as indicated in figure 3.2.4.

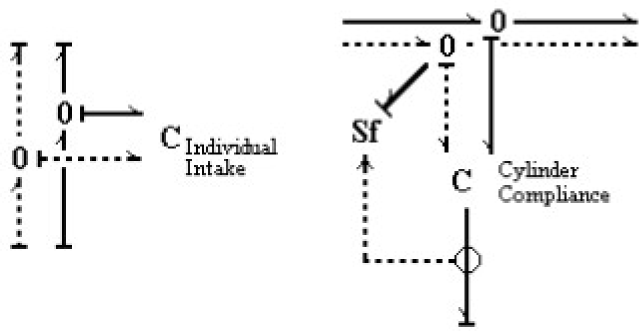

Figure 3.2.13: Bond Graphs of Thermal Fluid System Capacitors.

3.2.3 Modeling of Combustion and Specific Heats

The actual combustion process is far more complicated than the way it is modeled in this work. In a spark ignition ICE, it is desired to have the fuel and air brought into the cylinders as a homogeneous mixture. The combustion reactions take place in two steps. First, the hydrocarbon fuel is broken down into active radicals. Second, combustion reactions occur when the active radicals combine with the oxygen in the air. The spark is used to raise the energy of the fuel-air mixture above the activation energy required to form active radicals. In the time period just after the spark, there are not enough combustion reactions to raise the temperature and pressure of the cylinder, but the combustion reactions release enough energy to form an increasingly greater concentration of active radicals. This stage of the combustion period is known as ignition delay. At a certain point, the combustion proceeds rapidly enough to raise the temperature and pressure above the values that could be achieved by compression alone. The resulting emission concentrations will strongly depend upon the active radicals that are formed. This level of combustion theory explains both the rate of combustion and the formation of emissions.

Unfortunately, there are obstacles to using this level of theory in numerical analysis. First, the active radicals that result from the breakdown of hydrocarbon fuel are only known for methane and some other simple fuels. Furthermore, the formation of active radicals is influenced by chemical concentration gradients, temperature gradients, and momentum gradients, and each of these are also influenced by turbulence. Complex multi-dimensional (finite element based) fluid dynamics models can predict these phenomena to a limited extent, but not with great certainty. Without knowledge of the actual active radicals that have formed and without an accurate knowledge of the gradients and turbulence in the combustion chamber, the complex models used to predict the thermodynamics and emissions of an engine are at best a stochastic guess of the actual process.

The most complex engine model commonly used to predict combustion and thermodynamic phenomena in an ICE cylinder is KIVA III developed at Los Alamos National Laboratory [13]. While KIVA III does a respectable job of predicting emissions and thermodynamic properties, it is definitely not appropriate for drive cycle type performance simulations of an ICE. It divides a cylinder and its ports into thousands of finite elements. Gradients are determined from the properties that exists from cell to cell. Since the intermediate chains of active radicals are unknown for most fuels, it must use chemical equilibrium calculations to determine the concentrations after each time step. It runs very slow even on a supercomputer. One engine cycle can take anywhere from ten minutes to an hour and a half on a supercomputer. A complex code like this is more appropriate for detailed cylinder geometry design and heat transfer design.

A more appropriate scheme for simulation of vehicle performance is to model the combustion as an energy release rate using an empirical relation. The empirical relation used for this work is very similar to the Wiebe function [1] that is commonly used for this purpose. It involves no integration or search routines and is computationally fast. Since combustion phenomena are well understood qualitatively, it is easy to develop functions that do a good job of quantitatively estimating the correct energy release rate. The energy release rates modeled by these functions are adjusted through parameters that adjust the ignition delay period and the rate of combustion. Industrial manufacturers of engines have very precise data for energy release rates verses speed for most of their engines. When a new engine is being designed, the manufacturer will use energy release rates from a previous engine with similar geometry. Unfortunately, this extremely valuable data is proprietary information. Experience has shown that the cyclic variations in energy release rate that occur in actual engines do not result in significant variations in mean effective pressure [1]. Therefore, performance predictions should be close even if energy release rate predictions are not extremely close to actual rates. Flame speed increases with engine speed such that the energy release rate is somewhat constant with respect to crank angle degrees. Therefore, no speed correlation is used for spark advance. This is not serious, since, in the end, spark advance is adjusted experimentally, or adaptively, for each engine to achieve the maximum torque at each engine speed.

The empirical relation used for the combustion release is shown in equation 3.2.5. The product of heating value, Q_{HV}, in joules and crank angle speed, ω_{cr}, in degrees per second are in the numerator. The spark angle, θ_{sp}, in degrees starts at zero when ignition of the fuel begins and is reset to zero every full engine cycle. The flame duration angle in degrees, θ_{fd}, is the estimated flame duration for the combustion energy release.

$$\dot{E}_c = \frac{Q_{HV} \cdot \omega_{cr}}{1 + \exp(5 - 10 \cdot \theta_{sp} / \theta_{fd})}$$ **Equation 3.2.5**

In further consideration of simulation speed, the compositions of the unburned gases (air-fuel mixture) and the product gases were assumed to be frozen mixtures of ideal gases (the concentrations of these gases were considered constant). Thus, the specific heats (C_p and C_v), and the specific heat ratios (γ's) of these gas mixtures, which are used in the constitutive relations for the thermal fluid capacitances and resistances, are assumed to be functions of temperature only. This assumption provides adequately realistic performance predictions. The of C_p, C_v, and γ for both air and product gases are calculated as functions of temperature using the form of equation 3.2.6. The values used in this equation that curve fit each of the specific heats and each of the ratios of specific heats are shown in table 3.2.1 below [14].

$$f(T) = C_1 + C_2 \cdot T + C_3 \cdot T^2 + C_4 \cdot T^3$$ **Equation 3.2.6**

	Air			Products		
Parameter	C_p	C_v	γ	C_p	C_v	γ
C_1	900.39	613.29	1.4506	1072.86	782.26	1.4221
C_2	0.31904	0.31904	-1.6384e-4	0.3241	0.3241	-1.8752e-4
C_3	-8.9293e-5	-8.9293e-5	5.8378e-8	-2.1429e-4	-2.1429e-4	6.9668e-8
C_4	8.8328e-9	8.8328e-9	-7.3897e-12	9.7778e-8	9.7778e-8	-9.099e-12

Table 3.2.1: Specific Heat and Ratio of Specific Heats Parameters for Equation 3.2.6

During the intake and the initial phase of the compression stroke, the gases in the cylinder are mostly air and fuel. Some of the gases in the cylinder are product gases, or burned gases, that were not completely exhausted during the exhaust stroke. This small amount of leftover burned gas is called the residual. When combustion starts, the unburned gases start to combust, and the amount of burned gases in the cylinder change from the amount of residual gas to completely burned. During this time, the specific heat functions for unburned and burned gases are appropriately weighted by the burned fraction and unburned fraction in order to calculate the average specific heat of the cylinder gases.

3.2.4 Modeling of Heat Transfer

Modeling of the actual temperature gradients and heat transfer in every location of the engine and cooling system is possible, but this would be an arduous task with very little return. Many of the heat transfer correlations used to model these individual movements of thermal energy can easily err as much as 30 to 40% [15], and such a detailed model would not be suitable for the type of simulation desired. When observing actual engine temperatures, it is found that the cylinder wall temperatures do not vary significantly over the operational ranges of the engine [1]. The cooling system can easily be designed to maintain a fairly constant and optimal cylinder wall temperature for the operational range of the engine. Thus, the most significant heat transfer mechanism is the heat transfer from the gases to the cylinder walls. Woschni has developed an empirical correlation that has proven to be accurate for predicting this heat transfer [1]. The correlation and its related terms are described below.

$$h = K_1 \frac{P_{cyl}^{0.8}}{B^{0.2} T_{cyl}^{0.53}} \left[K_2 \overline{S}_p + K_3 \frac{V_{sw} T_{ref}}{P_{ref} V_{ref}} (P_{cyl} - P_{mot}) \right]^{0.8}$$

Equation 3.2.7

$\mathbf{P_{cyl}}$ is instantaneous cylinder pressure (kPa); **B** is bore (m); $\mathbf{T_{cyl}}$ is instantaneous cylinder temperature (K); Sp is mean piston speed (m/s); $\mathbf{V_d}$ is displacement volume; $\mathbf{T_{ref}}$, $\mathbf{P_{ref}}$ and $\mathbf{V_{ref}}$ are reference values for temperature, pressure and volume, respectively, that are stored just before the beginning of combustion; $\mathbf{P_{mot}}$ is the motoring pressure; and the **K** constants are as follows:

	$\mathbf{K_1}$	$\mathbf{K_2}$	$\mathbf{K_3}$
During Gas Exchange:	3.26	6.18	0
During Compression:	3.26	2.28	0
During Combustion and Expansion:	3.26	2.28	0.00324

Along with other vehicle accessories, the power to run the cooling system components can be modeled as a variable power drain on the engine output.

3.2.5 Modeling of Translational and Rotational Mechanics

The translational mechanics in the ICE model are straight forward with the exception of one difficulty. The translational mechanics in the ICE model are concerned with the piston motion only. The forces encountered by the piston result from the pressures in the cylinder and crank case, the resistance forces from the rings, and the forces from the connecting rod. It is desirable to regard the connecting rod as a rigid member. If it was modeled with a capacitance (i.e. a compliance, or the inverse of a stiffness), it would be a very small capacitance, and a very small time step would have to be used for the simulations. If it is regarded as rigid, the inertia of the piston causes the resulting differential equation for the piston to be in derivative causality once it is connected to the rest of the model [7]. This derivative causality is avoided by lumping the piston's inertia effects to the crank shaft and the mechanical bus. The crank shaft will see each piston as an angle dependent rotational inertia.

The crank shaft and rods work together as transformers from translational to rotational motion. Equations 3.2.8 illustrate the kinetic energy stored in the pistons in translational and rotational form. Jp_{eq} is the equivalent polar moment of inertia at the flywheel due to flywheel and piston inertia, $\boldsymbol{\omega}$ is the rotational velocity of crank shaft, **r** is the crank radius, **L** is the rod length, θ is the crank shaft angle. According to energy conservation, these two energies must be equal. Eliminating the 1/2 on each side and then dividing both sides by the square of the rotational velocity leaves the equivalent rotational inertia for the pistons. Now that this inertia is in the rotational part of the system, it is non-linear and is a function of crank shaft angle. The rotational mechanics also include a constant rotational inertia in the form of an engine flywheel. The equivalent rotational inertia of each piston is added to the constant inertia of the flywheel, and the result is a single time dependent lumped inertia for the entire rotational part of the engine model.

$$\tfrac{1}{2} Jp_{eq}(t)\omega^2 = \tfrac{1}{2} Mp \cdot \left(r \cdot \sin\theta + \frac{r^2 \cdot \cos\theta \cdot \sin\theta}{\left(L^2 - r^2 \sin^2\theta\right)^{1/2}} \right)^2 \omega^2$$

Equations 3.2.8

$$Jp_{eq}(t) = Mp \cdot \left(r \cdot \sin\theta + \frac{r^2 \cdot \cos\theta \cdot \sin\theta}{\left(L^2 - r^2 \sin^2\theta\right)^{1/2}} \right)^2$$

The output shaft is regarded as rigid for the same reason that the connecting rods were regarded as rigid. Therefore, for simplicity and speed of simulation, the engine's rotational system is assumed to have no compliances. However, this makes the lumped inertia an actual part of the mechanical bus. Therefore, this inertia is passed to the mechanical bus for use in the determination of rotational acceleration, velocity and angle of the rotational mechanical bus (i.e. the crankshaft).

3.2.6 Complete Bond Graph Model

The individual bond graphs formed above and the heat transfer and combustion relations are represented in a large bond graph sub-model shown in figure 3.2.6, for the thermal fluid section of the engine that is shown in figure 3.2.5. Atmospheric temperature and pressure are sources of effort for the pseudo bonds. These feed into the throttle valve which is a variable resistance. Mass and energy of atmospheric air accumulate in the intake manifold, so it is treated as a constant capacitance. The air flow transitions from the manifold to the intake port passages and encounters a change in cross-sectional area and thus a constant resistance to flow. Air between the beginning of the intake port and the intake valve can accumulate in the intake port's volume, so a constant capacitor is added. A variable resistance is added for the intake valve which is opened and closed according to the valve timing scheme. The bond coming out from this resistance feeds energy flow and mass flow into the cylinder at the zero junctions. The zero junctions are used here, because the net flows into the cylinder are the result of intake and exhaust flows. The zero junctions also indicates the common pressure and temperature of the cylinder for the pseudo bonds connected to it. At the temperature and energy flow pseudo bond, combustion is added as a source of energy flow. A resistance for heat transfer is placed directly next to the "**C**" for the cylinder, because Woschni's heat transfer correlation is a function of variables from all three of the cylinder's bonds. A variable resistance is placed on the other side of the cylinder's zero junctions for the exhaust valve. The cylinder's volume can change, so a variable volume thermal fluid capacitance is used. The connections to the pressure and volume flow bond of the cylinder capacitance will be discussed later. All that remains is the constant capacitance and resistance of the exhaust port, and the constant capacitance and resistance of the exhaust manifold. Note that each manifold contains connections for the other passages to the other cylinders in the engine.

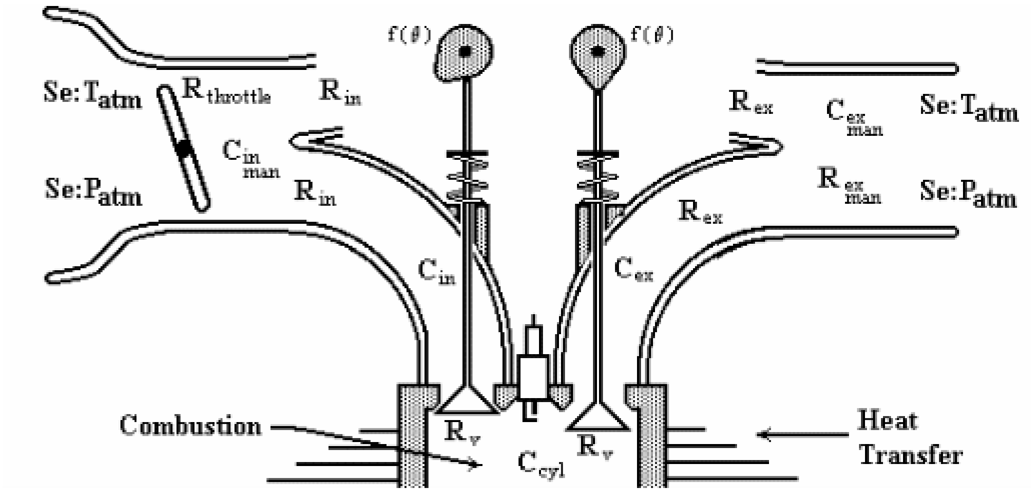

Figure 3.2.14: Thermal Fluid Section of a Four Stroke ICE.

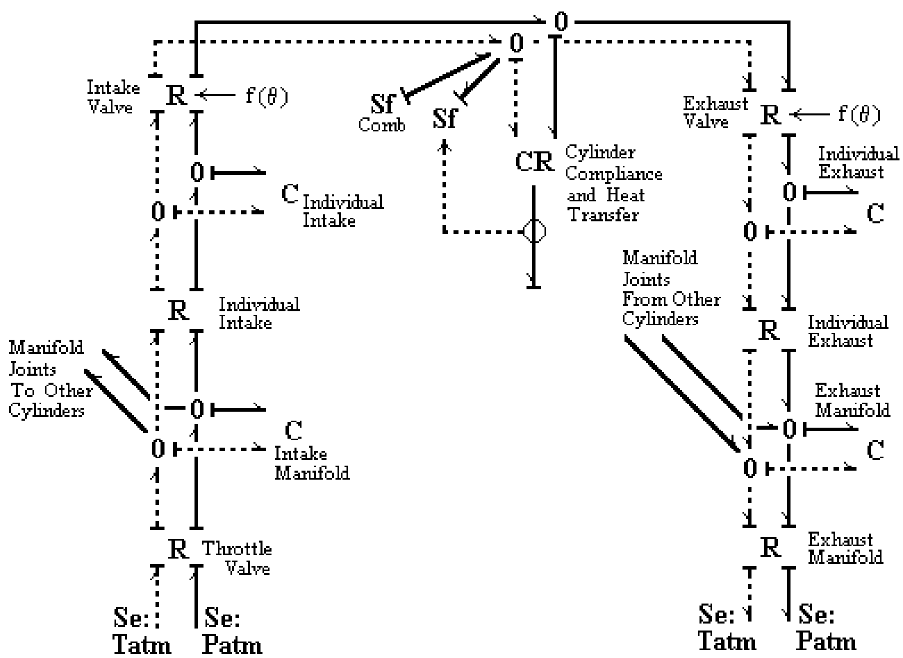

Figure 3.2.15: Bond Graph of Thermal Fluid Portions of a Four Stroke ICE.

Figure 3.2.7 shows the addition of the translational and rotational mechanics to the bond graph of figure 3.2.6. Note also that some additional thermal fluid features have been added: ring leakage and crank case venting resistances; and crank case capacitance. The net pressure on the piston (the difference between cylinder and crank case pressure) is determined at the **1** junction. The resultant pressure is then passed through the transformer which has the piston area for a modulus. The bond below the transformer is comprised of force and velocity. Some of this power is dissipated through the resistance supplied by the piston rings. This resistance is composed of coulombic and viscous friction effects. The remaining power is transferred through the modulated transformer (representing the crank shaft) and is converted into rotational power via the non-linear modulus given within the parentheses of Equations 3.2.8. The torque from the other pistons is added at the one junction where some of the rotational power is dissipated to the resistive element shown. This resistive element can include coulombic and viscous friction effects, and windage effects. The remaining power is sent to the inertias indicated: the flywheel inertia; the crank shaft inertia; the piston inertias converted to equivalent rotational inertias using equation 3.2.8. As stated previously, these inertias will be lumped with any other inertias associated with the mechanical bus at this point to determine the rotational velocity of the bus.

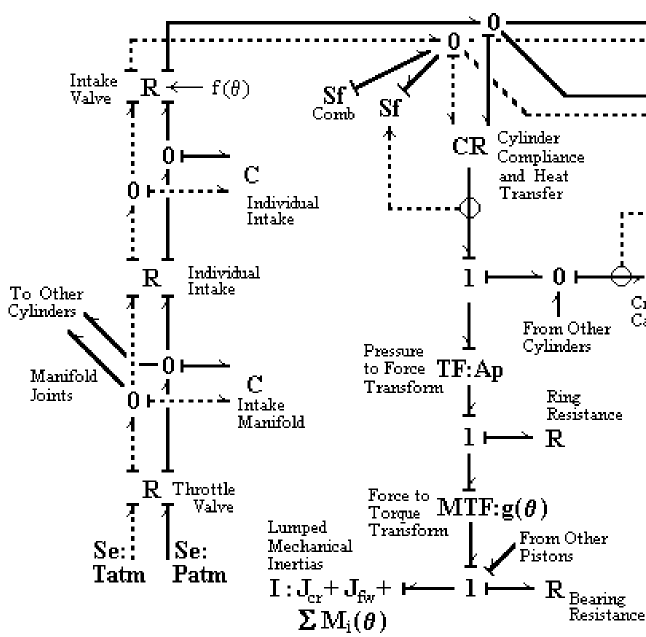

Figure 3.2.16: ICE Bond Graph of Figure 3.2.6 with the Additions of Translational and Rotational Mechanics.

A similar method would be followed to develop a bond graph model for a two stroke engine bond graph. A drawing of a simple two stroke engine is shown in figure 3.2.8. The bond graph model for this portion of the two stroke engine is shown figure 3.2.9.

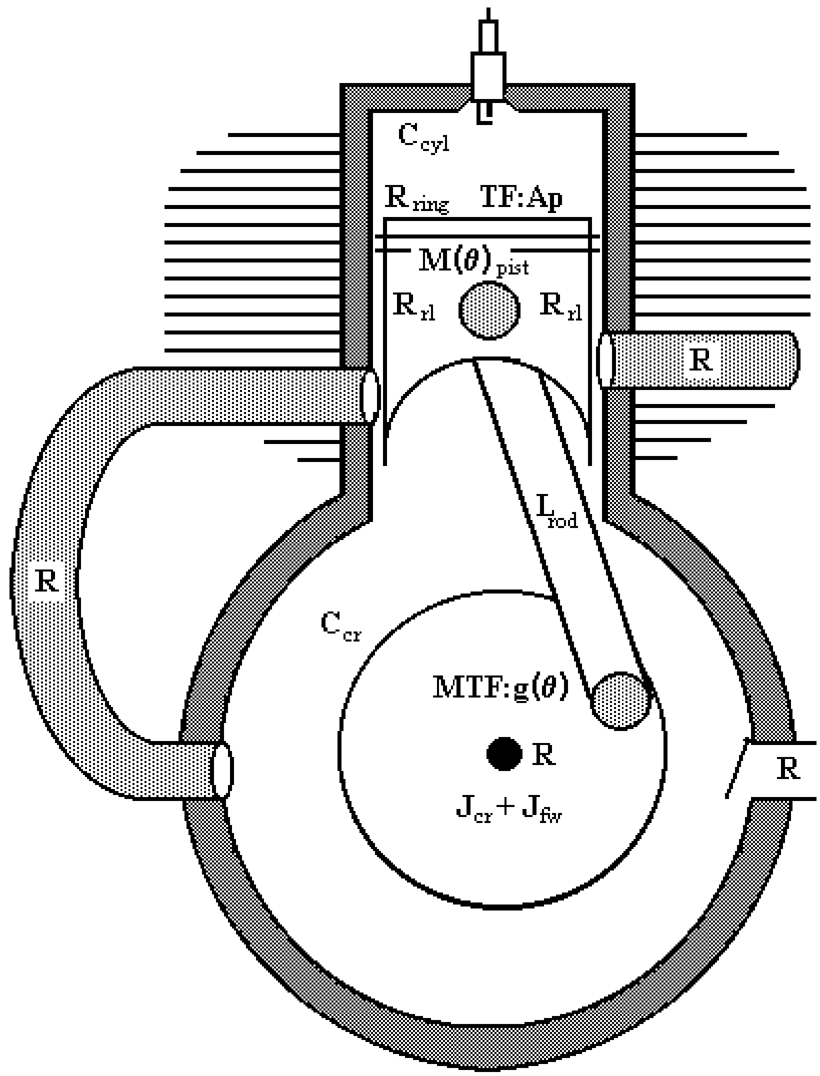

Figure 3.2.17: Drawing of a Simple Two Stroke Engine.

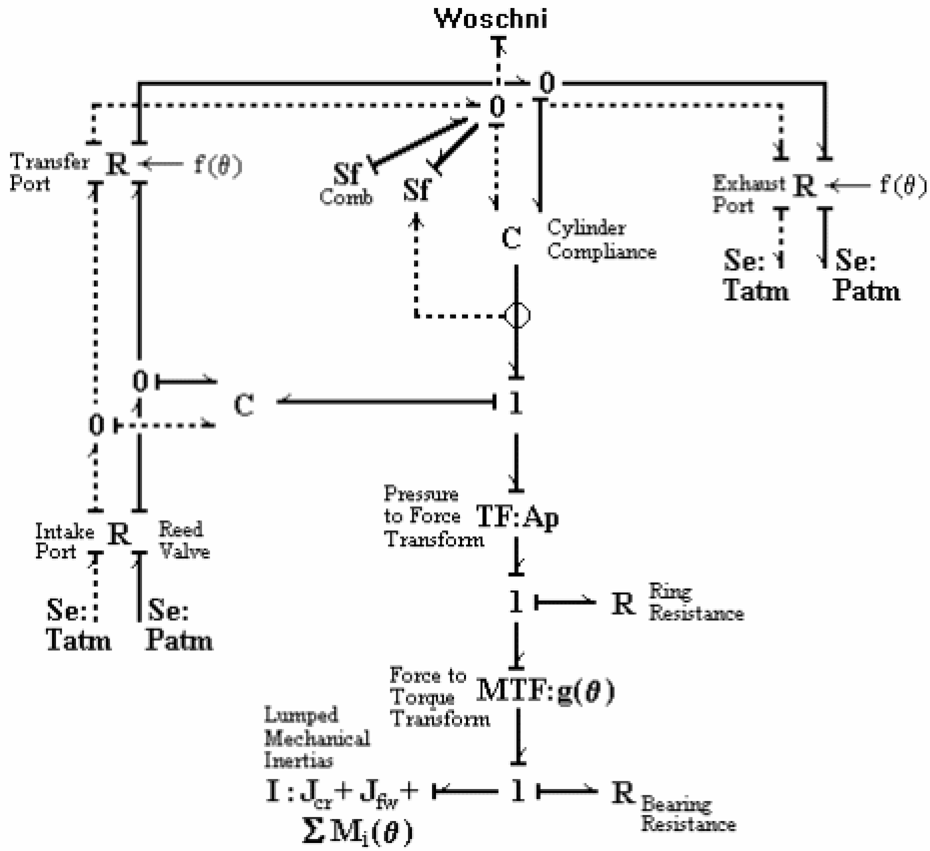

Figure 3.2.18: Bond Graph of a Simple Two Stroke Engine.

3.2.7 Choosing ICE Configuration and Parameter Values

Guidelines for choosing engine configurations and parameter values for the various design parameters in an engine are given in Appendix B. These guidelines were mostly taken from [1]. Choosing engine parameter values is not an exact science. However, the performance predictions of the engine models are good enough to indicate whether the desired performance characteristics will be met by the chosen engine parameters. Furthermore, the tables and guidelines provided in [1] are very useful in helping one develop an initial understanding of how various changes in design parameter values will effect the engines performance.

3.2.8 Coding and Simulation of Complete ICE Models

The ICE sub-component models were all verified by individual simulation for proper values and characteristics. Then the sub-components were arranged to match the configuration of a Honda 500cc Ascot motorcycle engine, and the sub-component parameter values were set to closely match those of this engine [16]. The specific parameter values for the Ascot can be found in Appendix B. The Ascot engine configuration for the thermal fluid portion of the engine is shown in figure 3.2.10. The mechanics portion of the engine is typical. The bond graph model for this engine configuration is shown in figure 3.2.11.

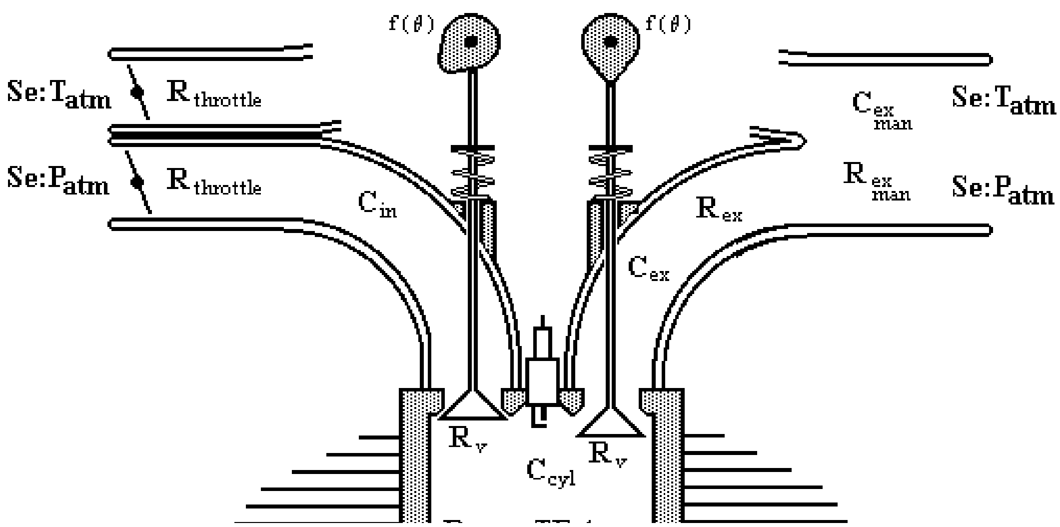

Figure 3.2.19: Illustration of Ascot Configuration.

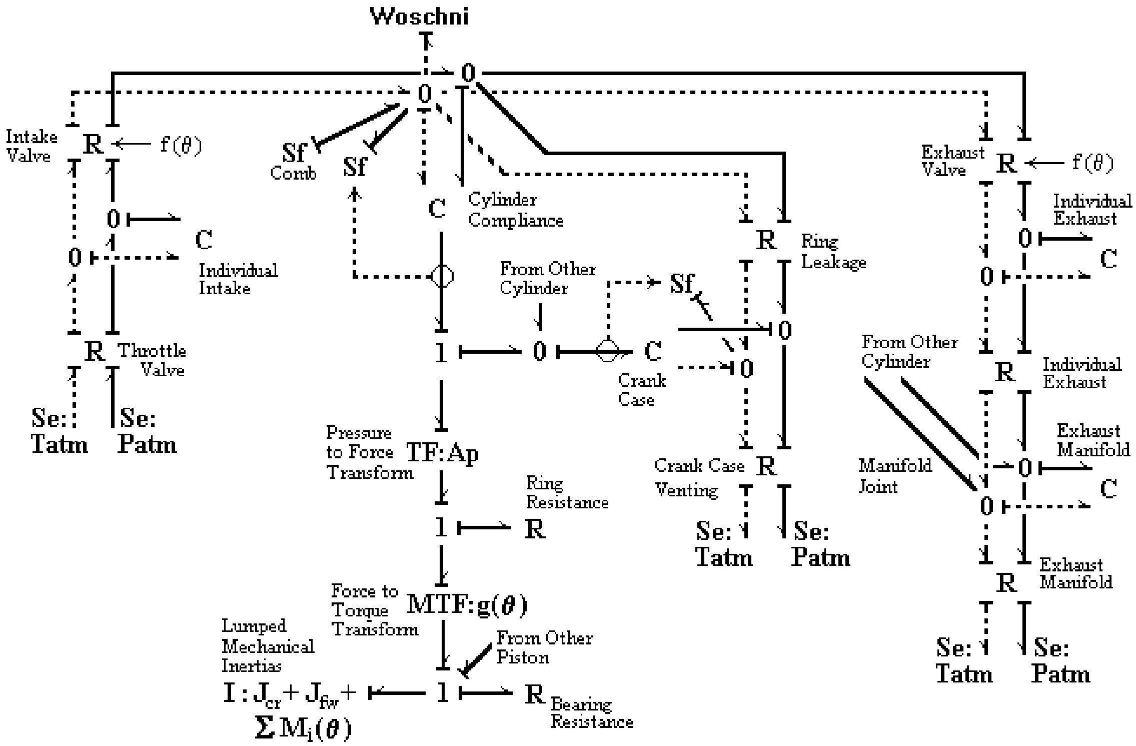

Figure 3.2.20: Ascot Configuration Showing One of Two Thermal Fluid Paths and Connections to the Other Thermal Fluid Path.

An explanation of how to reduce bond graph models to mathematical statements is given in Appendices A and D. Appendix C presents a mathematical reduction of an engine model to mathematical statements. The ACSL graphical models for the Ascot engine model will be presented here. The code for each of the power blocks is given in Appendix E. Figure 3.2.12 shows the power blocks for one cylinder and piston set connected to their associated elements for air and exhaust flow. Note that with the exception of the Cylinder and Piston power block, each of the blocks represents a separate bond graph element. The Cylinder and Piston power block contains code for modeling combustion, heat transfer, transformations across the piston area, ring resistance, and transformation from translational to rotational realms through the crankshaft. Furthermore, each pseudo power bond is represented by two connecting lines between the power blocks that represent the values carried by the power bonds.

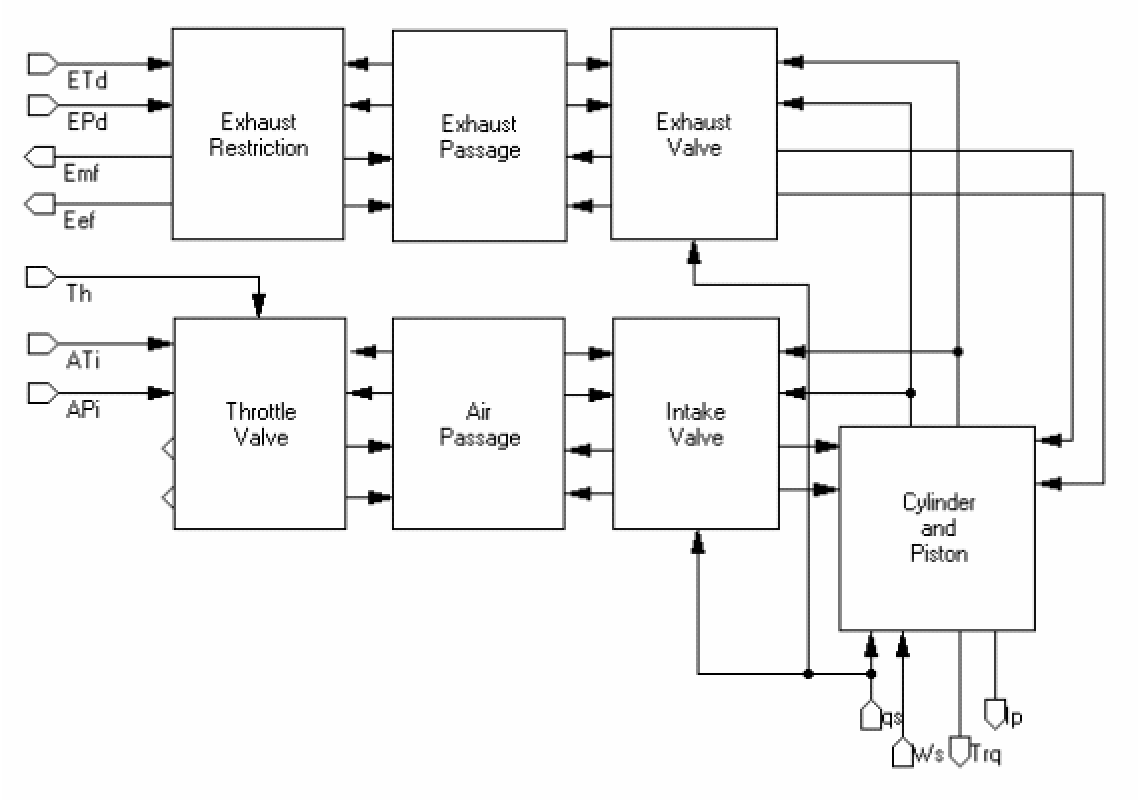

Figure 3.2.21: ACSL Power Blocks for One Thermal Fluid Path and its Associated Mechanics.

Each of the two thermal fluid paths are identical in the Ascot engine. Therefore, this set of power blocks can be grouped together, copied and pasted to form the second path. These paths will be referred to as Ascot Paths. With the exception of the number of the cylinder, which is used for timing calculations, the parameters are identical. This grouped set of power blocks can also be stored as one example of an engine thermal fluid path and placed in a digital library for future use. The values of the parameters associated with each block can be changed or adjusted as desired at any time.

Figure 3.2.13 shows the connection of the two separate Ascot Path power blocks to the rest of the engine components and to other systems. The individual exhaust ports are connected to the exhaust manifold. The throttle valves and the exhaust manifold are connected to the atmospheric conditions, which are sources of effort. The engine is controlled by the throttle valve whose signal comes in at the upper left corner of figure 3.2.13 labeled “th”. The mechanical bus communicates the crank speed to the engine through the port labeled “w”, and the engine communicates its torque to the mechanical bus through the port labeled “trq”. The crank speed is integrated to determine the instantaneous crank angle for various calculations in the Cylinder and Piston power blocks.

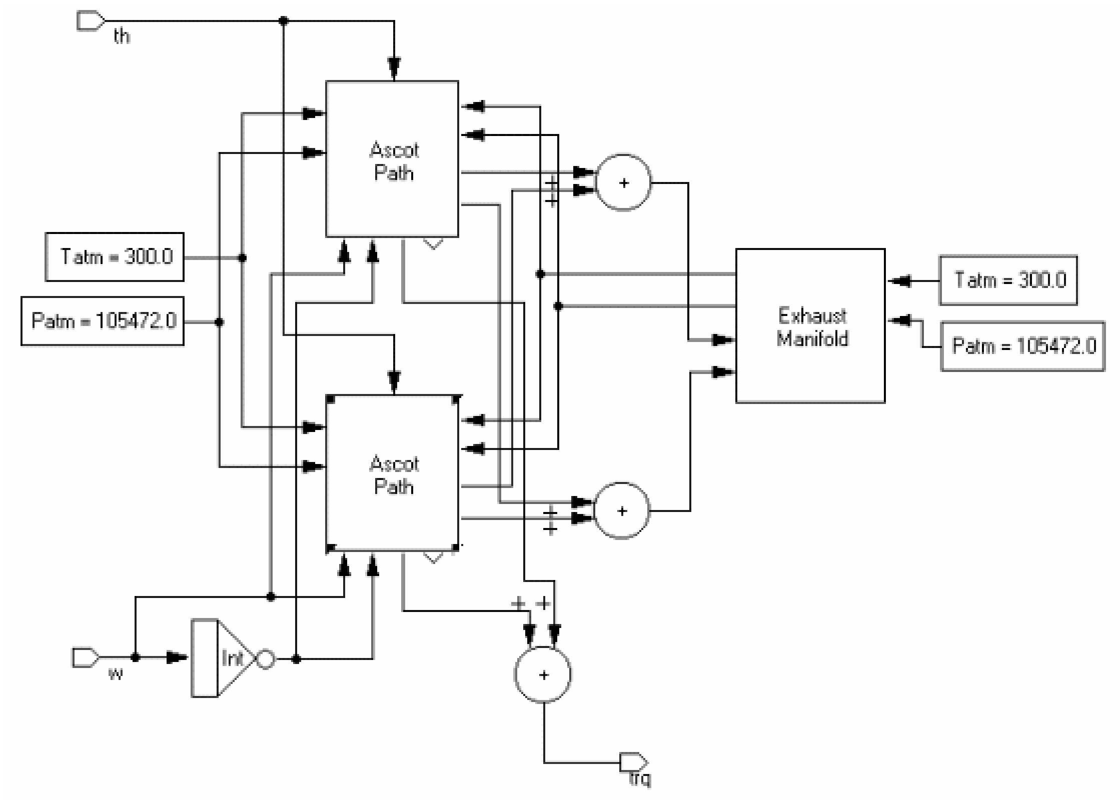

Figure 3.2.22: Complete Ascot Engine Model in the ACSL Graphic Modeller.

The graphical model of the Ascot engine was grouped together into one compound block labeled “2 Cylinder 500cc” to form the single block shown in figure 3.2.14. Note this block is connected to the Engine Interface power block that handles the calculations necessary to carry out the rigid-modular-discontinuous connection scheme described previously. This block is then grouped to form the single block representing the entire engine that is ready to be fitted into the rigid-modular-discontinuous connection scheme.

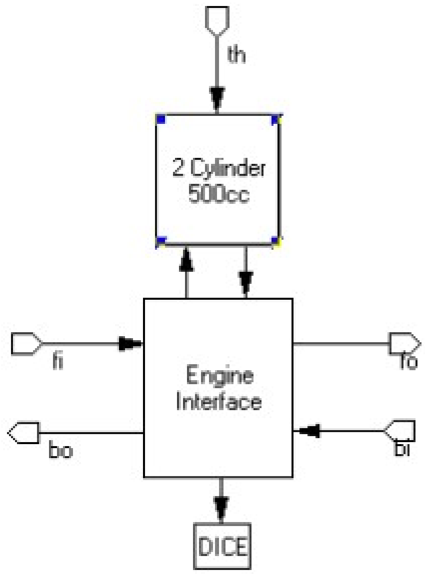

Figure 3.2.23: Grouped Ascot Engine Connected to an Engine Interface for the Rigid-Modular-Discontinuous Connection Scheme.

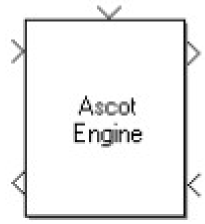

Figure 3.2.24: Grouped version of Figure 3.2.14.

3.2.9 Model Validations

The simulated torque of the Ascot engine model was optimized by varying spark timing, flame duration, and valve timing which helped to validate that model exhibited realistic sensitivities. Pressure-volume and torque speed plots were also made to validate that the model exhibited proper dynamic characteristics. The torque speed plot was also used to validate that the model gave realistic torque predictions. To further validate the model, it was simulated in the vehicle simulation test bed presented in section 4.2 to compare the predicted vehicle performance to actual reported performance values for speed, acceleration and fuel consumption.

It is not possible to accurately re-produce the pressure-volume characteristics in an engine cylinder unless the model properly balances the energy supply and energy loss mechanisms in the cylinders. Comparisons with plots in [1] and [17] show that the characteristics of the plot shown in figure 3.2.16 are in good agreement with actual ICE pressure-volume measurements. The mean effective pressure at this speed for this engine is 9.5 atmospheres which is in good agreement with measurements in actual engines of this size.

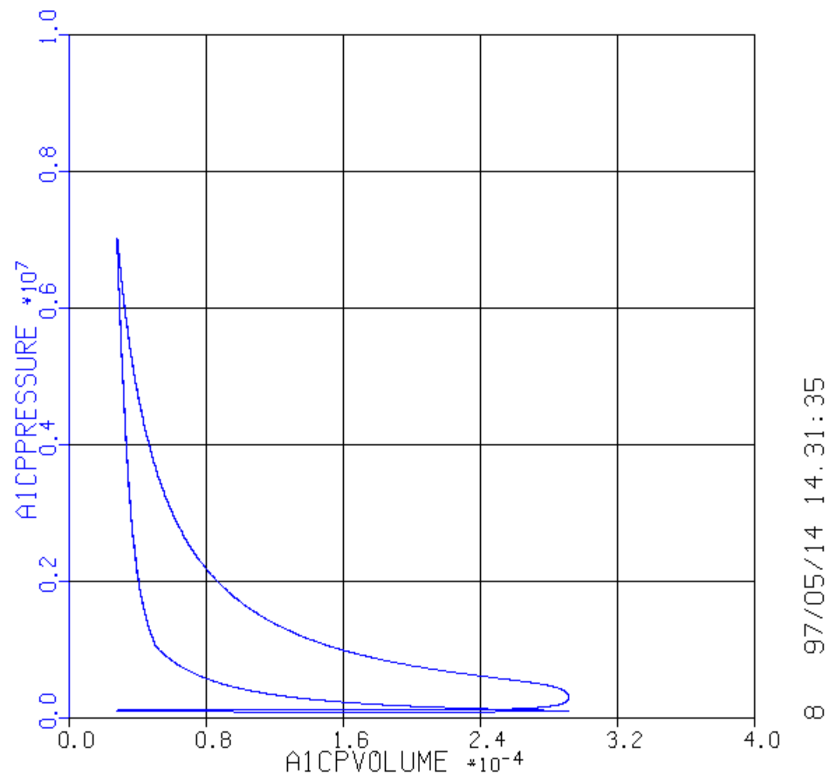

Figure 3.2.25: Pressure (Pa) verses Volume (m^3) Curve for the Honda Ascot Motorcycle Engine Model Operating at 742 rad/sec.

Honda claims that the Ascot produces 47 bhp (35 kW) at 9000 rpm (942 $^{rad}/_{sec.}$) which results in a torque of 37 Nm. Figure 3.2.17 shows a torque of 38.1 Nm at 942 $^{rad}/_{sec}$. This results in an error of 3%. While this error is within the realm of measurement error, it should also be pointed out that the simulated engine has a 42cc greater displacement than the Ascot, and the simulated engine does not consider the lower pressure that exists at the tail pipe as vehicle speed increases. Since this was the only torque value available, it was necessary to validate the remainder of the curve to typical SI ICE torque speed curve characteristics. This curve shown in figure 3.2.17 has the proper characteristic compared to those shown in [17] and [1].

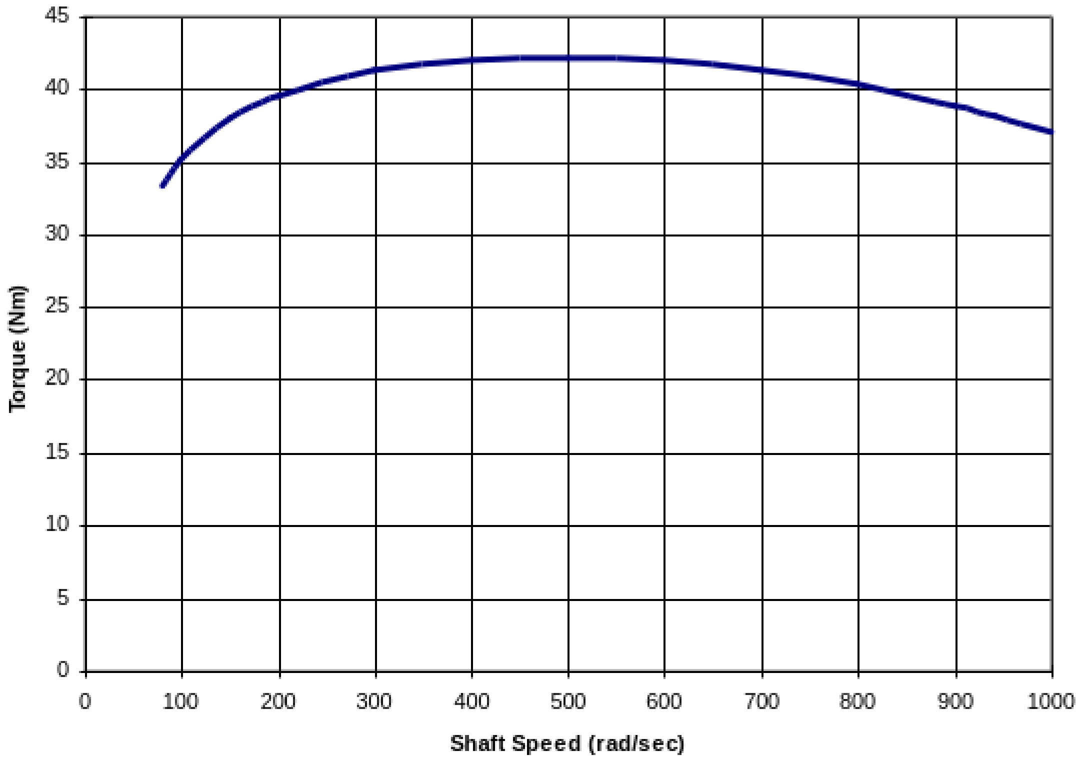

Figure 3.2.26: Torque Speed Curve for the Ascot Engine Model Operating between 100 and 1000 rad/sec.

The power block for the Ascot engine model was placed into the virtual Ascot motorcycle described in section 4.2 for further performance evaluation. The parameters for vehicle dynamics are estimates of the actual Ascot motorcycle parameters and are considered to be adequately close to the parameters that existed for the published tests [16]. Estimates for vehicle dynamics based on published data [17] and educated estimates were as follows: 0.7 for drag coefficient; 0.01 for friction coefficient, 270 kg for mass which includes a 78 kg (172 lb.) rider; and 0.75 m^2 for frontal area. An actual ¼ mile maximum acceleration test was completed in 13.63 seconds at which point the motorcycle was traveling 93.65 mph [16]. The simulated Ascot reached 93.65 mph in 13.68 seconds when it was at 0.22 miles. At ¼ mile the simulated Ascot reached a speed of 97.4 mph in a time of 14.74 seconds. These small differences are mostly due to the small errors in the actual and estimated vehicle parameters. Along this same reasoning, the test driver probably leaned forward during the test to reduce his cross-sectional drag area. This was not considered in the simulation. Furthermore, it is probable that the actual driver shifts gears faster than the test bed's simulated driver.

The experimental fuel consumption test for the Ascot was obtained on a test loop. It is assumed that the motorcycle encountered slight head winds, tail winds, and varying gradients on this test loop. The simulation did not consider these factors, because they were not listed in the test results. Also, the speeds on this drive cycle are unknown. The Ascot's measured fuel consumption for this test loop was 60 mpg. The vehicle test bed predicted a 100 mpg fuel consumption without head winds or gradients during a 65 mph cruise.

This difference should not be surprising. Given the Ascot's configuration, the type of carburetors used for this engine, and the small throttle angle used for this cruising speed, it is expected that poor mixing of air and fuel would take place in the intake. This poor mixing results in the need for a higher fuel to air ratio to achieve adequate power. One could expect to get 100 mpg from this engine if fuel injectors are used that provide good atomization of the spray. To test this theory, the author simulated a 3 liter Ford Taurus SHO cruising at 70 mph. The engine in this vehicle uses fuel injectors that atomize the fuel well. The measured fuel consumption for highway was 26 mpg [18]. The simulated fuel consumption was 26.4 mpg.

3.2.10 Summary

It is desirable to have ICE models that behave realistically. The engine models developed from the sub-component models exhibited sensitivities and revealed critical design parameters comparable to those in real ICE's and predicted ICE performance with good accuracy. These features are important to making the ICE sub-component models good tools for the design of HVPP's in a virtual setting. Although spark advance was constant verses speed in the developed models (due to the constant flame duration combustion model that was explained above), the modeled engine's torque prediction was sensitive to this setting. In order to further improve accuracy of the predicted torque, optimal valve timing for both the exhaust and intake valves of the cylinders had to be found. The optimal values found for valve timing were in the same range of values used for real engines. This is encouraging, because studies of variable valve actuation can be, and have been, performed with these models, to improve engine performance. The performance of the modeled engines could also be improved by balancing the volumes of the intake and exhaust ports and by adjusting the configuration of the overall intake and exhaust systems in the same fashion as with real engines. The models were accurate for fuel consumption predictions when good mixing of fuel and air are achieved by the final design. The models do not however account for bends and roughness of the intake and exhaust channels. They only predict the effects of cross-sectional area and volume changes of these passages.

3.2.11 Conclusions

The level of ICE modeling and modularity proposed and developed in this work was first used herein. It has also been successfully used in another HVPP model for which the author originally developed this model. To the best knowledge of the author, a more detailed level of modeling has not been previously used in the dynamic simulation of HVPP's which makes the HVPP models presented in this work significant. The best tradeoffs between detail, accuracy, modularity, and current simulation speed capabilities were utilized to develop models that would meet the current objectives. The modeled ICE sub-components allow easy reconfiguration of ICE models and should provide accurate performance predictions for any size engine. Optimal values found for valve timing were in the same range of values used for real engines. Also, variable valve actuation can be, and have been, performed with these models, to improve engine performance. Because the models have thus far proven to be accurate and show realistic dynamics with respect to valve timing changes, values found from variable valve actuation studies should provide good direction for setting initial timing verses speed values for prototype ICE's used in HVPP's. The fuel consumption predicted by the models should be accurate for engines that will provide near ideal mixing of the fuel and air. The models cannot predict fuel consumption that results from poor mixing. This should not be a concern for engines used in hybrid vehicles, because fuel efficiency is always a significant concern, and any engine that does not provide good mixing of the air and fuel would not be meeting the essential objectives of a HVPP. The simplifying assumptions used in the models did not diminish their predictive capabilities. These assumptions also did not diminish the ability of the models to exhibit realistic sensitivities to parameter value changes. These finding were important to this work, because without these simplifying assumptions, the models would be slowed to impractical speeds for HVPP performance predictions and would therefore not be practical design tools.

3.3 Electric Machine Modeling

Dynamic DC machine modeling is accurate to within 1% [19]. Therefore, no studies were conducted to validate DC machine models used in this work. Induction motors are more difficult to design, model and control than DC machines. Thus, the majority of this section is devoted to discussions relevant to induction machine (IM) modeling, design and control.

The development of an IM model that can meet the modeling objectives is presented in this section using generalized - bond graph modeling techniques. The electrical, magnetic, and mechanical processes in the machine are modeled as separate, discrete regions or processes. The model is adequately accurate for the purposes of this work and is able to display realistic performance characteristics.

Design parameter values were estimated for an existing production IM used in vehicle applications to validate the IM model. Simulation predictions using the model and the estimated design parameters were good, and the simulated characteristics were like those one would measure in a real machine. Also, the modeled IM exhibited correct sensitivities to design changes. The IM model's responses to variable speed control are presented in section 4.2 where the IM powered EV is covered, and the modeled IM behaved as a real IM would behave with this type of control.

Electric machine performance is highly dependent upon the power electronics that control them. Machine control logic will dictate whether the machine is used to its best capabilities or not [20]. Separately excited DC machines provide excellent flexibility in control. IM's have not typically been used in traction applications, but are gaining in popularity in this field, because new power electronic schemes have been developed to control them [21] [22]. When implementing motor control logic in the models used in this work, it was important to limit the models for the power electronic controls to that which can be practically implemented. However, because of the flexibility and options currently available in power electronics, there are very few things that can be imagined which cannot be implemented.

The power electronics used in machine control can have their own peculiar dynamics. They can also have a notable effect on the performance of a vehicle power plant even though their efficiency is quite high. Thus, these systems are worthy of a more detailed study in a work such as this. However, it was not in the original scope of this work to model such dynamics. Therefore, these effects should be added to future developments of this HVPP modeling scheme.

3.3.1 Generalized View and Decomposition of Electric Machines

The generalized view of separately excited DC machines and squirrel cage rotor IM's will be discussed in this section. Transformer modeling will also be discussed to aid the reader in understanding the development of the IM models.

3.3.1.1 Separately Excited DC Machines

The field of a separately excited DC machine consists of inductance and resistance [19]. The inductance can also be decomposed into the turns around the pole core times a magnetic permeance. The turns would be modeled as a generalized gyrator, and the permeance as a generalized capacitance [7]. Saturation of the field pole should also be considered. The result of this model would be a current that would be used to determine the flux value of the field poles, $\boldsymbol{\phi_f}$.

However, the flux paths in a DC machine cause very small magnetic permeances. This results in a very small inductance for the field windings. Compared to the time response of the mechanics in vehicle performance modeling, the transient effects of the field can be safely neglected. Furthermore, the power passing through the field is very small compared to the power passing through the armature. Therefore, the field will be modeled as part of the machine's voltage/torque constant $\mathbf{K_a}\boldsymbol{\phi_f}$, and it will be assumed that it can changed instantaneously by the control logic. However, one should make sure that the values of $\mathbf{K_a\phi_f}$ are limited to practical levels that would not allow the field poles to become severely saturated.

The armature of a separately excited DC machine consists of inductance, $\mathbf{L_a}$, resistance, $\mathbf{R_a}$ [19], one additional effect. The interaction of the moving armature coils with the field flux causes a back electro-motive-force (emf) at the motor terminals. This effect is modeled as a modulated gyrator where the modulus of the gyration is simply $\mathbf{K_a\phi_f}$. The resulting bond graph model for a separately excited DC machine is shown in figure 3.3.1. The mechanical side of the motor includes the rotational inertia of the armature and load, $\mathbf{J_{a+load}}$, the constant torque from the load, $\mathbf{T_{load}}$, and the mechanical resistance to rotation of the armature shaft, $\mathbf{R_b}$.

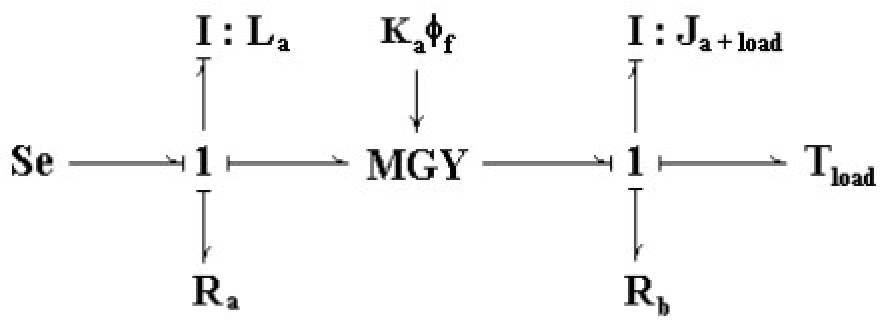

Figure 3.3.27: Bond Graph Model of a Separately Excited DC Machine.

3.3.1.2 Transformer and Squirrel Cage Rotor Induction Motor Modeling

Accurate dynamic models of IM's are very slow, and usually depend upon finite element models [23]. Simple IM models, that are used for control studies, are derived using an electrical circuit that models the combined effects of the electrical, magnetic and mechanical dynamics. The modeling criteria stated in the introduction requires an IM model with practical simulation speeds, good accuracy, and discrete decomposition of the IM and its processes. Therefore, the electrical, magnetic, and mechanical effects were modeled separately, and the transformations between these different physical realms where modeled using principles of energy conversion. This methodology will first be applied to the dynamic modeling of transformers to aid the reader in understanding the development of IM models.

The presentation of the equations will follow the physical causality shown later in the bond graph models. Because the bond graph deals with all three physical realms encountered in an electrical machine (i.e. electrical, magnetic and mechanical), and because the explanations of the equations follow the causality of the bond graphs, this explanation will differ from traditional explanations of IM's [19]. Careful observation will reveal that the explanations herein are not extremely different if one uses a generalized perspective. The explanation herein simply approaches the subject of IM modeling from a different viewpoint.

Consider an ideal transformer (i.e. one without leakage) and its respective bond graph shown in figure 3.3.2. A single resistance on the secondary and an air gap are used to make this explanation more analogous to an induction motor. The source of effort, an AC voltage, encounters the resistance of the windings and is then converted by the windings into a magnetic flux rate in the core. A gyrator is used to model this conversion, because an effort is converted to a flow by the gyrator modulus. In this particular case, an electrical voltage is converted to a magnetic flux rate in inverse proportion to the number of coils [7] [24]. There is a common flux and flux rate in the core according to transformer physics. Thus the permeance, or reluctance, of the core, which behaves as a generalized capacitance, is attached to a **1** junction. The flux built up in the core divided by the permeance of the core results in a magnetomotive force, MMF. The common flux rate also encounters the secondary coils, the second gyrator, of the transformer. The secondary coils convert the magnetic flux into a voltage across the secondary coils. The current in the secondary coil is found using the secondary resistance and Ohm's law. The resulting current in the coils times the number of secondary coils, the second gyrator modulus, causes another MMF in the core. The two MMF's are added together at the magnetic **1** junction for the core. This resultant MMF in the primary coils, the first gyrator, sets the flow (i.e. the current) in the primary coils.

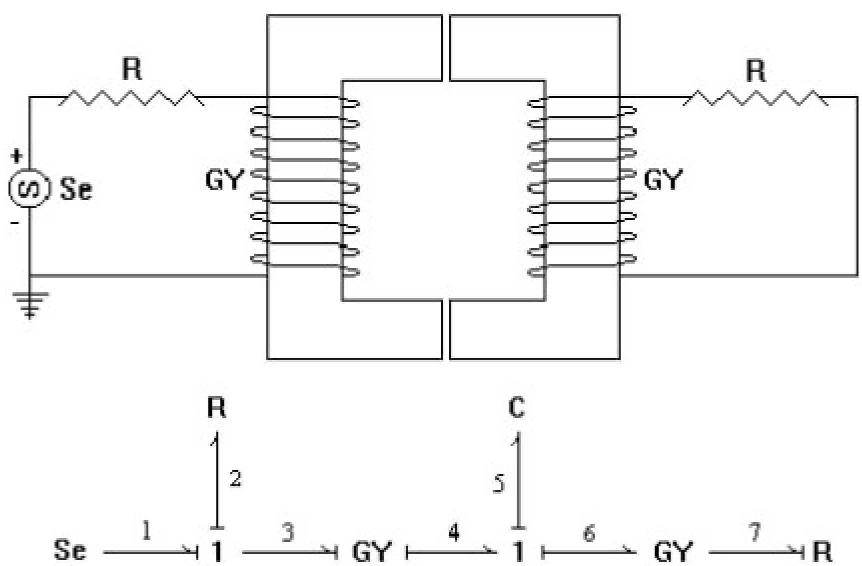

Figure 3.3.28: Bond Graph Model of an Ideal Transformer with Air Gaps and a Secondary Resistance.

In the assignment of causal strokes to this bond graph, an arbitrary choice of causality had to be made which alerts the modeller that he must either set up an implicit relation or do an algebraic reduction [7] of the equations. The equations corresponding to the numbered bonds of the bond graph are in table 3.3.1. The e's and f's in the table stand for generalized efforts and flows that should be understood through correlation with the bond graph and system drawing. The implicit relation is applied to the magnetic **1** junction where a generalized form of Kirchhoff's voltage law is applied to calculate a residual at each time step. The residual is used to determine the current in the primary coil.

When simulated, this transformer predicted the proper dynamic characteristics, and no error could be determined between the actual measurements and the simulated predictions for the magnitudes of primary and secondary current and voltage once the simulation reached steady state conditions. There was a notable, but small, amount of error between the measured and simulated phase shift between current and voltage, because the transformer leakage was not modeled.

Effort Equations						
e1=Se	e2=f1*R_1	e3=e1-e2	e4=e5+e6	e5=q5/C	e6=GY_2*f6	e7=GY_2*f6
Flow Equations						
f1=f3	f2=f3	f3=impl(res)	f4=GY_1*e3	f5=f4	f6=f4	f7=e7/R_2
Residual Equations						
res=f3*GY_1-q5/C-e6						
Integral Equations						
q5=integ(f5)						

Table 3.3.2: Equations for Dynamic Simulation of the Ideal Transformer in Figure 3.3.2.

These same principles used to model this ideal transformer were applied to develop an IM model. (This IM model will be referred to henceforth as an Ideal IM). This model was studied in detail for several weeks. It was very promising for steady state predictions and was computationally fast. But, the model finally proved to be unsuitable when simulating transients. It was found that leakage must be modeled to achieve accurate predictions and characteristics of the transient dynamics. Therefore, the model will not be discussed further here, but the ACSL code for it is in Appendix F.

The transformer above will now be altered to include leakage flux predictions of both the primary and secondary windings. Figure 3.3.3 illustrates a transformer that has leakage. The leakage phenomena additions to the bond graph are shown as **C** elements. It is important to note that leakage flux in electrical machines is not a loss mechanism (i.e. no energy is dissipated from the system due to leakage) [7].

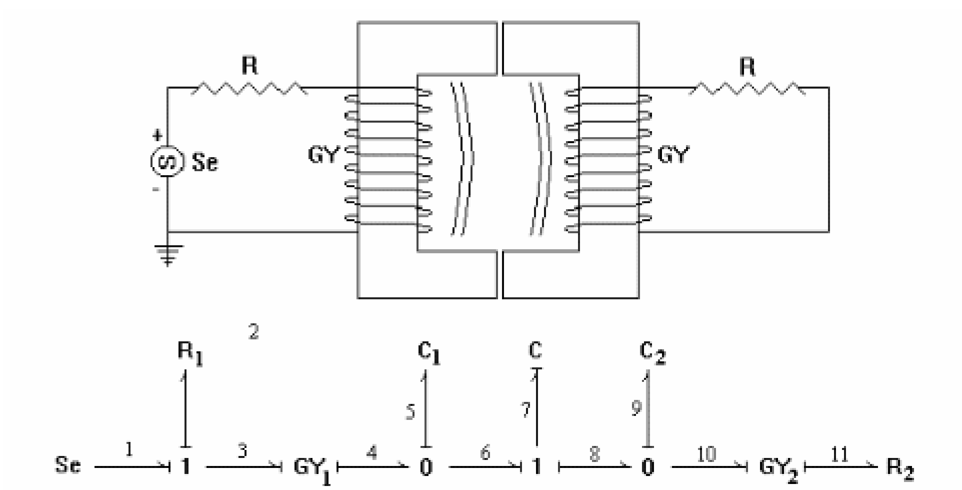

Figure 3.3.29: Transformer with Flux Leakage and its Bond Graph.

The equations for the Bond Graph of figure 3.3.3 are shown in table 3.3.2. The C element in derivative causality that models the air gap and core reluctances was handled using the implicit relation shown in the table. The simulation results for this transformer also showed the proper dynamic characteristics, and no error could be determined between the actual measurements and steady state predictions for the magnitudes of primary and secondary current and voltage. There was also no notable error between the measured and simulated phase shift between current and voltage.

Effort Equations					
e1 = V	e2 = R1*f3	e3 = e1-e2	e4 = e5	e5 = q5/C1	
e6 = e5	e7 = e6-e8	e8 = e9	e9 = q9/C2	e10 = e9	e11 = R2*f11
Flow Equations					
f1 = f3	f2 = f3	f3 = e4/N1	f4 = e3/N1	f5 = f4-f6	
f6 = f7	f7 = implc(res)	f8 = f7	f9 = f8-f10	f10 = e11/N2	f11 = e10/N2
Residual Equations					
res = f5/c1-f9/c2					
Integral Equations					
q5 = integ(f5,0.0)			q9 = integ(f9,0.0)		

Table 3.3.3: Equations from the Transformer with Flux Leakage Bond Graph in Figure 3.3.3.

The techniques used to model the transformer with leakage will now be applied to model an IM. However, some complications are now introduced. The primary now becomes a stator with three phases that set up a rotating magnetic flux in the machine. This flux causes a primary magnetomotive force, MMF 1, to be developed as the flux encounters the reluctances of the machine. The secondary is now a squirrel cage rotor. The squirrel cage rotor is not a simple coil, but it is a network of low resistance copper bars connected together. The rotating flux from the stator causes an AC voltage to be induced along the rotor bars and current flows in the rotor bars. The rotor bar currents cause the rotor to develop a secondary magnetomotive force, MMF 2. A resultant MMF from MMF 1 and MMF 2 determines the amount of current drawn from each stator phase. These two MMF's and the magnetic angle between them, cause a torque to be developed which moves the rotor. This is a causal viewpoint of the IM physics. The transition from transformer model to IM model will now be explained using this causal viewpoint. The resulting model will be very similar to the transformer model that includes leakage. The model will be explained in two steps. The first will be a qualitative overview using the development of the bond graph to explain the physical flows of energy through the machine. The second step will be an analytical explanation the detailed mathematics used to simulate the machine.

Consider the delta wound stator shown in figure 3.3.4. Using electrical circuit and magnetic bond graph modeling techniques, it is a simple matter to develop the bond graph shown in figure 3.3.5.

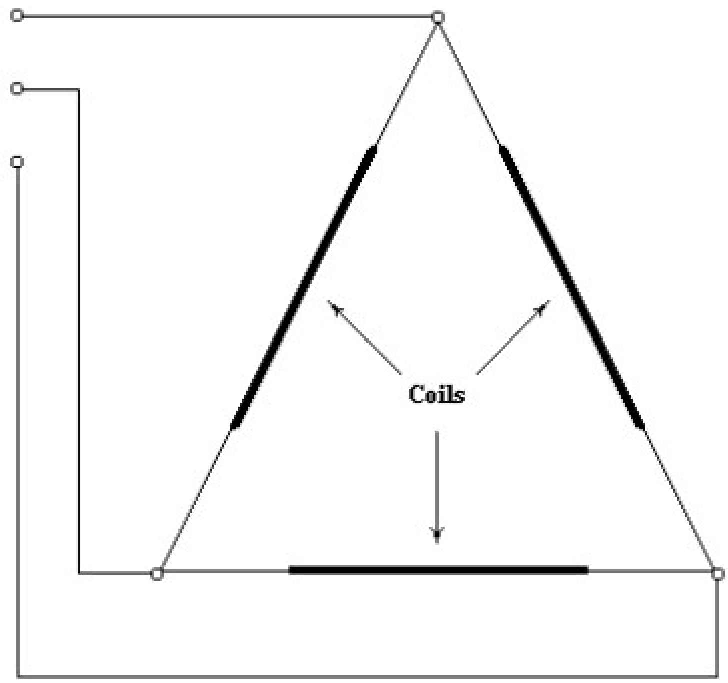

Figure 3.3.30: Delta Wound Stator Configuration for an Induction Machine.

At this point, the energy has gone from the voltage sources, **SE**, to the nodes of the stator windings, through the resistances of the coils, **R**, and through the coils, **GY's**. As the energy flows through the coils, a magnetic flux rate, **δϕ/δt**, is established. Before moving onto the other magnetic considerations, this bond graph will be simplified. This simplification is not necessary, but will serve to make the resulting model more clear for the sake of presentation.

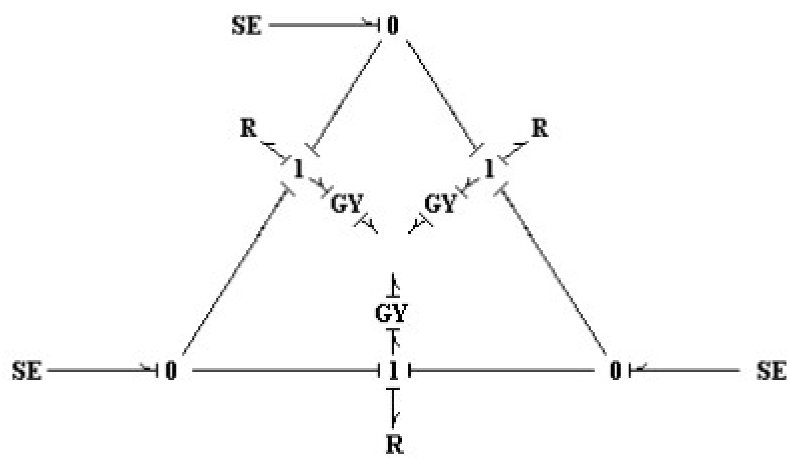

Figure 3.3.31: Bond Graph for a Three Phase Delta Wound Stator.

Since phase voltages for any type of winding are easily derived, it will be assumed that phase voltage is applied directly to each coil. In the case of a delta connection, the phase voltage equals the line to line voltage. Thus the bond graph of figure 3.3.5 can be changed to the form shown figure 3.3.6. This bond graph has the advantage of being generic to any type of stator winding. One would consider the number of parallel paths per phase to multiply the number of branches in the bond graph as necessary.

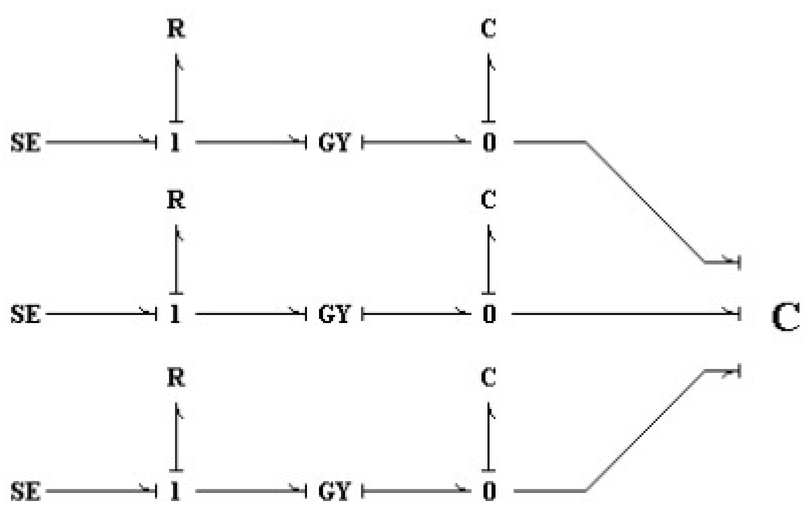

Figure 3.3.32: Simplification of Figure 3.3.5's Bond Graph to use Phase Voltages as the Sources of Effort.

The energy on the other side of the **GY's** in figure 3.3.5 is magnetic. The energy then encounters the region of the machine where stator flux leakage can occur. The diversion of flow to the flux leakage paths is handled by the **0** junctions to the right of the **GY's**. The permeance for the stator flux leakage is represented by the **C** elements connected to these **0** junctions. Following a causal viewpoint, the **δφ/δt** developed from the voltage across the coils, **GY's**, minus the **δφ/δt** that is passed on to the **C** field yields the amount of leakage **δφ/δt**. This **δφ/δt** leakage is then integrated to give a flux and divided by the total leakage permeance per stator phase to give a MMF. Note that the total leakage effects per stator phase does not include any leakage effects from the rotor in this particular development. Those leakage parameters will be handled separately below. The MMF's at the 0 junctions for each stator bond graph branch are directed back through the **GY**'s, and the MMF's divided by the **GY** modulus defines the current in each of these branches.

The energy not diverted to the stator flux leakage paths is passed through the stator teeth and then across the air gap. The large **C** element represents the combined reluctances of the stator teeth, air gap and rotor teeth. The method for determining the non-linear instantaneous reluctances for the stator and rotor teeth will be explained after the rotor model has been explained. The reluctance of the effective air gap is constant and linear and depends upon the physical parameters of the machine [25] [19].

The MMF's into the large **C** element from each branch in figure 3.3.6 are decomposed into **d** and **q** components (i.e. x and y) [21], [19]. The **d** components from each branch are summed, and the **q** components from each branch are summed to obtain a resultant stator MMF along the **d** axis and a resultant stator MMF along the **q** axis. An explanation of how the resultant stator MMF **d** and **q** components are used is given after the rotor model has been explained.

Consider a simple squirrel cage rotor like the one shown in figure 3.3.7. For simplicity, only four bars are used in this explanation.

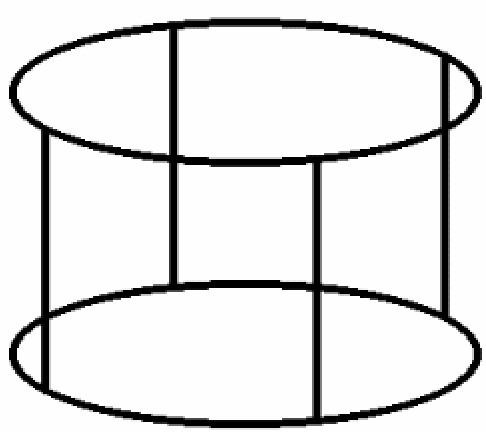

Figure 3.3.33: Simple Squirrel Cage Rotor Used to Explain Induction Motor Model Development.

The bond graph for this squirrel cage electrical circuit is shown in figure 3.3.8 without causality strokes. According to rules of bond graphs [7] and some simplifying assumptions, this bond graph can be simplified in 3 steps.

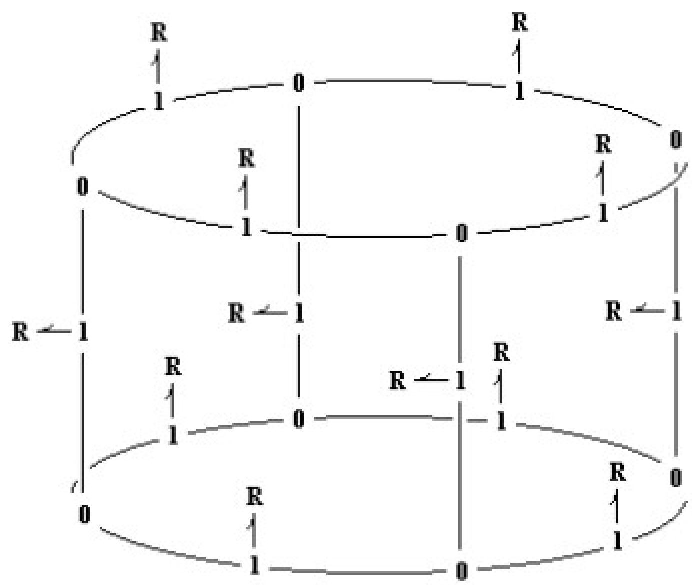

Figure 3.3.34: Bond Graph Model without Causal Strokes for the Squirrel Cage Rotor in Figure 3.3.7.

First, the resistances of the end ring segments are typically very small compared to the resistances of the rotor bars. Therefore, the first simplification (which is temporary) assumes that these end ring segments have negligible resistance, and the two end rings will be regarded as nodes as shown in figure 3.3.9 (a). Small resistance changes in the rotor circuit can alter the performance and dynamic characteristics of the IM significantly [19]. Therefore, it is desirable to maintain some estimate of the effects that the end rings have on the squirrel cage circuit.

The effects of the end ring resistance can be included in the rotor bars. The overall power loss of the end rings at rated power is obtained using traditional methods of IM design [25]. This power loss is added to the estimated power loss of all the rotor bars at rated power to yield a total power loss for the squirrel cage at rated power and rated current. This total power loss is divided by the square of the rated current and the number of rotor bars to yield an equivalent resistance for each rotor bar. This adjustment to the resistance of the rotor bars allows the use of the above simplification without disregarding the effects of the end ring resistance.

According to the rules of bond graphs, the symmetry of the bond graph in figure 3.3.9 (a) allows the operation indicated in figure 3.3.9 (b). The one node in the bond graph of figure 3.3.9 (b) can be regarded as the reference point in this circuit and thus eliminated [7] to give the separate bond graph resistance elements for each rotor bar as shown in figure 3.3.9 (c).

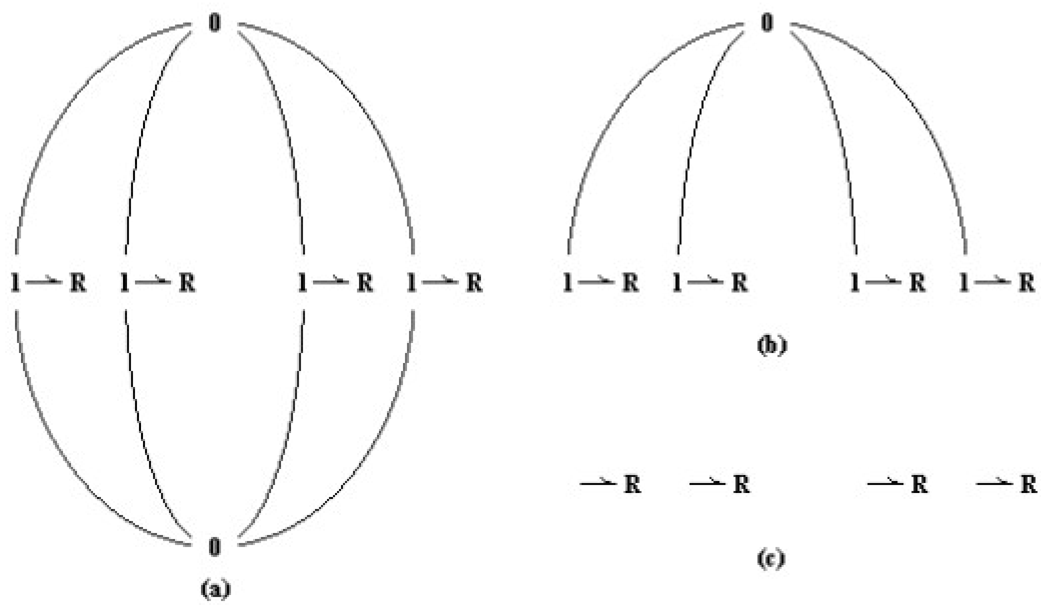

Figure 3.3.35: Illustration of Steps to Simplify the Bond Graph Shown in Figure 3.3.8.

The remainder of the IM bond graph can now be explained using the above simplifications of the squirrel cage rotor and the complete bond graph model shown in figure 3.3.10. After receiving energy from the stator circuit, the energy stored in the large **C** field is directed to two other paths: the mechanical elements connected to the machine; and the squirrel cage rotor circuit.

The squirrel cage rotor physics are represented by the portion of the bond graph that lies to the right of the large **C** field element. The magnetic variables connected to the **C** field are in derivative causality. The method of dealing with the mathematical details of this arrangement will be discussed later. For now, consider that a sinusoidal distribution of discrete $\delta\phi/\delta\tau$'s, contained in the power bonds leaving the right side of the **C** field, interact with the rotor core and squirrel cage circuit. The number of these power bonds (i.e. energy flow paths) is equal to the number of rotor bars.

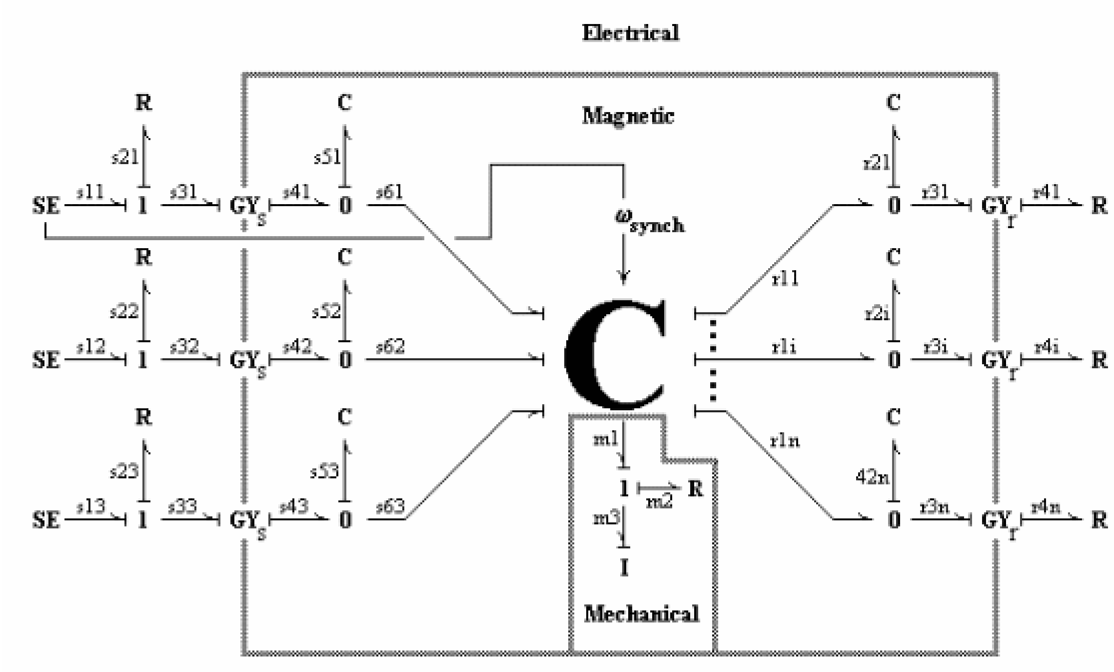

Figure 3.3.36: Induction Motor Bond Graph

Still moving to the right through the bond graph, these power bonds connect to **0** junctions. This junction deals with the rotor leakage **δϕ/δt**. The **δϕ/δt** distribution in the machine (from the C field) that is not passed onto the rotor core (**δϕ/δt** to the right of the **0** junctions described below) jumps through the copper in the rotor slots [19] and is considered leakage **δϕ/δt**. Each of the leakage **δϕ/δt** are integrated and then divided by a multiple of the rotor slot leakage permeance to yield an MMF from each rotor tooth. These rotor MMF's are used by the **C** field, and by each of the rotor energy flow paths as shown by the bond graph.

For the **C** field, these MMF's are decomposed into **d** and **q** components as was previously done for the MMF's of each stator branch. The **d** components from each branch are summed, and the **q** components from each branch are summed to obtain a resultant rotor MMF along the **d** axis and a resultant rotor MMF along the **q** axis. An explanation of how these resultant MMF's will be used is given later.

For the energy flow paths of the rotor circuit, these MMF's encounter the rotor bars. Each rotor bar can be thought of as a ½ turn coil. Therefore, each bar is considered to be a **GY** with a modulus of ½. Each bar is also considered to be a resistance, **R**, as shown in figure 3.3.10. The MMF's at the **0** junctions for each of the rotor bond graph branches is converted to a current through each of the **GY**'s. The current in each rotor bar times the resistance results in a voltage across each bar. The voltage across each bar is converted to a **$\delta\phi/\delta t$** by the ½ turn of the bar (i.e. the same rotor bar **GY**). This was the **$\delta\phi/\delta t$** used above for rotor leakage.

The **d** and **q** components found for the resultant stator MMF and rotor MMF are used in two ways. They are used to determine the angular distribution of the flux in the machine, **$\phi(\theta)$**, which, along with the synchronous and rotor speeds, helps to determine the angular distribution of flux rate in the machine, **$\delta\phi/\delta t(\theta)$**. This **$\delta\phi/\delta t(\theta)$** defines each of the **$\delta\phi/\delta t$**'s for the power bonds connected to the C field as described previously. They are also used to determine the torque of the machine. The **d** and **q** components of each resultant MMF are used to convert them to polar coordinates. Using the scalar magnitudes of the MMF resultants, the angle between these MMF's, and the instantaneous total reluctance encountered by the machine's flux (the non-linear physical value for the **C** field), the torque of the machine can be determined at any instant in time.

The first bond of the mechanical section in the IM bond graph is connected to the underside of the element representing the **C** field. Neglecting shaft compliance, the inertial and dissipative loads of the machine experience the same flow (i.e. the rotor speed). Thus, the power bonds for these loads and the torque determination described above are all connected to a **1** junction.

The equations for the IM model will now be obtained from the IM bond graph using the power bond labels. The equations are presented in table 3.3.3. The first characters for the power bonds (s, r, m) stand for stator, rotor and mechanical. The mechanical bonds are numbered. The stator bonds are numbered with bond number first and then stator branch number (this will usually be the phase number). The rotor bonds are numbered with bond numbers first and then the rotor bar number. Derivations for fs6I and fr1i are explained next. The equation for em1 is developed in [19].

<table>
<tr><th colspan="6">Effort Equations for Stator</th></tr>
<tr><td colspan="3">es11 = Se</td><td colspan="3">es21 = fs21*R</td></tr>
<tr><td colspan="3">es31 = es11 - es21</td><td colspan="3">es41 = es51</td></tr>
<tr><td colspan="3">es51 = qs51/C</td><td colspan="3">es61 = es51</td></tr>
<tr><td colspan="6">(Effort equations for the other branches are similar)</td></tr>
<tr><th colspan="6">Flow Equations for Stator</th></tr>
<tr><td colspan="3">fs11 = fs31</td><td colspan="3">fs21 = fs31</td></tr>
<tr><td colspan="3">$fs31 = es41/GY_S$</td><td colspan="3">$fs41 = es31/GY_S$</td></tr>
<tr><td colspan="3">fs51 = fs41 - fs61</td><td colspan="3">$fs61 = \omega_{synch} * \mathbf{C} * MMF_r * \sin(\boldsymbol{\theta}_{phase\ i} - \boldsymbol{\theta}_{MMFr})$</td></tr>
<tr><td colspan="6">(Flow equations for the other branches are similar)</td></tr>
<tr><th colspan="6">Integral Equations for Stator</th></tr>
<tr><td colspan="6">qs51 = integ(fs51)</td></tr>
<tr><th colspan="6">Effort Equations for Rotor</th></tr>
<tr><td colspan="3">er11 = er21</td><td colspan="3">er21 = qr21/C</td></tr>
<tr><td colspan="3">er31 = er21</td><td colspan="3">er41 = fr41*R</td></tr>
<tr><td colspan="6">(Effort equations for the other branches are similar)</td></tr>
<tr><th colspan="6">Flow Equations for Rotor</th></tr>
<tr><td colspan="3">$fr11 = \omega_{slip} * \mathbf{C} * MMF_r * \sin(\boldsymbol{\theta}_{bar\ i} - \boldsymbol{\theta}_{MMFr})$</td><td colspan="3">fr21 = qr21/C</td></tr>
<tr><td colspan="3">er31 = er21</td><td colspan="3">er41 = fr41*R</td></tr>
<tr><td colspan="6">(Flow equations for the other branches are similar)</td></tr>
<tr><th colspan="6">Integral Equations for Rotor</th></tr>
<tr><td colspan="6">qr21 = integ(fr21)</td></tr>
<tr><th colspan="6">Effort Equations for Mechanics</th></tr>
<tr><td colspan="6">$em1 = \mathbf{C} * MMF_1 * MMF_2 * Poles/2 * \sin(\boldsymbol{\theta}_{mmf1} - \boldsymbol{\theta}_{mmf2})$</td></tr>
<tr><td colspan="3">em2 = fm3*R</td><td colspan="3">em3 = em1 - em2</td></tr>
<tr><th colspan="6">Flow Equations for Mechanics</th></tr>
<tr><td colspan="2">fm1 = fm3</td><td colspan="2">fm2 = fm3</td><td colspan="2">fm3 = pm3/I</td></tr>
<tr><th colspan="6">Integral Equations for Mechanics</th></tr>
<tr><td colspan="6">pm3 = integ(em3)</td></tr>
</table>

Table 3.3.4: Equations from Bond Graph in Figure 3.3.10.

The resultant MMF for the machine, MMF_r, is found using the d and q components of the rotor and stator MMF's described previously. The resultant flux of the machine is found by dividing the MMF_r by the reluctance of the machine which is the value for the **C** field. The resultant flux is distributed sinusoidally about the circumference of the air gap. The amount of resultant flux seen by any coil in the machine (i.e. stator coils, or the ½ turn of the rotor bars) is described by equation 3.3.1.

$$\phi_{coil} = \phi_R \cdot \cos(\theta_{coil} - \theta_{\phi_R}) \qquad \textbf{Equation 3.3.1}$$

The angles are referenced from the machine's angle datum (usually the d axis). The first angle, θ_{coil}, is the electro-magnetic angle to the centerline for the coil of interest, and θ_{ϕ_R} is the angle to the resultant flux.

The **C** field is in derivative causality. Normally, derivative causality requires algebraic reduction or implicit operations. However, consider what happens if we take the time derivatives of equation 3.3.1 so that the **C** field supplies flows (i.e. flux rates) to the power bonds attached to it. Taking the time derivatives of equation 3.3.1 with respect to a given stator coil yields equation 3.3.2 (a). Taking the derivative of equation 3.3.1 with respect to a given rotor bar yields equations 3.3.3 (b). The second terms on the right side of the equal signs for equation 3.3.2 (a) and equation 3.3.3 (a) are considered negligible compared to the first terms to the right of the equal signs. Therefore, these terms are dropped, and equation 3.3.2 (b) and equation 3.3.3 (b) are used. This is fortunate, because the time derivative of the resultant flux would be hard to find analytically and would probably be unstable if determined numerically. Note, that in equations 3.3.2, the time derivative of any stator coil angle is zero, which leaves only the time derivative of the resultant flux angle. In steady state, this derivative is the synchronous rotational velocity, and in transients, this derivative deviates only slightly from the synchronous rotational velocity. The time derivative of any bar angle is the rotor rotational velocity. Thus, in equations 3.3.3, the time derivative of the two angles yields the slip velocity.

$$\phi_{si} = \phi_R \cdot \sin(\theta_{si} - \theta_{\phi_R}) \cdot \omega_{synch} + \dot{\phi}_R \cdot \cos(\theta_{si} - \theta_{\phi_R})$$ **Equation 3.3.2 (a)**

$$\phi_{si} = \phi_R \cdot \sin(\theta_{si} - \theta_{\phi_R}) \cdot \omega_{synch}$$ **Equation 3.3.2 (b)**

$$\phi_{bi} = \phi_R \cdot \sin(\theta_{bi} - \theta_{\phi_R}) \cdot \omega_{slip} + \dot{\phi}_R \cdot \cos(\theta_{bi} - \theta_{\phi_R})$$ **Equation 3.3.3 (a)**

$$\phi_{bi} = \phi_R \cdot \sin(\theta_{bi} - \theta_{\phi_R}) \cdot \omega_{slip}$$ **Equation 3.3.3 (b)**

With the flux distribution throughout the machine known, the amount of flux passing through each rotor and stator tooth is known at any time in the simulation. The teeth are divided into several slices. Each slice could have a different cross-sectional area, and, therefore, each slice experiences a different flux density. Using data from the manufacturer of the magnetic steel in the machine, the magnetic reluctance of each slice can be determined from the local flux density using lookup tables. The reluctances of the slices of a single tooth can be summed directly because they share a common flux. Once the reluctances of each tooth are known, a cosine distributed weighted average of the rotor teeth and stator teeth reluctances is determined. This type of average relates these reluctances directly to the resultant flux of the machine. The sum of these two tooth reluctance averages and the air gap reluctance yield the effective total reluctance of the C field with respect to the peak of the resultant flux in the machine.

The ACSL code developed for this IM model can be found in Appendix G. Note that there are several arrays used to simplify the repetitive calculations of the values for the different branches of the stator and rotor.

3.3.2 Modularity and Configurations

Many values can be altered in a squirrel cage IM, but the basic configuration of the IM does not change. Therefore, modularity of induction motor components was not considered critical in the coding of this model. Thus, there is only a single ACSL power block for the IM model.

3.3.3 Validation

Because DC Machine models are extremely accurate [19], no validation of the separately excited DC machine model was deemed necessary. Presentation of simulation studies using the Ideal IM model and the IM model with leakage are given below. Further presentation of the simulated dynamic characteristics of the IM with leakage model are provided in the IM powered EV section.

The ideal IM model that was mentioned above was used to simulate a free acceleration of an 18 kW nominal power induction motor powered from batteries. It's torque verses rotor speed is shown below in figure 3.3.11. The smaller slope near synchronous speed is due to the recovery of battery voltage. The normal breakdown torque for a high efficiency motor of this size is approximately 150 Nm. The peak torque in this plot is 260 Nm. If simulated batteries had not been used to power this IM model, a more unrealistic peak torque would have been achieved. However, the ideal IM model is a good educational tool, it is computationally fast, and it makes fair steady state predictions. Also, as one can see, the free acceleration characteristics (when powered by the batteries) are similar to actual IM's. Plots similar to this one, where IM's are simulated without leakage, can be found in [26].

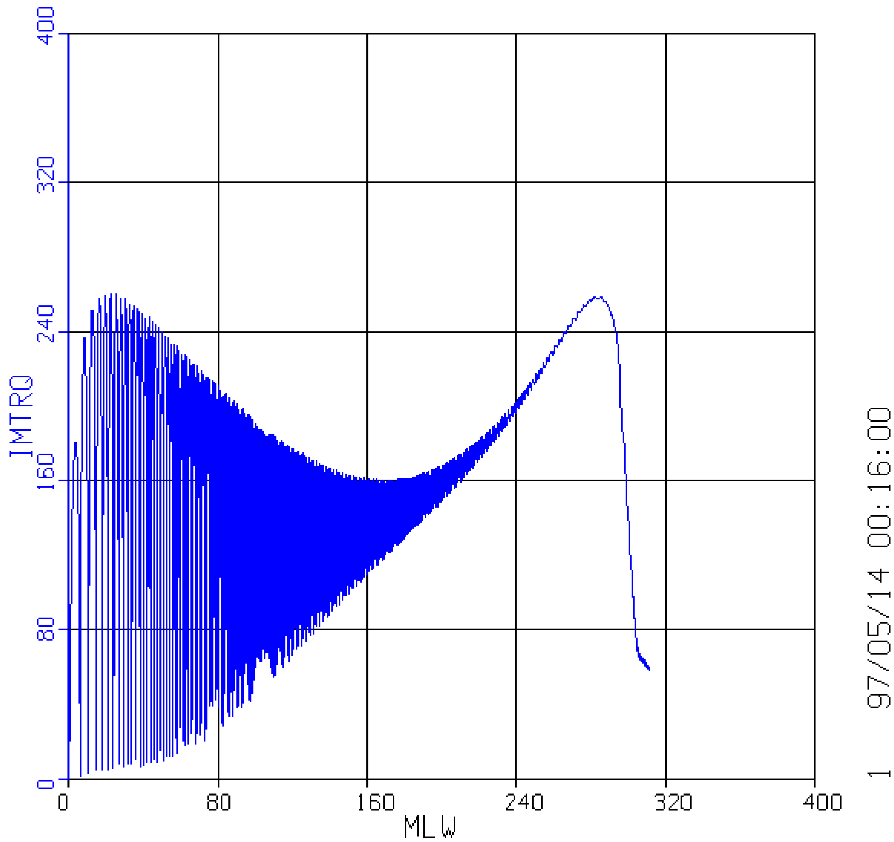

Figure 3.3.37: Torque (Nm) verses Rotor Speed (rad/sec) Predictions Using the Ideal IM Model for a 18 kW Nominal Power IM Powered From a Simulated Battery Bank of 39 Sears Batteries.

Design parameter values for a popular IM used in vehicle applications were estimated to validate the IM model of figure 3.3.10. The IM is made by the Solectria Corporation. The reported ratings of this machine are 312 volt peak controller voltage, 18 kW nominal power, 70 kW maximum power, 40 Nm nominal torque, 140 Nm maximum torque, 3000 rpm rated speed, 12,000 rpm maximum speed. The design techniques used to determine design parameter values that could meet these specifications can be found in [25]. Data sheets with the resulting design parameter values are in Appendix H.

The predictions using the model and the estimated design parameters were good. The simulated motor was found to have a breakdown torque of 145 Nm and a top speed of approximately 12,000 rpm using a peak controller voltage of 320 volts. The simulated characteristics for the modeled machine were like the characteristics one would expect to measure from a real machine. Much of the findings and operating characteristics are presented in this section. Other results regarding response to variable speed control will be presented in the section covering the IM powered EV.

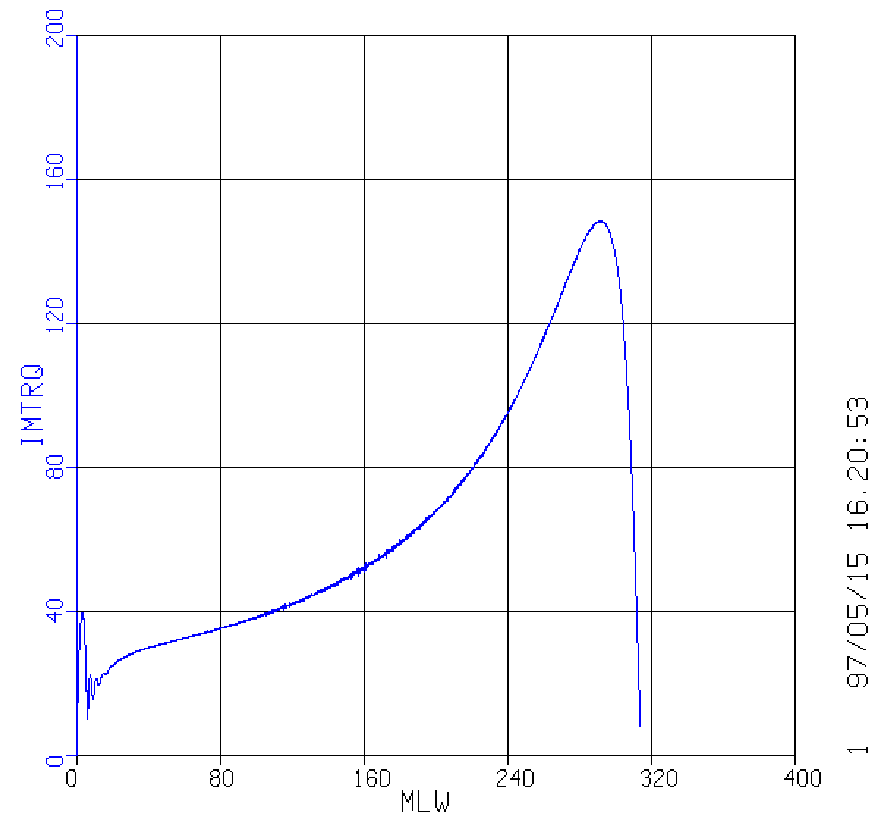

Figure 3.3.38: Torque (Nm) verses Rotor Speed (rad/sec) in a Free Acceleration of a 18 kW Nominal Power IM without End Ring Adjustment to the Rotor Bar Resistance.

The first simulation of this machine was a free acceleration with a small viscous load. The torque speed results are shown in figure 3.3.12. Free acceleration simulations are useful, because free acceleration characteristics are very close to steady state characteristics for smaller machines [26]. The end ring resistance adjustment was not included in this plot. The free acceleration of this machine with the end ring resistance adjustment is presented later. Note that the peak torque of this machine for this free acceleration is 148 Nm. This simulation used an ideal voltage source that increased at a rate of ($1-e^{-40*t}$).

Figures 3.3.13 through 3.3.18 are also shown to present the simulated characteristics of this 18 kW nominal power IM. The electrical power drawn by the IM during the free acceleration of this first simulation is shown, along with the torque, verses IM rotor speed in figure 3.3.13. The mechanical power used by the IM is shown, along with the electrical power drawn, verses IM rotor speed in figure 3.3.14. Terminal current and electrical power verses rotor speed are shown in figure 3.3.15. Volt amps and terminal current are shown figure 3.3.16. Phase Voltage and Phase Current of the IM at idle are shown in Figure 3.3.17 indicating a small power factor at idle.

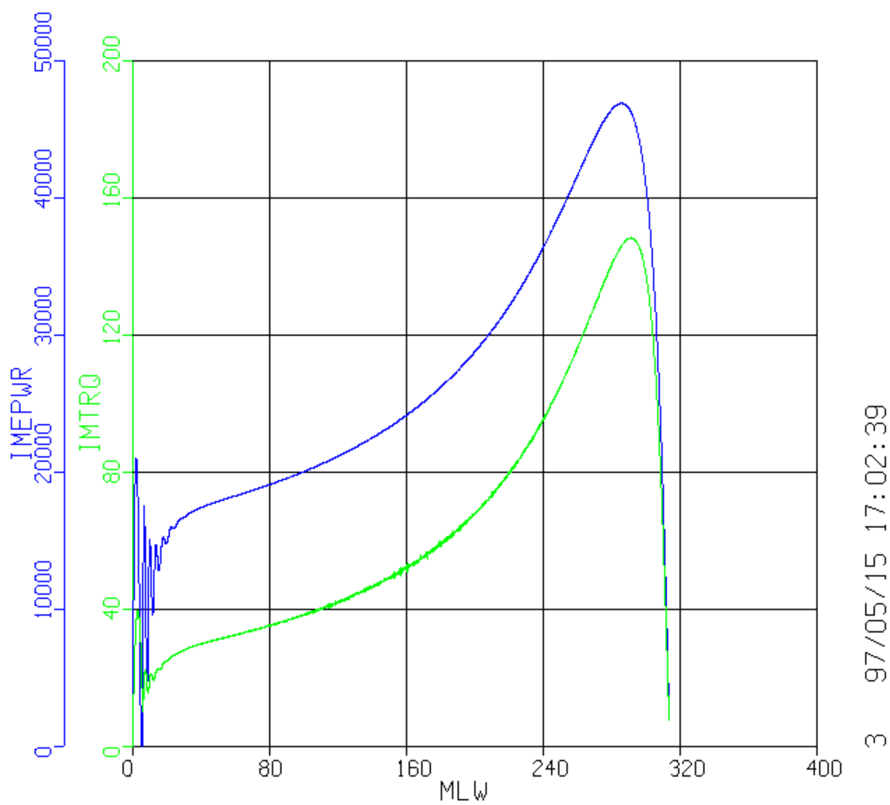

Figure 3.3.39: Electrical Power (watts, solid line) and Torque (Nm, dotted line) verses Rotor Speed (rad/sec) in a Free Acceleration of a 18 kW Nominal IM.

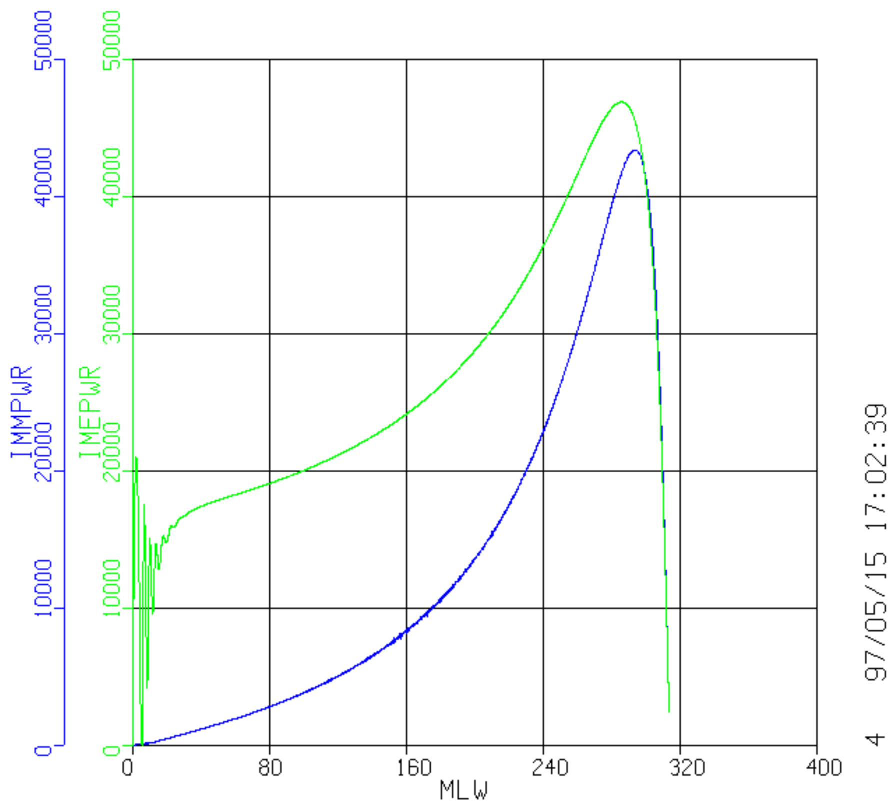

Figure 3.3.40: Mechanical Power (watts, solid line) and Electrical Power (watts, dotted line) verses Rotor Speed (rad/sec) in a Free Acceleration of a 18 kW Nominal IM.

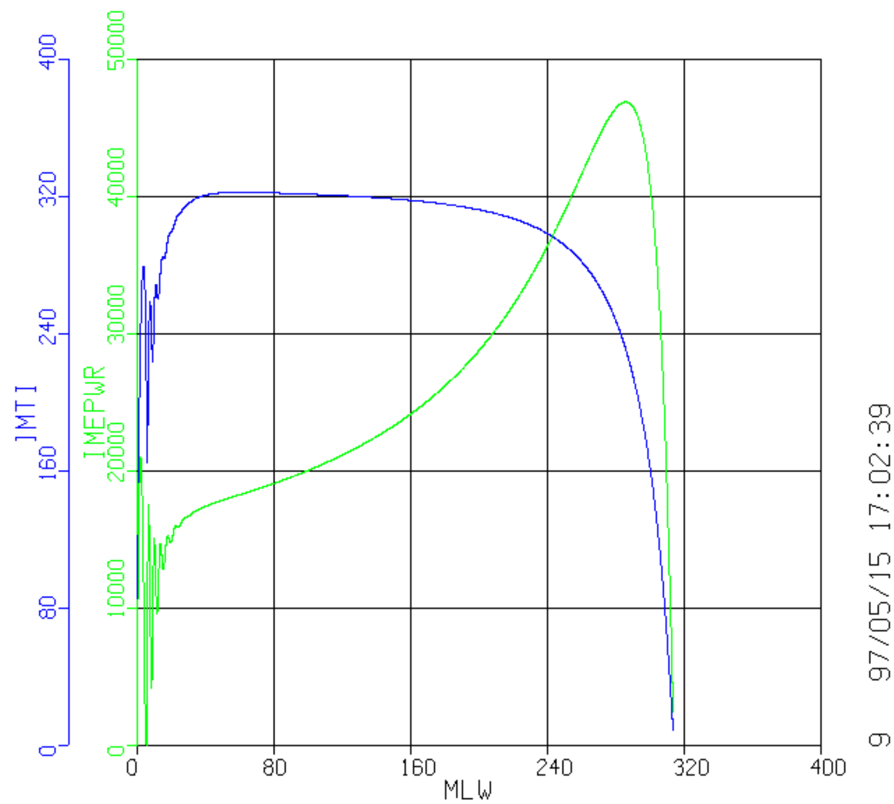

Figure 3.3.41: Terminal Current (amps, solid line) and Electrical Power (watts, dotted line) verses Rotor Speed (rad/sec) in a Free Acceleration of a 18 kW Nominal IM.

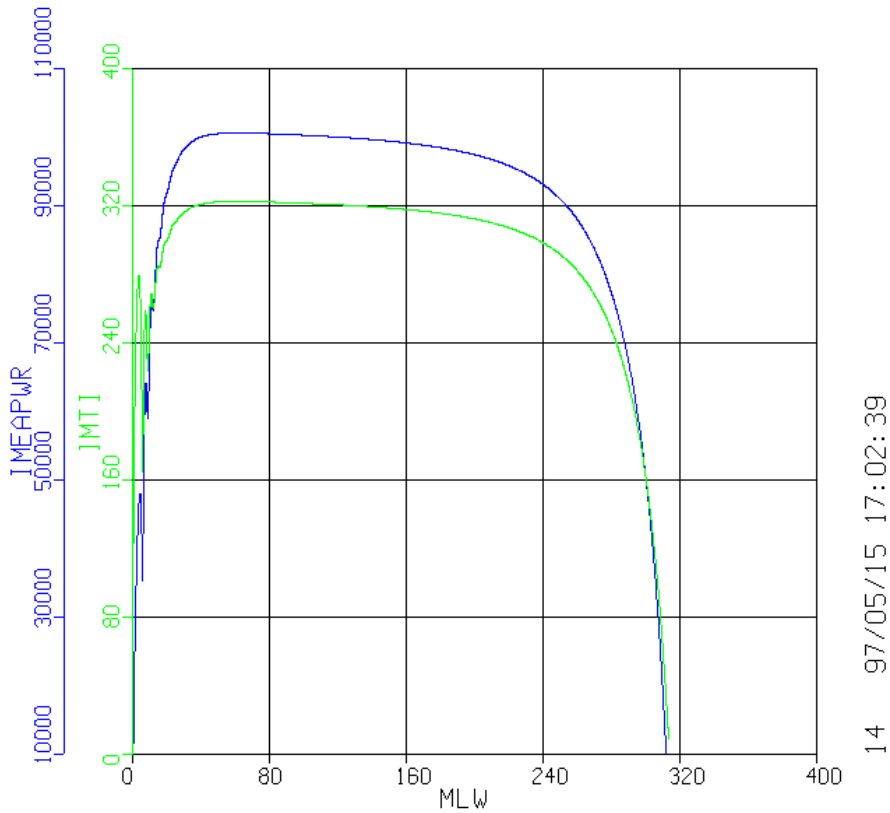

Figure 3.3.42: Volt Amperes (watts, solid line) and Terminal Current (amps, dotted line) verses Rotor Speed (rad/sec) in a Free Acceleration of a 18 kW Nominal Power IM.

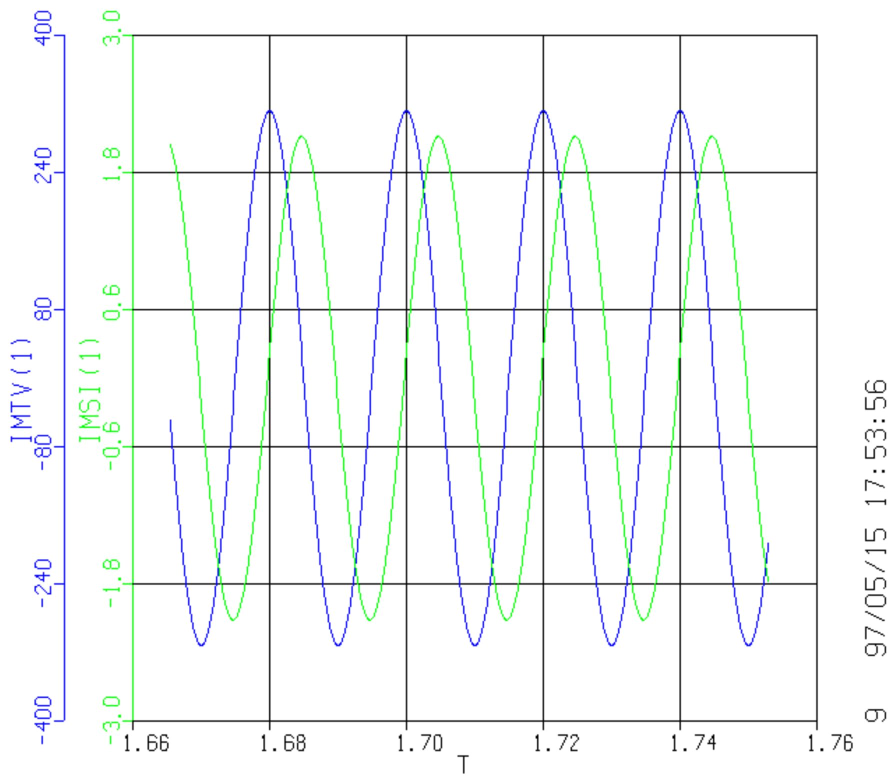

Figure 3.3.43: Phase Voltage (volts, solid line) and Phase Current (amps, dotted line) verses Time (seconds) for a 18 kW Nominal Power IM at idle.

Each of the plots in figures 3.3.13 through 3.3.17 are from simulations where the end ring resistance adjustment was not used. However, end ring resistance was not found to have a significant effect on the characteristics of these plots. A plot of this same motor design simulated with the end ring adjustments made to the rotor bars is shown in figure 3.3.18. Note that the peak torque has reduced slightly, and the torque at low speeds has increased compared to the plot shown in figure 3.3.12. This is what would be expected by increasing the rotor resistance [19]. The motor had a pull-out torque of 145 Nm, and an idle power factor of 0.1. All characteristics appeared correct.

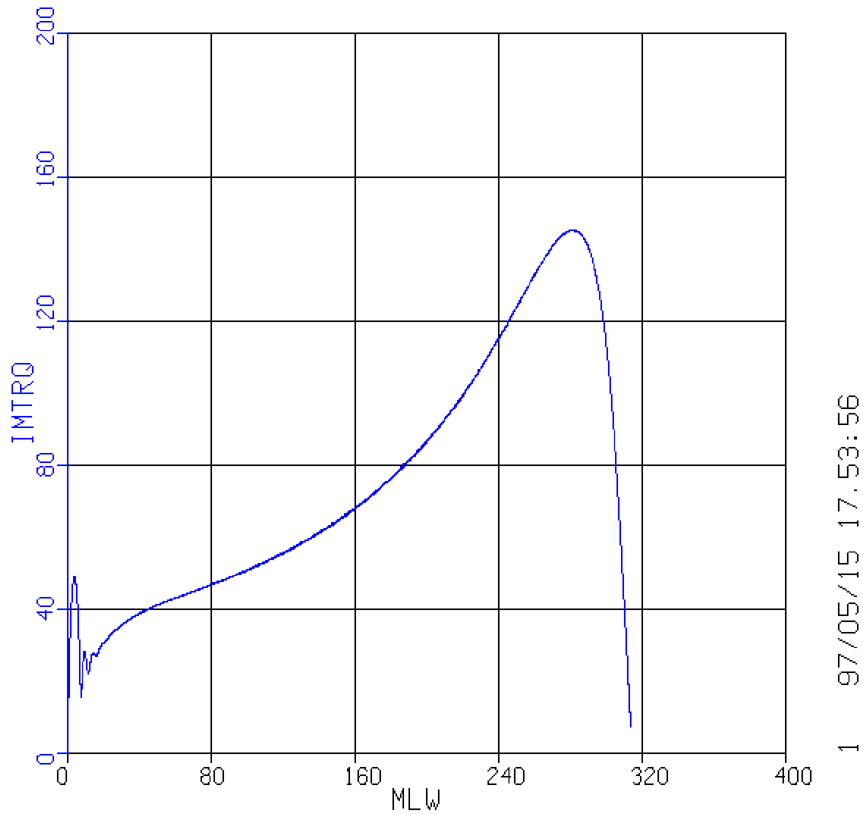

Figure 3.3.44: IM Torque (Nm) verses Rotor Speed (rad/sec) for the Free Acceleration of a 18 kW Nominal IM with the End Ring Resistance Adjustment Made to the Rotor Bars.

Powering an IM from an ideal voltage source is unrealistic. Any voltage supply will experience a dip when an IM of any significant rating is started. Therefore, free acceleration simulations using battery models (that will be presented in section 3.4) were performed to further observe the predicted characteristics using the model. This simulation also helped to study the battery model. A total of 26 lead acid batteries were used which yield an open circuit voltage of 325 volts (the IM design specified a nominal voltage of 312 volts peak, 220 rms. Appendix H). Plots for torque verses speed, shown in figures 3.3.19 and 3.3.20, are broken into two portions to show more detail. These plots illustrate that in order to acquire peak torques and prevent excessive voltage drop in the batteries, the designer will need to oversize a vehicle battery bank. This will be addressed further in the battery modeling section and in the sections covering EV modeling and simulation.

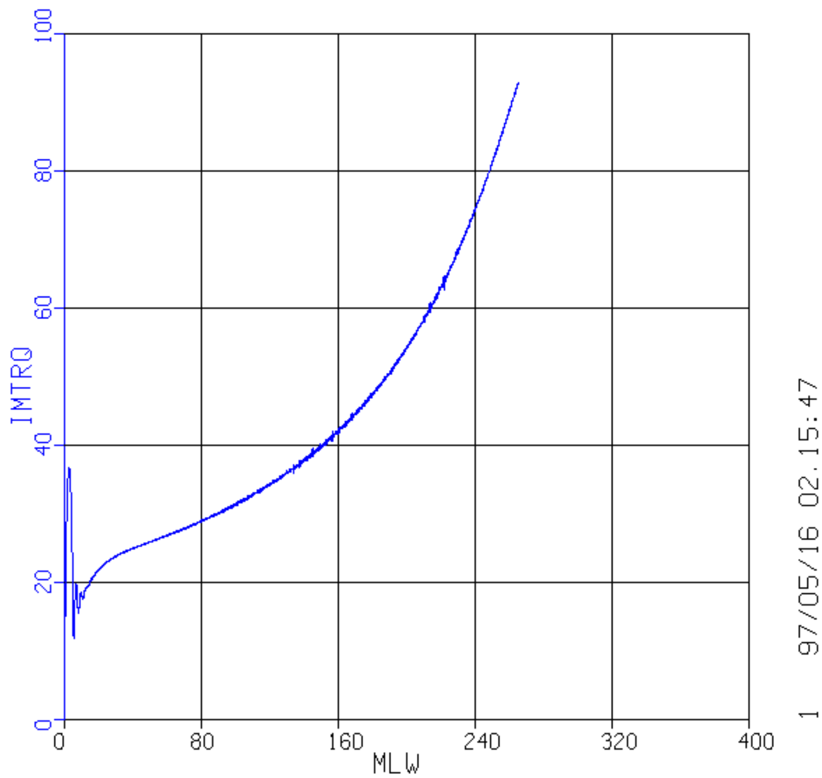

Figure 3.3.45: Torque (Nm) verses Rotor Speed (rad/sec) for a 18 kW Nominal IM Powered by 26 Lead Acid Sears Batteries.

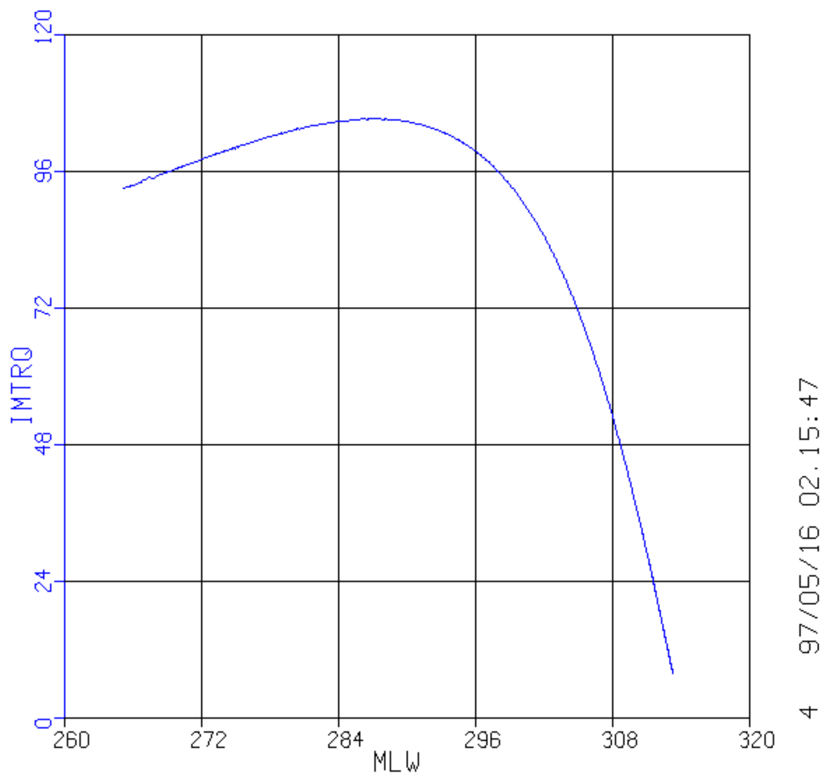

Figure 3.3.46: Torque (Nm) verses Rotor Speed (rad/sec) for a 18 kW Nominal IM Powered by 26 Lead Acid Sears Batteries.

3.3.4 Summary

DC Machine models do not require validation, because they are very accurate when compared to experimental results. An IM model that could meet the modeling objectives of component / process level decomposition was developed using the generalized approach and bond graph modeling techniques. The electrical, magnetic, and mechanical processes in the machine were modeled as separate, discrete regions or processes. The model proved to be adequately accurate for the purposes of this work and to reproduce realistic performance characteristics. It showed the proper sensitivity to design parameter changes. However, in a squirrel cage IM design, design parameters cannot be changed easily without affecting many other design parameters, so a careful IM design process was followed when adjusting IM design parameters to ensure that the interrelations of design change effects were properly considered [25]. The

IM model requires more computation time than any of the other models in this work, but the speed was found to be tolerable. Ten seconds of dynamic simulation required 3 hours to run on a Digital VAX Alpha computer.

Design parameter values for an existing production IM used in vehicle applications were estimated to validate the IM model. Simulation predictions using the model and the estimated design parameters were good. The simulated characteristics for the modeled machine were like the characteristics one would expect to measure from a real machine, and the modeled IM exhibited sensitivities to design changes that would be experienced in experimentation. Results regarding response to variable speed control are presented in the section covering the IM powered EV.

3.3.5 Conclusions

The contribution of this IM model is that it is the first IM model developed using the generalized approach and bond-graph modeling techniques where the electrical, magnetic, and mechanical processes in the machine were modeled as separate, discrete regions or processes. The model's decomposition and generalized nature make it an ideal tool for a multi-disciplined design team for the reasons explained in the introduction. It shows realistic sensitivities to design parameter changes.

The model lies between the two most common methods of IM modeling presently used: equivalent circuit models and finite element models. Equivalent circuit models are computationally fast and adequately accurate, but they were avoided, because they do not meet the stated objectives, since they mask the magnetic and mechanical processes. Decomposing the machine into electrical, magnetic, and mechanical processes and modeling these separate processes allows a better understanding of the processes, and better visualization of state variables, in their respective realms at any time in the simulation. This was another important element of the modeling that was explained in the introduction. Even with this level of decomposition, the developed model is not detailed enough to predict all of the phenomena that affect the performance of the machine. Finite element models would be better suited for this purpose, but, given present computational speed on the fastest machines available, these models are not well suited for vehicle performance simulations. However, given the recent history of microprocessor computational speed increases, and the predictions for speed improvements in the near future (which have been on track over the last year), it is only a matter of time before engineers will be using finite element based models for performance predictions as well. If this era arrives in the near future, the author feels that the IM model developed in this work should have value as an academic tool, because, in that era of greater computational speed, this IM model will allow the students of IM's to visualize the separate realms of energy that exist in actual IM's with exceptional computational speed and reasonable accuracy.

3.4 Battery Modeling

If used in a hybrid power plant, batteries are the most sensitive component to the design, coordination and performance of the plant. They can influence the design of every power supply component. This is due to two primary things: their weight; and their voltage variations. Batteries have the highest power density of any other device in the power plant. (Power density is defined to be kg/kW). And, a battery bank for an electric vehicle can vary by 200 volts depending upon the transient.

Battery voltage is pulled down during any energy discharge. Hard accelerations pull battery voltage down severely. It is possible to damage, or drastically reduce, the terminal voltage of a battery if too much current is drawn. This requires special attention in the design of the electric machine controls for any EV or HVPP using batteries.

During charging, voltage rises. Hard regenerative braking pushes battery voltages very high. However, battery voltage during charging must be kept from going too high to avoid harming the batteries. Batteries can be designed to handle faster charging transients, so that more energy can be regained in regenerative braking. But even then, batteries put limits on the amount of energy that can be regained in regenerative braking.

Voltage variations between transients put special demands on electric machine design and electric machine control. Electric machines must be larger and more robust to reliably and effectively handle these large voltage ranges. This can significantly influence the weight and/or volume of the power plant. And, the effects on machine design may be such that regenerative braking is deemed too troublesome.

Objectives chosen for the plant performance will influence the choice of battery mass. Tradeoffs are incurred between the required battery mass and the size of other components. A designer can be more sure of the power balance he has chosen, if he has a good battery model for use in the simulation of his proposed design. Thus, in order to meet the objectives of this work, a good dynamic battery model is necessary.

Finite element models are in use by battery designers that concentrate on the design of individual cells. These types of models are currently not computationally appropriate for vehicle performance simulations. Empirical models exist, but they are not based on cell design geometry and chemical reactions. There are various levels of equivalent circuit models being used in simulation studies [27]. Some of them can be adjusted quite easily and appropriately with a basic knowledge of current energy capacity and power density limitations [28] [29]. Based on this information, the most accurate and flexible equivalent circuit model that could be found was used for this research.

The chosen model is an accurate equivalent circuit model that is based on first principles. It proved to be extremely valuable in meeting the objectives of this work. Adequate simulation accuracy can be achieved by making small adjustments to the nonlinear functions published with the model. It is easy to code, and it is computationally fast.

3.4.1 Battery Model

The equivalent circuit battery model chosen was developed at the University of Lowell in Massachusetts [28]. It was developed for use in the simulation of systems requiring batteries to store and deliver electrical energy. It uses nonlinear elements that emulate the essential characteristics of battery phenomena. It is very accurate and computationally fast. The best accuracy is obviously achieved when the nonlinear functions for a specific battery are experimentally identified. But, with a basic knowledge of how cell design affects battery performance, standardized nonlinear functions can be tailored to effectively predict the performance of a battery whose performance has not been measured.

The equivalent circuit battery model used is shown in figure 3.4.1 (a). It uses nonlinear functions to represent the charging, discharging, and self discharging resistances, and the battery capacitance. Each of these nonlinear components is a function of open circuit voltage, and the combination of them properly reproduces the important phenomena known to exist in battery operation.

The battery capacitance is modeled as a nonlinear capacitance that is a function of its own voltage. This requires an implicit integration to calculate open circuit voltage at each time step. In this work, unlike the publication, a sigmoid function was used to model the capacitance function. This allowed modifications of the capacitance function that were quicker than adjustment of lookup tables. As open circuit voltage drops, so does capacitance. Dropping the capacitance value over a discharge cycle makes the modeled battery voltage follow the voltage drop characteristics of a real battery.

The battery self discharge resistance is modeled as a nonlinear function of open circuit voltage. This resistance is much larger than the charge and discharge resistances and is connected in parallel with the battery capacitances. This arrangement properly models the open circuit discharge characteristic of a battery. A lookup table that scaled values found in [28] was used to model this non-linear function. Self discharge resistance is lowest when open circuit voltage is high, and gradually shifts to a higher value as the open circuit voltage drops.

Resistances during charging are much higher than those experienced during discharging. Therefore, one set of look-up tables is used during charging, and another is used during discharging. These lookup table also contained scaled values from [28].

During charging, battery voltage rises. Once the charge is stopped, the open circuit voltage falls below the last voltage seen during charging. A linear capacitance was used to model this phenomena. It is linked in parallel to half of the charge/discharge resistance.

3.4.2 Bond Graph and Equations

The bond graph for the equivalent circuit is shown in figure 3.4.1 (b). Several of these battery bond graphs can be linked together as shown in figure 3.4.1 (c) to form a bank of batteries. This can add a significant number of implicit integrations to the simulation.

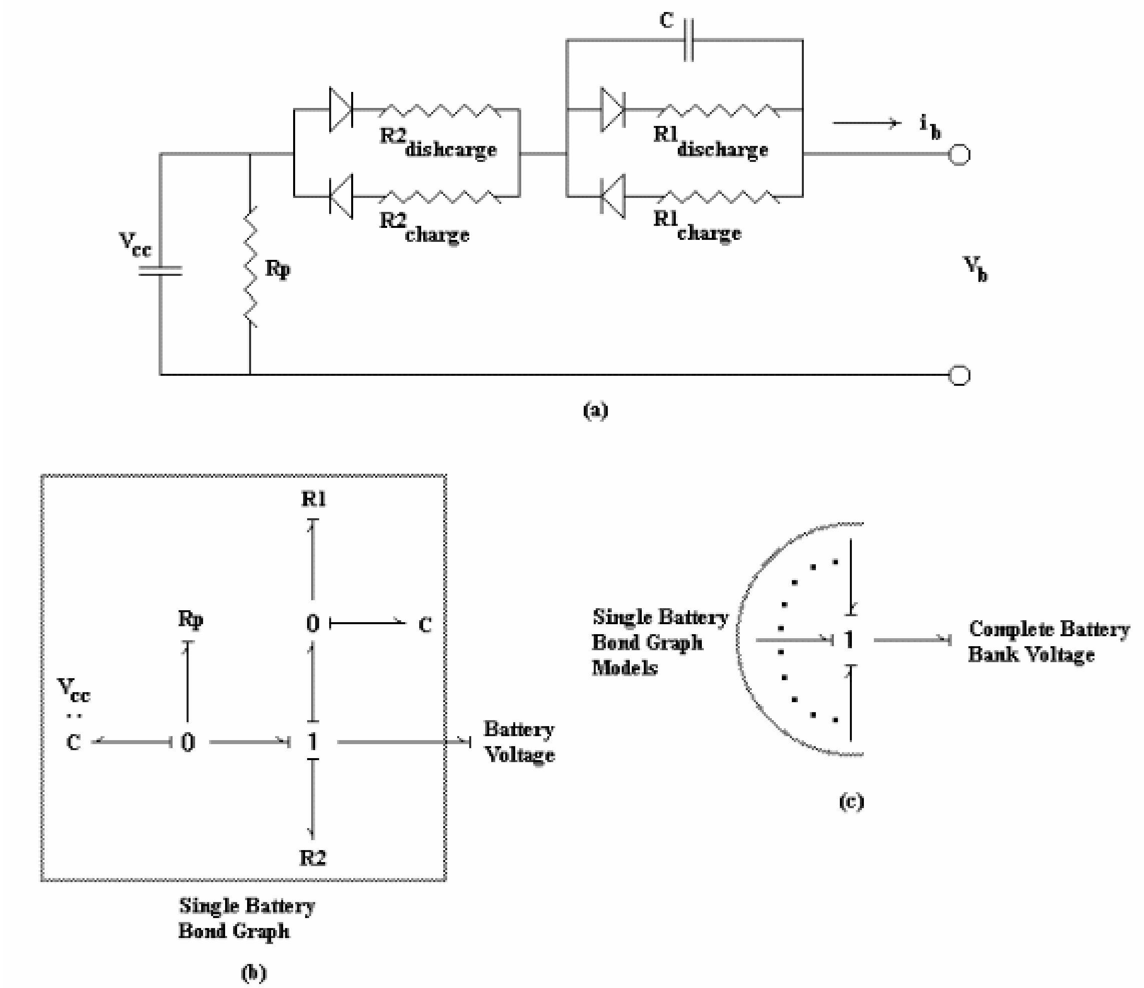

Figure 3.4.47: (a) Battery Schematic Model, (b) Single Battery Bond Graph Model, (c) Battery Bank Bond Graph Model.

Multiplication factors used on one battery model can be used to properly reproduce the dynamics of a battery bank. The battery voltage of one battery can be multiplied by the number of batteries in the series paths of the battery bank. The current being fed back to the one battery model can be divided by the number of parallel paths in the bank. This will increase simulation speed by reducing the number of implicit integrations. The power blocks used for this scheme are shown in figure 3.4.2. The code for this model is in Appendix I.

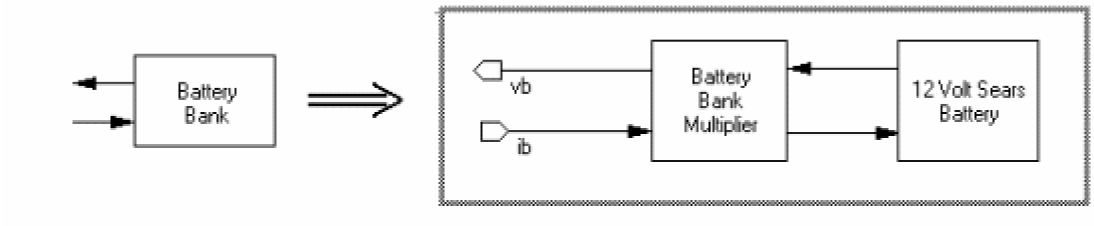

Figure 3.4.48: Battery Bank Power Blocks.

3.4.3 Validation of Model

The developers of this battery model obtained the data to identify and curve fit the functions for the model elements using a voltage controlled current source [28] [29]. The methods for obtaining the functions of the model elements are explained in [29]. Batteries were not tested using transients as severe as those occurring in electric vehicles. Furthermore, the lead acid batteries in the reference did not exhibit power densities similar to lead acid batteries used in electric vehicles. Therefore, the values in the lookup tables that were used to represent the non-linear functions were all scaled by the same values until the modeled battery performance matched the power density specifications given for the battery to be used in this present work. This type of scaling was deemed acceptable and accurate, because the model adequately decomposes the battery performance into discrete phenomena, and the predictions of the model were set to match known specifications.

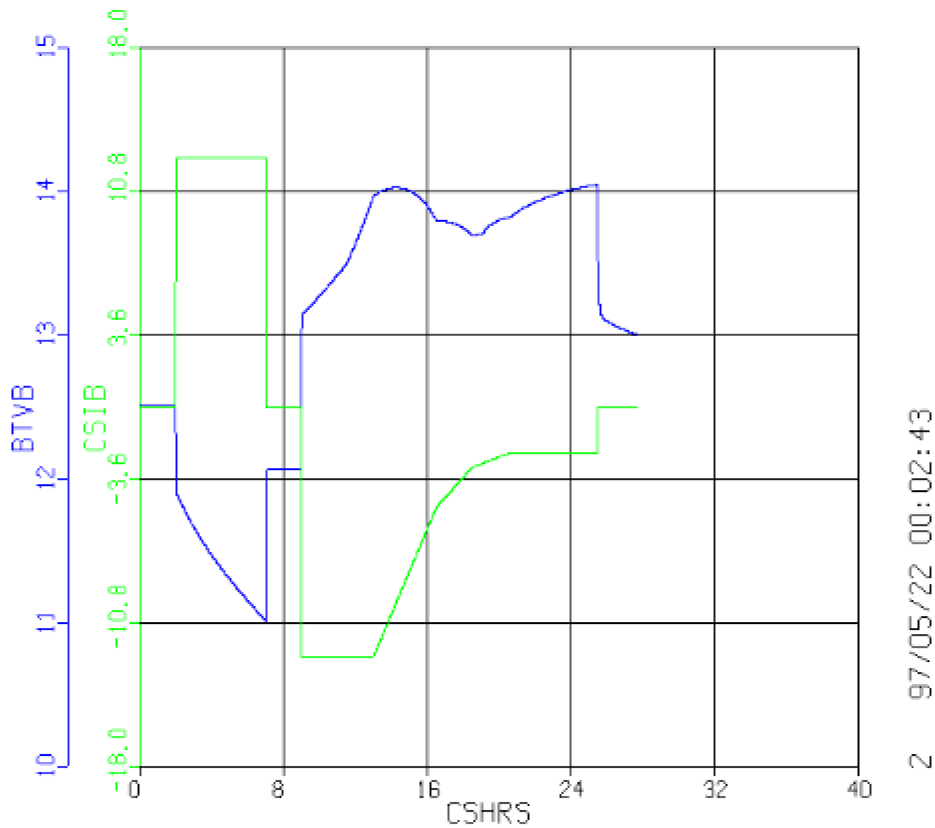

Figure 3.4.49: Battery Model Voltage Response (volts, solid line) and Input Current (amps, dotted line) verses Time (hours) for the Battery Model and Specifications Used in this Work.

When comparing the plot in figure 3.4.3 to the similar plots in [28], one can see that the only significant difference occurs between 13 and 25 hours on the charging cycle. This difference is due to open loop verses closed loop simulation. The authors of [28] used a closed loop voltage controlled current source. The battery model herein was tested open loop using estimated values of current from the plots provided in [28]. Thus, small deviations from the currents used in the reference can result in significant voltage differences.

3.4.4 Summary

Finite element battery models are currently the only battery models that can model the actual physical processes in the battery cells. However, finite element battery models are currently not computationally appropriate for vehicle performance simulations. Currently, the best battery model that can be used for a work such as this is a good equivalent circuit model. Therefore, the most accurate and flexible equivalent circuit model that could be found was used.

This model is based on first principles, and it is comprised of discrete elements that emulate typical battery phenomena. The model is not a contribution of this work. It was obtained from literature. Other than one implicit calculation, it is easy to code, and it is computationally fast. It uses a few simple statements and small lookup tables for the nonlinear parameters. The battery capacitance was modeled using a variable sigmoid function.

As claimed by the authors who developed the model, adequately accurate simulation predictions could be achieved by making small adjustments to the capacitance based on knowledge of a given battery's energy storage capacity and power density. Since the developers did not test the battery model for the more severe transients that occur in an EV, it was necessary to adjust the functions for nonlinear resistances to achieve an accurate prediction for power density. (More accurate results can be achieved by experimentally identifying the nonlinear parameters for specific batteries of interest).

This model proved to be extremely valuable to the objectives of this work. The most influential interface sensitivities encountered were due to the batteries and the most critical design parameters of the HVPP's studied included effects related to the batteries. They had a strong influence on the design of the plant. This, of course, is not a new finding. What is important at this point is that the developed models are consistent with known facts in EV and HVPP design.

3.4.5 Conclusions

This model is not a contribution of this work, and the initial aim of the work did not include creation of a battery model, but it was necessary to have a good battery model to fulfill the overall objectives of this work. Even though this model is an equivalent circuit model, and the explanation of how the objectives would be fulfilled dictated that these types of models should be avoided, this battery model is appropriate for this work considering the current state of battery modeling. It does not model the actual chemical reactions and processes in the battery, but it does give the end user a good indication of the difficulties that will be encountered when using batteries in vehicle power applications. This makes it an important tool for meeting the objectives of this work.

4VALIDATION OF THE MODELING METHODOLOGY USING SIMULATIONS OF NON-HYBRID POWER PLANT VEHICLES

Simulation of single power plant vehicles proved to be very valuable to this work. Developing the correct balance of power through the design and control of power supplies for a HVPP is difficult and requires a prudent approach. Very simple models are used first to help identify large scale parameter values such as power, torque, speed and drive train ratio requirements. Then, single power plant vehicles are simulated using the detailed power supply models to gain experience in simulated dynamic operation of the detailed power supplies. This experience includes identifying interface sensitivities and critical design parameters which can be identified in an isolated setting with a faster simulation. These single power plant vehicles also provided further validation of the sub-component models developed in section 3. Controls developed for single power plant power supplies will be similar to local controls for similar power supplies that will be placed into the HVPP designs. All of these factors help to provide good initial guidance when designing the HVPP's. These single power plant vehicle simulations can also be used to compare performance to simulated HVPP's. And, they help illustrate the application of the function system diagram and bond graphs to familiar systems, so that their application to HVPP design can be better understood.

When a vehicle power plant designer considers all of the functions, requirements, and criteria to be met, he will find that acceleration specifications are the most demanding aspect of the design. Therefore, all power plants in this study were designed to meet a certain acceleration specification. Some of the vehicles were also tested on an idle, acceleration, cruise, deceleration, and idle drive cycle.

Considering the purpose of the vehicle, the designers can estimate the proposed vehicle mass without its power supplies. The design requirements and criteria established by the design team, or the customer, are then used to determine the power supply ratings. There are no simple calculations to determine required mechanical power supply ratings. Torque and power output change over the speed range of the power supply. In some cases this is due to limitations of the power supply. In other cases this is due to limitations of the energy source. Control of power supplies is also shifted into different modes in an effort to optimize the use of the power supply over the speed range of the vehicle. This further complicates the estimation of required ratings. Also, vehicle mass is increased as power is increased. Thus, power supply requirements must be determined by simulation. However, the simulations used to make initial determinations of power supply ratings can be very simple.

The detailed models used in this work are very slow. They are valuable when an accurate performance prediction of a proposed design is needed. They are also valuable when used to give direction in improving the performance of a proposed, or existing, design. But, they are not practical for making initial estimates of power supply ratings and gear ratios. A simple simulation that considers the mass of the vehicle, the power densities of the power supplies and energy sources, and the gear ratios is more appropriate. These types of simulations were conducted using Microsoft Excel spreadsheets and will be presented in each section below.

Caution should be exercised in the use of these simple spreadsheet simulations. They can instill a false sense of accuracy, because, sometimes, they are as accurate as published results. However, they cannot account for the changes in efficiency with speed that occur in most power supplies. Most of the time, the spreadsheet simulations underestimate the power requirements.

The main introduction set forth a presupposition that a certain level of modeling would adequately achieve the objectives of this work. This presupposition was partially validated in section 3, and this section also serves to further validate this presupposition. This is achieved by illustrating two things that were partially illustrated in section 3. One, the models accurately predict performance. Two, the models exhibit realistic sensitivities to changes in design, operational and control parameter values.

This section is also used to demonstrate the usefulness of the models in the design process. This was initially explained in section 3 for each of the power supply component models. It is further illustrated here by applying the developed design and modeling methodologies to existing vehicle designs for which some level of performance is known beforehand. Then parameters are altered to achieve improved performance. The studies performed herein are not meant to be comprehensive. They are only meant to illustrate how complete applications of the methodologies set forth can aid in improving the design of vehicle power plants.

4.1Conventional Vehicle

The primary purpose of this conventional vehicle section was validation of the driver model. This driver model is the most complicated version of the driver models used throughout this work. It must properly handle clutch actuation to avoid stalling or over speeding the engine during starts, stops, and gear shifting. It was also necessary to validate the MRD scheme by checking for correct speed correlations throughout the drive train. However, this model provided two additional benefits. First, it provided further validation of the accuracy of the engine modeling methods. Second, it provided a virtual environment for observing sensitivities in engine operation in preparation for HVPP designs.

4.1.1Application of Design Methodology

The concept of a conventional vehicle powered by an ICE are applied to the structure of the function system diagram as shown below in figure 4.1.1. Note that the only bi-directional energy storage is the mass of the vehicle. The mass stores kinetic energy and seeks to maintain vehicle velocity constant.

Although not shown, the mass is actually connected to another transformer - its cross-sectional area. The connection to the cross-sectional area would be considered the velocity of the car. This transformer dissipates a portion of the vehicle's kinetic energy to the atmosphere. These processes are not shown, because they are common to all vehicles, and designers are painfully aware that these factors must be considered. The ICE is shown as a segmented transformer, because there are multiple transformations of energy that occur as energy passes through it.

In this common concept, the ICE converts a mixture of air and fuel into rotational kinetic energy. This energy is passed through the transmission (TRANS) and then to the wheels of the car. The interface of the tires with the road, convert the rotational kinetic energy of the wheels into translational kinetic energy of the vehicle. This energy is dissipated by brakes via heat transfer to the atmosphere when a significantly rapid deceleration is desired by the driver.

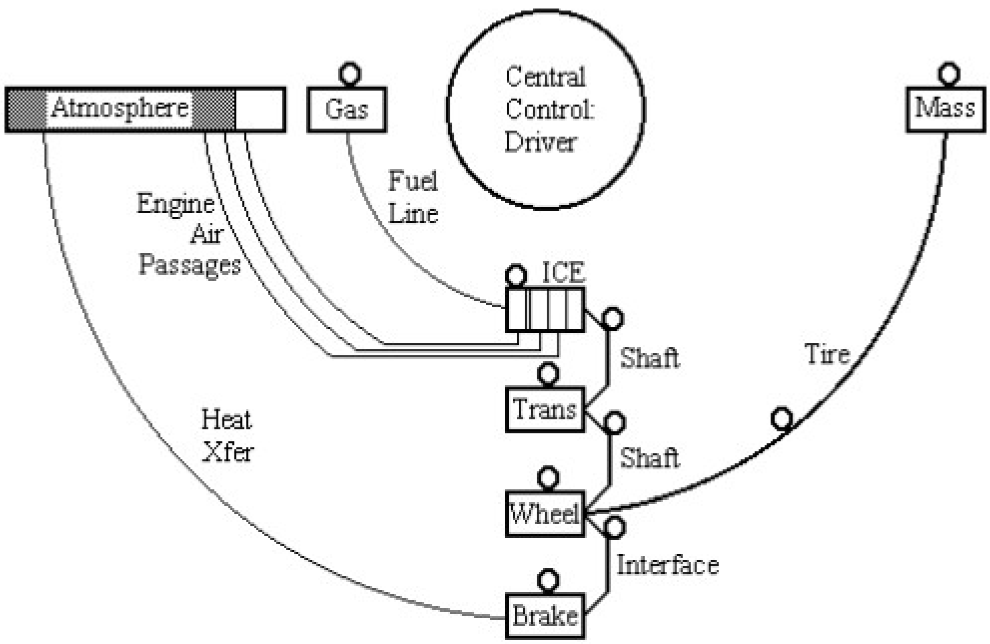

Figure 4.1.1: Conventional Vehicle Concept Applied to the Function System Diagram.

4.1.2Bond Graph Model

This vehicle's bond graph can be formed directly from the conventional vehicle system diagram and is shown in figure 4.1.2. The causality in the bond graph points out that the efforts are passed in the forward direction (i.e. to the left) and the resulting flows are passed backwards from the vehicle. There is one modulated transformer for the transmission. All other transformer ratios are constant.

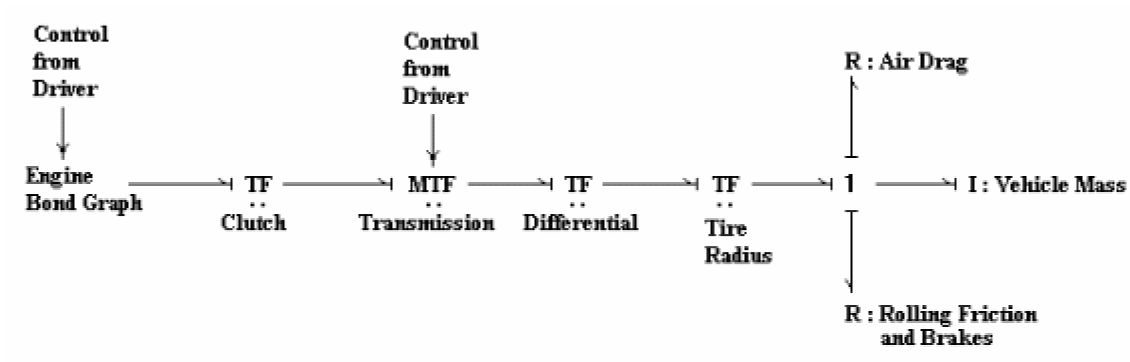

Figure 4.1.2: Conventional Vehicle Bond Graph.

Vehicle mass is determined by adding the mass of each power supply to the mass of the vehicle. To estimate the mass of the power supplies, one multiplies the maximum rated power by an estimate of the power density. This estimated power density would fall within a range of power densities for that type of device. In this first example, the overall vehicle mass is known, and the power rating of the ICE is known. The vehicle mass can be determined using equation 4.1.1 and approximate power densities for the engine. In the remaining sections, it will be necessary to estimate vehicle mass and power supply power densities.

$$M_{Tot} = M_{Veh} + P_{ICE} \cdot \rho_{ICE}$$ **Equation 4.1.1**

where M_{Tot} is the total vehicle mass, M_{Veh} is the mass of the vehicle without power supplies.

For the simple spreadsheet simulations, the torque of the ICE was considered to be constant with respect to ICE rpm. This estimate is not bad. Actual torque profiles of ICE's verses speed are relatively flat. Engines are designed to yield required torques within a reasonable range of speed. Thus, the power at maximum rated speed can be determined by equation 4.1.2. In the equations and tables that follow, ρ is power density, A_f is frontal area of the vehicle, R_T is tire radius, GR is gear ratio, P is power, T is torque, ω is rotational velocity, C_D is aerodynamic drag coefficient, and C_F is rolling friction coefficient [17].

$$P_{ICE} = (T\omega)_{C_{ICE}}$$ **Equation 4.1.2**

Torque from the ICE is multiplied by the overall ratio of the drive train to determine the force applied to accelerate the vehicle as shown in equation 4.1.3. The overall drive train ratio includes the current gear ratio of the transmission that changes at set speeds, the ratio of the differential, and the inverse of the tire radius. The force to the vehicle is integrated and the resulting momentum is divided by the mass of the vehicle to determine the vehicle velocity. The vehicle velocity is multiplied by the overall ratio of the drive train to determine the ICE speed as shown in equation 4.1.4. The transmission gear is changed at the up shift rpm specified in the spreadsheet as shown in figures 4.1.1 and 4.1.2.

$$\sum F = T_{ICE} \cdot GR_{ICE} / R_T$$ **Equation 4.1.3**

$$\omega_{C_{ICE}} = V_C \cdot GR_{ICE} / R_T$$ **Equation 4.1.4**

Spreadsheet simulations were performed for a Ford Taurus SHO and a Honda Ascot Motorcycle. These simulations were not necessary to the objectives of this work. They were simply used to validate the usefulness of the simple simulations for estimating power supply ratings. The values used by the simple spreadsheet models for each of these vehicles are shown in tables 4.1.1 and 4.1.2 for the Ascot and Taurus SHO, respectively. The plots of velocity verses time are shown in figure 4.1.3 and figure 4.1.4 for the Ascot and Taurus SHO, respectively. The performance predictions of these simple models were very close to published performance data.

Ascot Motorcycle						**Conventional Vehicle Settings**					
M_{veh} (Kg)	**ρ_{ICE}** (Kg/w)	**A_f** (m^2)	**C_d**	**C_f**	**R_T** (m)	**ICE Torque Avg**	**Num Gears**	**Up Shift RPM**	**Dn Shift RPM**	**Cruise Speed**	
261.0	0.0	0.5	0.7	0.0	0.3	0.9	6.0	10000	2000	60.0	
M_{tot} (Kg)	**M_{tot}** (lbs)	**P_{ICE}** (Kw)	**ω_{ICE}** (rpm)	**T_{ICE}** (N/m)	**V_{10}** (mph)	**1^{st} GR_{ICE}**	**2^{nd} GR_{ICE}**	**3^{rd} GR_{ICE}**	**4^{th} GR_{ICE}**	**5^{th} GR_{ICE}**	**6^{th} GR_{ICE}**
272	600	45.45	7000	62.00	81.05	18.510	12.620	10.010	8.290	6.960	6.030

Table 4.1.1: Ascot Motorcycle Settings for Simple Simulation.

Taurus SHO						**Conventional Vehicle Settings**					
M_{veh} (Kg)	**ρ_{ICE}** (Kg/w)	**A_f** (m^2)	**C_d**	**C_f**	**R_T** (m)	**T_{ICE} Avg**	**Num Gears**	**Up Shift RPM**	**Dn Shift RPM**	**Res.**	**Res.**
1030	3.5E-03	2	0.33	0.015	0.267	1	5	8000	2000		
M_{tot} (Kg)	**M_{tot}** (lbs)	**P_{ICE}** (Kw)	**ω_{ICE}** (rpm)	**T_{ICE}** (N/m)	**V_{10}** (mph)	**1st GR_{ICE}**	**2nd GR_{ICE}**	**3rd GR_{ICE}**	**4th GR_{ICE}**	**5th GR_{ICE}**	**6th GR_{ICE}**
1475	3252	127.23	4500.00	270.000	69.15	16.018	10.429	6.836	5.090	3.743	-

Table 4.1.2: Taurus SHO Settings for Simple Simulation.

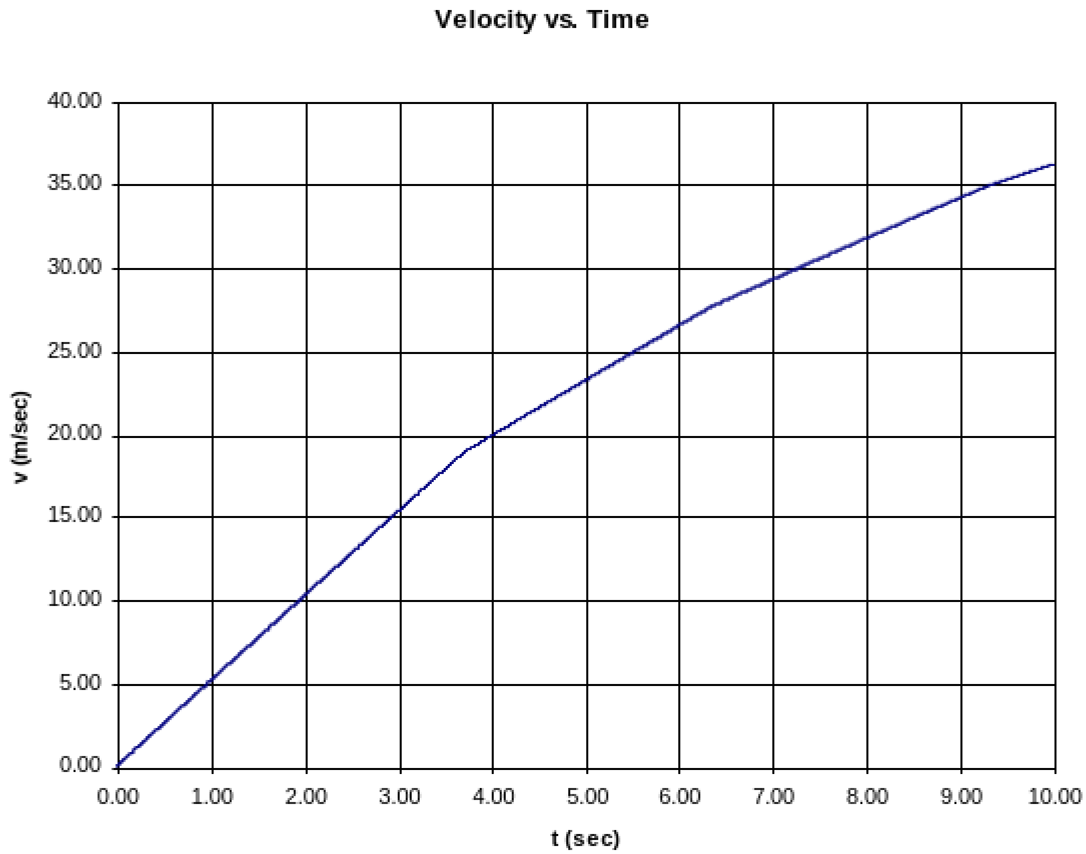

Figure 4.1.3: Velocity verses Time for Ascot Motorcycle Simple Simulation.

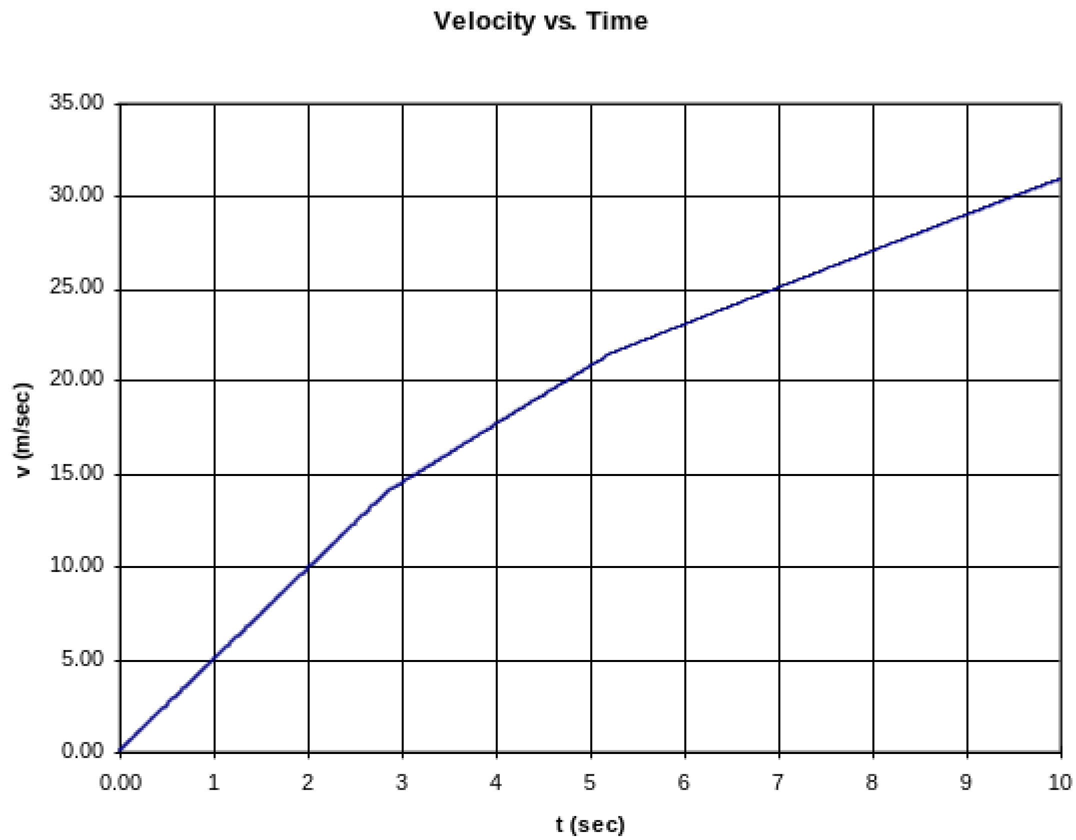

Figure 4.1.4: Velocity verses Time for Taurus SHO Simple Simulation.

4.1.3Graphic Model for Detailed Ascot Simulation

The bond graph model is followed in the construction of the ACSL graphic model. The combination of MRD power blocks and the detailed ICE power block used to construct the virtual Ascot motorcycle are shown in figure 4.1.5. The code for each of the power blocks can be found in the previously mentioned appendices. Note the DCAR block connected to the Vehicle Mass and Drag Block. This is a simple block used to reset the momentum of the vehicle directly preceding any disengagement of the clutch for gear changing or vehicle stopping. A similar block is contained inside the Ascot Engine compound block. There are two new blocks in the virtual Ascot test bed that have not been previously discussed.

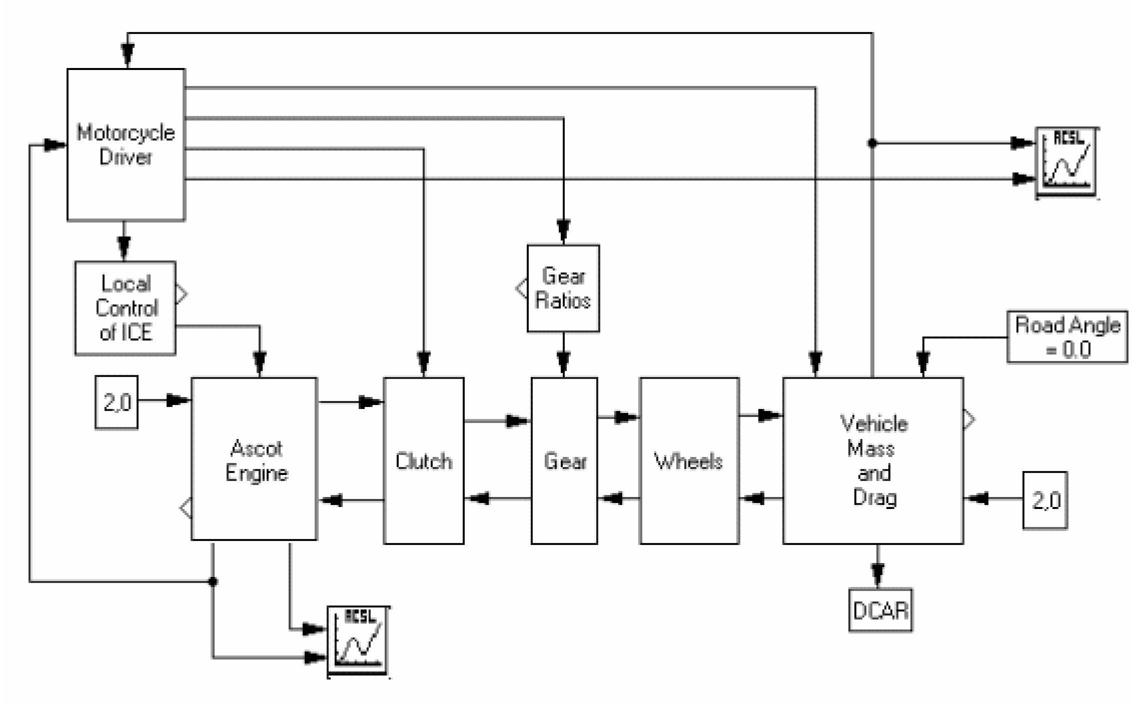

Figure 4.1.5: Virtual Ascot Motorcycle Test Bed for ICE Power Plant Performance Evaluations.

The first new block is the Motorcycle Driver, or Conventional Driver, power block. The code for this block is contained in Appendix J. This driver block is the most complicated of all the vehicle driver blocks. It simulates the driver accelerating and braking, engaging and disengaging the clutch, and shifting gears. All of these actions must be coordinated properly by the driver, and this block seeks to emulate a driver's performance of these actions. A desired drive cycle is entered into the block. The drivers torque command for the engine originates from a proportional, integral, derivative (PID) controller that receives and input of the difference between actual and desired velocities. The clutch and gears are operated according to the rpm's of the engine and the rpm's specified for shifting.

The second new block is the Local Control of ICE block. This block simply takes the torque command from the driver and determines the amount the throttle valve of the engine should be opened. Upper and lower limits for the throttle are included in the block to ensure a limited throttle area and a proper idle setting. Code for this block can be found among the ICE component models code sections in Appendix E.

4.1.4Simulations and Validation

The Ascot motorcycle model was simulated first for the short drive cycle test. Figure 4.1.6 contains a plot of motorcycle velocity and driver's desired velocity verses time. It is not hard for the Ascot in simulation, or real life, to follow this drive cycle, because of the motorcycle's high power to weight ratio. Other power plants will exhibit greater difficulties.

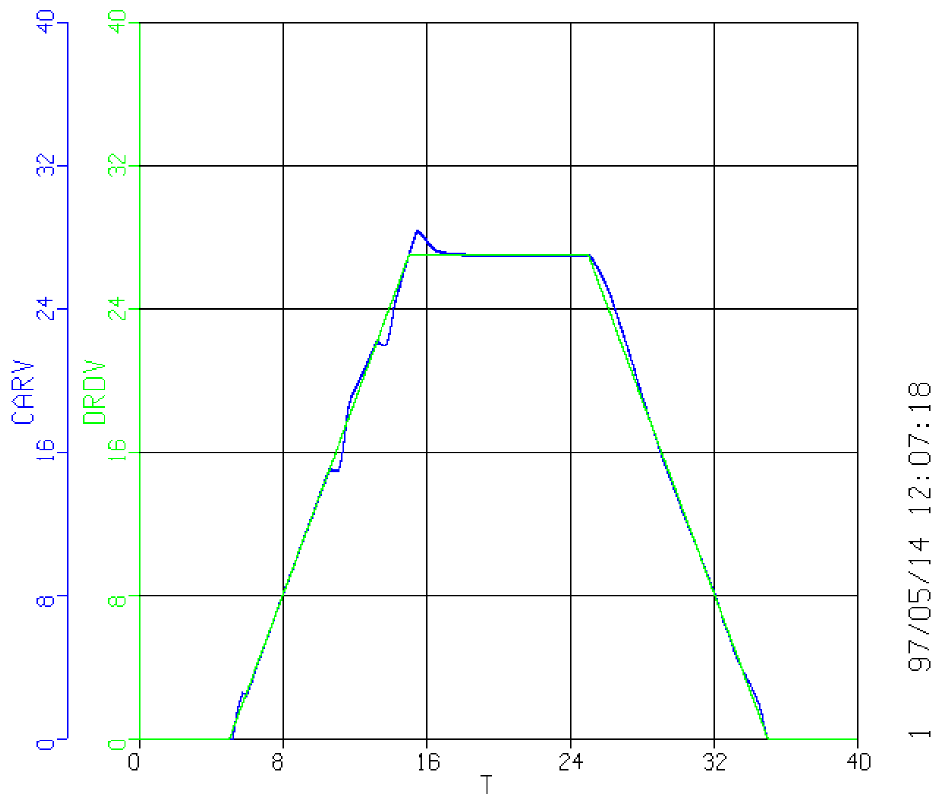

Figure 4.1.6: Velocity (m/sec, solid line) and Driver's Desired Velocity (m/sec, dotted line) verses Time (sec) from Simulation of the Ascot Motorcycle on the Short Drive Cycle.

The next plot for the short drive cycle shown in figure 4.1.7 shows the engine rpm together with the motorcycle velocity verses time. Note the predictions of engine rpm variations with gear changes and clutch actions.

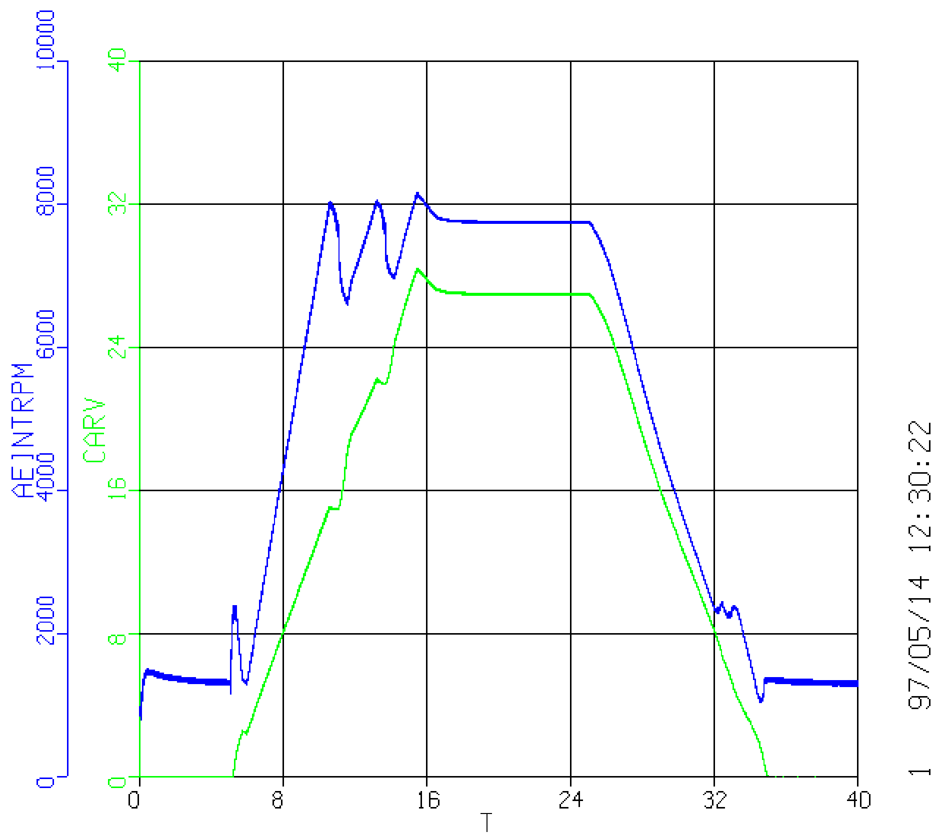

Figure 4.1.7: Engine RPM (solid line) and Vehicle Velocity (m/sec, dotted line) verses Time (sec) from Simulation of the Ascot Motorcycle on the Short Drive Cycle.

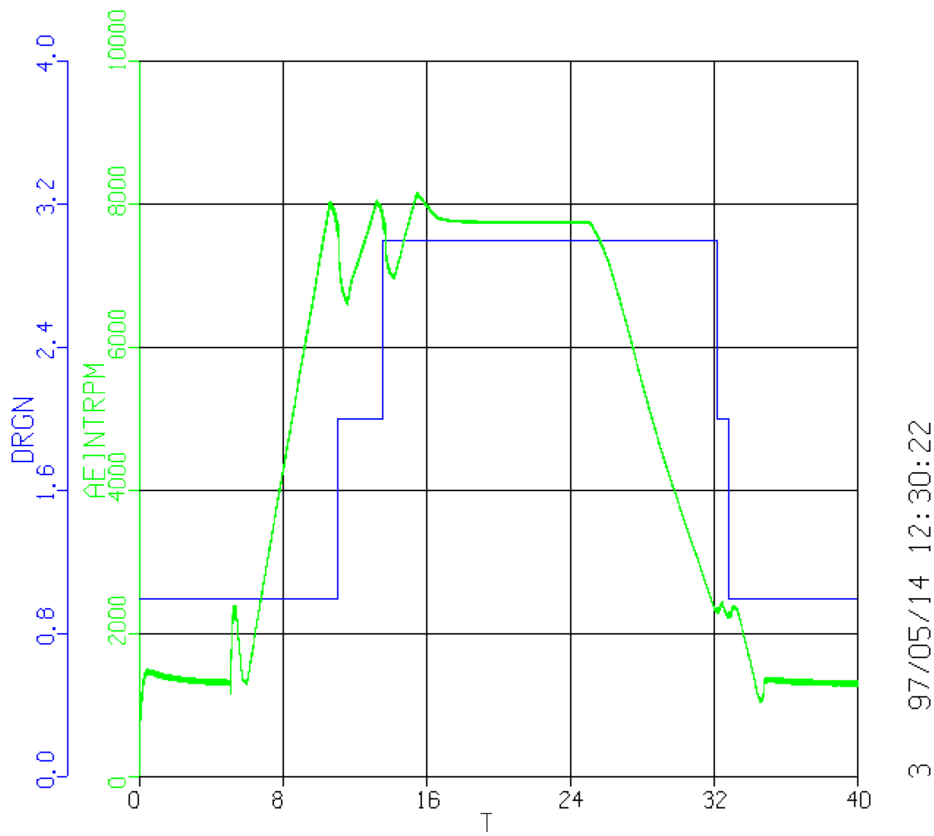

Figure 4.1.8: Gear Number (solid line) and Engine RPM (dotted line) verses Time (sec) from Simulation of the Ascot Motorcycle on the Short Drive Cycle.

The gear changes and the clutch operation are shown along with the engine rpm to better illustrate these correlations in figure 4.1.8 and 4.1.9, respectively.

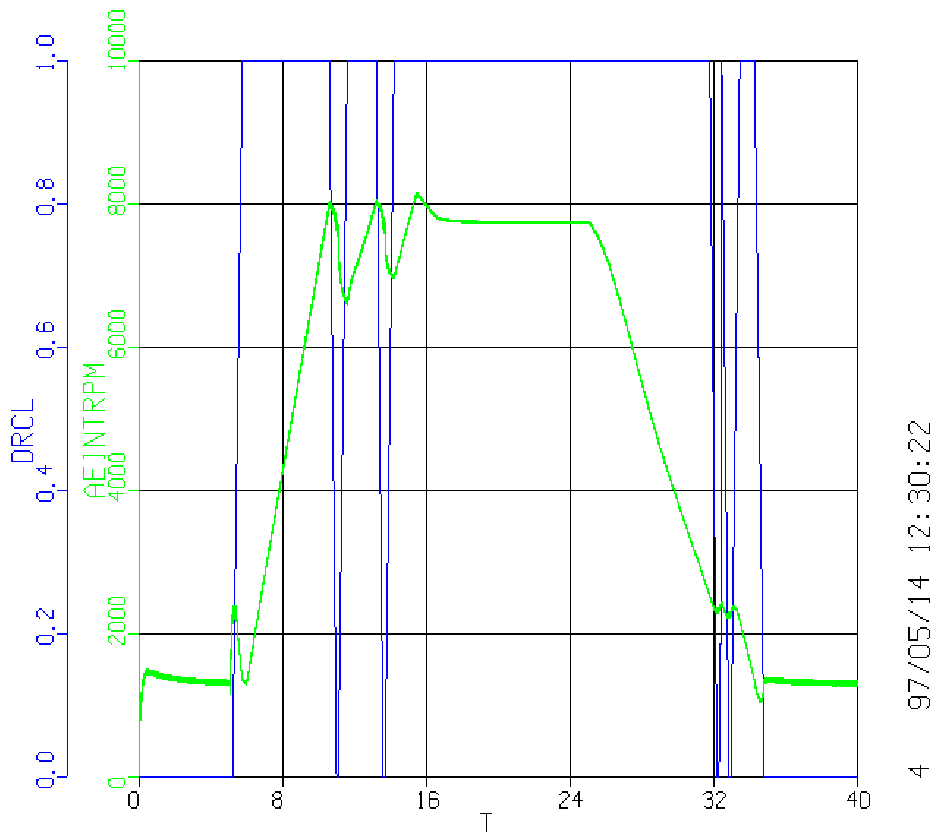

Figure 4.1.9: Clutch (solid line) and Engine RPM (dotted line) verses Time (sec) from Simulation of the Ascot Motorcycle on the Short Drive Cycle.

The next simulation of the Ascot engine was a maximum acceleration. The start time for the velocity measurements was 1 second.

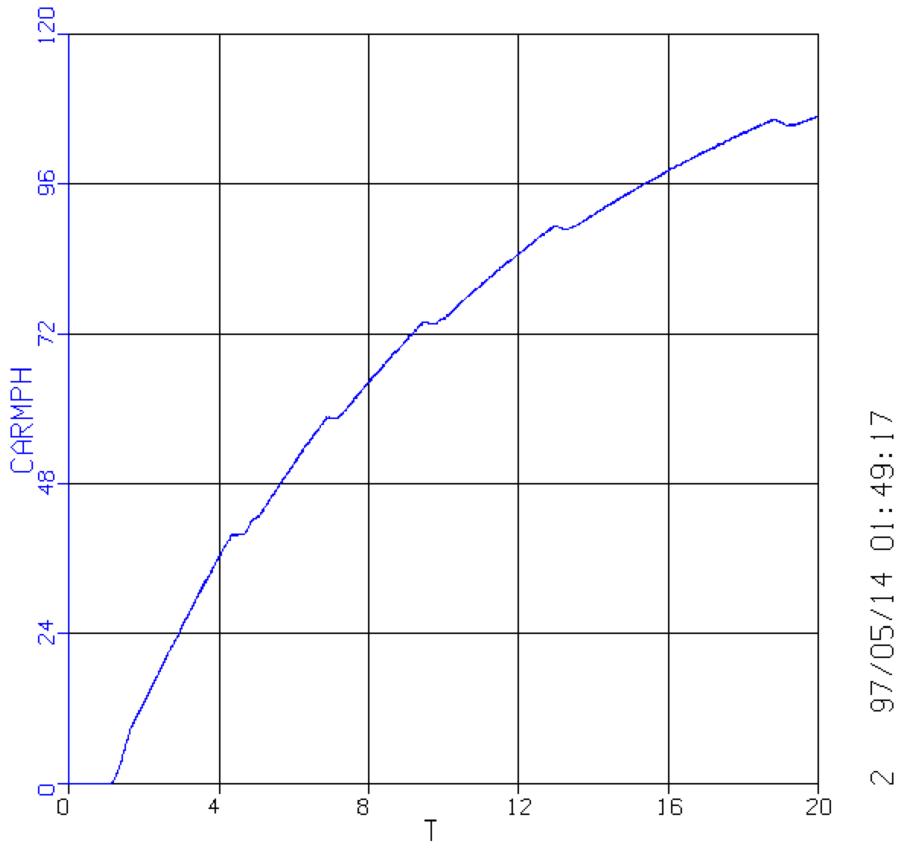

Figure 4.1.10: Velocity (mph) verses Time (sec) from Simulation of the Ascot Motorcycle on a Maximum Acceleration.

The velocity verses time predictions for this simulation are shown in figure 4.1.10. The measured speeds of the Ascot were found in [16]. Comparisons between the simulated and actual values can be found in table 4.1.3. Other validation results for the ICE/Motorcycle model are reported in Section 3.2.

Simulated and Actual Ascot Motorcycle Speeds							
Time to:	**30 mph**	**40 mph**	**50 mph**	**60 mph**	**70 mph**	**80 mph**	**90 mph**
Actual	2.0	2.9	4.0	5.3	7.2	9.5	12.3
Simulated	2.6	3.2	4.8	5.5	7.5	9.8	12.5

Table 4.1.3: Simulated verses Actual Times to Speed for the Ascot Motorcycle Model.

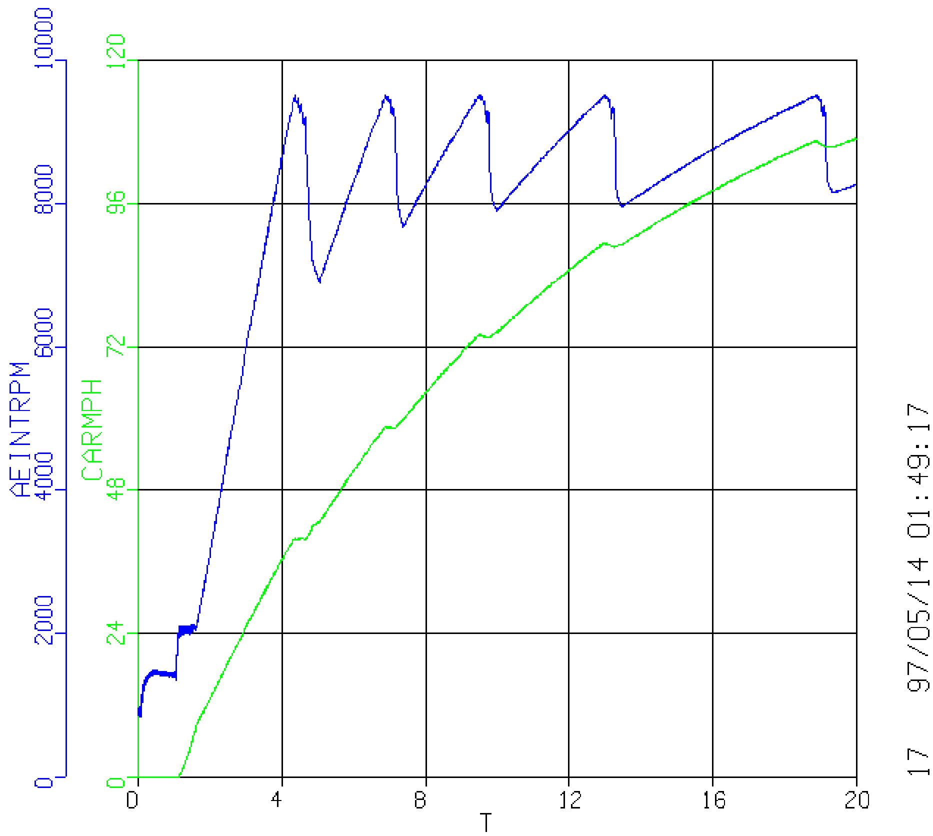

Figure 4.1.11: Engine RPM (solid line) and Velocity (mph, dotted line) verses Time (sec) from Simulation of the Ascot Motorcycle on a Maximum Acceleration.

The correlations of engine rpm and motorcycle velocity for the maximum acceleration simulation are illustrated in figure 4.1.11. The correlations of gear number and engine rpm are shown in figure 4.1.12.

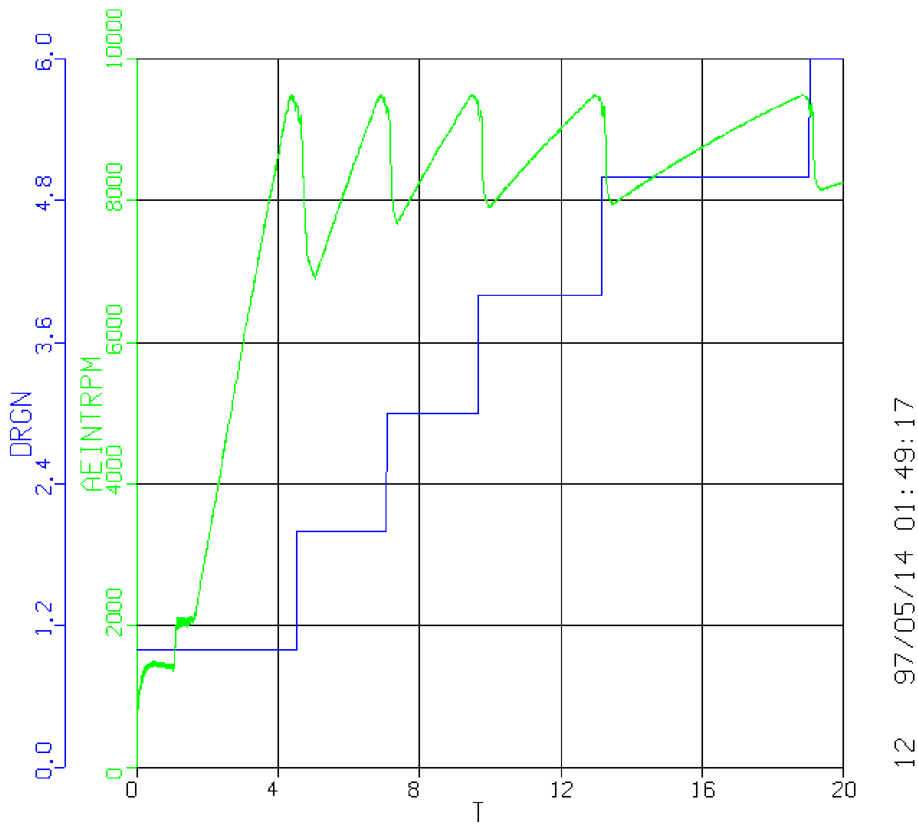

Figure 4.1.12: Gear Number (solid line) and Engine RPM (dotted line) verses Time (sec) from Simulation of the Ascot Motorcycle on a Maximum Acceleration.

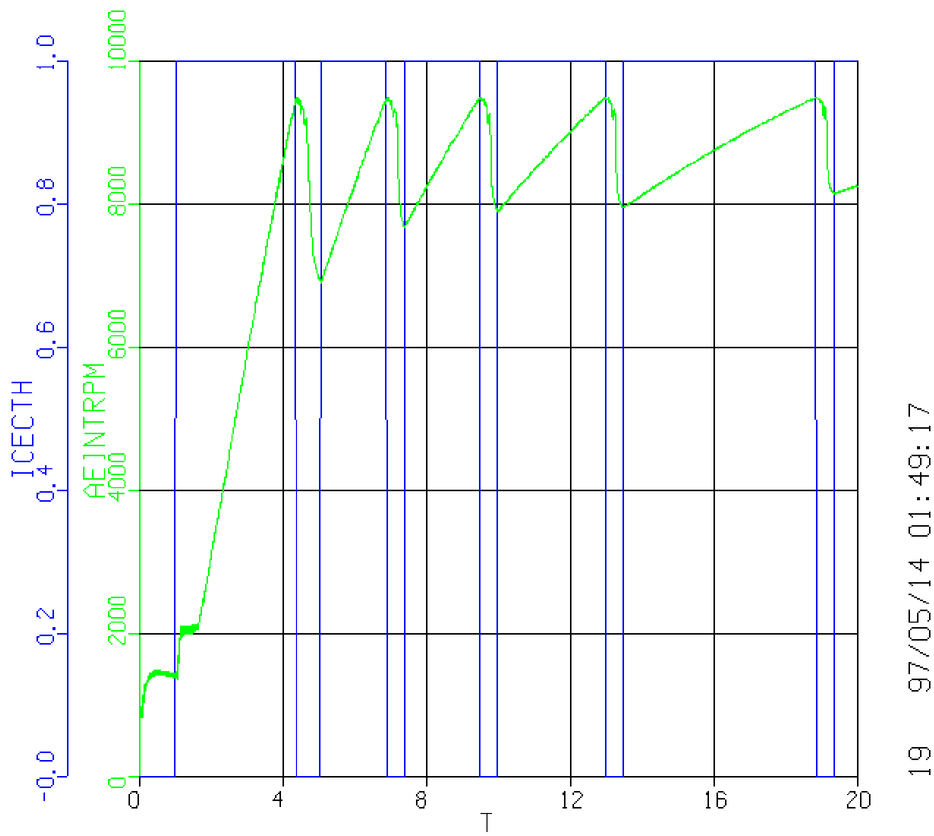

Figure 4.1.13: Throttle Actuation (solid line) and Engine RPM (dotted line) verses Time (sec) from Simulation of the Ascot Motorcycle on a Maximum Acceleration.

The correlation of throttle actuation and engine rpm is shown in figure 4.1.13 for the Ascot's maximum acceleration. Correlation of clutch actuation and engine rpm is shown in figure 4.1.14.

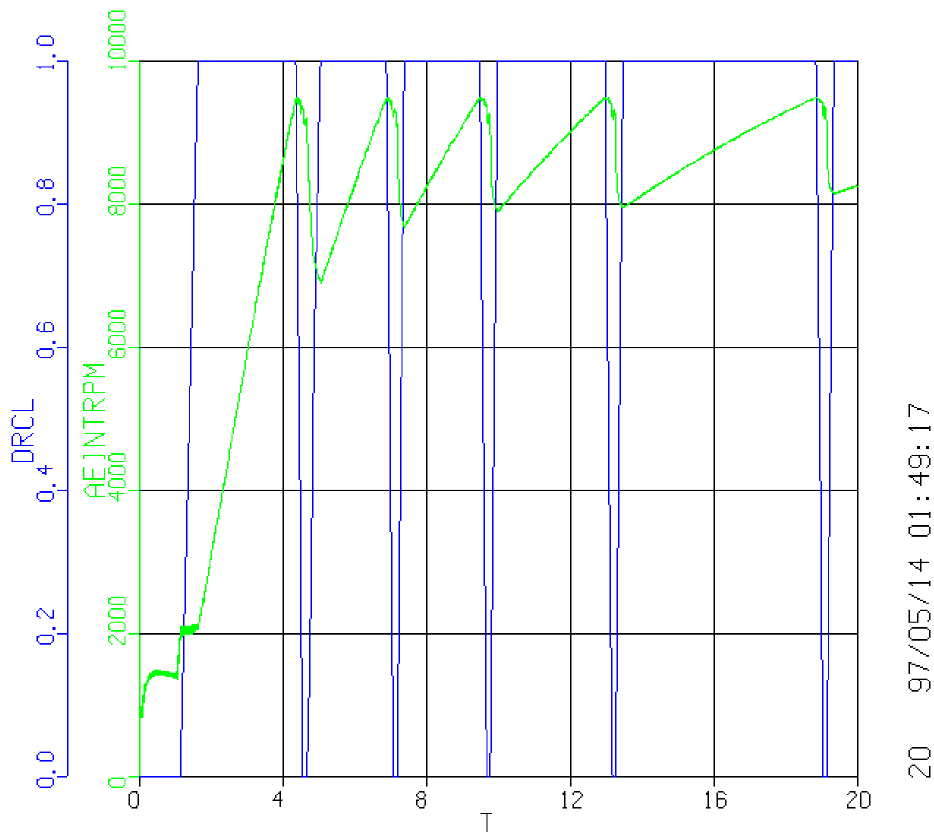

Figure 4.1.14: Clutch Actuation (solid line) and Engine RPM (dotted line) verses Time (sec) from Simulation of the Ascot Motorcycle on a Maximum Acceleration.

4.1.5Summary

The first application of the design and modeling methodology was presented in this sub-section. The function system diagram was applied to an existing concept. Illustration of its usefulness will become more apparent as the other designs in this section, and the designs in section 5, are reviewed and/or developed. The simple model and the bond graph model for the vehicle were derived from system diagram. Then the ACSL graphic model was derived from the detailed system model. The MRD drive train scheme allowed rapid construction of this model from sub-component modules, accommodated the dependencies within the model, and properly handled discontinuities during clutch actuations for starting, stopping and gear shifting.

The engine models exhibited critical control and operational parameter sensitivities comparable to those of real engines. Section 3.2 discusses the observed sensitivities in detail. The main sensitivities observed in this test bed were the driver modeling and driver settings and how they affected engine performance. Settings for pre-clutch engagement rpm's and clutch disengagement rpm's proved to be extremely sensitive. Most readers will readily identify with this fact from their own driving experiences. Clutch and throttle actuation during gear shifting was also very sensitive. All three of these common actions must be coordinated carefully. Fortunately, for control system engineers, these problems are normally handled by the driver, or partially by an automatic transmission. However, the experience gained in developing the driver model for this vehicle model was crucial to the other driver models developed. Furthermore, the development of driver control logic will be similar to automatic clutch, gear shifting and ICE control systems that might be developed in the future.

4.2Electric Vehicles

Two EV's were simulated in this section. Each EV used design specifications that were very close to the GM Impact. This was done to provide a means of validating this work's methodologies when synthesizing the electrical sub-component models to form a virtual vehicle. The first vehicle uses a dc machine. The second vehicle uses an IM. Both vehicles had battery bank masses approximately equal to the Impact's battery bank mass.

4.2.1Application of Design Methodology

The concept of an EV applied to the function system diagram is shown in figure 4.2.1. Note that there are now two energy sources that can handle bi-directional energy flows: the vehicle mass; and the batteries. Batteries deliver electrical energy to the electric machine (EM) to be transformed into rotational kinetic energy. This energy is passed through the transmission (TRANS) and then to the wheels of the car. The interface of the tires with the road, convert the rotational kinetic energy of the wheels into translational kinetic energy of the vehicle. This energy can potentially be transformed and transmitted back to the batteries. The batteries are charged from an external power source (PWR). If this regenerative braking does not adequately decelerate the car, the brakes must be used, and the kinetic energy of the vehicle is dissipated via heat transfer to the atmosphere.

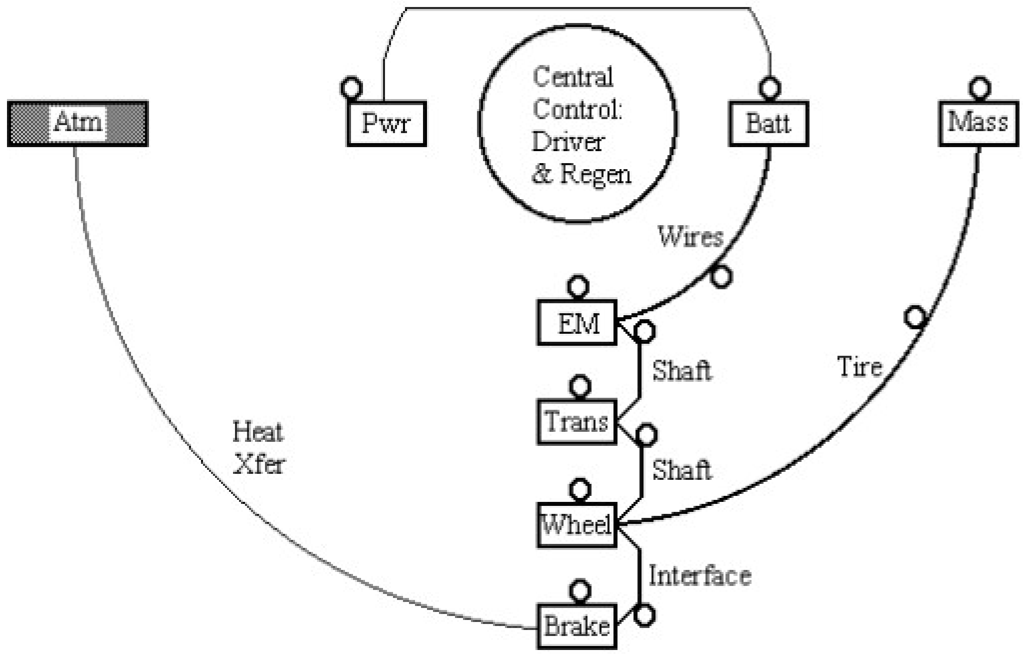

Figure 4.2.15: Electric Vehicle Concept Applied to a Function System Diagram.

4.2.2Bond Graph Model

The EV vehicle bond graph shown in figure 4.2.2 is formed directly from the EV system diagram shown in figure 4.2.1. In this example, a constant ratio transmission is used. However, with the flexibility of the models, the model can be quickly changed to include a variable ratio transmission and clutch. As with the conventional vehicle, the causalities of the model indicate that the efforts are passed from left to right, and the flows are passed from right to left. Note the input/output causality used for the general electric motor bond graph. The causality difficulties that would normally be introduced by the inertias are handled by the MRD connection scheme. The inertias are simply passed through the MRD components to be handled as described in section 3.1. And, although the MRD drive train scheme can give velocity outputs at any point in the drive train, the bond graph indicates that the inertial lumping is done with the vehicle mass. However, the MRD scheme takes care of inertial dependencies, so the designer doesn’t need to concern himself with proper lumping.

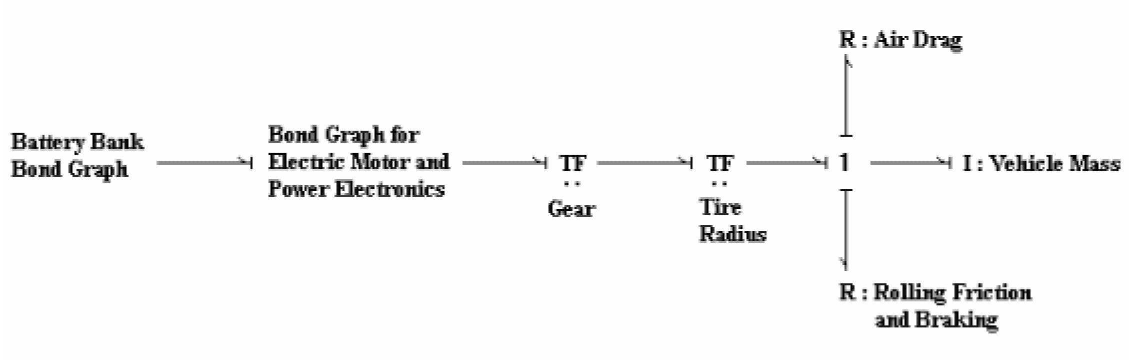

Figure 4.2.16: Bond Graph of an Electric Vehicle.

4.2.3DC Motor Powered EV

4.2.3.1Initial Estimation of Motor Ratings and Gear Ratios

The total mass of the vehicle is calculated as shown in equation 4.2.1, where P_{MOT} is the power rating of the electric motor, and ρ_{MOT} and ρ_{Batt} are the power densities of the electric motor and batteries, respectively, taken from table 5.1.1. The batteries must be $1/\eta_{MOT}$ heavier to account for power lost in the motor.

Equation 4.2.1

$$M_{Tot} = M_{Veh} + P_{MotMax}\left(\rho_{MOT} + \frac{\rho_{Batt}}{\eta_{MOT}}\right)$$

The electric motor is designed to meet a certain nominal power for a base speed. The motor may be overrated for short periods of time (e.g. 300% + higher powers during an acceleration). Using the nominal power, the overrating factor and the base speed, the maximum torque of the motor can be determined. Thus maximum power is replaced by the desired maximum torque specification that will meet acceleration criteria and the base speed as shown in equation 4.2.2.

Equation 4.2.2

$$M_{Tot} = M_{Veh} + T_{MaxMOT}\omega_{b}\left(\rho_{MOT} + \frac{\rho_{Batt}}{\eta_{MOT}}\right)$$

Since dc machine models are simple, they pose no difficulties to a spreadsheet simulation. The voltage control for the simulation is described by equation 4.2.3. Unfortunately, the simple spreadsheet calculations assumes an ideal voltage source which is not the case with the batteries.

$$V_T = \begin{cases} T_{MaxEM} \cdot R_a / K_a\phi_f + K_a\phi_f \cdot \omega_r & \text{if} \quad \omega_r < \omega_b \\ V_{MAX} & \text{if} \quad \omega_r \geq \omega_b \end{cases}$$ **Equation 4.2.3**

The product of field flux, ϕ_f and motor constant, K_a, as a function of rotor speed is given by equation 4.2.4. This value is modified by the torque command (Tc - a number between 0 and 1) from the driver. Values for base flux, ϕ_b, and motor terminal voltage, V_T, are determined through iterations using the spreadsheet.

$$K_a\phi_f = \begin{cases} K_a\phi_b \cdot Tc & \text{if} \quad \omega_r < \omega_b \\ K_a\phi_b \cdot \dfrac{\omega_b}{\omega_r} \cdot Tc & \text{if} \quad \omega_r \geq \omega_b \end{cases}$$ **Equation 4.2.4**

The force to the road from the tires is calculated using the above values, the gear ratio for the electric motor's drive train, GR_{EM}, and the tire radius, R_T. The reaction forces, or road load, are due to air drag and rolling friction [17]. The motor rotor rotational velocity is simply the product of vehicle velocity, V, gear ratio, GR_{EM}, and tire radius.

$$\sum F = \left(\frac{(V_T - K_a\phi_f)}{R_a} \right) \cdot K_a\phi_f \cdot GR_{EM} / R_T - \frac{1}{2} C_D \rho_{air} A V^2 - M_T g C_F$$ **Equation 4.2.5**

Vehicle design parameters close to those of a GM impact were used in the estimation of dc motor ratings and gear ratios that would meet the GM impact acceleration (0-60mph in 8.5 seconds). These particular estimations were not as accurate as the simple simulations of the ICE powered vehicles, due to this simple model's inability to account for battery dynamics. However, these initial estimates were still good. They were close to the final values found using the more detailed models. A good method for estimating the number of batteries required by a power plant is explained in section 4.2.5.

Separately Excited DC	**Electric Vehicle Settings**

M_{veh} (Kg)	ρ_{batt} (Kg/w)	ρ_{em} (Kg/w)	T_{max} (N/m)	$\omega_{b\,flux}$ (rad/s)	$V_{t\,max}$ (volts)	η_{em}	**EMG Over Rating**	A_f (m^2)	C_d	C_f	R_T (m)
450	0.012	9E-04	220.3	314	220	0.90	1	2	0.19	0.01	0.267
P_{EMNom} (Kw)	M_{tot} (Kg)	M_{tot} (lbs)	i_{ab} (amps)	$K_a\phi_b$	R_a (ohms)	$\omega_{b\,volt}$ (rad/s)	V_{10} (mph)	**Battery Mass** (Kg)	ρ_{batten} (wh/Kg)	**Cruise Speed** (mph)	**Cruise Range** (miles)
69.180	1435	3163	324.0	0.680	0.020	314	65.12	830.166	25.0	75	115.4

Table 4.2.4: DC Powered EV Settings for Simple Simulation.

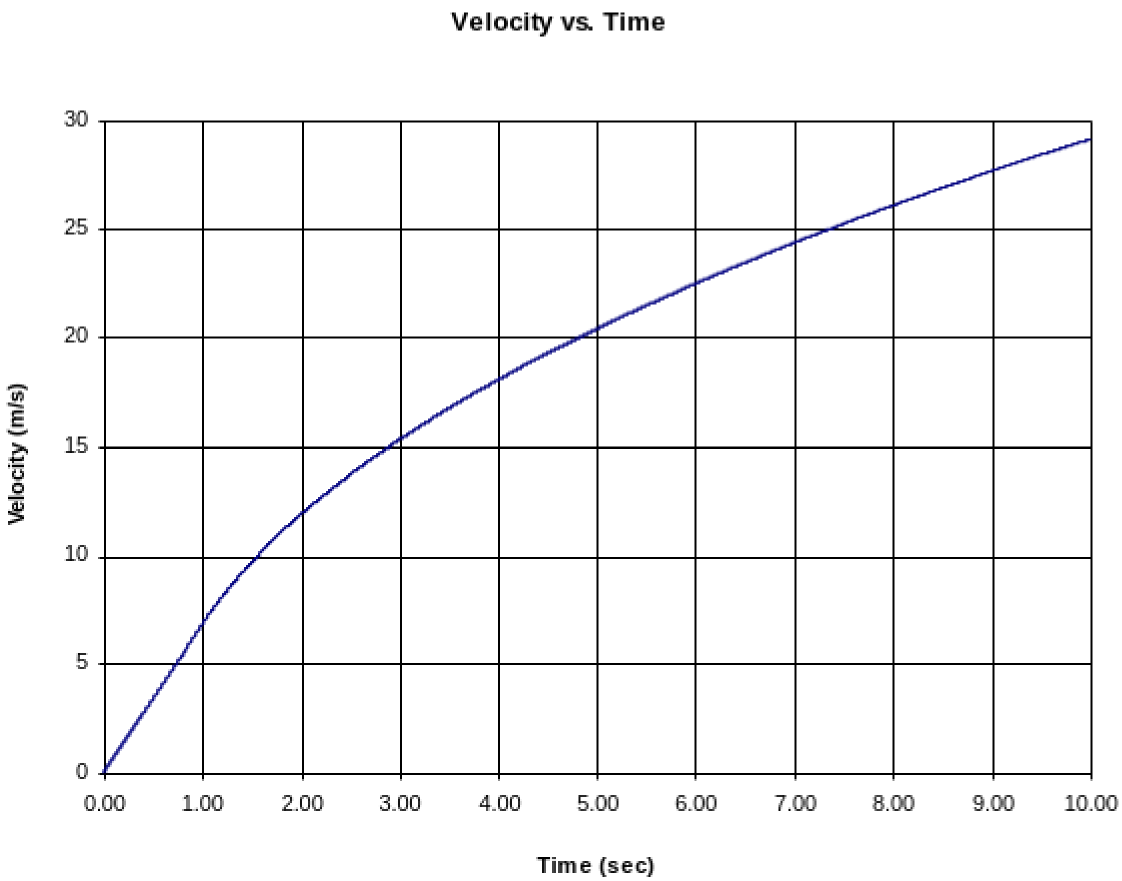

Figure 4.2.17: Velocity verses Time for Simple Simulation of the DC Motor Powered EV.

Most values for table 4.2.1 were previously described in section 4.1. Additional terms in table 4.2.1 are armature resistance, R_a, base armature current, i_{ab}, maximum terminal voltage $V_{t\,max}$, efficiency, h, and the subscripts em, b, and batt stand for electric machine, base point and batteries, respectively.

4.2.3.2DC Motor Control

The first attempt to design a controller was done with the naïve assumption that the battery voltage would not drop too severely during a heavy transient. The battery bank was sized to deliver close to the base voltage on the most severe acceleration. Voltage was raised with speed until the base point. Then, voltage was kept at the base voltage or at battery bank voltage, whichever was lower. A constant flux in the dc machine was applied until the base voltage was reached [30] [20]. Then, the flux was allowed to weaken beyond the base point to maintain a constant power. This constant power control was achieved in closed loop by measuring the battery voltage and rotor speed and adjusting $\mathbf{K_a\phi_f}$ to maintain constant power. This resulted in battery levels reaching conditions that would have damaged real batteries.

The final controller design used a feedback of rotor speed only, and calculated a flux for the machine. Voltage was controlled in the same manner as described above. The flux calculations for before and after base rotor speed, respectively, are shown in equations 4.2.6. In these calculations, $\mathbf{V_b}$, base voltage, and, $\mathbf{Pwr_{MAX}}$, maximum allowed power are constants. The armature resistance is $\mathbf{R_a}$, and the torque command is $\mathbf{T_c}$ which is a value between 0 and 1. The rotor speed is $\boldsymbol{\omega}$, and $\boldsymbol{\omega_b}$ is the base rotor speed.

$$K_a\phi_f = \frac{\left(V_b^2 - R_a \cdot Pwr_{MAX}\right)}{V_b \cdot \omega_b} T_c \qquad \textbf{Equation 4.2.6 (a)}$$

$$K_a\phi_f = \frac{\left(V_b^2 - R_a \cdot Pwr_{MAX}\right)}{V_b \cdot \omega} T_c \qquad \textbf{Equation 4.2.6 (b)}$$

This method of controlling the field in the machine provided a good balance of performance while preventing battery voltage from dropping too rapidly.

Regenerative braking was attempted, but it was deemed impractical. The stator of the dc machine would have to be increased significantly to be able to deal with the increased flux values necessary to charge the batteries at their inflated charging voltages. Furthermore, the battery voltages necessary to achieve a significant amount of braking torque would be harmful to the batteries.

4.2.3.3Graphic Model for Detailed DC EV Simulation

The ACSL graphic model of the dc motor powered EV was formed from the bond graph model and is shown in figure 4.2.4. The Separately Excited DC Machine compound power block contains the MRD interface to the MRD drive train. The Battery Bank compound power block contains the multiplier that adjusts output voltage and input current according to the battery bank configuration. Since no discontinuities are present in the drive train, none of the power blocks that handle discontinuities are present in the model. The EV driver is a simplified version of the conventional driver that was explained in the discussion of the conventional vehicle model. The driver model only passes on a torque command and a brake command.

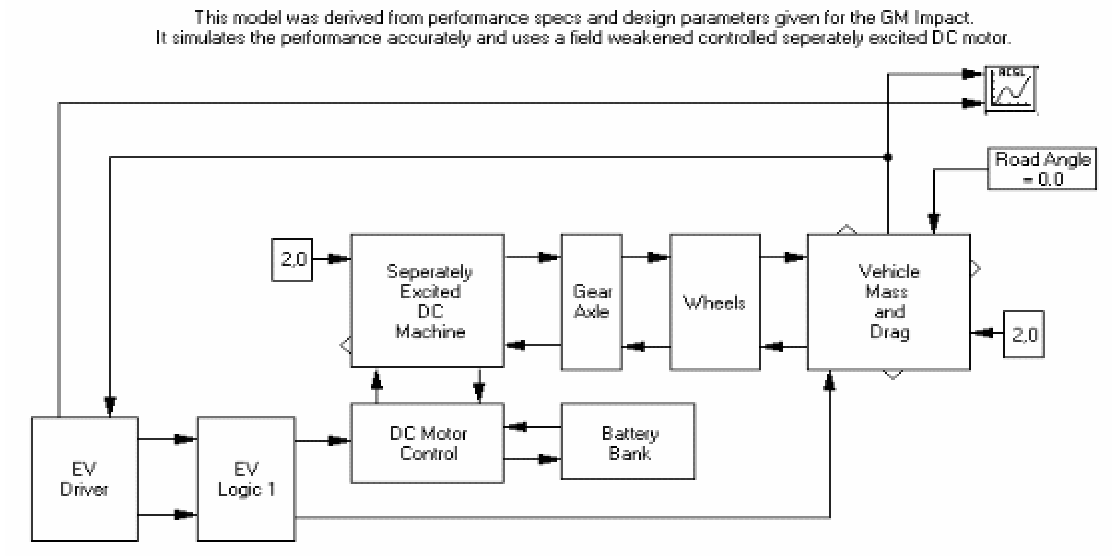

Figure 4.2.18: ACSL Graphic Model of DC Motor Powered EV.

4.2.3.4Simulations

The plots presented in this section are from the maximum acceleration and simple drive cycle simulations of the dc motor powered EV. This EV model is simple and computationally fast. No comparisons with other control methods or previous runs using earlier parameter values are presented here. These results are simply listed so that the reader can see that the models exhibit realistic operational characteristics. These results can also be compared to HVPP performances that are presented in section 5. The parameter values adjusted for this detailed simulation that are different from the simple simulation parameter values are vehicle mass (1530 Kg) and battery mass (1014 Kg). The value for $\mathbf{K_a\phi_f}$ is now calculated by equations 4.2.6, and the base value calculated from equation 4.2.6 (a) is 0.675 which made a notable performance difference.

The first group of plots are from the maximum acceleration simulation. The velocity of the dc motor powered EV verses time is shown in figure 4.2.5. Note that this plot shows the simulated vehicle reaching 27 m/sec (60 mph) in approximately 8.5 seconds. This is the acceleration spec for the GM Impact. The main difference in specifications between these two vehicles is that the Impact uses an IM.

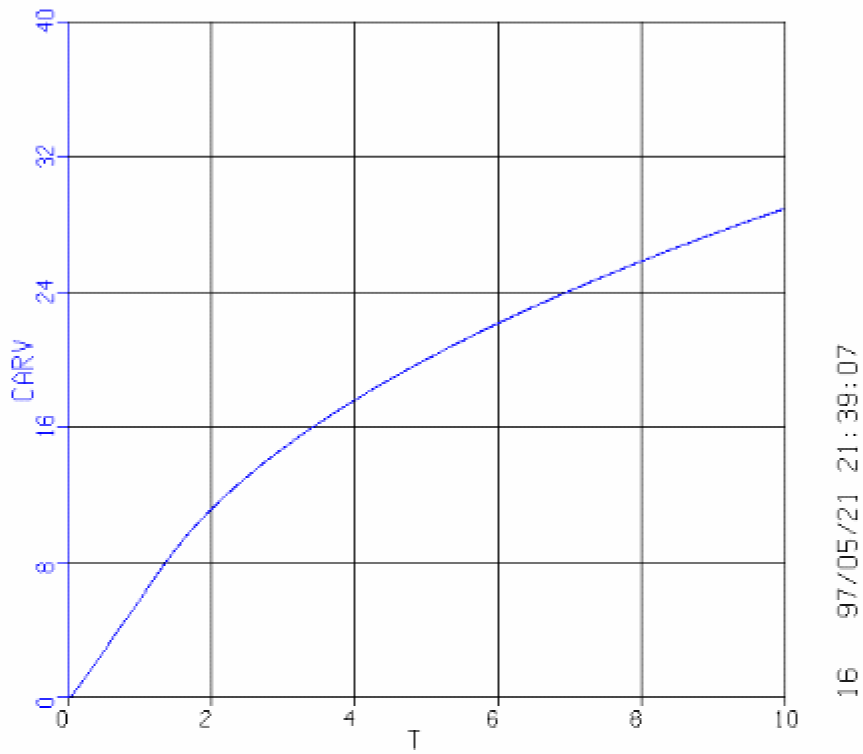

Figure 4.2.19: Velocity (m/sec) verses Time (sec) for the DC Motor Powered EV during Maximum Acceleration.

The motor controller output voltage verses dc motor rotor speed is shown in figure 4.2.6.

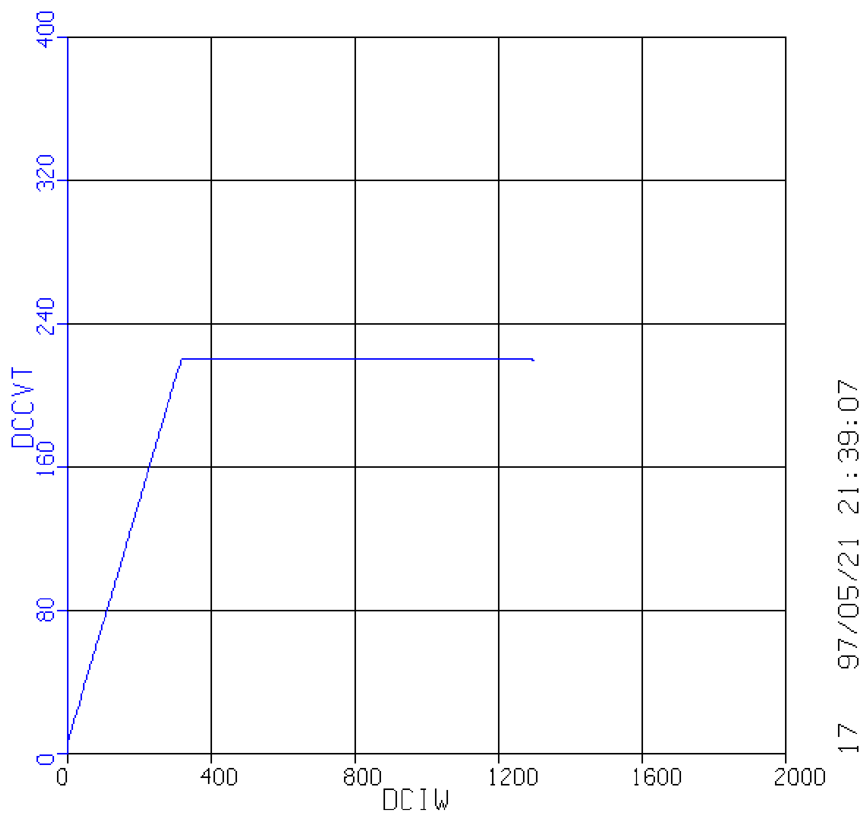

Figure 4.2.20: DC Motor Controller Output Voltage (volts) verses DC Motor Rotational Velocity (rad/sec) for the DC Motor Powered EV during Maximum Acceleration.

A comparison of the battery bank output voltage to the dc motor controller output voltage is shown in figure 4.2.7. Note that battery voltage drops down to the controller voltage and then stays at the controller voltage level. Correlate this plot to figure 4.2.8.

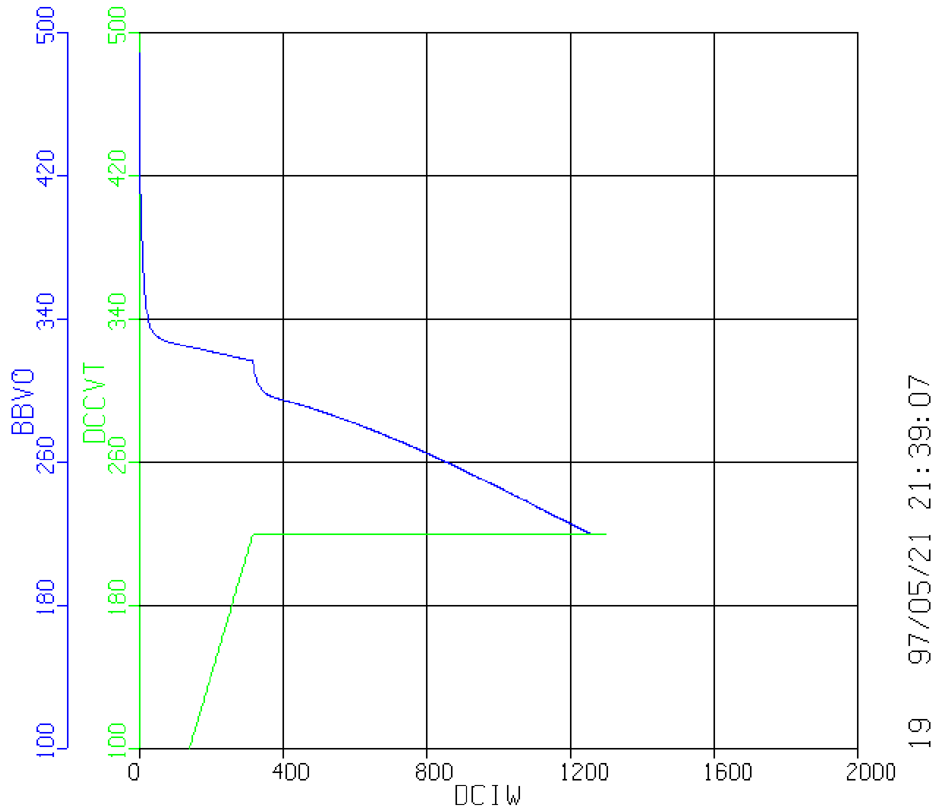

Figure 4.2.21: Battery Voltage (volts, solid line) and DC Motor Controller Output Voltage (volts, dotted line) verses DC Motor Rotational Velocity (rad/sec) for the DC Motor Powered EV during Maximum Acceleration.

Once battery voltage is at the controller voltage, the power drawn from the batteries decreases in accordance with the control scheme to protect the batteries. This is illustrated in figure 4.2.8.

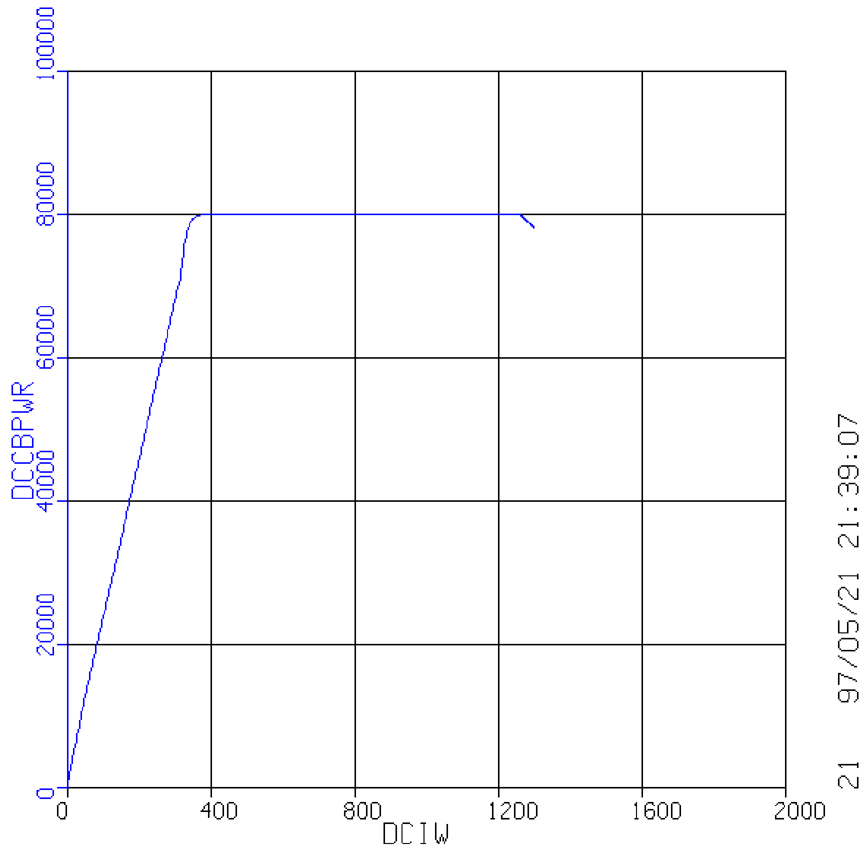

Figure 4.2.22: Power Drawn from Batteries (watts) verses DC Motor Rotational Velocity (rad/sec) for the DC Motor Powered EV during Maximum Acceleration.

DC motor torque and flux control during the maximum acceleration simulation are illustrated in figure 4.2.9.

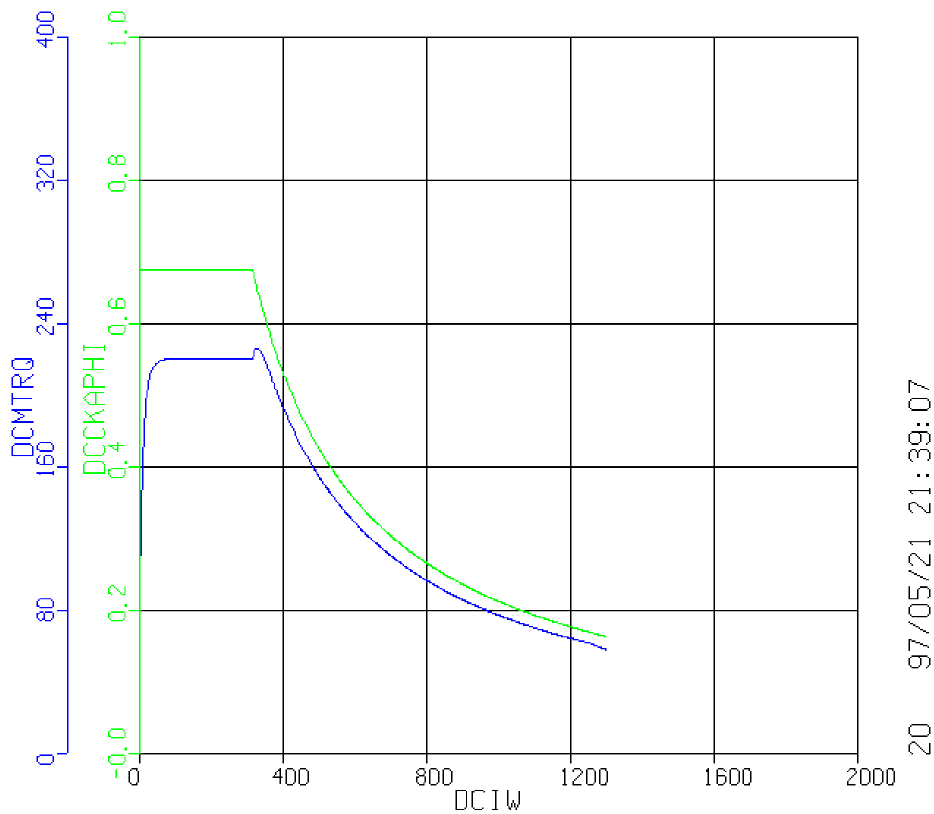

Figure 4.2.23: Torque (Nm, solid line) and Motor flux (dotted line) verses DC Motor Rotational Velocity (rad/sec) for the DC Motor Powered EV during Maximum Acceleration.

The next set of plots show results of simulating the dc motor powered EV through the simple drive cycle. The vehicle velocity and the driver's desired velocity are shown in figure 4.2.10.

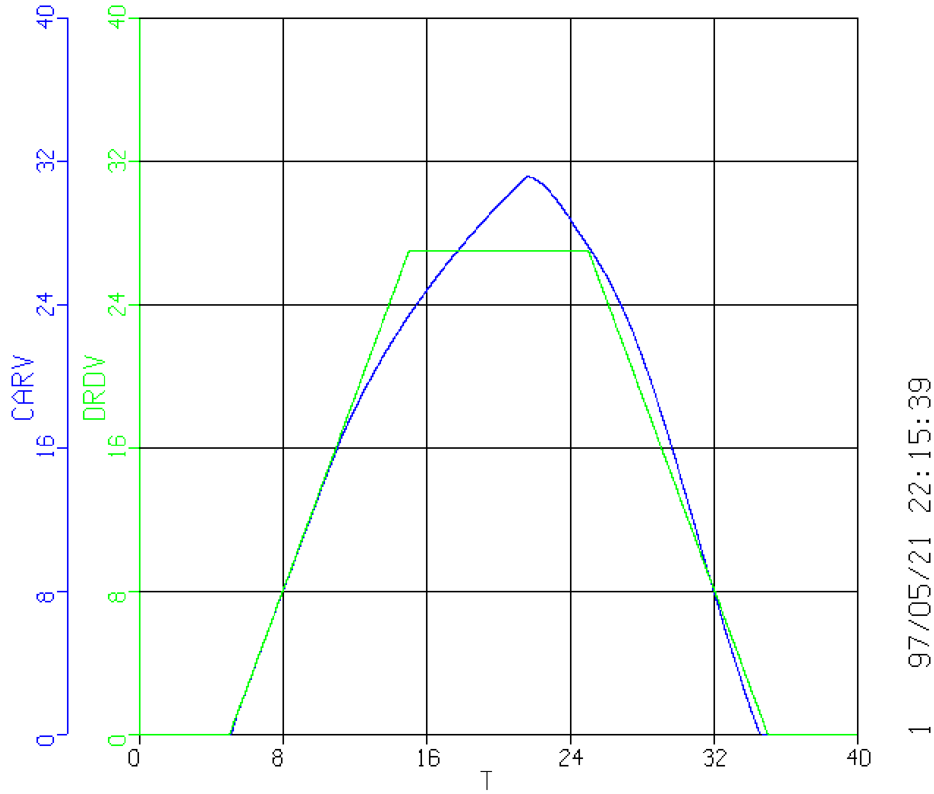

Figure 4.2.24: Car Velocity (m/sec, solid line) and Driver's Desired Velocity (m/sec, dotted line) verses Time (sec) for the DC Motor Powered EV during the Simple Drive Cycle.

Motor controller output voltage verses dc motor rotor speed is shown in figure 4.2.11.

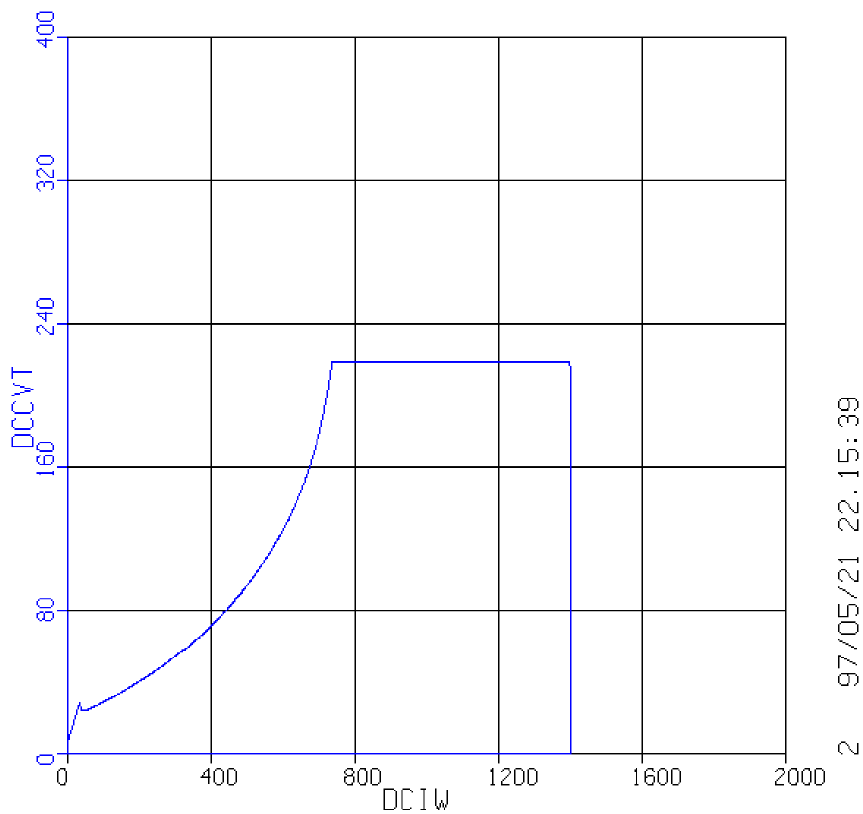

Figure 4.2.25: DC Motor Controller Output Voltage (volts) verses DC Motor Rotational Velocity (rad/sec) for the DC Motor Powered EV during the Simple Drive Cycle.

A comparison of battery bank voltage to this dc motor control output voltage verses rotor speed is shown in figure 4.2.12.

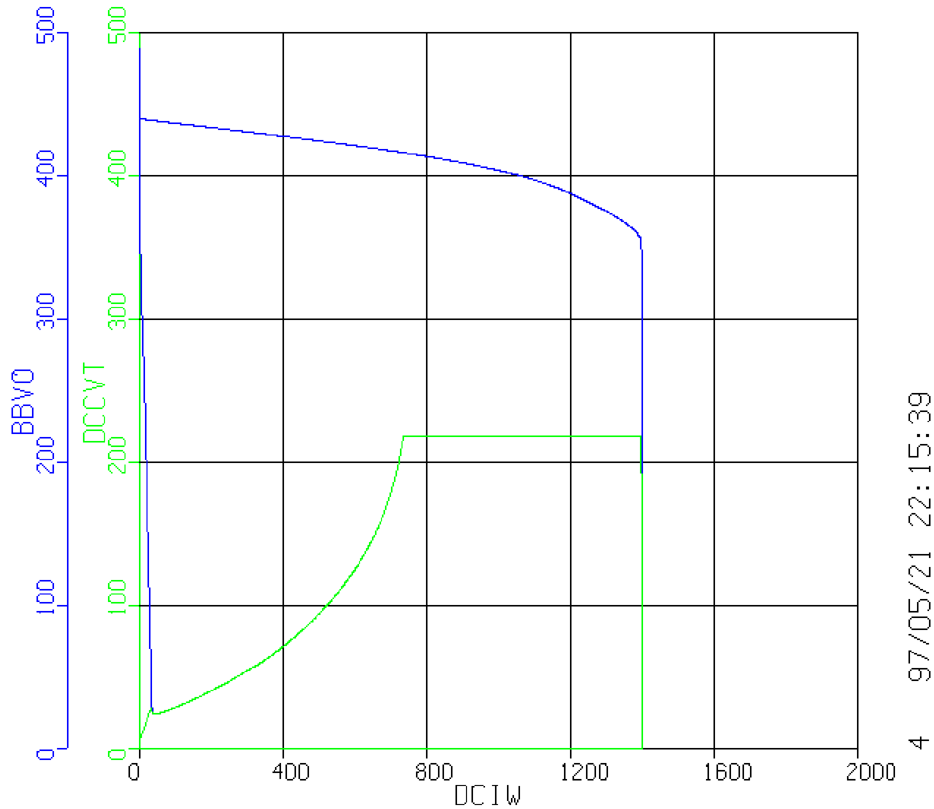

Figure 4.2.26: Battery Bank Voltage (volts, solid line) and Controller Voltage (volts, dotted line) verses DC Motor Rotational Velocity (rad/sec) for the DC Motor Powered EV during the Simple Drive Cycle.

Motor controller power verses dc motor rotor speed is shown in figure 4.2.13.

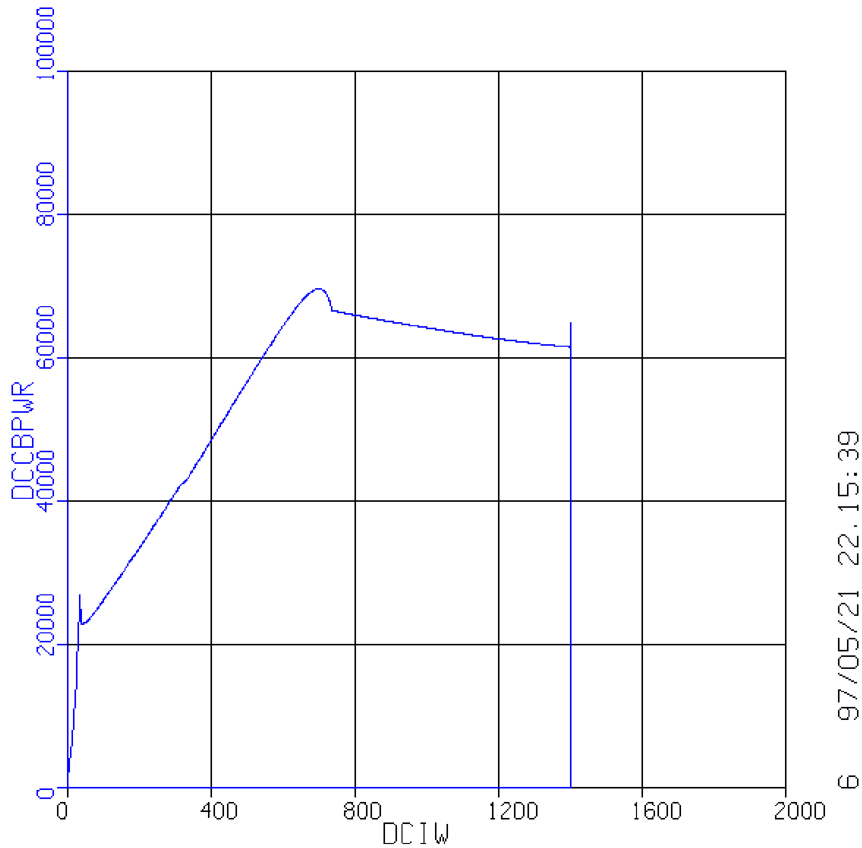

Figure 4.2.27: Power Drawn from Batteries (watts) verses DC Motor Rotational Velocity (rad/sec) for the DC Motor Powered EV during the Simple Drive Cycle.

And, a correlation of dc motor torque and field control is shown in figure 4.2.14.

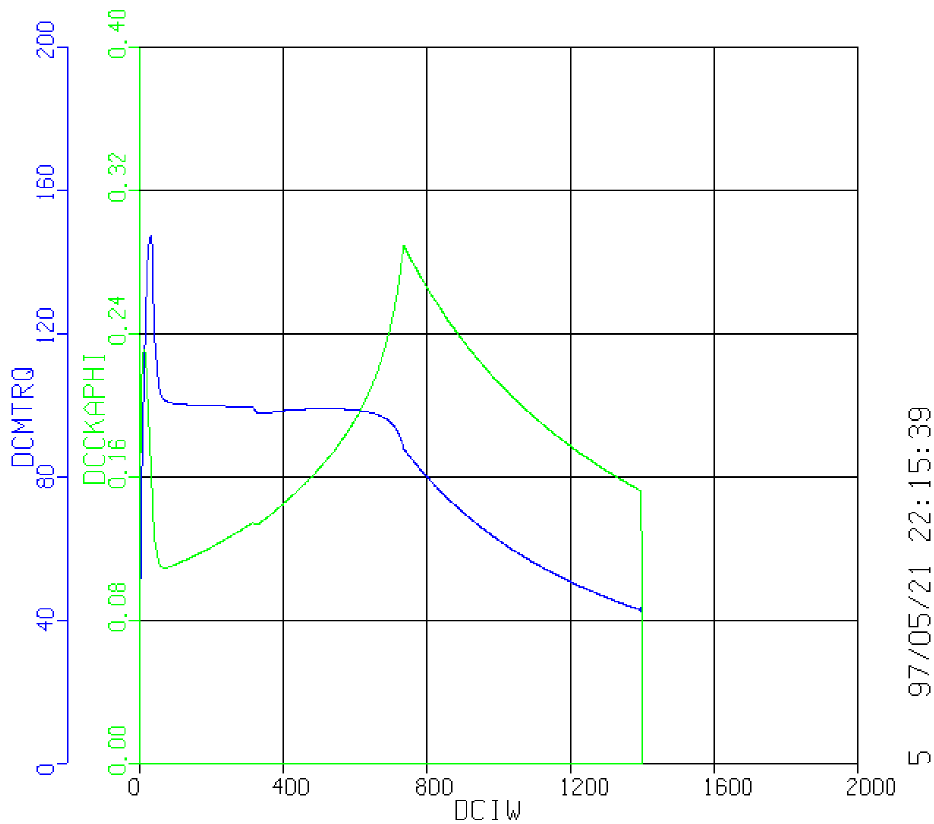

Figure 4.2.28: DC Motor Torque (Nm, solid line) and Motor Flux Value (dotted line) verses DC Motor Rotational Velocity for the DC Motor Powered EV during the Simple Drive Cycle.

4.2.3.5Summary

The simulations of the dc motor powered EV provided experience in the synthesis of a battery bank, electric machine, and an electric machine controller. This synthesis showed that this model with these sub-components also exhibited critical control and operational parameter sensitivities comparable to those of real EV's. The most important knowledge gained from these simulations was that the sensitivities between battery bank and motor had to be carefully handled in the design of the dc motor controller. The models behaved realistically enough that vehicle, power supply and controller designs developed herein would give excellent direction toward the initial pre-experimental construction of the vehicle. The simulation results predicted the same acceleration performance of the GM Impact when design parameters similar to those of the Impact were used. The MRD drive train scheme also allowed rapid construction of this model from sub-component modules and accommodated the dependencies within the model. Since there were no discontinuities in the drive train during the simulated operation of the plant, the MRD scheme was not required to handle any discontinuities during the simulation.

4.2.4Induction Motor Powered EV

4.2.4.1Initial Estimation of Motor Ratings and Gear Ratios

Vehicle design parameters close to those of a GM impact were used in the estimation of IM ratings, gear ratios, and battery mass that would meet the GM impact acceleration (0-60mph in 8.5 seconds). The values for the simple simulation are shown in table 4.2.2. This particular estimation was also not as accurate as the simple simulations of the ICE powered vehicles, due to the simple model's inability to account for battery dynamics. However, these were also good initial estimates.

Vehicle mass estimations were made using equation 4.2.2. The summation of forces on the vehicle that affect its acceleration are illustrated by equation 4.2.7. Motor rotor rotational velocity is determined in the same way that it was for the dc motor.

$$\sum F = \begin{cases} T_{MaxEM} \cdot GR_{EM} / R_T - \frac{1}{2} C_D \rho A V^2 - M_T g C_F & \text{if } \omega_r < \omega_b \\ T_{MaxEM} \frac{\omega_b}{\omega_r} \cdot GR_{EM} / R_T - \frac{1}{2} C_D \rho A V^2 - M_T g C_F & \text{if } \omega_r \geq \omega_b \end{cases}$$

Equation 4.2.7

GM Impact Guesses					**Electric Vehicle Settings**					
M_{veh} (Kg)	**$\rho_{battpwr}$** (Kg/w)	**ρ_{em}** (Kg/w)	**T_b** (N/m)	**ω_b** (rad/s)	**A_c** (m^2)	**C_d**	**C_f**	**R_T** (m)	**GR_{EM}**	**η_{em}**
510	0.012	9E-04	80	320	2	0.19	0.01	0.267	12.000	0.90
P_{EMNom} (Kw)	**M_{tot}** (Kg)	**M_{tot}** (lbs)	**V_b** (m/s)	**V_{10}** (mph)	**EMG Over Rating**	**Battery Mass** (Kg)	**ρ_{batten}** (wh/Kg)	**Cruise Speed** (mph)	**Cruise Range** (miles)	**Cruise Power** (Kw)
25.600	1557	3433	7.120	65.92	3	921.6	20.0	75.0	99.5	13.9

Table 4.2.5: IM Powered EV Settings for Simple Simulation.

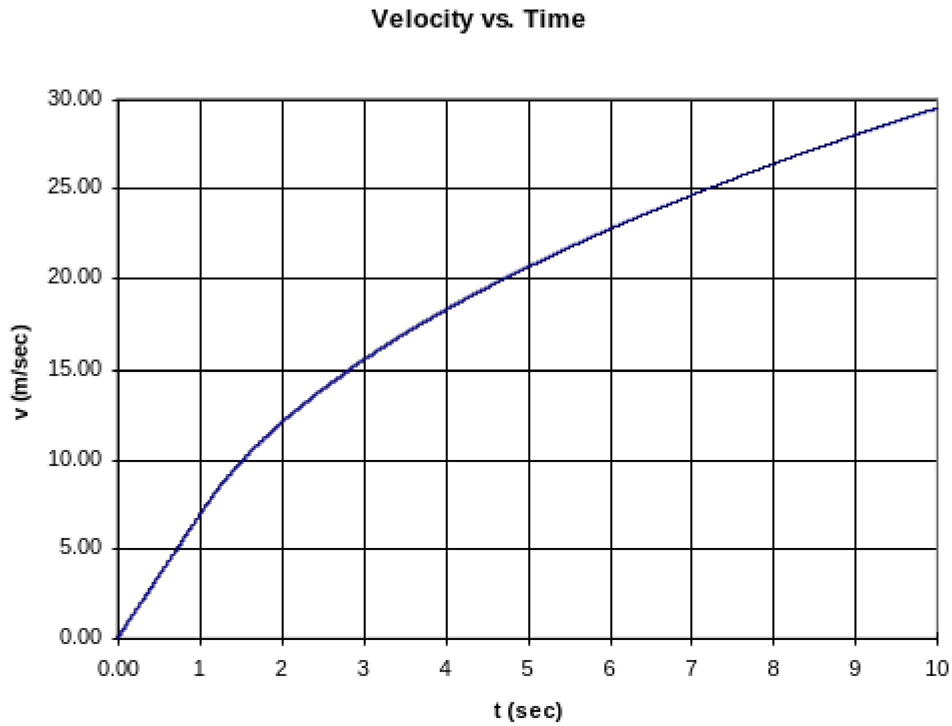

Figure 4.2.29: Velocity verses Time for the IM Powered EV Simple Simulation.

4.2.4.2Graphic Model for Detailed IM Powered EV Simulation

The ACSL graphic model of the IM powered EV formed from the bond graph model is shown in figure 4.2.16. The “Rectifier Inverter & Induction Machines” compound power block is shown in figure 4.2.17. Based upon the simple model simulations, it is appropriate to use two of the IM’s that were simulated in section 3.3. In fact, Solectria specifies use of two IM’s of this rating when similar power ratings are required. The torque and current gain blocks in this figure are used to multiply the number of IM’s without increasing the number of integrations. This helps to maintain the best possible simulation speed for the vehicle models when multiple IM’s of the same size are used. No discontinuity handling blocks are needed in this model.

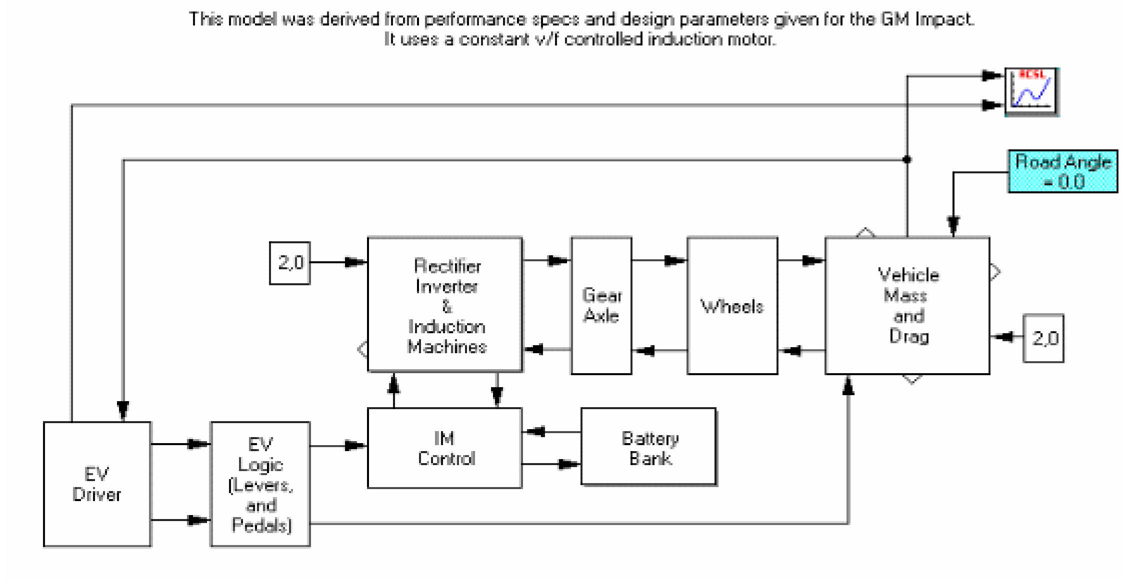

Figure 4.2.30: ACSL Graphic Model of DC Motor Powered EV.

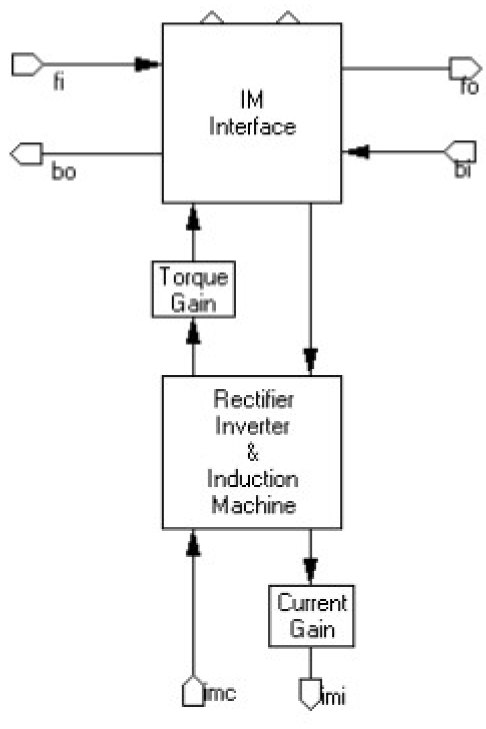

Figure 4.2.31: Exploded View of Compound Power Block for Induction Machines, their Inverter, and the Power Supply MRD Interface.

4.2.4.3Simulations of IM Powered EV and Induction Motor Control

These simulations provided two other validation tests for the IM model (other model validations were presented in section 3.3). An IM will encounter two speeds that limit its performance. It was important to verify that the simulated IM would go unstable if the controller logic did not account for these two speeds. These simulations also help to explain the development of an IM controller which is probably the most challenging task in the design of EV's and HVPP's. The parameter values adjusted for this detailed simulation that are different from the simple simulation parameter values are vehicle mass (1510 Kg) and battery mass (1014 Kg).

A variable speed controller for a real IM with must adapt its control for three different regions of speed. The first region of operation is the constant volts per hertz region [21]. In this region, torque and speed are controlled by raising the voltage at a nearly constant proportion to frequency to avoid saturation. A slight increase in voltage from this constant ratio must be made at lower frequencies. This is necessary to overcome the resistance of the stator windings enough to establish magnetic fields in the machine. Once the highest possible voltage is reached (a voltage limit that exists because of the power supply to the IM, or a voltage limit set by design limits of the IM), the second region of control is entered. The point at which this control is switched over is called the base point. Past the base point, the speed and torque of the IM are controlled by controlling the slip speed. This is a very sluggish region of control for some control schemes. If torque command is at the maximum, power is kept constant in this region, and torque must reduce with speed to keep power constant [30]. If torque command is less than the maximum, power is proportionally lower at a desired speed of operation. In these first two regions of variable speed IM operation, a controller is usually maintaining the torque below the breakdown torque [30]. However, as the synchronous speed is increased, reactances are increasing as well. A point is finally reached when the constant power at maximum torque command can no longer be maintained, because the breakdown torque is reached. If variations in breakdown torque with respect to synchronous speed are studied, one will find that a constant power is not maintained at the different breakdown torques for different speeds [30]. Therefore, at the speed where maximum power and breakdown torque meet, the controller must adapt for a new operational mode that will be called the natural mode (also none as high speed motoring) [30]. The point where this speed is reached will be called the natural point. From this point, the maximum torque allowed by the controller is dropped inversely to rotor speed. This region will be referred to as the natural region. Finally, a maximum speed is reached, for a given IM voltage, where the IM cannot run any faster. This is simply referred to as the maximum speed of the IM.

Rather than experimenting with the model to find the best initial voltage for the constant volts per hertz region, a PID controller was used to adjust terminal voltage to the IM that kept current at a level proportional to the desired torque of the machine. Once the base voltage was reached, this same PID control was scaled down and used to control slip. The natural mode was controlled as previously described, and the controller prevented operation above the maximum speed. The code used for this control is in Appendix G.

The first simulation presented only used two regions of control: constant volts per hertz to the base point; and slip control after the base point. No logic was developed to account for the natural mode. This was done to illustrate that the motor does in fact encounter the natural mode at a reasonable rotor speed. The rotor speed at which it was encountered was 3 times the base synchronous speed. Although not reported by Solectria, local experts confirmed that this was a reasonable value for a good IM design of this size. The natural mode was reached in approximately 4.5 seconds during a simulation of maximum acceleration. The vehicle acceleration stopped abruptly at this point as illustrated in figure 4.2.18.

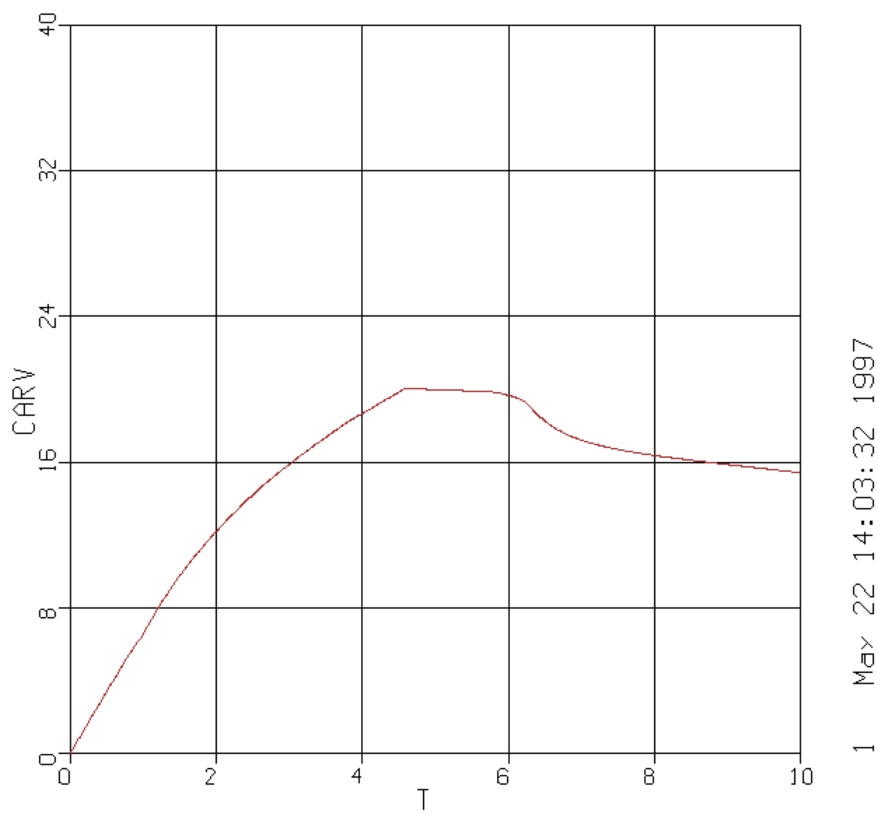

Figure 4.2.32: Car Velocity (m/sec) verses Time (sec) for the Induction Motor Powered Vehicle with No Natural Mode Adjustments.

Constant slip was used (20 rad/sec) until the voltage peaked. Afterwards, slip control was used as shown in figure 4.2.19. The slip control is sluggish, but works successfully because the vehicle mechanics are very slow. The control of slip went unstable once the natural region was entered and the slip past this point is not shown in figure 4.2.1 9. Notice the increased hunting of the slip control as the natural point is approached. The torque speed slope of an IM is much smaller near the breakdown point. Thus, as the control gets closer to the breakdown torque, the controller will try to make larger jumps to maintain the desired performance. Also notice the large initial jump when the controller converts to slip control. The method used to correct for this is explained in the last simulation presented for this vehicle. The presence of this anomaly does not adversely affect the IM or the controller, but it should be corrected, because it does cause a significant dip in the power drawn by the IM.

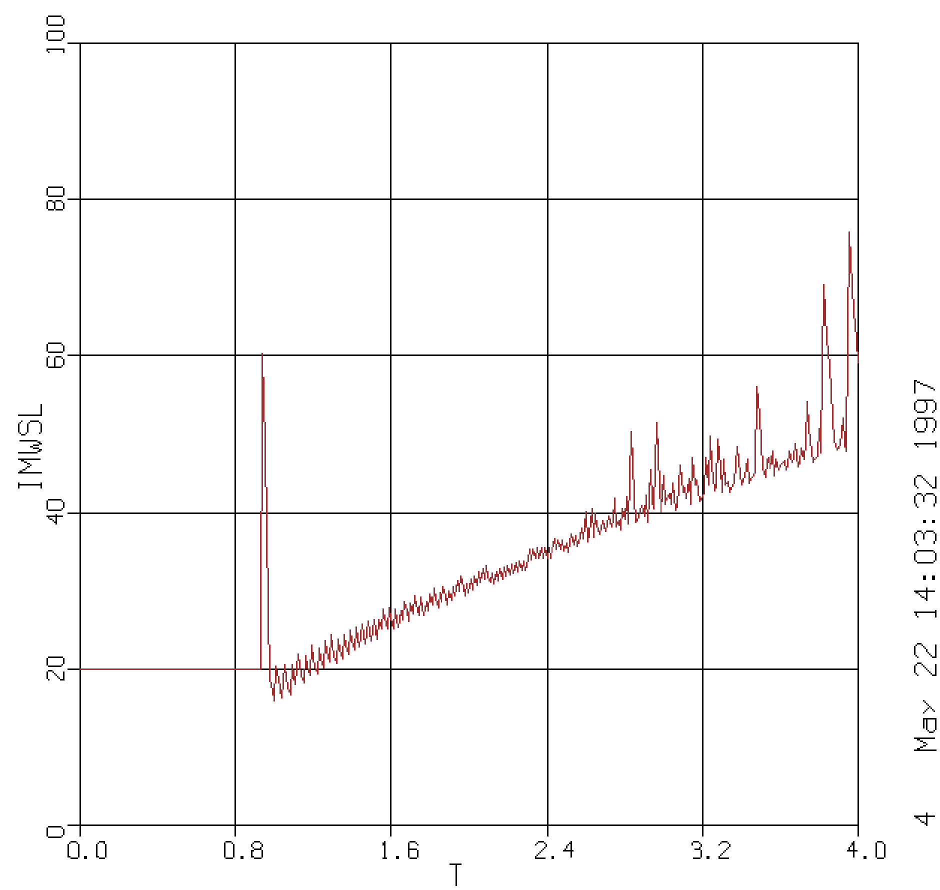

Figure 4.2.33: Slip Speed (rad/sec) verses Time (sec) for IM Powered EV Before the Natural Mode Region of the IM Was Reached.

The IM Control was adjusted to account for the natural mode, but control of maximum speed was neglected. The IM was able to move smoothly through the natural point as shown in figure 4.2.20. However, as the maximum speed was reached, the acceleration was halted abruptly at approximately 9.5

seconds. This occurred at a rotor speed of 12,241 rpm's (1282 rad/sec). The Solectria IM emulated for this work was reported to have a 12,000 rpm maximum rotor speed.

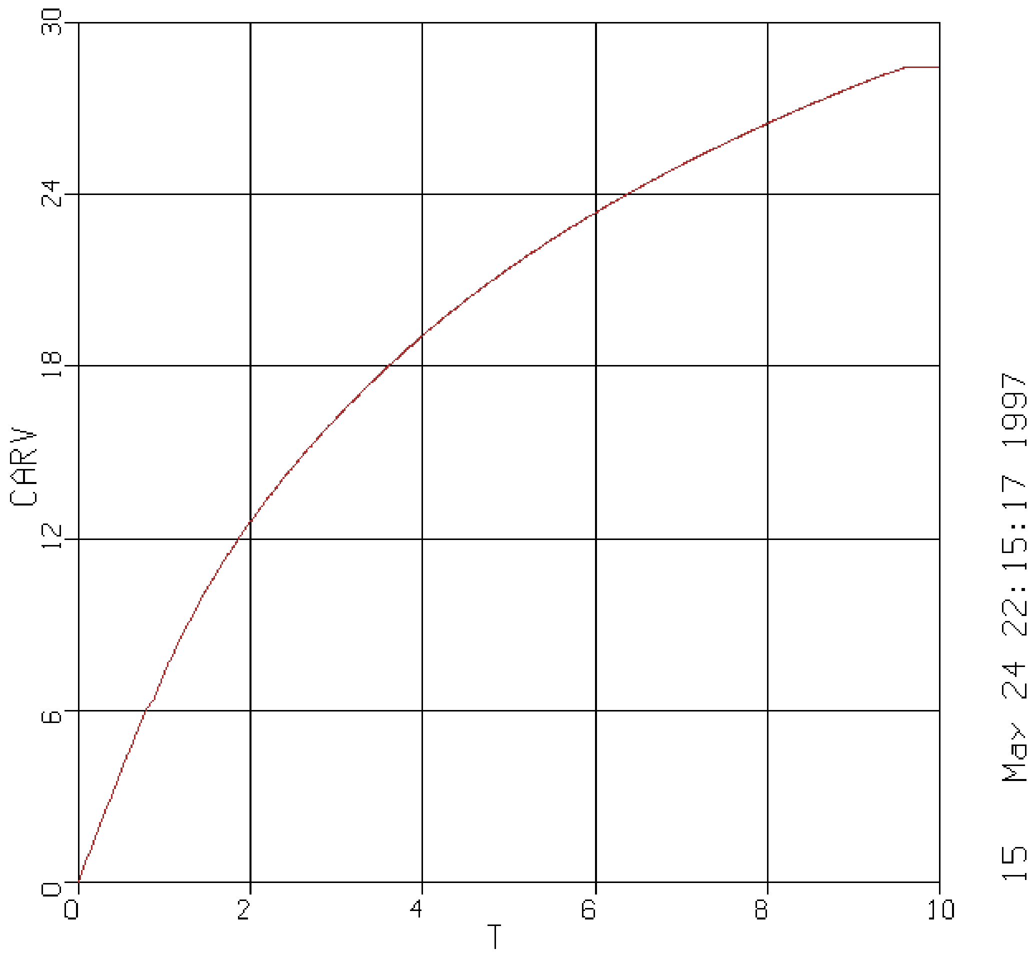

Figure 4.2.34: Velocity (m/s) verses Time (sec) during Maximum Acceleration of IM powered EV through the Three Regions of IM Variable Speed Operation and No Control of Maximum Speed.

Power drawn from one of the two IM's used in this simulated EV is shown in figure 4.2.21. This plot illustrates the drastic drop in IM power that occurs when trying to exceed the maximum speed of the machine for a given voltage.

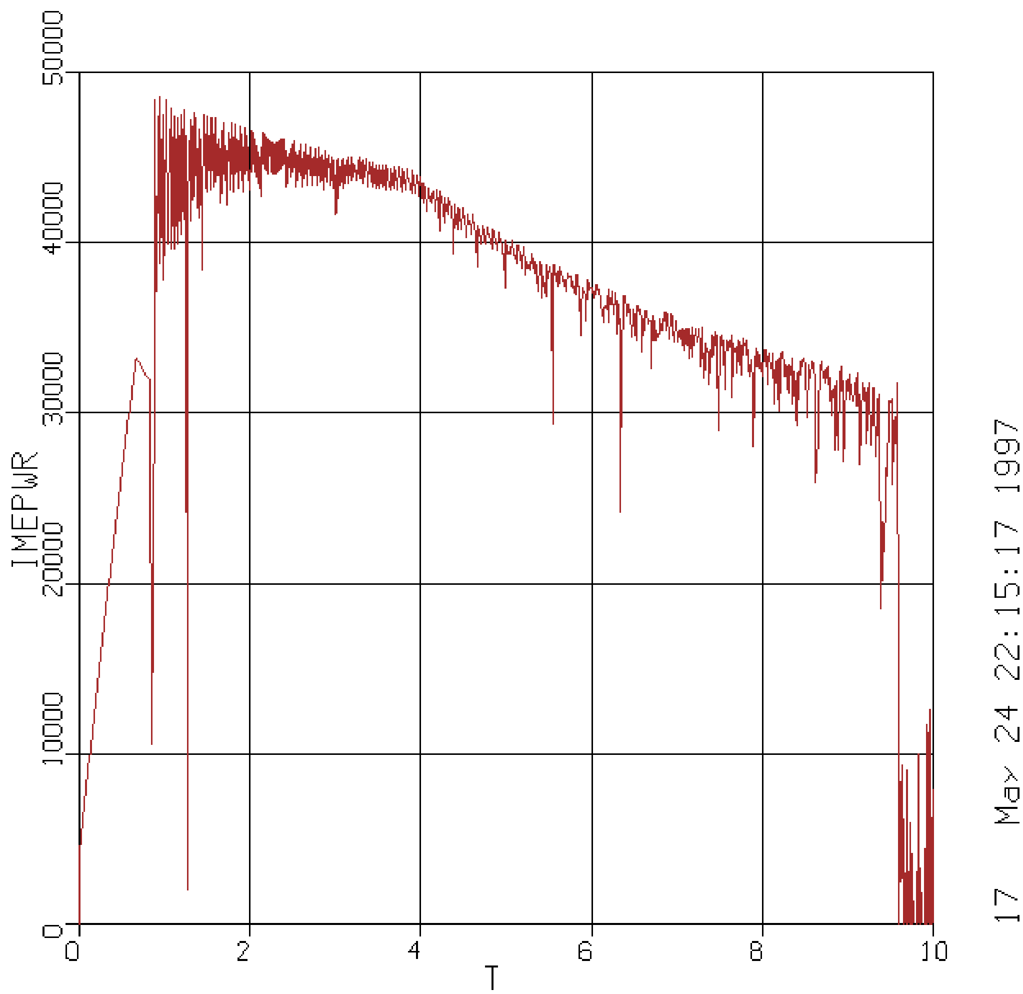

Figure 4.2.35: Electrical Power Drawn (watts) verses Time (sec) from One IM during Maximum Acceleration of IM powered EV through the Three Regions of IM Variable Speed Operation and No Control of Maximum Speed.

The total current drawn from the batteries by one of the IM's in the simulated EV is shown in figure 4.2.22. This current was used as the input to the PID controller.

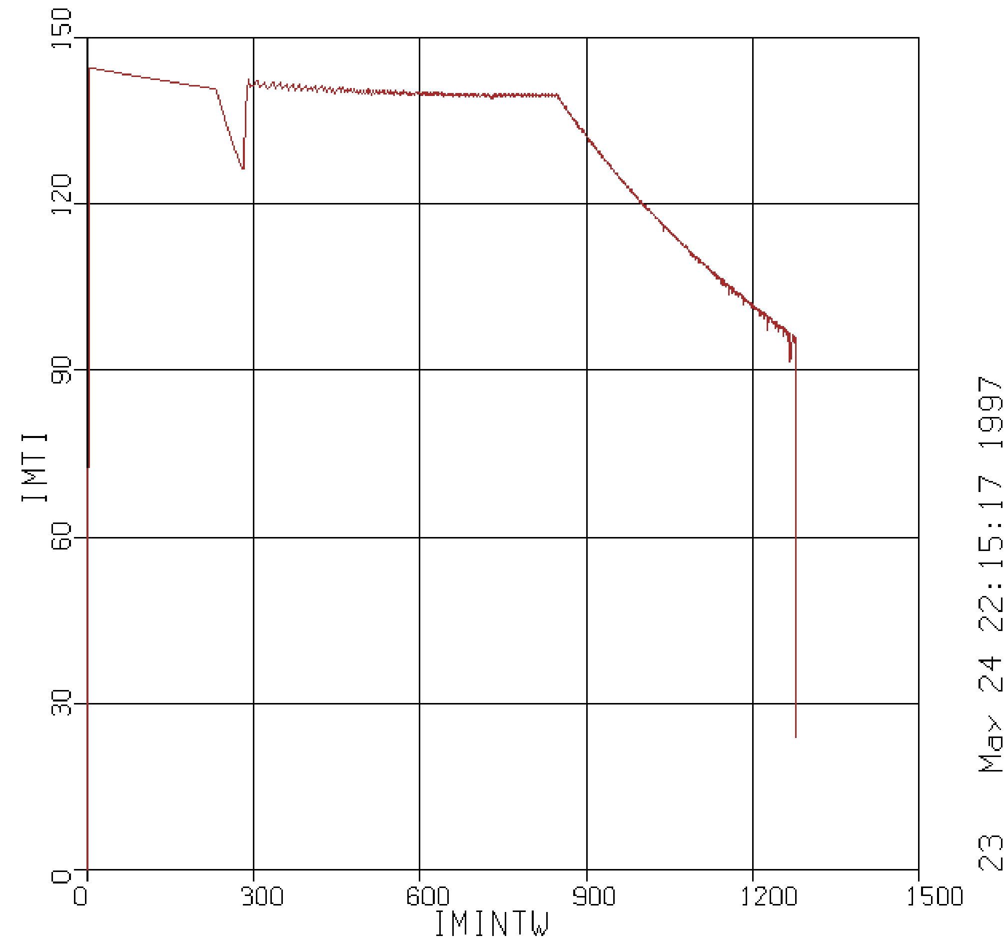

Figure 4.2.36: IM Current (amps) verses Rotor Speed (rad/sec) during Maximum Acceleration of IM powered EV through the Three Regions of IM Variable Speed Operation and No Control of Maximum Speed.

The large drop in current resulted in the PID controller trying to raise slip to an unreasonably high amount near the maximum speed as shown in figure 4.2.23.

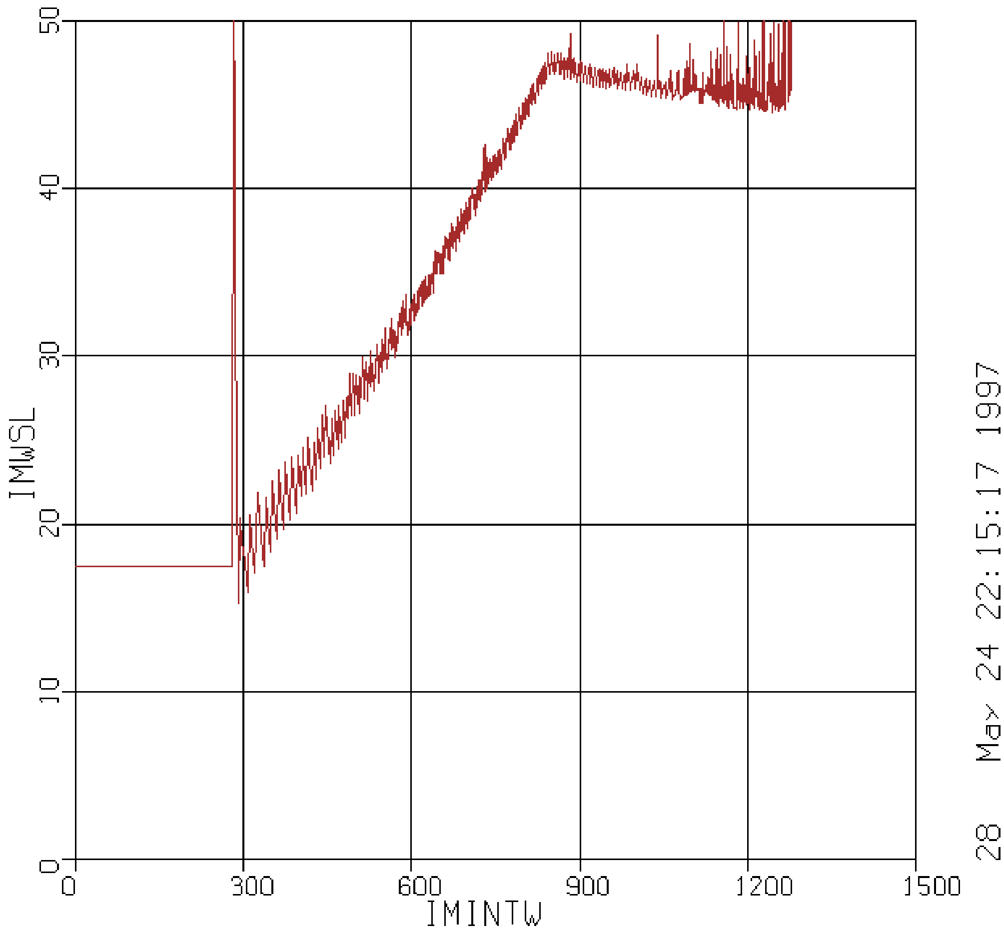

Figure 4.2.37: IM Slip (rad/sec) verses Rotor Speed (rad/sec) during Maximum Acceleration of IM powered EV through the Three Regions of IM Variable Speed Operation and No Control of Maximum Speed.

The controller was modified one more time to control the maximum speed. This modification allowed the simulated vehicle to make a smooth transition when exiting the high side of the natural mode region. This smooth transition is illustrated in figure 4.2.24 at approximately 9.5 seconds. Note that this plot shows the simulated vehicle reaching 27 m/sec (60 mph) in approximately 8.5 seconds. This is the acceleration spec for the GM Impact.

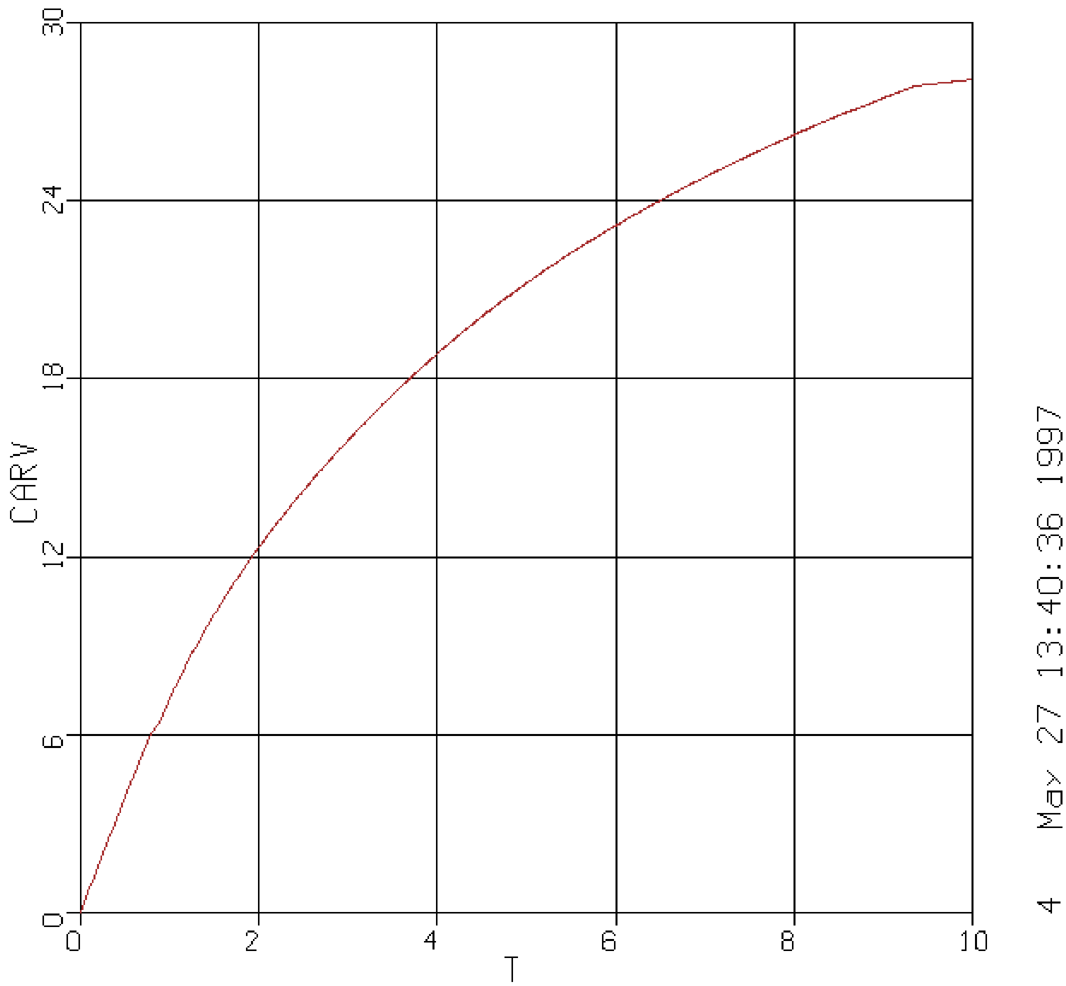

Figure 4.2.38: Car Velocity (m/sec) verses Time (sec) during Maximum Acceleration of IM powered EV through the Three Regions of IM Variable Speed Operation and Control of Maximum Speed.

The drop in control of slip as the maximum speed is reached is evident in the plot of slip speed verses rotor speed shown in figure 4.2.24. The characteristics of this slip control are consistent with variable speed IM control characteristics illustrated in [30].

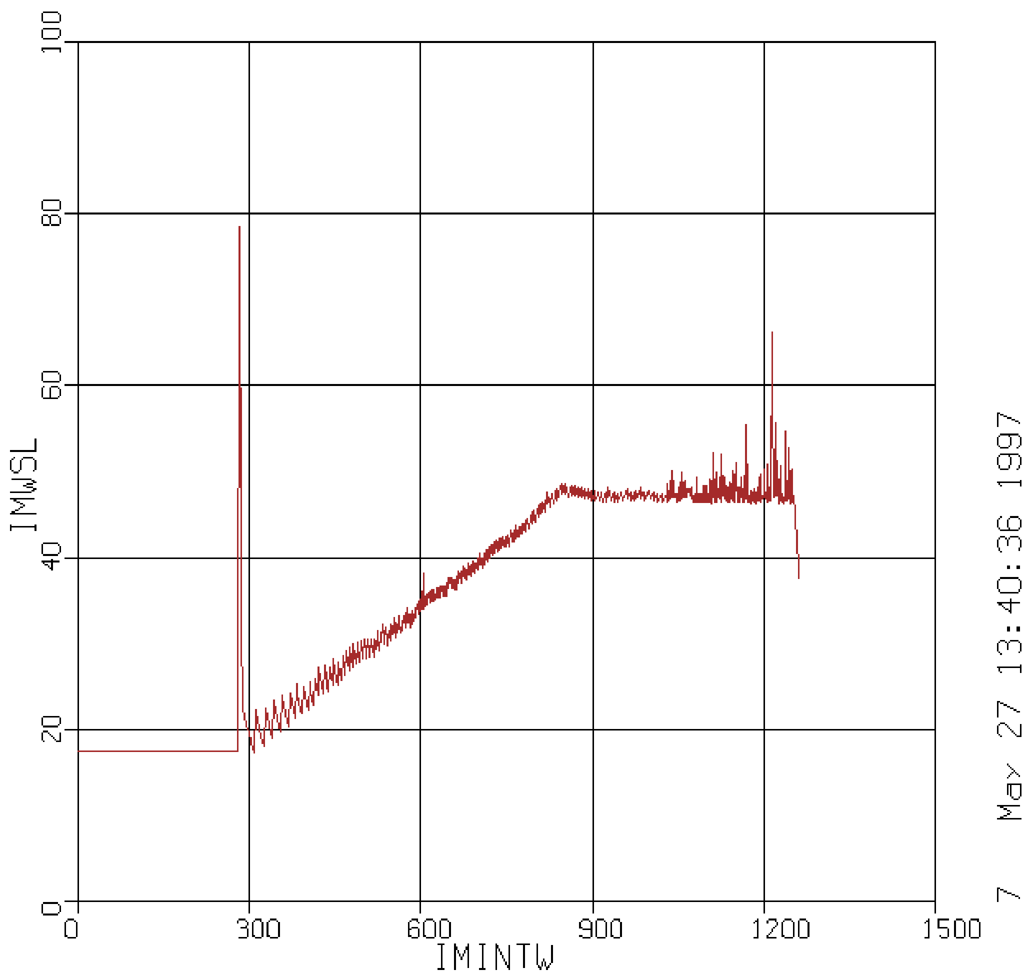

Figure 4.2.39: Slip Speed (rad/sec) verses Rotor Speed (rad/sec) during Maximum Acceleration of IM powered EV through the Three Regions of IM Variable Speed Operation and Control of Maximum Speed.

The last simulation for this vehicle was a maximum acceleration to a cruising speed. The velocity of the vehicle verses time is shown in figure 4.2.25. The correspondence of vehicle velocity to IM slip speed for this particular simulation is shown in figure 4.2.26.

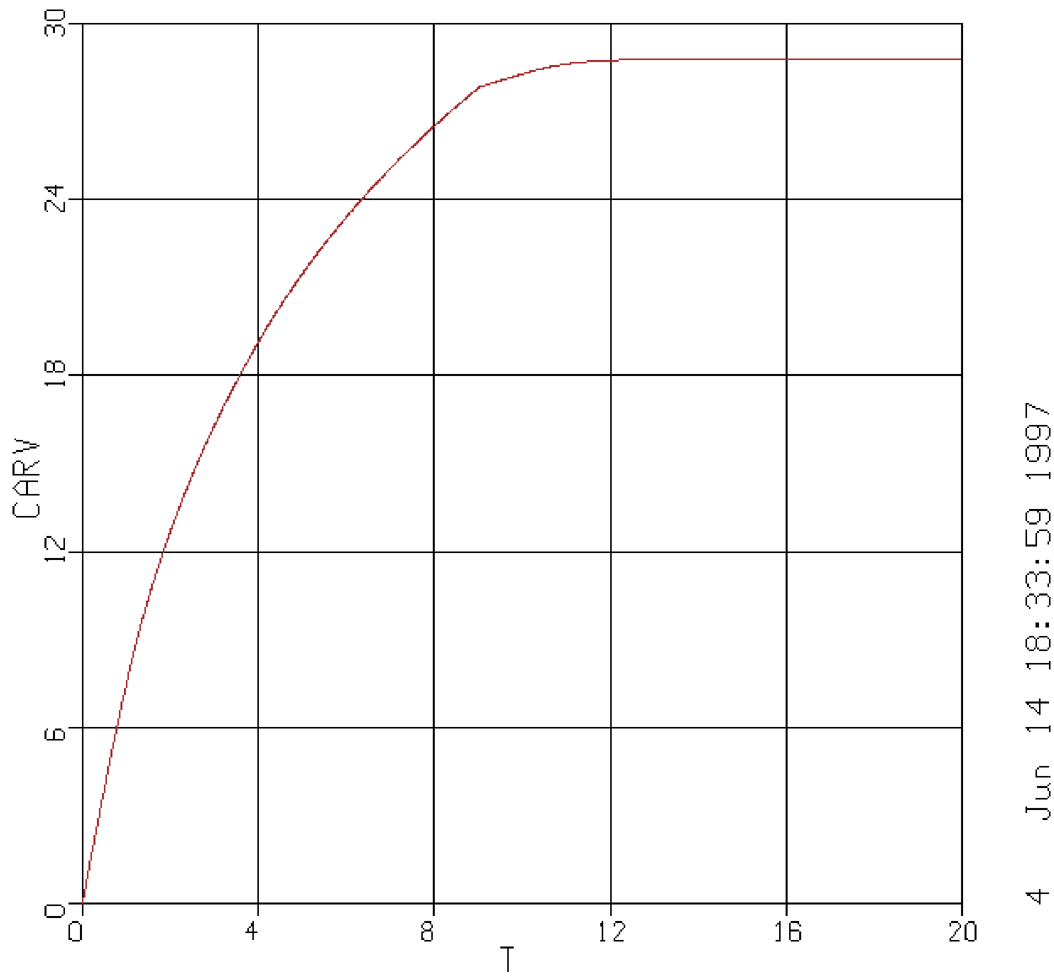

Figure 4.2.40: Velocity (m/sec) verses Time (sec) during Maximum Acceleration to a Cruising Speed for the IM powered EV with Final Improvements to the IM Controller.

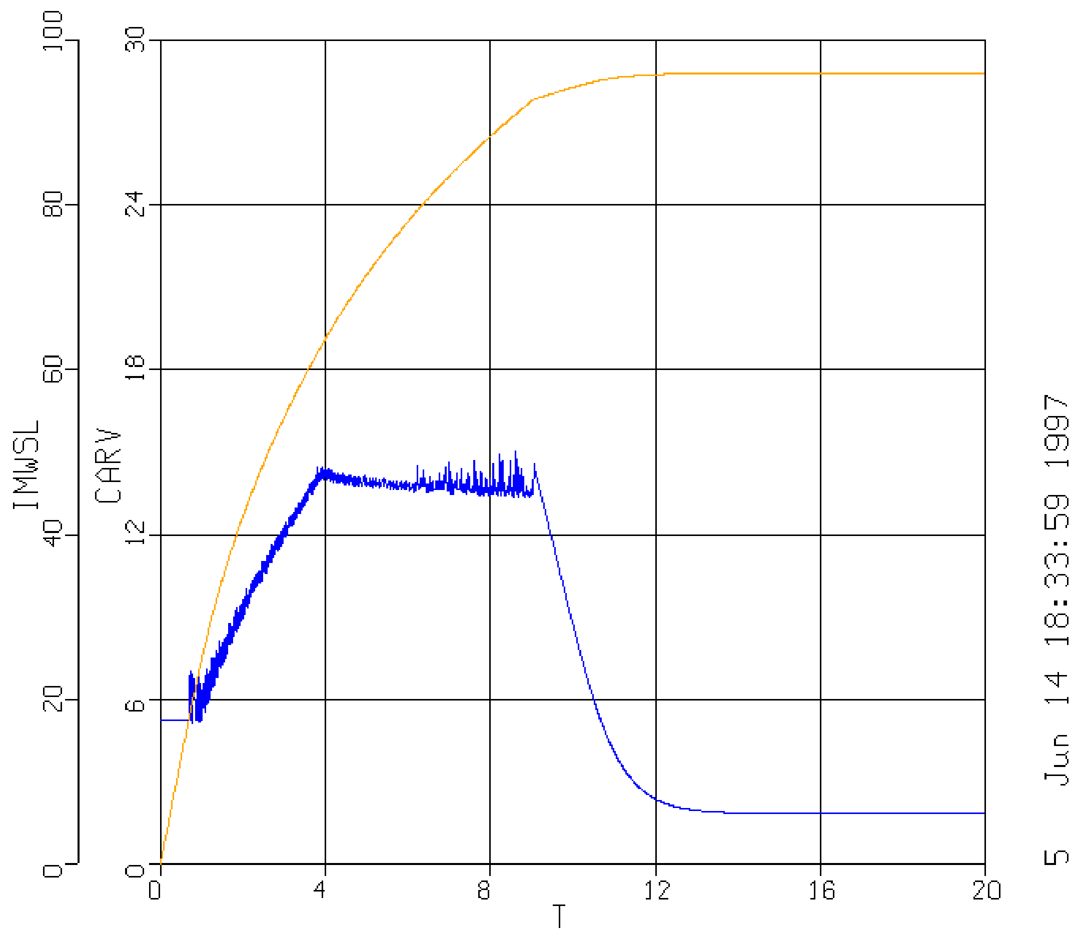

Figure 4.2.41: IM Slip Speed (rad/sec, solid line) and Car Velocity (m/sec, dotted line) verses Time (sec) during Maximum Acceleration to a Cruising Speed for the IM powered EV with Final Improvements to the IM Controller.

Note that the conversion to slip control does not cause the spike in slip that was seen previously. Adjustments made to the constant slip used in the first IM control region, and adjustments to the control of voltage that included considerations of the battery bank voltage, eliminated this anomaly. The plot in figure 4.2.27 helps to explain this.

Previously, the conversion between the two control regions across the base point were set to a certain synchronous frequency. When the base point was reached, the controller set the voltage to the IM to the base voltage, or to the battery voltage, whichever was less. Depending upon the transient, there was no guarantee that the PID controller would not go above this base voltage before reaching the base frequency, and it did in the previous simulations. Therefore, the control was changed to allow voltage variations until the maximum safe voltage for the IM was reached, or until the current battery bank voltage was reached as shown in figure 4.2.27. After reaching the maximum voltage currently allowed, which could change with time due to battery dynamics as shown in figure 4.2.27, the controller would control the slip. The details for the logic and the code can be found in Appendix G.

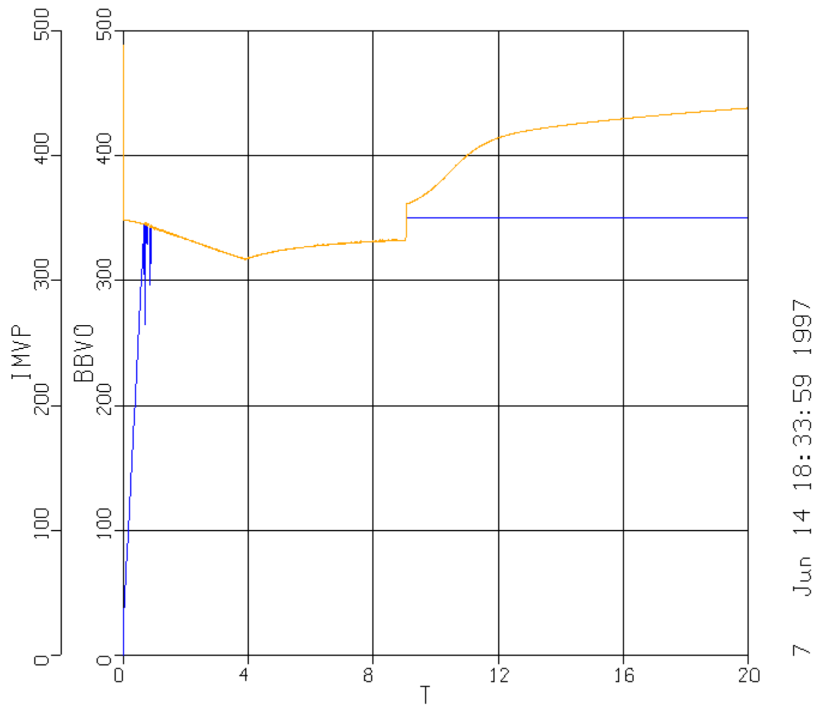

Figure 4.2.42: IM Controller Voltage (volts, lower line) and Battery Bank Voltage (volts, higher line) verses Time (sec) during Maximum Acceleration to a Cruising Speed for the IM powered EV with Final Improvements to the IM Controller.

4.2.4.4Summary

In addition to exhibiting realistic sensitivities to design changes and accurate performance predictions as shown in section 3.3, the IM model is exhibiting realistic sensitivities to variable frequency control and is exhibiting realistic dynamic behavior predictions in this section. Therefore, it should be good in helping determine critical control and operating parameters in the HVPP model analyses. It proved to be valuable in the process of developing variable speed IM controls in this section.

It should be pointed out that the GM Impact uses one IM with a maximum power rating of 102 kW. The EV in this subsection used two IM’s with ratings and design parameters equivalent to those given in section 3.3 and Appendix H. The maximum power and torque capabilities of these two IM’s and the maximum power density of the simulated battery bank must be close to the ratings of the respective components in the Impact in order to reproduce the results. It is unfortunate for this work that more accurate design data for the Impact could not be obtained for validation of this overall model.

Unfortunately, the IM model is the slowest of all the component models being used. However, ACSL is very portable, and simulations involving IM's were ran on more powerful university computers over the campus network. The time it took these models to run was reasonable (usually much less than overnight for 40 seconds or less simulation time). The MRD drive train scheme also allowed rapid construction of this model from sub-component modules and accommodated the dependencies within the model. Since there were no discontinuities in the drive train during the simulated operation of the plant, the MRD scheme was not required to handle any discontinuities during this simulation either. The simulation results predicted the same acceleration performance of the GM Impact when design parameters similar to those of the Impact were used.

4.2.5Discussion on Batteries

The batteries have proven to be the most sensitive device in the plants studied. This means that the battery model is in fact very valuable. Without it, the simulation studies of sensitivities between plant power supplies would not be nearly as valuable.

A reliable means of estimating the mass of batteries required for a certain vehicle was found that works well in all of the cases studied in this dissertation. The desired base voltage is first multiplied by 1.5. This gives the open circuit voltage of the battery bank. This voltage is divided by the open circuit voltage per battery to be used which gives the number of batteries in the bank. The number of batteries is then multiplied by the mass of each battery to determine the mass of the battery bank. The number of batteries can then be adjusted from this point to achieve the best simulation results possible.

4.2.6Conclusions

The above studies indicate that the research objectives are being successfully met. The component models, when used in non-hybrid power plant vehicle models, gave accurate performance predictions when compared to existing plants with power supplies of equivalent ratings. The presupposition that component level modeling would result in adequate accuracy for design and design directions appears to be correct from analyses performed in this section and in section 3. A special point of interest is that the realistic actions of the models occasionally provide frustrations similar to those that might be experienced in experimentation and development. The next section will utilize the sub-component models in the virtual construction of HVPP models.

5HYBRID VEHICLE POWER PLANT MODELS AND SIMULATIONS

The developments of sections 2 and 3 provide the necessary building blocks to construct virtual HVPP's. Examples of power plant simulations given in section 4 illustrated the synthesis of these building blocks to form virtual vehicle power plants for design analysis. Comparisons between the simulated data from the examples in section 4 to data for vehicles with similar power plants demonstrated that the sub-component models make accurate predictions and display realistic dynamics, and showed that the models were useful design tools. Therefore, the sub-component models are considered to be adequately validated at the present time.

Models of the discrete sub-components are based upon design parameters. The accuracy of such model modules, when scaled, is trustworthy. This is not to say that further validation of the models is undesirable. It is desirable to validate the models for a wider range of design parameters and power ratings. However, the power ratings of power supply components used in HVPP's do not change significantly in size for automobiles and only slight design changes to the models used in this work were necessary. Furthermore, validations were performed on sub-components that had ratings close to, or equal to, the component ratings used in these studies. Thus, more time was invested in demonstrating the utility of the methods. Further validations will be performed as this work progresses in the future.

In the complete HVPP design process, the design team would start with the general need statement and then move on to the function structure that includes the essential functions of any HVPP. After considering their specific requirements, criteria and objectives, they would extend the function structure to address their more specific objectives. As the team develops trial concepts, they would be applied to the structure of the function system diagram. The function system diagram is an abstract tool and framework that helps the team to compare the current strengths and weaknesses of the concepts and architectures that they are considering. Then, the simple simulation methods used to determine power ratings, gear ratios and vehicle mass are applied to the trial concepts. These simple simulations are the ideal tool for this stage of the design process where the initial trial concepts are still being rejected, accepted, or refined [6]. The most promising concepts are then applied to the virtual test environment using the detailed sub-component models.

The HVPP models synthesized from the sub-component models can be used to study how design, operational and control parameters affect the performance characteristics of the various HVPP configurations being considered. These models are considered to be virtual test beds whose configurations can be easily and quickly changed. A complete hybrid power plant model has a large number of design, control and operating parameters. Each component of the plant will have its own unique responses to these parameters. Fundamental references covering the theories of each of these components explain in significant detail which parameters have the greatest effects on performance parameters. Using this knowledge, and the knowledge a designer would gain from simulations of single power plant vehicle models, the appropriate design, operational and control parameters of a HVPP model can be varied until the plant has achieved an acceptable, or optimal, performance. Furthermore, as the designers use the model, they will be able to observe any operational anomalies that require redesign of the sub-components, redesign of the control logic, or that require more careful attention during prototype construction.

A note of caution is in order here. A good designer would take great care in designing a prototype before having it constructed. He would make sure that he had considered all of the functions that must be fulfilled by the design. He would repeatedly question the configurations of the design to make sure it was good and sound. He would check and recheck calculations to make sure that the system will operate correctly, so that valuable time and material are not wasted in a major redesign. This same type of care should be taken when developing the detailed HVPP models. It is easy, and takes little time, to construct these models using the developed modeling tools. But, simulating them, adjusting parameters, and re-simulating them takes a significant investment of time. A thorough analysis should be made to determine good initial parameters for the designs virtual. Careful analysis of each simulated performance should be made before adjusting the model's parameters to improve performance. The models and methodologies of this work cannot take the place of a good designer who applies good design methods. They can only help a good designer develop and compare his concepts in an abstract setting and test his concepts in a virtual test environment.

The complete process of refining a specific HVPP design until it achieves optimal or near optimal performance is a long and complete work in itself as explained in the introduction. The goal of this work was to take a major step in creating flexible and accurate tools that could help designers perform such optimizations. Thus, no attempts were made to validate whether or not optimal performance has been achieved. The focus of this section is to illustrate the application of these tools, and to present how they help to identify critical design parameters and the relationships and sensitivities among the design, operating and control parameters. This will be done by applying the methods to four different HVPP configurations. Each concept is first applied to the function system diagram to further illustrate its use. Bond graph models are formed from each system diagram, and simple simulations are used to make initial estimates of power supply ratings. Detailed models are then formed for each concept using the Bond Graph models, and unique design improvement scenarios are presented for each configuration model. Since a given vehicle's acceleration criterion is the most demanding criterion on the design, maximum acceleration transients are used to demonstrate the modeling methods. The models have been used in, and are capable of making predictions for, other drive cycle transients. Since section 3 demonstrated that the sub-component models exhibit proper sensitivities with regard to changes in their own design parameters, this section will serve to demonstrate the utility of the models with regard to changes in control systems and plant architecture.

5.1Design - Function System Diagrams

The function system diagram graphically illustrates the relationships that exist between the functions of the function structure. It provides a framework for considering and refining concepts. Once specific HVPP concepts are applied to this visual tool, the diagram helps to illustrate how power is transmitted and coordinated in the system. Designers would preferably want all energy sources to be bi-directional with no limitations. Existing technological limitations often prevent this, because current design objectives cannot be solely met by existing devices with this capability. However, these devices can be used to partially fulfill the objectives, and they do show promise for the future as developers continue to improve their capabilities. Coordinating these and other devices to achieve a desired end is the gestalt of HVPP design. The function system diagram is used to consider alternative concepts that might improve upon the weaknesses of a current configuration and meet the design objectives. Once the relationships are made clear with the diagram, the designers use their experience, and the knowledge of others, to identify large scale parameters and to speculate on which parameters will be the most sensitive. The design team can then consider designs for passive or active control concepts that can be used to compensate for these sensitivities. The general forms of the two most common hybrid power plant configurations are applied to the function system diagram. Component weaknesses are then considered and discussed. Then, the simple models and the detailed models are derived from these system diagrams. The model simulations are then used to find the parameter values that will provide proper plant operation.

5.1.1Parallel Hybrid Vehicle Power Plant

The gestalt of the parallel hybrid concept is to add the torques from two power supplies to achieve the desired performance [5]. This arrangement is shown in figure 5.1.1. In this configuration, the engine can take advantage of the high efficiency of the mechanical drive train. The engine connection to the gears, shafts and wheels of the drive train is controlled with the clutch. The battery and electric motor are coupled into the transmission and are primarily used to accelerate the vehicle. Since the electric motor is used to accelerate the vehicle, the engine can be smaller. A smaller engine uses less fuel and will therefore have reduced emissions. If regenerative braking is deemed to be practical, the electric motor and batteries can be used to help decelerate the vehicle as well. Charging, during driving, is achieved by running the electric motor in generator mode. During this mode of operation, the engine is supplying the road load power [1] and the mechanical power required for electrical power generation.

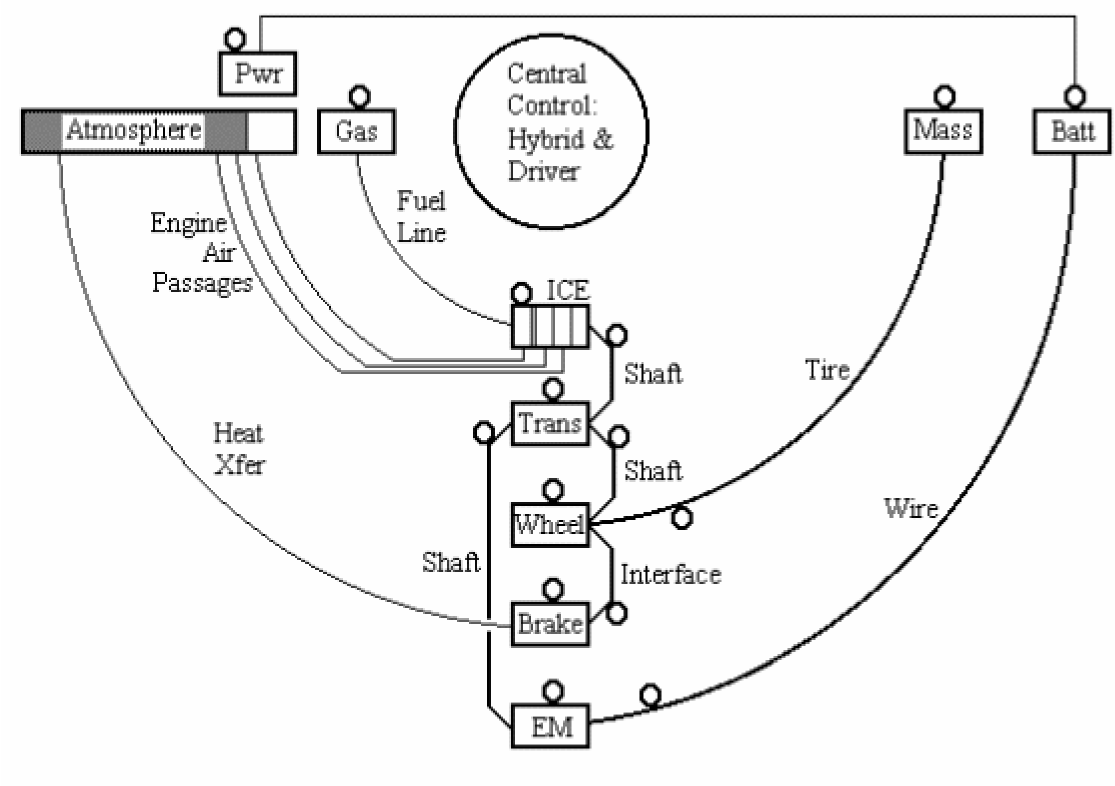

Figure 5.1.1: Application of the Parallel Hybrid Concept to the Function System Diagram.

Engineers have proposed fixed and variable transmissions for the engine in this configuration. It is desirable to reduce the weight of the car by eliminating the variable transmission. When this is done, the driver has no control over the engine speed and the engine’s torque cannot be utilized well at lower vehicle speeds. Furthermore, the engine cannot even be utilized below certain speeds, because, with a fixed gear ratio, the clutch must be engaged at a higher vehicle speed to avoid stalling the engine. Therefore, this configuration is simulated with both fixed and variable transmissions in the detailed model test bed to contrast the performance of each. Other comparisons and modifications will be made between parallel hybrid plants using dc machines and induction machines.

5.1.2Series Hybrid Vehicle Power Plant

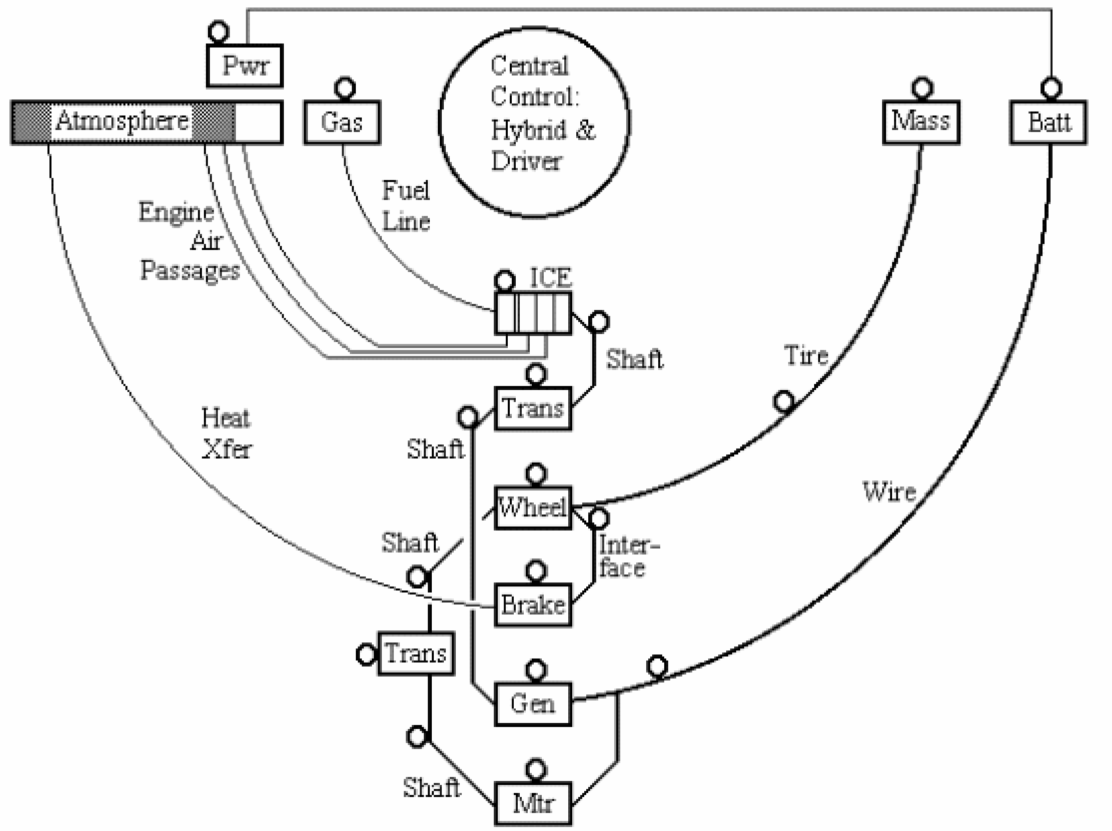

Figure 5.1.2: Application of the Series Hybrid Concept to the Function System Diagram.

The gestalt of the series hybrid concept is to charge the electrical storage system from one power supply and then run a primary traction power supply (e.g. electric motor) using the stored electrical energy [5]. This configuration is shown in figure 5.1.2. This vehicle configuration is typically regarded as an EV with an onboard charging system. It takes advantage of the good torque speed characteristics of electric motors and the simplistic design of an electric vehicle. The electric motor is connected directly to the wheels of the car through the fixed gears and shafts of the drive train. The engine is typically ran at a constant speed to turn an electrical generator that charges the batteries. This results in greater engine efficiency and thus greater fuel efficiency and lower emissions. If regenerative braking is deemed to be practical, the electric motor and batteries can be used to help decelerate the vehicle as well.

Since this vehicle is typically designed as an EV with an onboard charging system, the engine / generator set is not considered to be useful in high power transients. The engine / generator set is primarily used to charge the batteries over a longer time at the batteries most efficient charging rate. This type of power exchange does not present a major challenge to the design of a hybrid vehicle power plant. The control and coordination of power supplies is simple. For this reason, series hybrids are considered easier to control and design.

The design of an appropriate engine / generator set for a typical series HVPP may present some interesting dynamics. However, it is expected that the design of this sub-system would not be significantly aided by the type of modeling developed in this work. A simpler design scheme should be more appropriate and time efficient. Since the typical series hybrid is essentially an EV, the virtual EV test beds developed and presented in the previous section can be used to study such a system with a few simple modifications. These modification would primarily be the addition of a simple power supply that intermittently charges the batteries and an addition to the vehicle weight for the charging system.

In order to better illustrate the application of the design and modeling methodologies that have been developed, an atypical series HVPP was studied using the detailed models. This series plant is designed to utilize more power from the ICE / generator set and to use a smaller battery bank. This makes the vehicle significantly lighter than the typical series HVPP, because the power density of the engine / generator set is lower than that of the batteries. The author is not trying to promote this configuration. He simply wants to better illustrate the utility of the developed modeling tools. This type of HVPP will also be called an electrical parallel HVPP.

5.1.3Considerations

Consider a collection of vehicles with different power plants that have the same sizes (i.e. dimensions of volume) and performance ratings (i.e. acceleration, speed, range, etc.). The hybrid vehicles in this collection will tend to weigh significantly more than conventional vehicles, and approximately the same as EV's if the EV's are allowed to have a smaller range. Parallel HVPP's using larger ICE's with variable transmissions would weigh less than all the other vehicles except the conventional vehicle. The electrical parallel HVPP would be comparable to the parallel HVPP due to its reduced battery mass. These weight differences are primarily due to the batteries as seen by the comparisons of power densities shown in table 5.1.1.

	Power Densities, ρ	
Component	**Low (kg/kW)**	**High (kg/kW)**
Electric Motor	1.5	2.0
Electric Generator	1.5	2.0
Electric Batteries	10.0	18.0
ICE	2.5	3.5
Drive Train	0.1	0.3

Table 5.1.1: Power Densities of Common Components found in HVPP's.

Even though the mass of a vehicle is an important consideration, it is not the primary concern in the design of a HVPP. The concern is to improve fuel economy, reduce emissions and maintain or surpass the level of performance the market has come to expect. In order to improve fuel economy and reduce emissions, the size of the engine must be reduced well below the sizes found in comparable conventional vehicles. The new power supply components must be properly blended to maintain or surpass the expected performance. But, the right balance of vehicle power, weight and performance can only be found through simulation analysis and experimentation. The later sections will demonstrate the remaining simulation analysis tools that are used to help determine this balance.

The function system diagram will have its greatest utility in future work when it is used to compare, reject and refine concepts that will be considered for mass production. However, its usefulness can be further illustrated here. Consider, the discussions regarding regenerative braking in sections 3.4 and 4.2. Most batteries make regenerative braking difficult and sometimes impractical. The power density of batteries results in another significant problem in HVPP design. The battery mass must be inflated sufficiently to handle, or partially aid in, the acceleration transients. Figures 5.1.3 and 5.1.4 are used to demonstrate these difficulties. The batteries are enlarged to illustrate their power/energy density, and they have also been moved to the unidirectional energy source side of the diagram in figure 5.1.3, because, without regenerative braking, the EV has no means to recharge the batteries while driving.

In EV's and HVPP's, it is desirable to have a bi-directional energy source, which has a much lower power density than batteries, that can be used to deliver and recover energy during high power transients. The design team may consider several devices. It is acceptable for these devices to have high energy densities as long as they have low power densities. The system diagrams in figures 5.1.3 and 5.1.4 have been adapted from previous diagrams to bring these issues into focus. If batteries are primarily used in a HVPP during transients, they could feasibly be replaced by these low power density devices. If this is possible, the vehicle weight can be significantly reduced. The low power density bi-directional energy storage devices indicated in the diagrams will be investigated in future studies using the modeling methods of this work to determine optimal interfacial techniques.

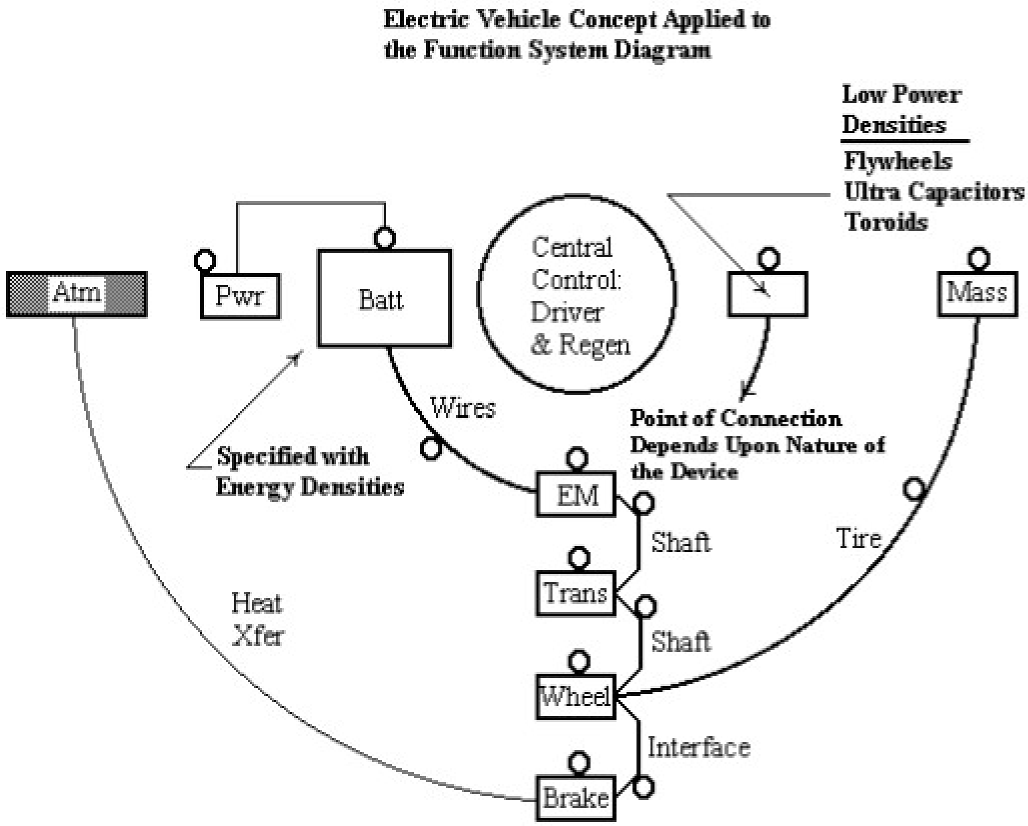

Figure 5.1.3: EV Concept Applied to Function System Diagram with Potential Future Concepts Added.

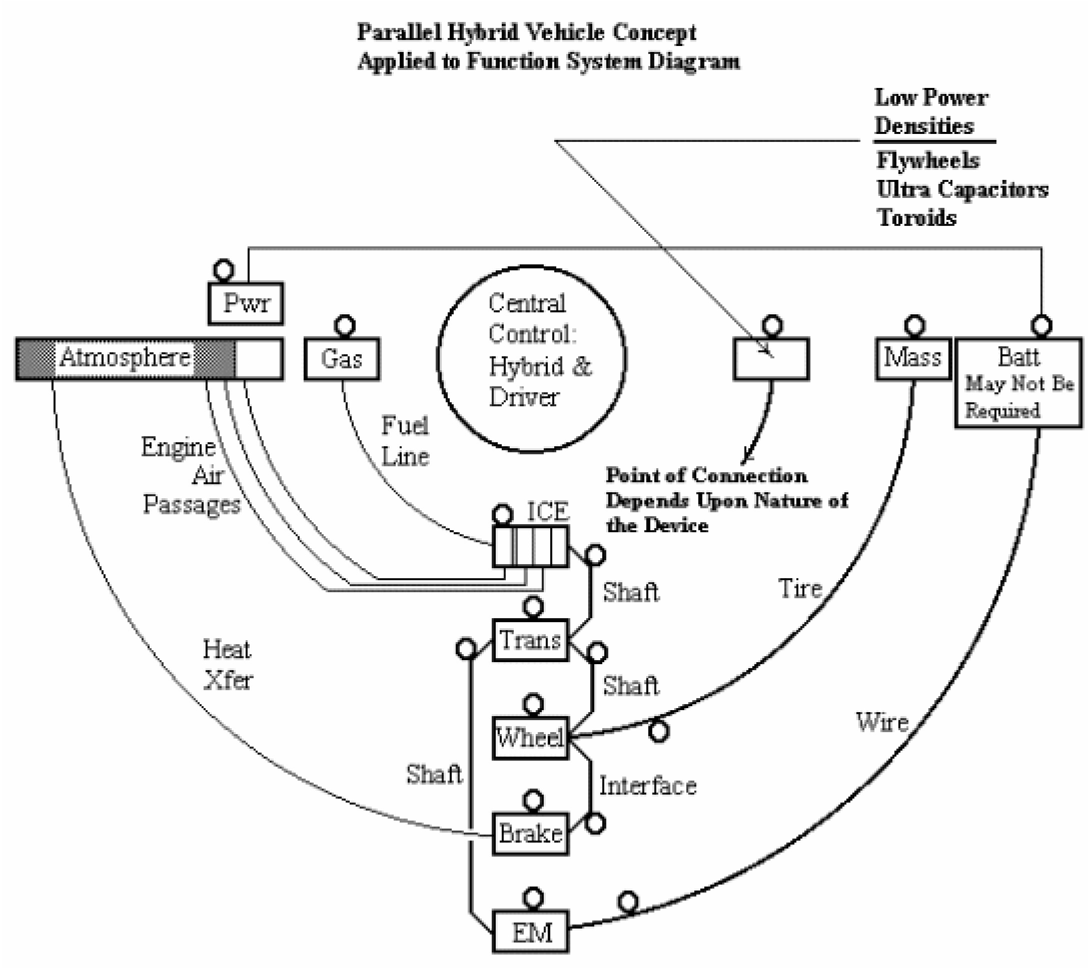

Figure 5.1.4: Parallel HVPP Concept Applied to Function System Diagram with Potential Future Concepts Added.

5.2Bond Graph Models

Bond graph models are developed using the system diagrams of section 5.1. The bond graphs bring attention to important aspects of the vehicle model. If any dependency problems exist in the model, the application of causalities to the bond graph points this out immediately. This aspect of bond graphs was discussed in sections 3.2 and 3.3 during the development of the detailed models. The causalities also communicate the state variable inputs and outputs of the sub-component models contained in the bond graph model. The bond graphs illustrate the relationships and transfer of energy between the components of the plant. For this same reason, they are useful in helping form the ACSL graphic models.

As with the EV bond graph in section 4, the dependencies indicated by the causalities that would normally be introduced by the interface of various drive train inertias are accomodated by the MRD connection scheme. Thus, the input/output causality used for the individual power supply bond graphs do not indicate the derivative causality that would normally be encountered. The inertias are simply passed through the MRD components to be handled as described in section 3.1. The bond graph indicates that the inertial lumping is done with the vehicle mass. However, a velocity at any point in the drive train can be output by the MRD scheme.

5.2.1 Parallel Hybrid

The bond graph for the parallel hybrid configuration is shown in figure 5.2.1. The detailed bond graph models for the engine, battery bank and electric motor are found in sections 3.2, 3.3 and 3.4, respectively. Torque from the engine is transmitted through the clutch and increased through the transmission and passed to the first **1** junction. The battery bank bond graph sends a voltage to the electric motor bond graph. The electric motor bond graph's torque output is passed through its constant gear and then passed to the first **1** junction. The **1** junction represents the physical coupling that adds the two torques from the two power supplies together. The torque output from the coupling, the **1** junction, is increased by the differential and then converted to a large force on the road through the tires. The velocity, determined by integrating the sum of the forces on the vehicle's equivalent mass and then dividing by the equivalent mass (i.e. Newton's third law), is converted to a rotational velocity through the tires. This velocity is then increased by the differential to define the rotational velocity of the coupling's **1** junction. This velocity is increased by the gear ratios in the two paths back to the power supplies. The velocities of the power supplies are used by the models to determine various state variables. Current is determined in the electric motor bond graph and sent to the battery bank model. This model is used to form the ACSL graphic models for the parallel hybrid power plants below.

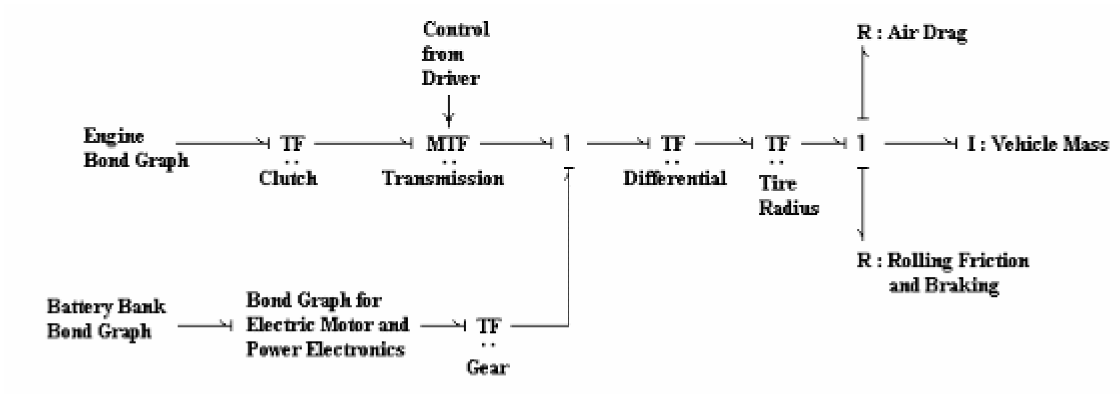

Figure 5.2.5: Parallel Hybrid Vehicle Bond Graph.

5.2.2Series Hybrid

The bond graph for the series hybrid configuration is shown in figure 5.2.2. The detailed bond graph models for the engine, battery bank and electric motor are found in sections 3.2, 3.3 and 3.4, respectively. Torque from the engine, after being reduced by any mechanical losses in the model, is delivered to the inertia of the generator armature and flywheel. There may not be a flywheel, but the ACSL graphic models allow for this additional inertia. Newton's third law of motion is used to determine the rotational velocity of the armature and flywheel. The velocity of the armature passes through the **MGY** that has a modulus of the product of machine constant and field flux and gives a voltage output to the second **1** junction which represents the common flow of armature current. The sum of voltages to the armature inductance at this **1** junction (the voltage from the MGY minus the voltage drop across the armature resistance minus the battery voltage) are integrated and divided by the armature inductance to determine the current from the DC generator. The current from the generator minus the current drawn by the electric motor determine the amount of current into, or out of, the battery bank at the **0** junction. The battery bank model determines the battery bank voltage from the current. The battery bank voltage determines the available voltage to the power electronics of the electric motor. The voltage from the power electronic control system goes to the electric motor bond graph. The electric motor bond graph outputs a torque that is increased by the gear and is converted to a force by the wheels. The vehicle velocity and its feedback through the drive train are determined in the same manner as the parallel hybrid vehicle velocity was. The rotational velocity of the electric motor is used by its model to determine various state variables including the current. This current is determined in the electric motor bond graph and sent to the **0** junction where the battery bank current was determined. This model is used to form the ACSL graphic models for the series hybrid power plants below.

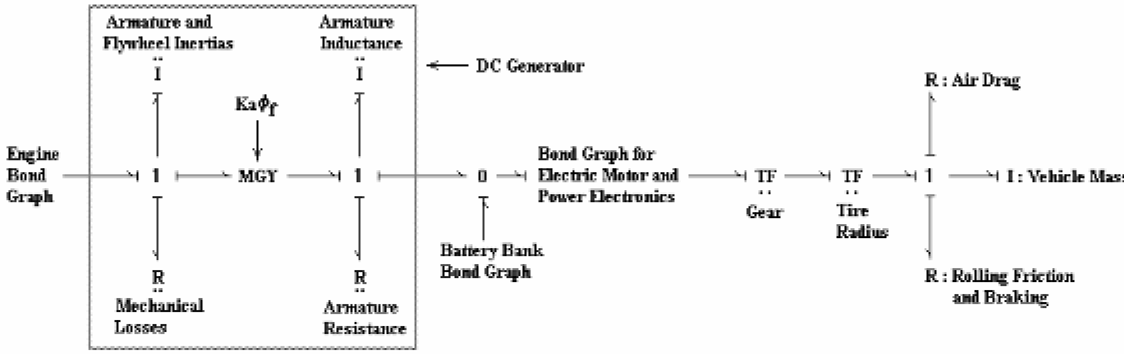

Figure 5.2.6: Series Hybrid Vehicle Bond Graph.

5.3Initial Design Analysis - Initial Parameter Value Estimates

Hybrid vehicle mass, power supply ratings and performance are interdependent parameters. The power and torque from the power supplies vary with speed and time. Power supply ratings affect the mass of the vehicle. Thus, estimates for parameter values are made based on the performance predictions from simulations using models. This saves time and money in costly experimentation. However, simulations using the detailed models are too slow to be practical for parameter value estimation. Simpler models are used to make initial parameter value estimates. Once predictions of detailed plant dynamics are observed with the detailed models, further adjustments to parameter value estimates can be intelligently made. The development of the simple models and the methods of estimating hybrid vehicle mass are presented in this sub-section.

5.3.1Simple Model for Parallel Hybrid Vehicle Power Plant

The mass of the parallel hybrid vehicle is determined by equation 5.3.1. The power from the batteries needs to be a little higher than that of the electric motor to compensate for the motor's efficiency which can be inferred from the bond graph model in figure 5.2.1.

$$M_{Tot} = M_{Veh} + P_{ICE} \cdot \rho_{ICE} + P_{EM}\left(\rho_{EM} + {\rho_{Batt}}/{\eta_{EM}}\right) \qquad \textbf{Equation 5.3.1}$$

In this design, the power from the ICE will be designed to sustain the maximum desired cruising speed, V_c, on a level grade. The power requirement at the maximum cruising speed is defined by the road load and the cruising speed as shown in equation 5.3.2. This power specification can be divided into an engine torque/speed specification. The engine speed is directly related to the velocity of the vehicle through the engine's gear ratio and the tire radius as shown by equation 5.3.3. The power specification of the electric machine is handled in the same way that it was in section 4 and is shown in equation 5.3.4. The speed of the electric motor is handled in a fashion similar to equation 5.3.3 but with the gear ratio that is unique to the electric motor.

$$P_{ICE} = \left(\frac{1}{2} C_D \rho_{air} A_f V_C^2 + M_{Tot} g C_F\right) V_C = RoadLoad \cdot V_C = (T\omega)_{C_{ICE}}$$ **Equation 5.3.2**

$$\omega_{C_{ICE}} = V_C \cdot GR_{ICE} / R_T$$ **Equation 5.3.3**

$$P_{EM} = T_{MaxEM} \omega_b$$ **Equation 5.3.4**

Combining equations 5.3.1 through 5.3.5 and isolating the total vehicle mass yields the expression shown in equation 5.3.5.

$$M_{Tot} = \frac{M_{Veh} + \left(\frac{1}{2} C_D \rho_{air} A V_C^3\right) \rho_{ICE} + T_{MaxEM} \omega_b \left(\rho_{EM} + {\rho_{Batt}}/{\eta_{EM}}\right)}{1 - g C_F V_C \rho_{ICE}}$$ **Equation 5.3.5**

The summation of forces accelerating the mass of the vehicle are found using the power supply torque specifications, the gear ratios, the tire radius, the base rotor speed specification, the rotor speed, ω_r, and road load value as shown in equation 5.3.6.

$$\sum F = \begin{cases} T_{ICE} \cdot GR_{ICE}/R_T + T_{MaxEM} \cdot GR_{EM}/R_T - \text{RoadLoad} & \text{if } \omega_r < \omega_b \\ T_{ICE} \cdot GR_{ICE}/R_T + T_{MaxEM} \dfrac{\omega_b}{\omega_r} \cdot GR_{EM}/R_T - \text{RoadLoad} & \text{if } \omega_r \geq \omega_b \end{cases}$$

Equation 5.3.6

These equations were used in a simple spreadsheet simulation of a parallel hybrid vehicle. Parameter values were changed until the acceleration specifications could be reasonably met or exceeded. The final parameter values are shown in table 5.3.1. The resulting performance for these parameters is shown in figure 5.3.1.

Parallel Hybrid Vehicle Settings												
M_{veh} (kg)	**ρ_{batt}** (kg/w)	**ρ_{em}** (kg/w)	**ρ_{ICE}** (kg/w)	**T_b** (N/m)	**ω_b** (rad/s)	**A_c** (m^2)	**C_d**	**C_f**	**TR** (m)	**GR_{ICE}**	**GR_{EM}**	**V_{mc}** (m/s)
930	0.012	9E-04	3E-03	60	320	2	0.33	0.015	0.267	5	12	46
$P_{EM\,Max}$ (kW)	**M_{tot}** (kg)	**P_{ICE}** (kW)	**ω_{ICE}** (rpm)	**T_{ICE}** (N/m)	**V_b** (m/s)	**M_{tot}** (lbs)	**P_{PP}** (kW)	**V_{10}** (mph)	**EMG Over Rating**	**T_{ICE} Avg**	**Max Air Drag** (N)	**Batt Mass** (kg)
19.2	1845	51.84	8227	60.2	7.120	4067	71.04	60.1	3	1.1	855.4	691

Table 5.3.2: Parameter Values for a Simple Simulation of a Parallel Hybrid Vehicle Power Plant.

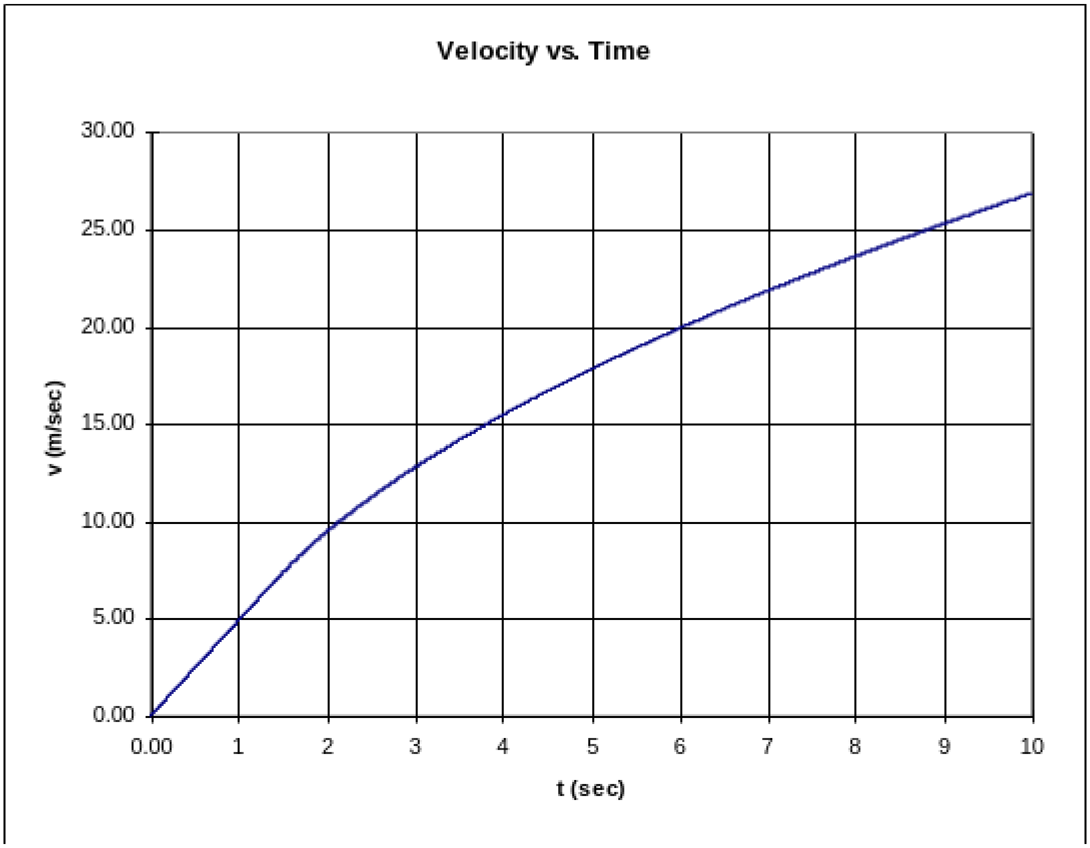

Figure 5.3.7: Predicted Acceleration Performance of a Parallel Hybrid Vehicle Using Parameter Values from Table 5.3.1.

5.3.2Simple Model for Series Hybrid Vehicle Power Plant

The mass of the series hybrid vehicle is determined using equation 5.3.7. The power required from the batteries is the maximum power of the motor minus the maximum power of the generator. The reasons for this are discussed in section 5.1.4. Since the battery mass is being calculated using the motor power, the motor power must be divided by the efficiency of the motor which can be inferred from the bond graph in figure 5.2.2.

$$M_{Tot} = M_{Veh} + P_{ICE} \cdot \rho_{ICE} + P_{GEN} \cdot \rho_{GEN} + P_{MOT} \cdot \rho_{MOT} + \left(\frac{P_{MOT}}{\eta_{MOT}} - P_{GEN} \right) \cdot \rho_{Batt}$$

Equation 5.3.7

The engine specifications are designed to meet a desired steady state road load as was done with the parallel hybrid. But, the power from the ICE, must pass through the generator, and the power from the generator must pass through the electric motor to deliver power to overcome the road load. During each of these transmissions, power is reduced by the efficiency of each device. Using these considerations, and the specifications explained by equations 5.3.2 and 5.3.4, the total mass of the vehicle is estimated using equation 5.3.8.

$$M_{Tot} = \frac{M_{Veh} + \left(\frac{1}{2}C_D\rho_{air}AV_C^3\right)\cdot\left(\frac{\rho_{ICE}}{\eta_{GEN}\cdot\eta_{MOT}} + \frac{\rho_{GEN}}{\eta_{MOT}}\right) + T_{MaxMOT}\omega_b\left(\rho_{MOT} + \frac{\rho_{Batt}}{\eta_{MOT}}\right)}{1 + gC_F V_C\left(\frac{\rho_{Batt}}{\eta_{MOT}} - \frac{\rho_{ICE}}{\eta_{GEN}\cdot\eta_{MOT}} - \frac{\rho_{GEN}}{\eta_{MOT}}\right)}$$

Equation 5.3.8

All of the power plant's power must pass through the electric motor. Therefore, the electric motor specifications, the gear ratio, the tire radius and the road load calculations are used for the simulation of the simple dynamic model. These calculations are shown by equation 5.3.9.

$$\sum F = \left.\begin{matrix} T_{MaxEM}\cdot GR_{EM}/R_T - \text{RoadLoad} \\ \\ T_{MaxEM}\dfrac{\omega_b}{\omega_r}\cdot GR_{EM}/R_T - \text{RoadLoad} \end{matrix}\right\} \begin{matrix} \text{if} \quad \omega_r < \omega_b \\ \\ \text{if} \quad \omega_r \geq \omega_b \end{matrix}$$

Equation 5.3.9

These equations were used in a simple spreadsheet simulation of a series hybrid vehicle. Parameter values were changed until the acceleration specifications could be reasonably met or exceeded. The final parameter values are shown in table 5.3.2. The resulting performance for these parameters is shown in figure 5.3.2.

Electrical Parallel / Series Hybrid Vehicle Settings													
M_{veh} (kg)	**ρ_{batt}** (kg/w)	**ρ_{em}** (kg/w)	**ρ_{ICE}** (kg/w)	**T_b** (N/m)	**ω_b** (rad/s)	**A_c** (m^2)	**C_d**	**C_f**	**R_T** (m)	**GR_{ICE}**	**GR_{EM}**	**V_{mc}** (m/s)
930	0.012	9E-04	3E-03	80	320	2	0.33	0.015	0.267	5	12	43
P_{EM} Nom (kW)	**M_{tot}** (kg)	**P_{ICE}** (kW)	**ω_{ICE}** (rad/s)	**T_{ICE}** (N/m)	**V_b** (m/s)	**M_{tot}** (lbs)	**P_{PP}** (kW)	**V_{10}** (mph)	**EMG Over Rating**	**T_{ICE} Avg**	**Max Air Drag** (N)	**Batt Mass** (kg)
26	1705	42.93	805	53.308	7.120	3758	68.53	61.61	3	1.0	747.5	406.5

Table 5.3.3: Parameter Values for a Simple Simulation of a Electrical Parallel / Series Hybrid Vehicle Power Plant.

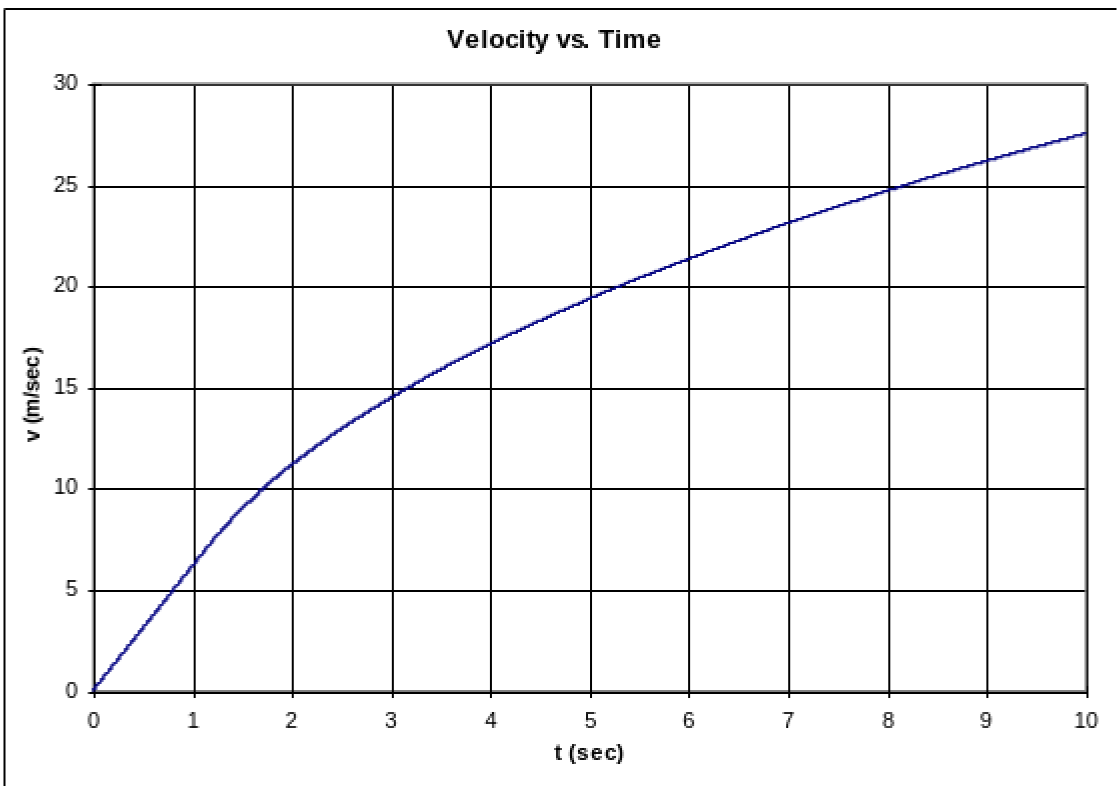

Figure 5.3.8: Predicted Acceleration Performance of an Electrical Parallel / Series Hybrid Vehicle Using Parameter Values from Table 5.3.2.

5.3.3Remarks

When the initial estimates using the simple models were compared to the final estimates using the detailed models, they were more diverse than the initial and final estimates made for the single power plant vehicles. Previously, these differences in estimations were primarily due to the simple models' inability to account for battery dynamics. However, there are additional reasons for this diversion when simulating the HVPP's. The exchange and coordination of power supply dynamics in a HVPP cannot be adequately predicted by the simple models. Therefore, larger adjustments were necessary when using the detailed models to meet the performance specifications. But, estimations of parameter values for the HVPP's using the simple models still proved to be helpful, because they saved time in the use of the detailed models.

5.4Graphic Model Synthesis of HVPP Components

ACSL graphic models were built from the MRD components and the detailed power plant sub-component models. These graphic models were formed by following the bond graph models for series and parallel configurations. These bond graph models were derived from the system diagrams. Each of the HVPP models in this section use a gasoline powered ICE, one or two electric machines and a bank of batteries. Each plant architecture was altered by using first a dc traction motor and then an IM.

5.4.1Parallel Hybrid Plants

The first two HVPP concepts to be presented are a parallel HVPP that uses a dc traction motor, figure 5.4.1, and a parallel HVPP that uses an induction traction motor, figure 5.4.2. The two traction motor controllers were not set up to do regenerative braking due to limitations with the batteries that were previously discussed in section 3.4 and 5.1. If regenerative braking were performed, only a minimal amount of braking force could be achieved due to these battery limitations. The power blocks labeled "HEV Engine," "Separately Excited DC Machine," and "Rectifier Inverter & # Induction Machine(s)" (where # is the number of IM's used) are compound power blocks that contain their respective power supply models and MRD power supply interface blocks. Local control exists for each power supply, and central control is accomplished by both the "Hybrid Driver" power block and the "Hybrid Logic #" power block where # is a version number. Code for all Driver and logic control power blocks can be found in Appendix J. Because a clutch is present, state variables throughout the drive train will need to be reset anytime the clutch starts to disengage for reasons discussed in section 3.1.

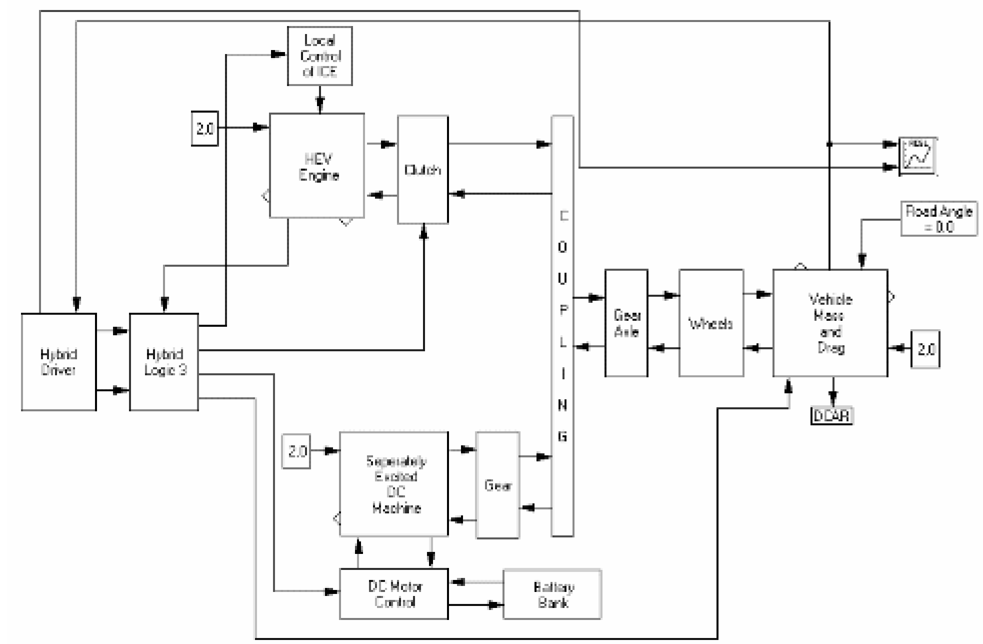

Figure 5.4.9: ACSL Graphic Model for a Parallel Hybrid Vehicle Power Plant that Uses a DC Traction Motor.

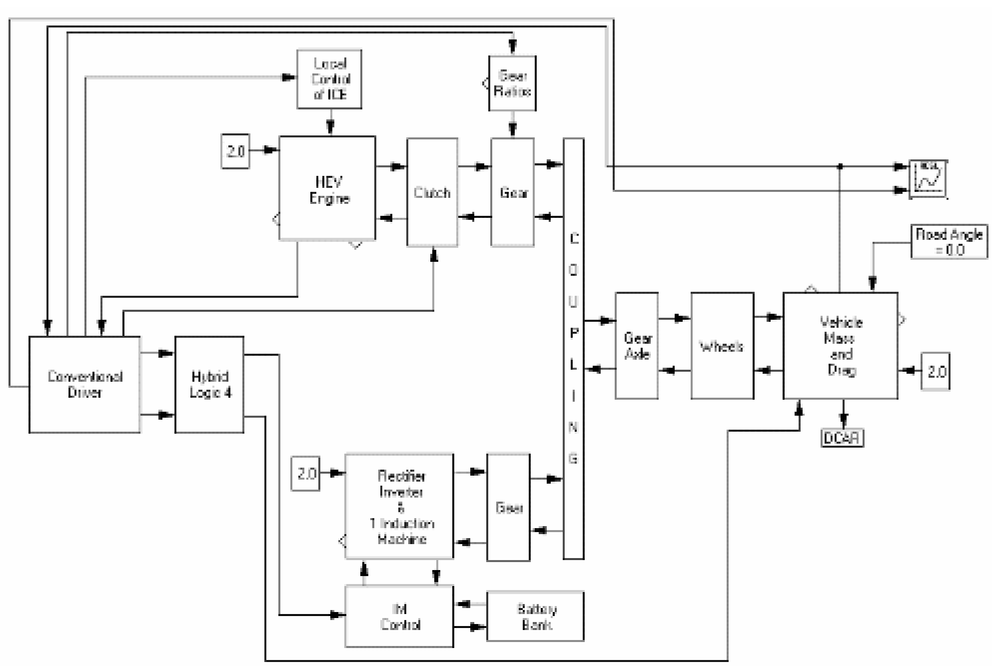

Figure 5.4.10: ACSL Graphic Model for a Parallel Hybrid Vehicle Power Plant that Uses an Induction Traction Motor.

5.4.2Series Hybrid with DC Motor

The second two HVPP concepts to be presented are a series HVPP that uses a dc traction motor, figure 5.4.3, and a series HVPP that uses an induction traction motor, figure 5.4.4. This configuration is also referred to as an electrical parallel HVPP, because, for these studies, the dc generator will be running more often so that battery mass can be reduced. Again, the two traction motor controllers were not set up to do regenerative braking due to battery limitations and due to the minimal amount of braking force that can be achieved. And, again, the power blocks labeled “HEV Engine,” “Separately Excited DC Machine,” and “Rectifier Inverter & # Induction Machine(s)” are compound power blocks containing power supply models and MRD power supply interface blocks. Local control exists for each power supply, and central control is partially applied by the driver. The other controller labeled “EV Logic #” is the same essential controller used for the electric vehicles. Power coordination is crucial for this configuration, but it can be adequately achieved by the local controllers. Therefore, there is no specific hybrid controller logic. Since no clutch is present in this configuration, resetting of state variables will not be necessary.

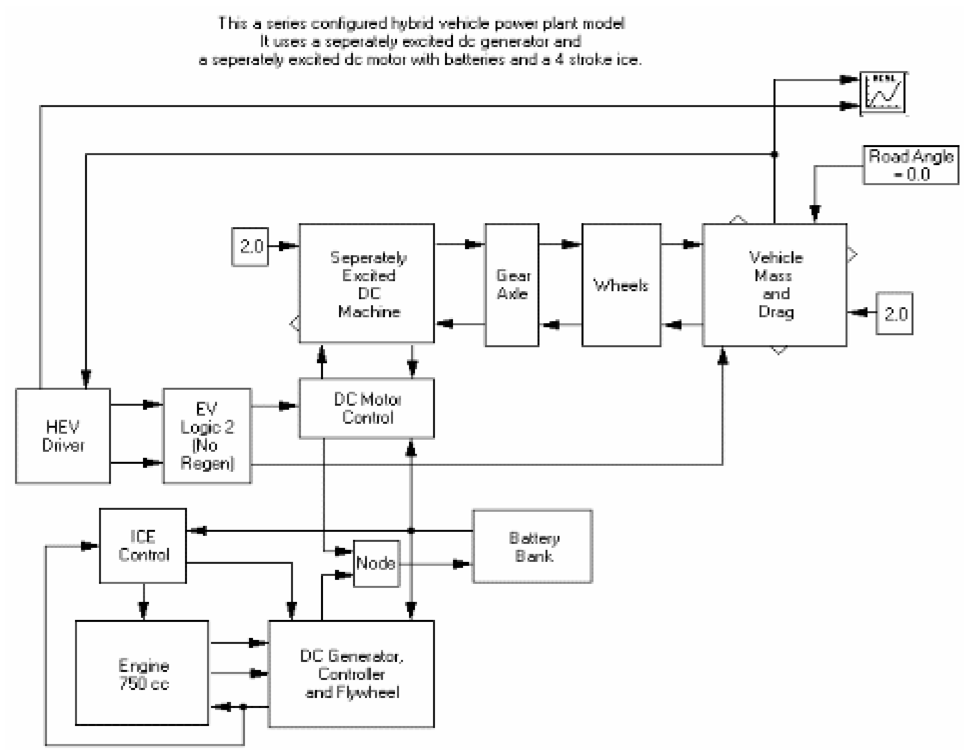

Figure 5.4.11: ACSL Graphic Model for an Electrical Parallel / Series Hybrid Vehicle Power Plant that Uses a DC Traction Motor.

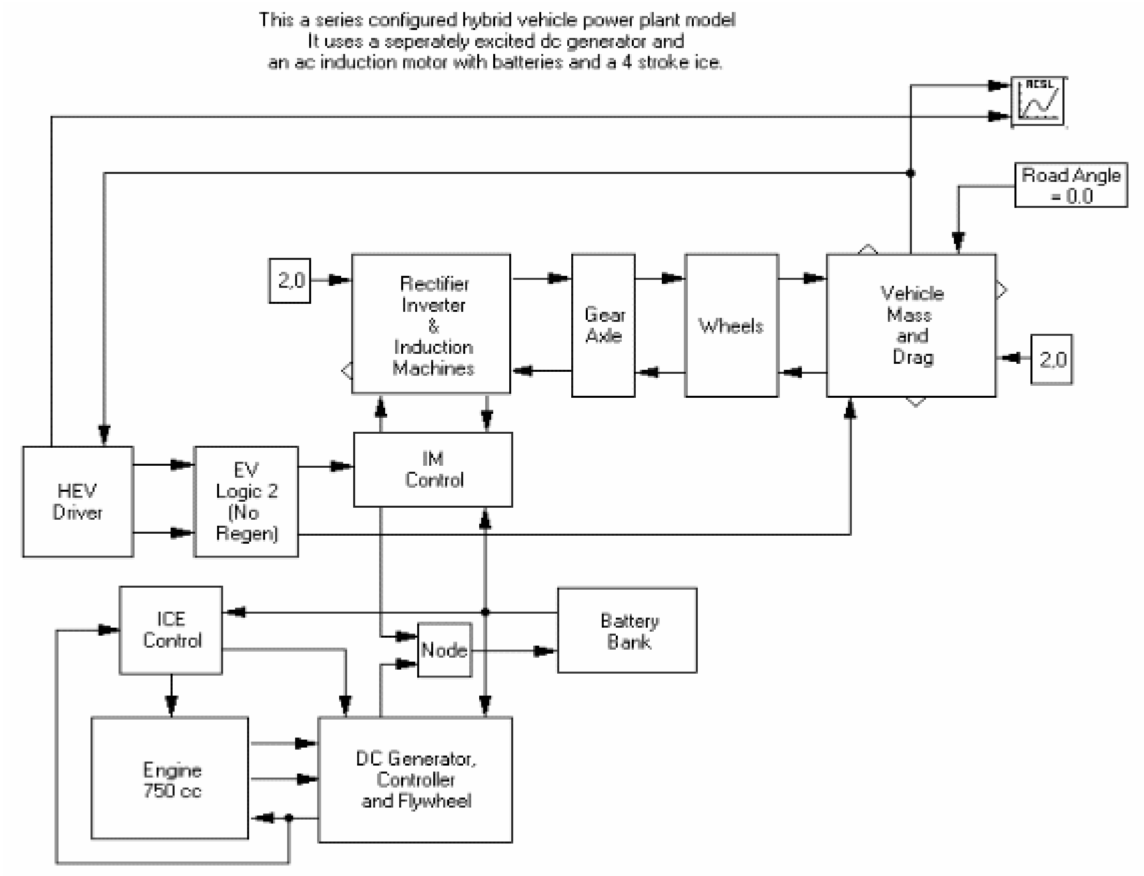

Figure 5.4.12: ACSL Graphic Model for an Electrical Parallel / Series Hybrid Vehicle Power Plant that Uses an Induction Traction Motor.

5.5Design of the Hybrid Vehicle's Power Supply Components

Specific methods of designing the individual power supplies are too lengthy to cover in this work. The method used in this work to design ICE's were derived from [1]. An overview of these methods can be found in Appendix B. The methods used in this work to design electric machines can be found in [25]. Only existing battery designs were used in this work. But, guidelines in battery design can be found in [31].

The induction motor used for the modeling studies and validations in section 3.3 was suitable for the HVPP's simulated in this section. The parallel HVPP in figure 5.4.2 uses one IM of this design. The series plant in figure 5.4.4 uses two of these IM's.

It was necessary to use a larger ICE engine than the Ascot for the plants used in this study. This engine's intake system configuration is also different from the Ascot's engine configuration. It uses a single throttle valve on an intake manifold to feed two intake ports. The configuration is adequately illustrated by the ACSL graphic model for this engine which is shown in figure 5.5.1. The specific parameter values developed for this model can be found in Appendix B. The torque speed plot at wide open throttle for this engine is shown in figure 5.5.2.

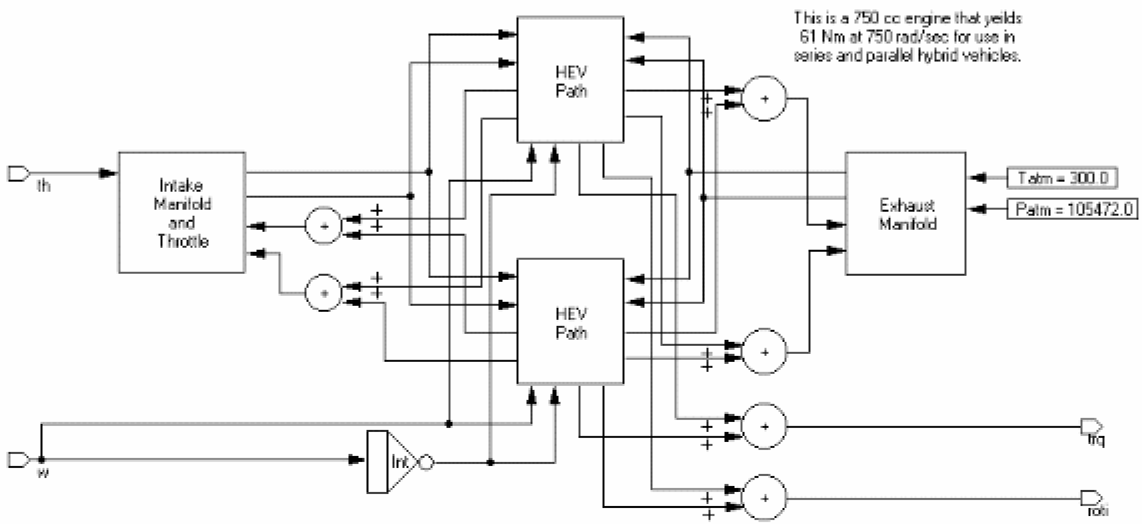

Figure 5.5.13: ACSL Graphic Model for the Engine Used in the HVPP Models.

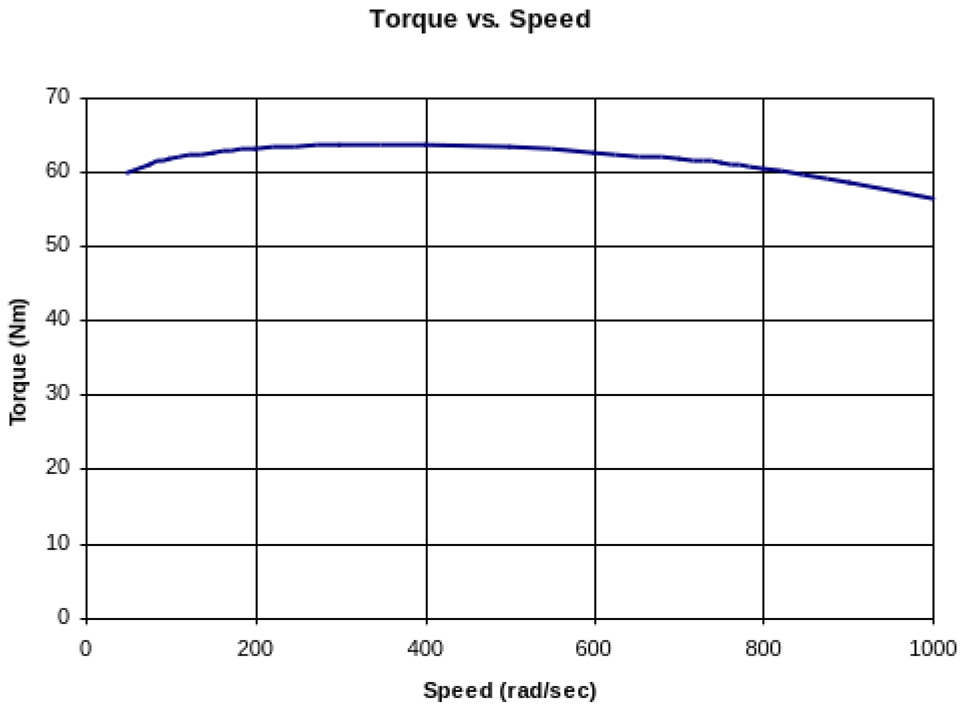

Figure 5.5.14: Predicted Torque Speed Characteristics for the Engine Used in the HVPP Models.

5.6Simulations

There are essentially two stages in the development of the detailed models. The first stage involves balancing the power supply ratings and coordinating the multiple power supplies to achieve stable operation. The second stage involves adjustment of the design parameter values to improve the predicted performance of the HVPP.

Achieving proper coordination of the power supplies was the most difficult task in the first stage. The problems with this coordination existed at the local controller level for the parallel electric / series hybrid. It was necessary to alter typical control schemes for these devices, so that they would work properly in a HVPP configuration. These redesigns proved to be interesting sensitivity studies. Each of the parallel hybrids were initially stable.

Balancing power supply ratings was not a problem for these configurations. The simple simulations used to make initial parameter value estimates proved to be good for estimating the proper balance of power supply ratings. However, due to speed dependent performance parameters and variations in efficiency, the power supply ratings were over specified by 10% to 15%. This resulted in adequate power supply ratings for each configuration. The detailed power supply designs were derived from these estimated power supply ratings, and the parameter values from the detailed designs were used in the detailed models.

The second stage was to identify sensitivities between design and performance parameters. This involves finding design parameters that significantly affect the performance parameters of interest. Once found, these design parameters are adjusted to improve the predicted performance parameters. In these studies, adjustments were made to the configuration, the controllers and the drive train parameters to illustrate the utility of the models. In a real design scenario, a designer would also adjust power supply parameters to achieve the desired performance. But, power supply parameters were not adjusted for the following reason. Acceleration was the performance parameter studied in this work to illustrate the utility of the modeling methods. It is well known that any design changes to the power supplies will affect this performance parameter. It is desirable to achieve the desired acceleration specification using the smallest power supply ratings possible. Therefore, the individual power supplies are designed to be as efficient and as small as practically possible, and then attempts to improve plant performance are made by trying to change configurations, control parameters and drive train parameters. However, several other performance parameters will be studied by the end users of these methods, and parameter value adjustments can be made to the power supply models while they are in the detailed models. But, it might be preferable to make some of these adjustments on individual power supply test beds to save time.

All the vehicles in this section were modeled using Ford Taurus vehicle parameters. The values for vehicle mass (including the driver) with no power supplies, aerodynamic drag coefficient, rolling friction coefficient, and frontal area are given in tables 5.3.1 and 5.3.2. Conventional drive train mass was assumed equivalent to hybrid power plant drive train mass.

5.6.1Parallel Hybrids

5.6.1.1Using a DC Motor

The first parallel hybrid vehicle used a 750 cc ICE, a separately excited dc machine with a maximum output of 45 kW, and 20 lead acid deep cycle batteries weighing 520 kg. The overall constant gear ratio from the engine to the wheels was 5.0. The overall constant gear ratio from the dc motor to the wheels was 12.0. This vehicle’s maximum acceleration is shown in figure 5.6.1.

In the first design of this plant, the engine throttle and clutch were controlled by the central control scheme. In this scheme and in this configuration, the gear ratio for the engine is constant and is designed to utilize the engine for high speed cruising. Therefore, the clutch engagement speed must occur at a faster vehicle speed than in a conventional vehicle configuration to avoid stalling the engine. The dc motor was utilized in acceleration transients only.

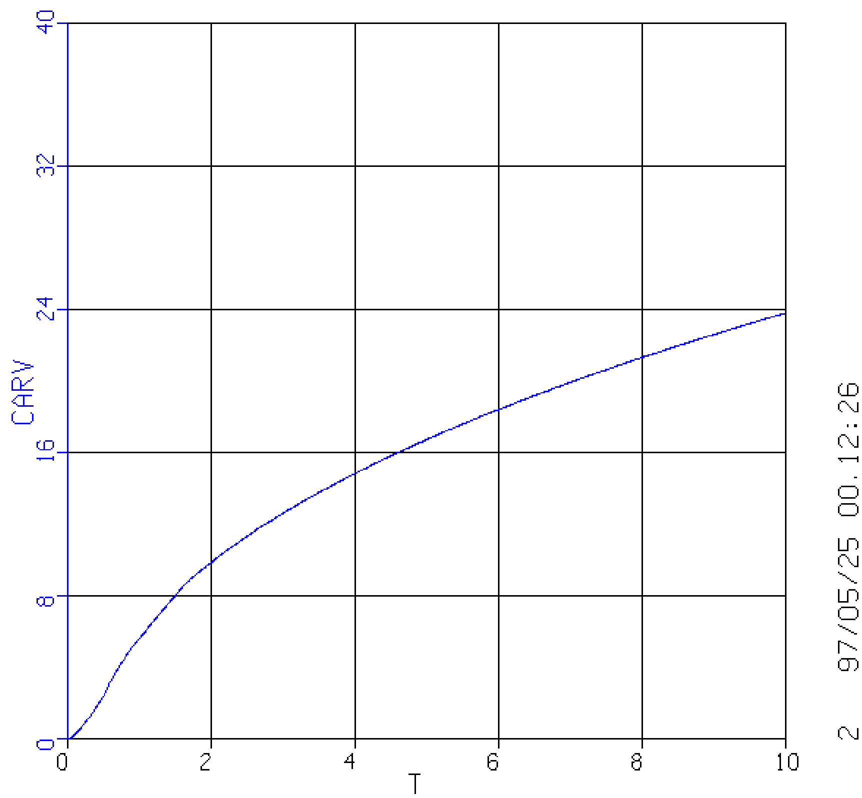

Figure 5.6.15: Velocity (m/sec) verses Time (sec) for Maximum Acceleration of the Parallel HVPP / DC Motor Design.

The motor controller voltage and the battery bank voltage are plotted together verses time in figure 5.6.2. Note that the battery bank voltage drops to a low of 75 volts during the acceleration transient. The initial open circuit voltage of the battery bank is approximately 250 volts. This calculates to a 70% drop in voltage for the transient. This may seem excessive, but it is typical for maximum EV transients.

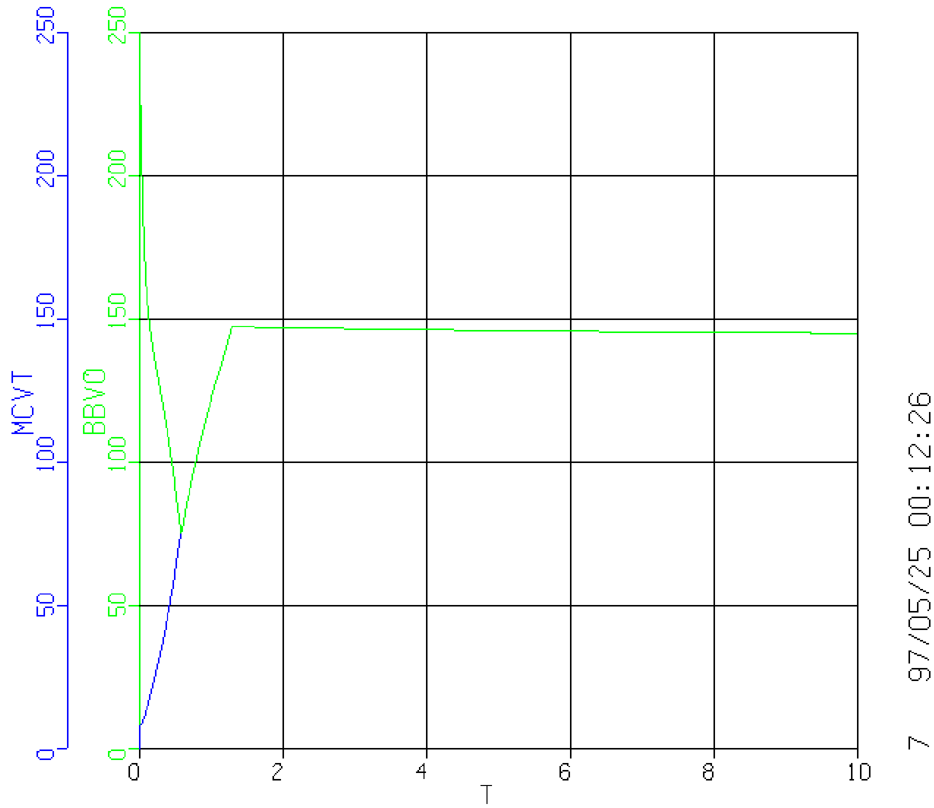

Figure 5.6.16: Motor Controller Voltage (solid line) and Battery Bank Voltage (dotted line) verses Time (sec) for Maximum Acceleration of the Parallel HVPP / DC Motor Design.

Engine rpm and vehicle velocity are plotted together in figure 5.6.3. Note the hard downward spike in engine rpm that occurs at the beginning of the plot.

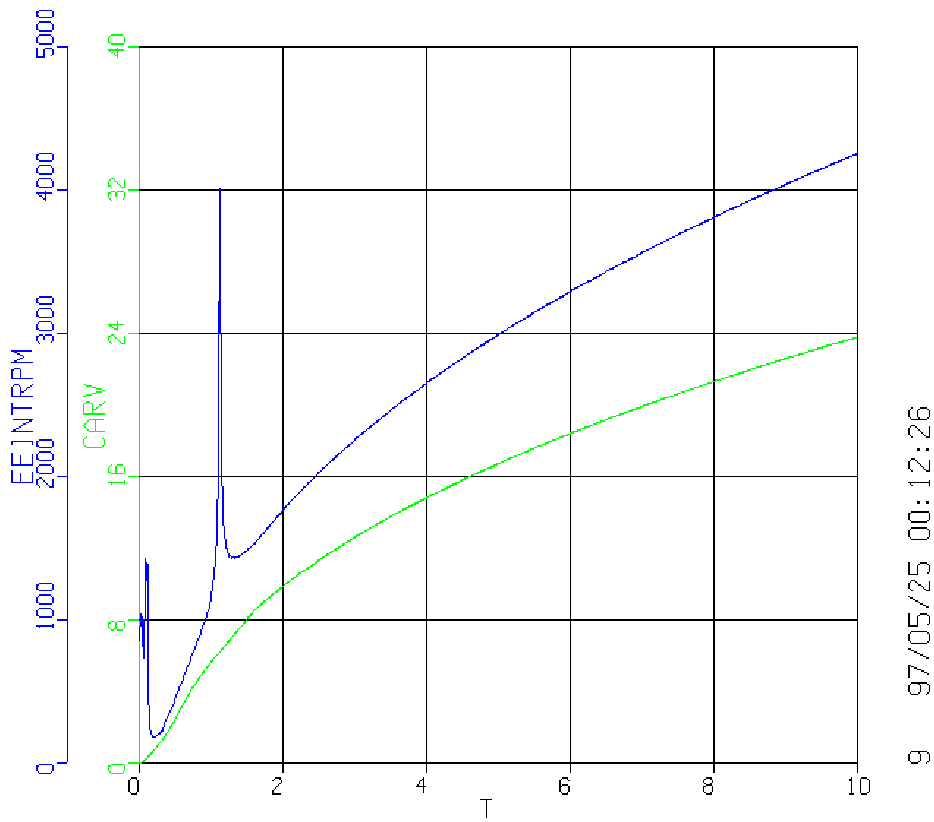

Figure 5.6.17: Engine RPM (solid line) and Vehicle Velocity (m/sec, dotted line) verses Time (sec) for Maximum Acceleration of the Parallel HVPP / DC Motor Design.

This downward spike is due to the clutch control scheme. The engine throttle, in this design, is not allowed to actuate until a certain vehicle speed is reached. Then, the clutch automatically engages at a certain rpm. This scheme did not account for drifts in rpm during initial engine starting. Thus, the clutch tried to engage the engine to the drive train when the vehicle speed was too low, and the engine rpm feel rapidly below the clutch disengagement set point, and the clutch disengaged. Once the vehicle speed reached the set point to actuate the engine throttle, the engine rpm rose rapidly, and the clutch engaged the second time. This entire scenario is further demonstrated using the plot of engine rpm and clutch actuation shown in figure 5.6.4.

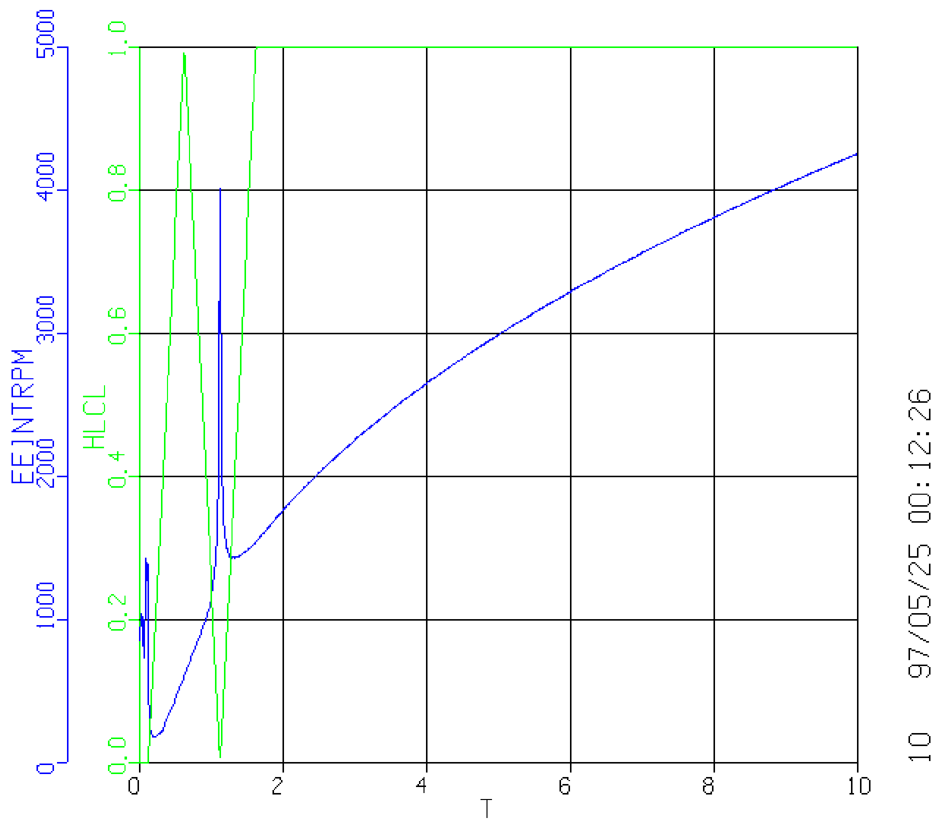

Figure 5.6.18: Engine Speed (RPM, solid line) and Clutch Actuation (dotted line) verses Time (sec) During Maximum Acceleration of the Parallel HVPP / DC Motor Design.

The first improvement in the acceleration performance of this vehicle was made by placing a variable transmission between the clutch and coupling to better utilize the engine's torque over a wider range vehicle speed range. Clutch and throttle control of the engine was given to the driver. The electric motor was used when the engine could not completely supply the driver's torque command. These changes to the virtual HVPP test bed are shown in figure 5.6.5.

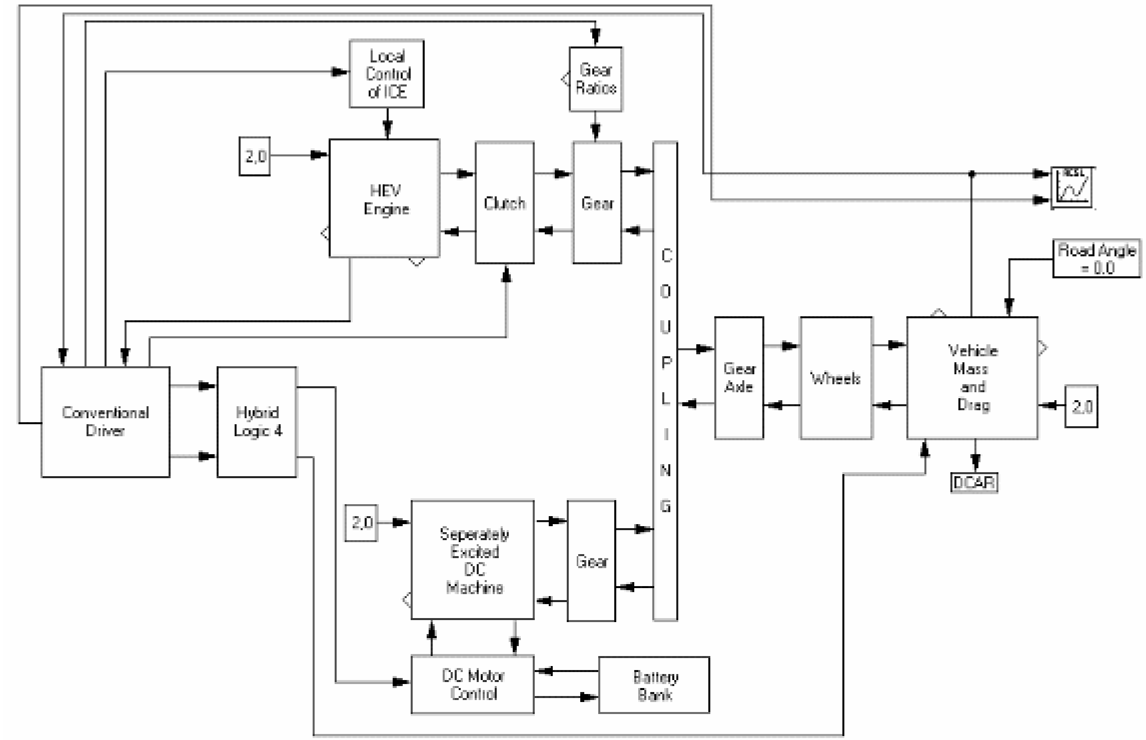

Figure 5.6.19: New Design for the Parallel HVPP / DC Motor.

The initial improvement in the acceleration resulting from these controller and configuration design changes is shown in figure 5.6.6. Note the flat spots in the vehicle velocity during gear shifting. These occur, because the electric motor is controlled by the driver's torque command, and the driver zeros his torque command during shifting. The simulated driver could also shift faster.

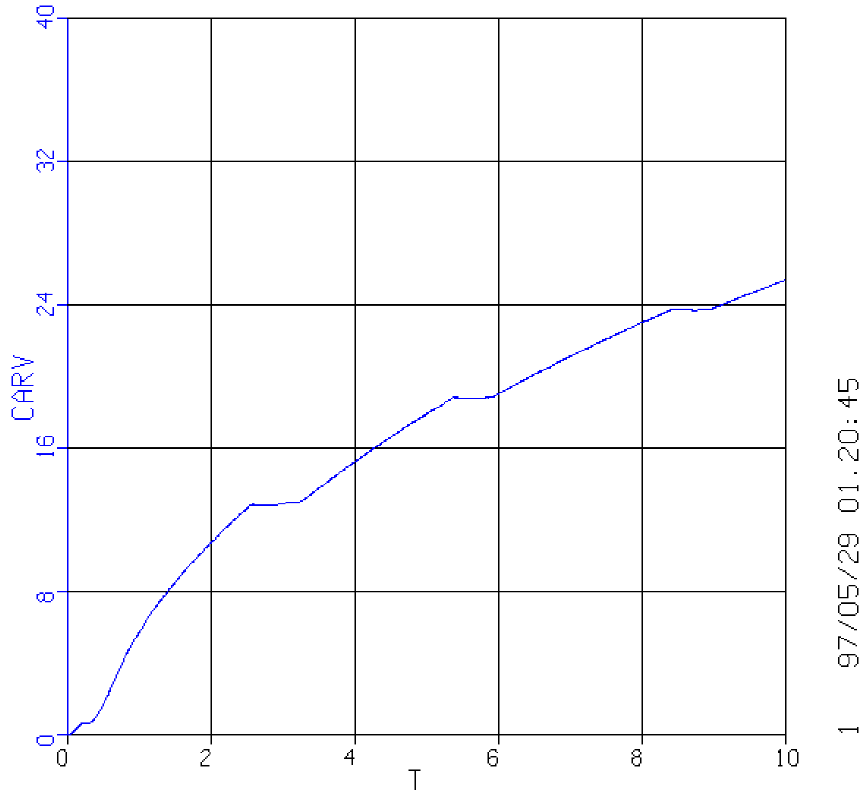

Figure 5.6.20: Velocity (m/sec) verses Time (sec) during Maximum Acceleration of the New Design for the Parallel HVPP with the DC Motor Off during Shifting.

These two considerations were applied to the model, and the resulting improvement in acceleration is shown in figure 5.6.7.

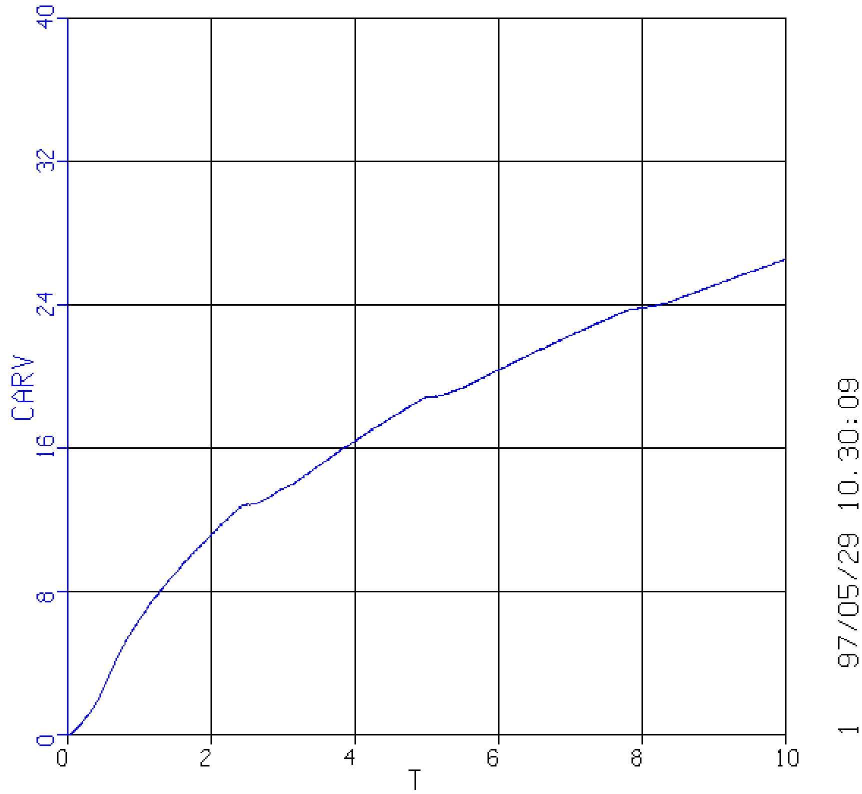

Figure 5.6.21: Velocity (m/sec) verses Time (sec) during Maximum Acceleration of the New Design for the Parallel HVPP with the DC Motor On during Shifting and with Faster Driver Shifting.

The battery bank voltage drop is only slightly reduced by the increased low vehicle speed utilization of the engine as shown in figure 5.6.8

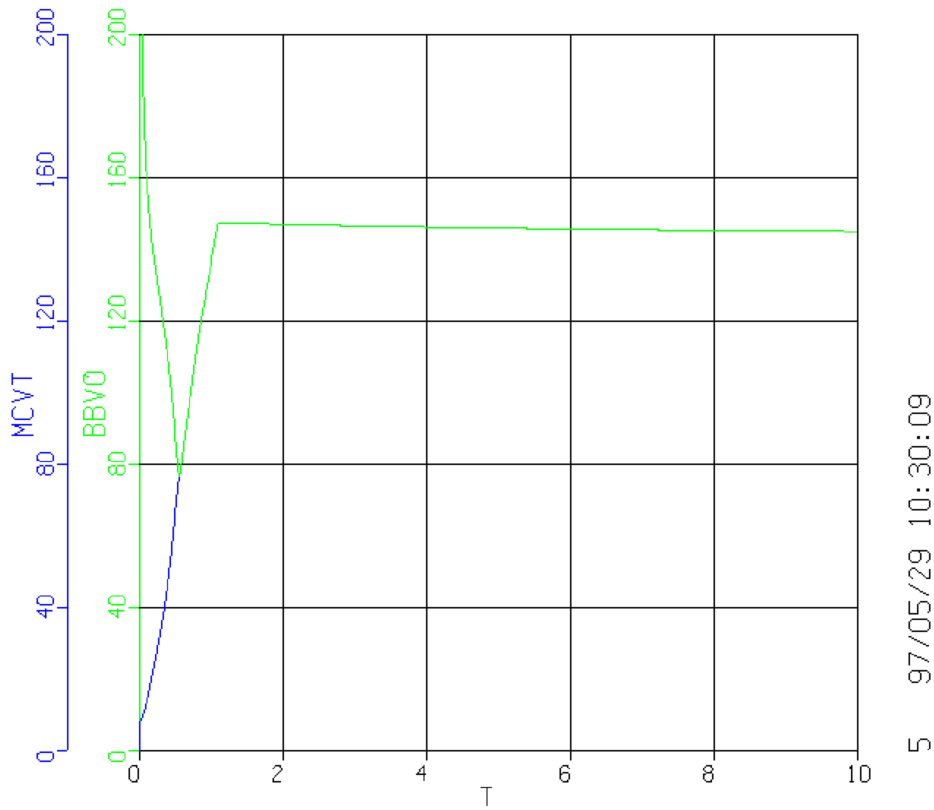

Figure 5.6.22: Motor Controller Voltage (solid line) and Battery Bank Voltage (dotted line) verses Time (sec) for Maximum Acceleration of the Parallel HVPP / DC Motor Design that Uses Gear Shifting for the ICE.

5.6.1.2Using an Induction Motor

The first design of the parallel HVPP that uses an induction motor was made using the final configuration and drive train design from section 5.6.1.1. The same parameters were used with one exception. The battery bank used 28 deep cycle batteries that were smaller than the ones used in the previous section, and the overall battery bank weighed the same.

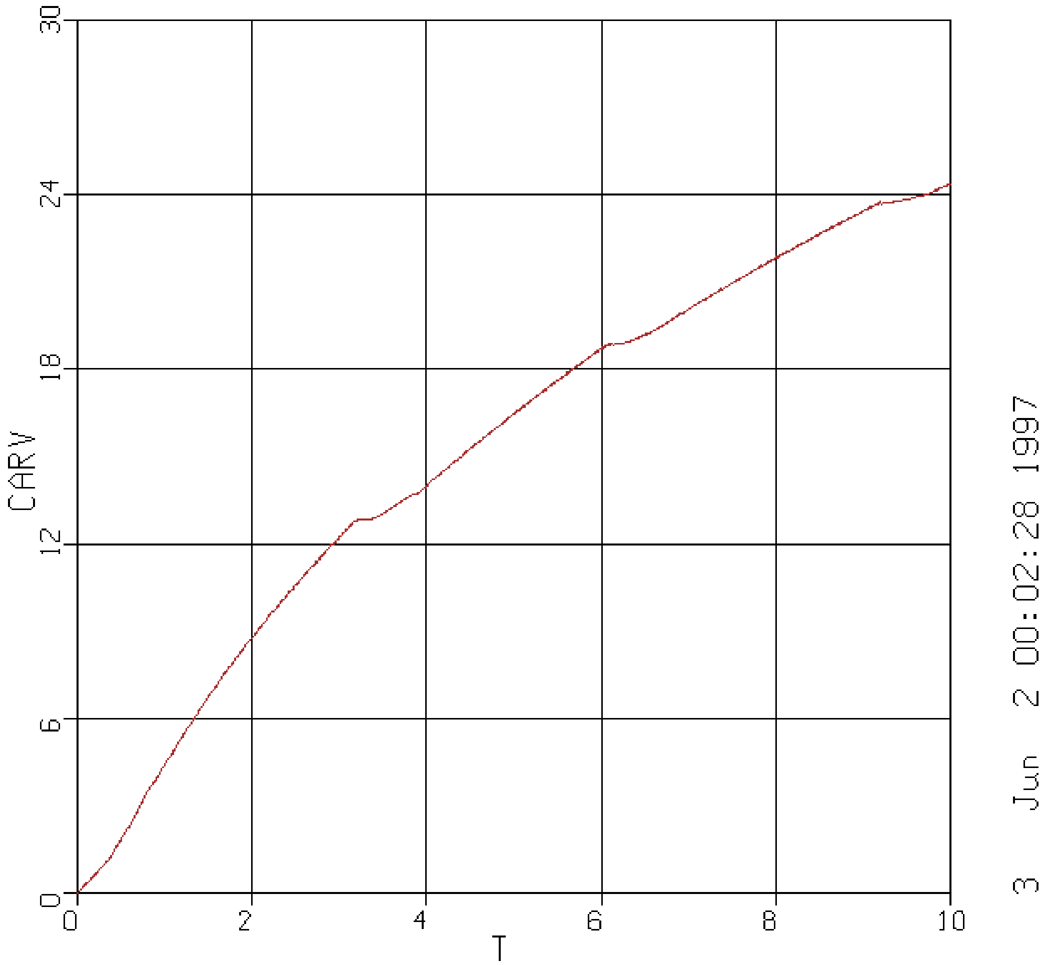

Figure 5.6.23: Velocity (m/sec) verses Time (sec) during a Maximum Acceleration of the Parallel HVPP with IM Design.

The acceleration for the initial design of this virtual plant is shown in figure 5.6.9.

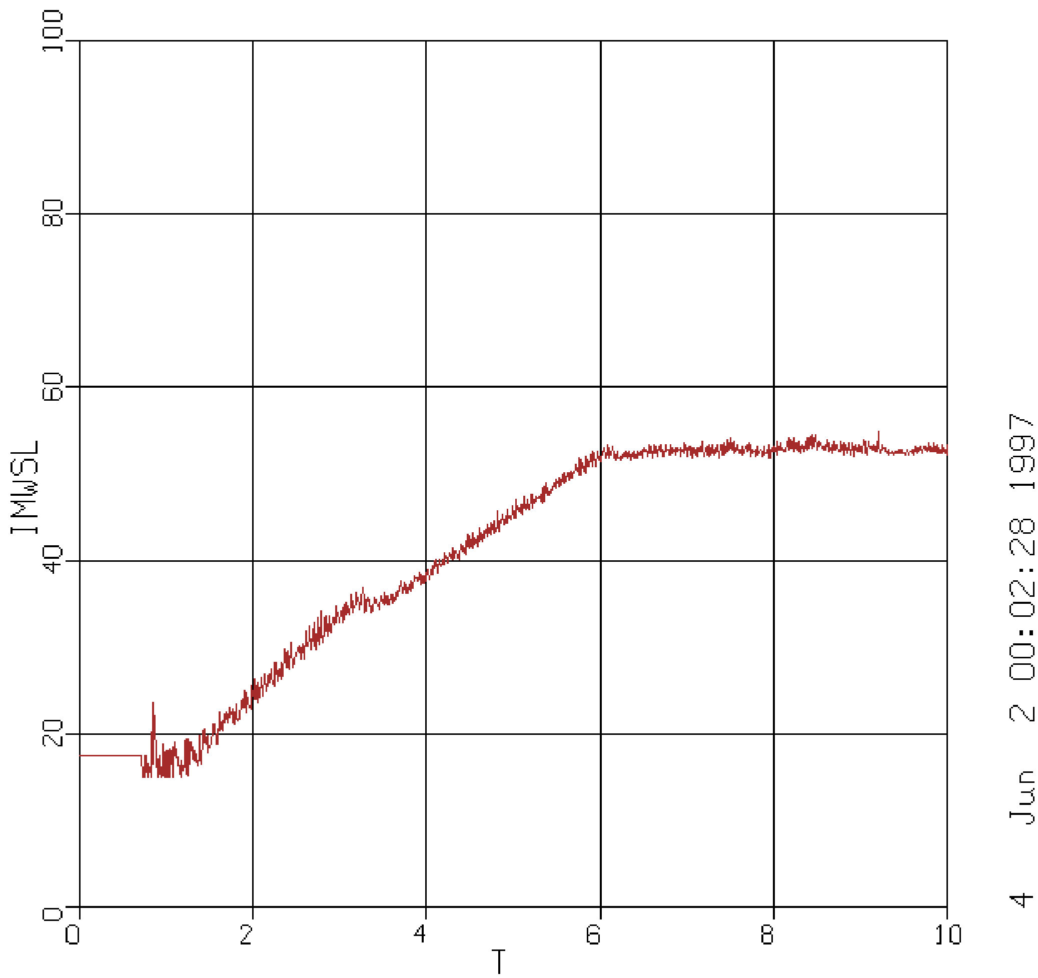

Figure 5.6.24: Slip Speed (rad/sec) verses Time (sec) for Maximum Acceleration of the Parallel HVPP / IM Design.

The slip speed of the IM during this acceleration transient is shown in figure 5.6.10. The slip could be higher without exceeding the breakdown torque as long as the voltage level of the batteries does not drop too significantly. The IM controller voltage and battery bank voltage for this transient are shown in figure 5.6.11. Note that the voltage drops to almost 280 volts. Based on this analysis, four more batteries will be added to the battery bank in the next simulation. This will add approximately 104 kg of batteries, copper cable and battery frame to the mass of the vehicle, but will allow the IM controller to draw more power at higher speeds. The higher power will be achieved by allowing a greater amount of slip and current draw in the IM.

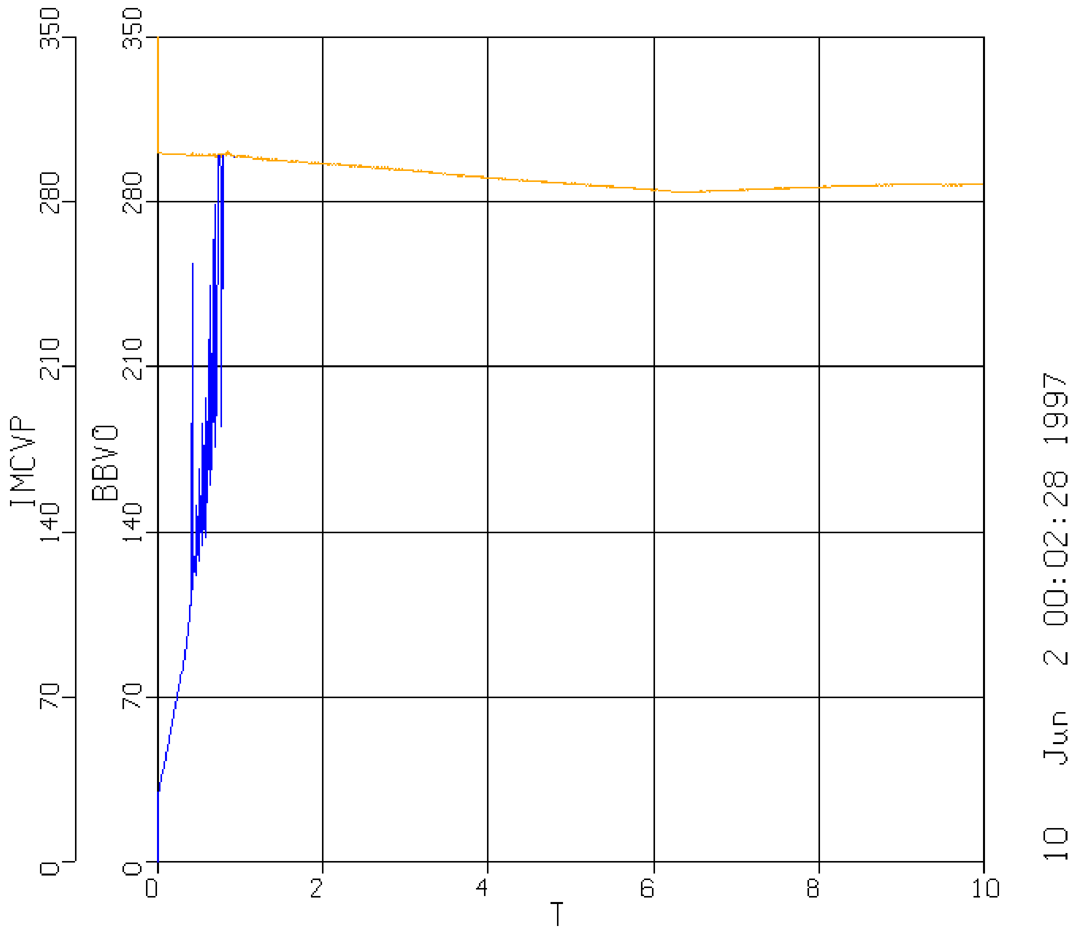

Figure 5.6.25: IM Controller Voltage (lower line) and Battery Bank Voltage (upper line) verses Time (sec) for a Maximum Acceleration of the Parallel HVPP with IM Design.

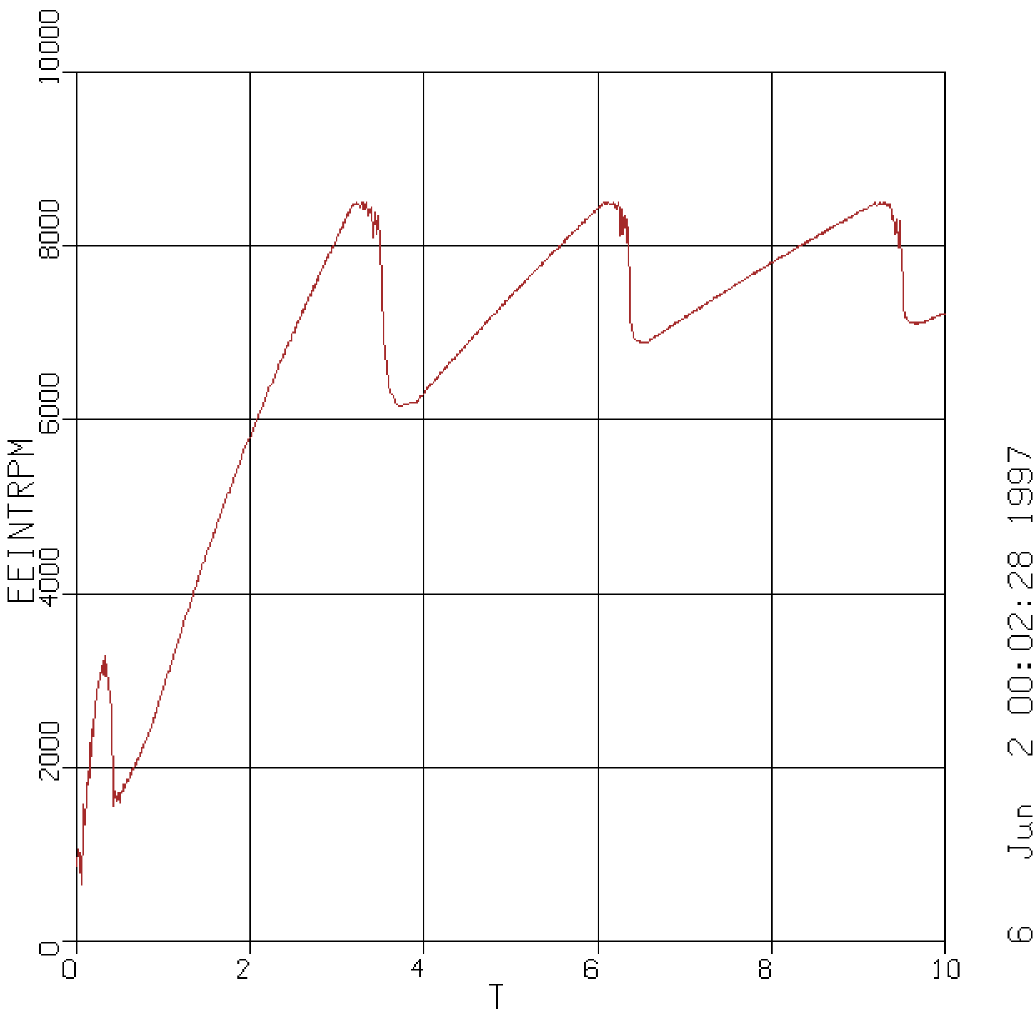

Figure 5.6.26: Engine RPM verses Time (sec) for Maximum Acceleration of the Parallel HVPP / IM Design.

Another control adjustment is also made to allow more power from the engine. The engine speed during the initial design's maximum acceleration transient is shown in figure 5.6.12. The engine can safely exceed the maximum rpm's indicated in figure 5.6.12 for short periods of time. Therefore, in the next simulation, the driver will shift at a slightly higher rpm. Furthermore, the first five gear ratios will be increased for the next simulation. This is done to achieve higher torques at the wheels, and thus greater vehicle acceleration, for lower vehicle speeds. The resulting improvement in vehicle acceleration due to the extra batteries, the increase IM power draw, higher gear ratios for the first five gears, and the driver shifting at higher engine rpm's is shown in figure 5.6.13.

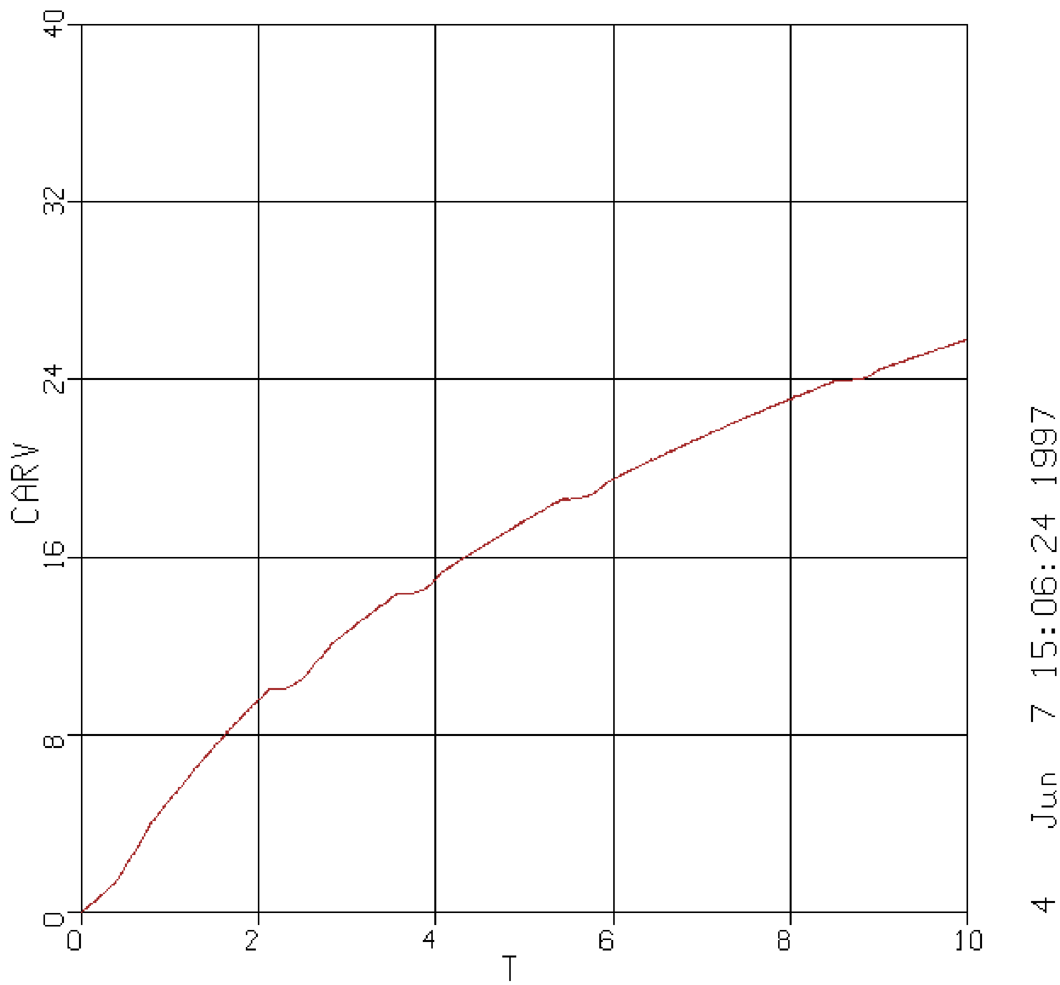

Figure 5.6.27: Velocity (m/sec) verses Time (sec) during Maximum Acceleration of the Parallel HVPP / IM Design after Controller, Battery Bank and Gear Ratio Changes.

After analyzing figure 5.6.14, that shows the IM controller voltage and the battery bank voltage, it seems that it might be possible to achieve even more slip without exceeding the breakdown torque. However, as more slip is used, more power is drawn and the battery bank voltage will drop even lower. This scenario will result in a lower available breakdown torque. Furthermore, the open circuit voltage will drop even lower with time. Therefore, it is best to be conservative at this point, and make sure that there is a good margin for available battery bank voltage.

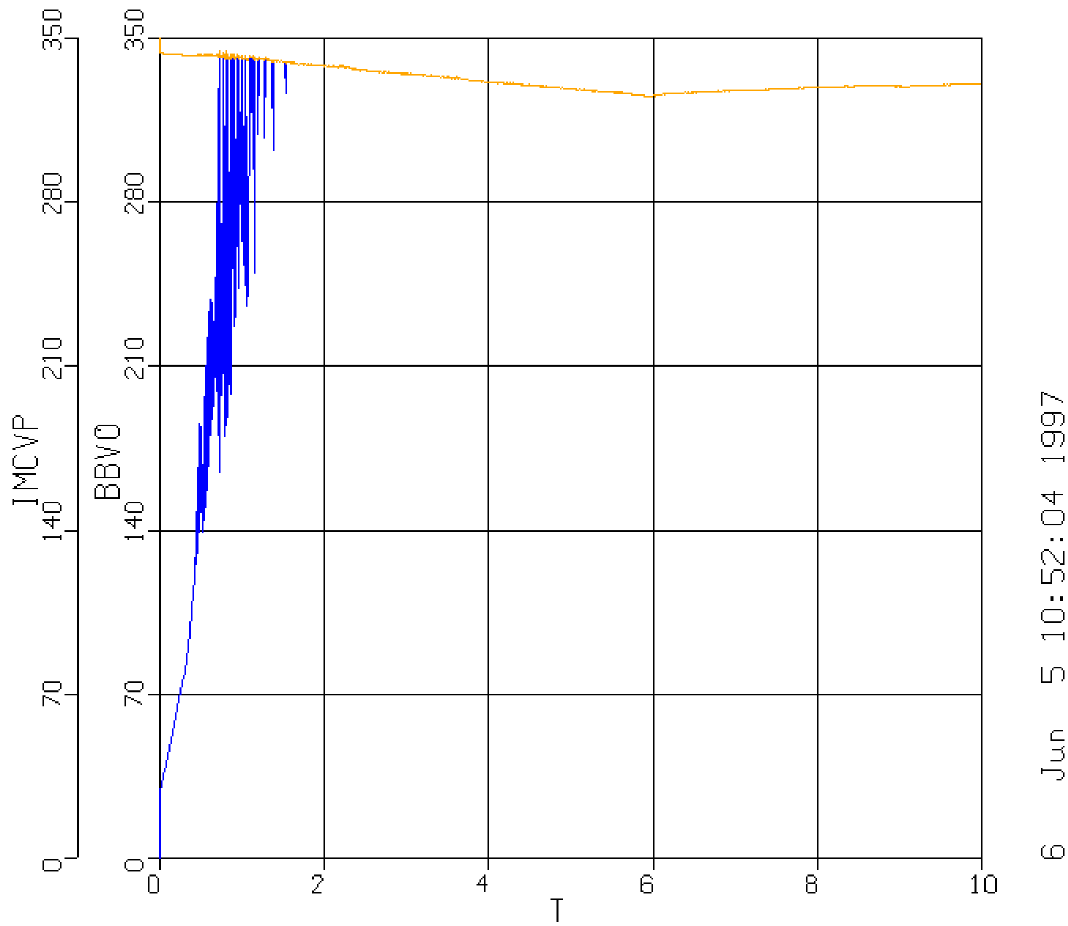

Figure 5.6.28: IM Controller Voltage (lower line) and Battery Bank Voltage (upper line) verses Time (sec) during Maximum Acceleration of the Parallel HVPP / IM Design after IM Controller, Battery Bank, and Gear Ratio Changes.

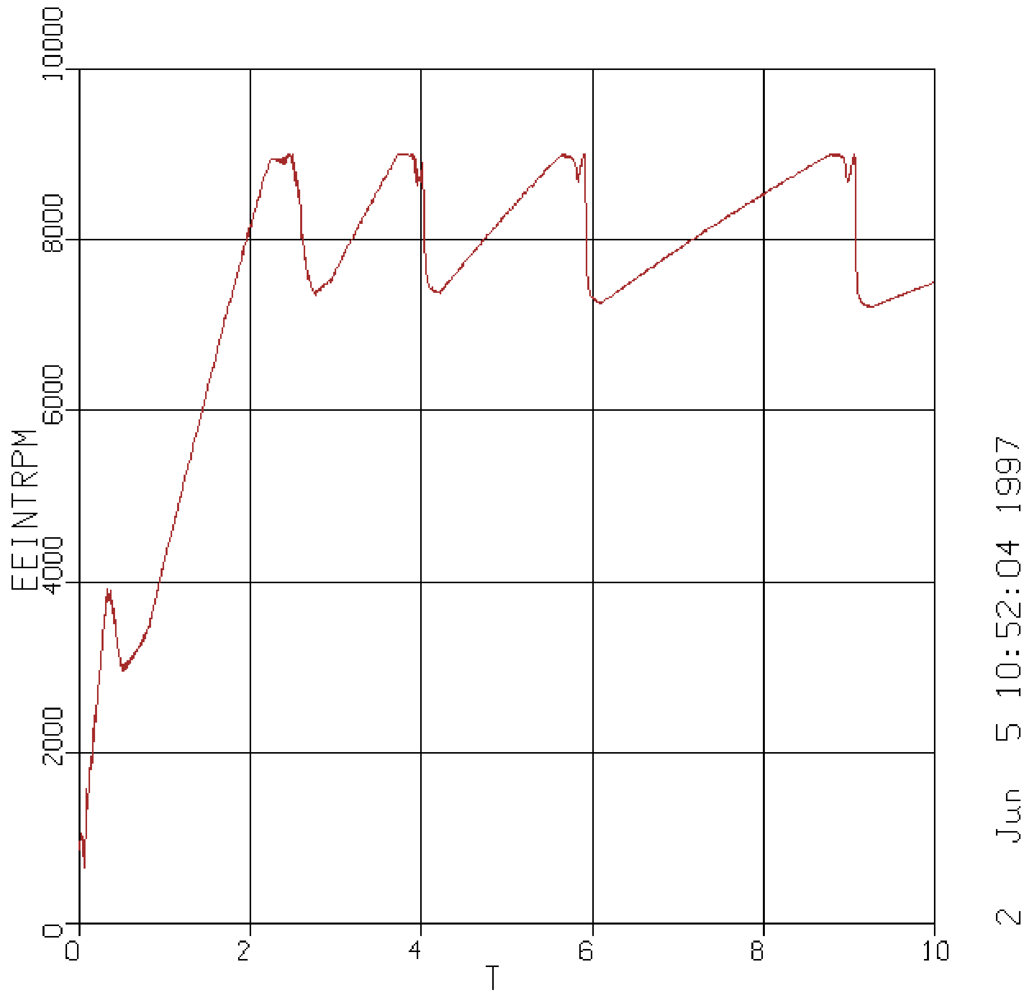

Figure 5.6.29: Engine RPM verses Time (sec) during Maximum Acceleration of the Parallel HVPP / IM Design after IM Controller, Battery Bank, and Gear Ratio Changes.

The effect of the gear ratio changes on the engine speed verses time for a maximum acceleration transient are shown in figure 5.6.15. The gear ratios for the first four gears were changed by the same percentage. The fifth gear was changed by a smaller percentage and the sixth gear was not changed. This allows improved low speed acceleration without reducing the vehicle's top speed.

5.6.2Electrical Parallel / Series Hybrids

The series HVPP is typically designed as an EV with an onboard charging system. With a few simple modifications, the virtual EV test beds developed and presented in the previous section would be more appropriate for studying such a HVPP. In order to better illustrate the usefulness of the design and modeling methodologies that have been developed, an atypical series HVPP was studied using the detailed models. This series plant is designed to utilize more power from the ICE / generator set and less power from the batteries. The battery bank is smaller, and the vehicle is lighter, because the power density of the engine / generator set is lower than that of the batteries. This design is not being promoted. It simply better illustrates the utility of the developed modeling tools. This type of HVPP is also called an electrical parallel HVPP.

5.6.2.1Using a DC Motor

The first electrical parallel HVPP (EP HVPP) used a 750 cc ICE, a 46 kW separately excited dc generator, a separately excited dc traction motor with a maximum output of 85 kW, and 20 lead acid deep cycle batteries weighing 520 kg. The dc generator was connected directly to the engine without a clutch. The overall constant gear ratio from the dc traction motor to the wheels was 12.0.

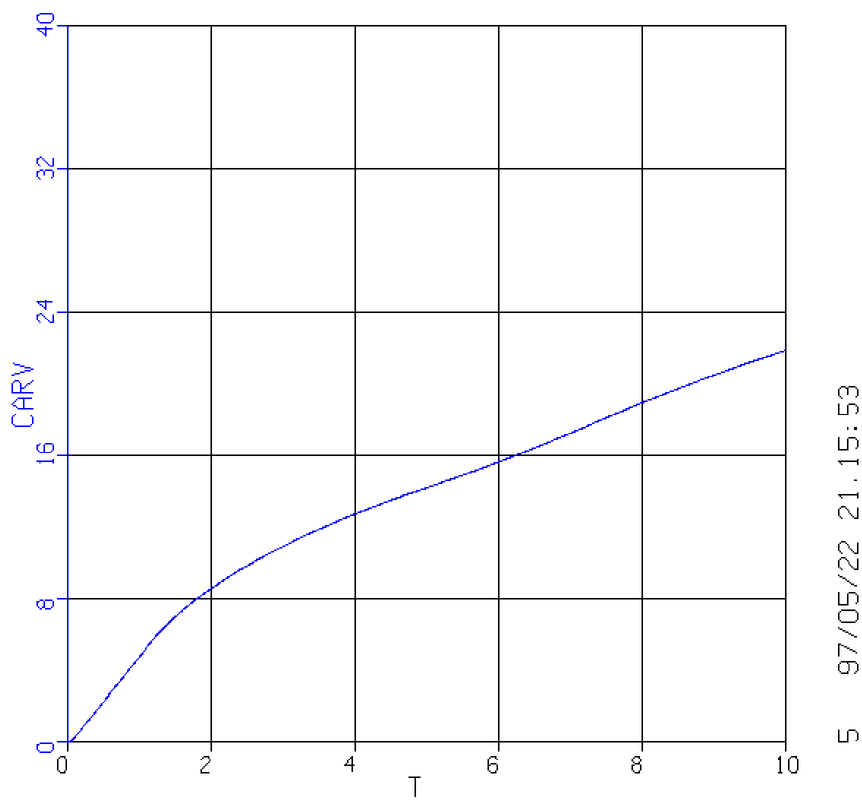

Figure 5.6.30: Velocity (m/sec) verses Time (sec) during Maximum Acceleration of the EP HVPP / DC Traction Motor Design.

In the first simulations of this plant, there was an obvious low power region between 2 and 8 seconds during the maximum acceleration shown in figure 5.6.16.

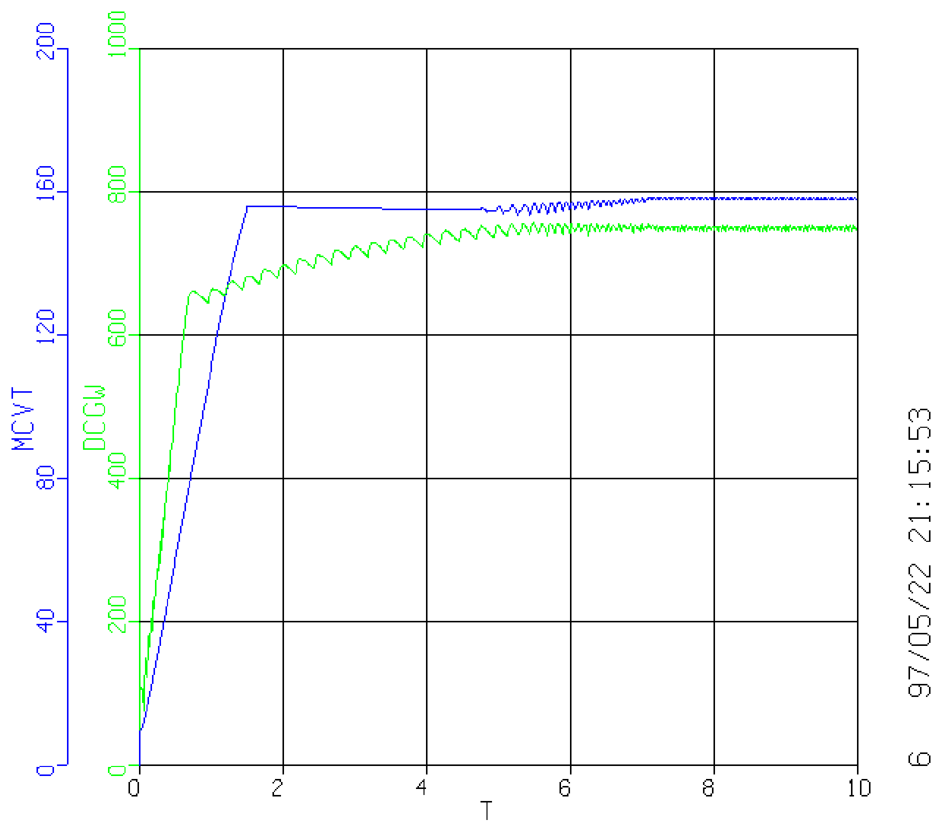

Figure 5.6.31: Motor Controller Voltage (solid line) and ICE / Generator Speed (rad/sec, dotted line) verses Time (sec) during Maximum Acceleration of the EP HVPP / DC Traction Motor Design.

To investigate the cause of the low power region, the motor controller output voltage and engine speed were analyzed first. These values are shown verses time in figure 5.6.17. The engine speed does not reach the desired operating speed of 750 (rad/sec) until approximately 5 seconds. The generator controller was set to give the highest output power at this speed. The DC motor controller was set to use a maximum voltage of 160 volts, and the motor controller output voltage is obviously being limited by the batteries.

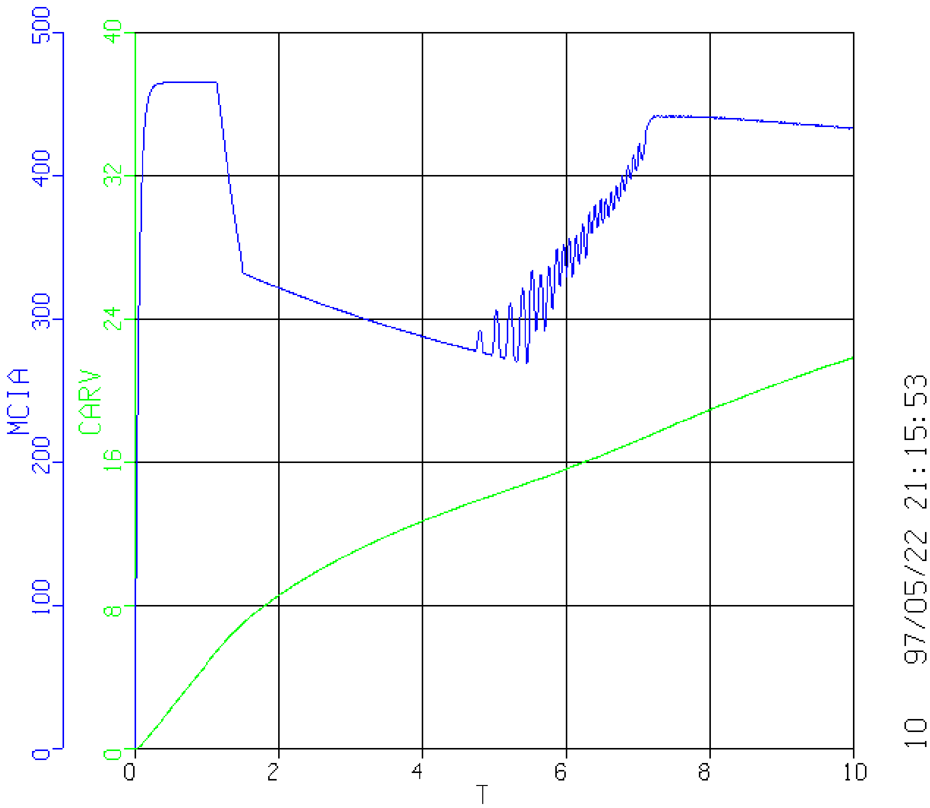

Figure 5.6.32: DC Motor Armature Current (amps, solid line) and Vehicle Velocity (m/sec, dotted line) verses Time (sec) during Maximum Acceleration of the EP HVPP / DC Traction Motor Design.

The next parameter to be analyzed was the dc motor armature current verses time shown in figure 5.6.18. The effect of the low power region is more obvious here, and is also seen in figure 5.6.19 for the dc motor output torque.

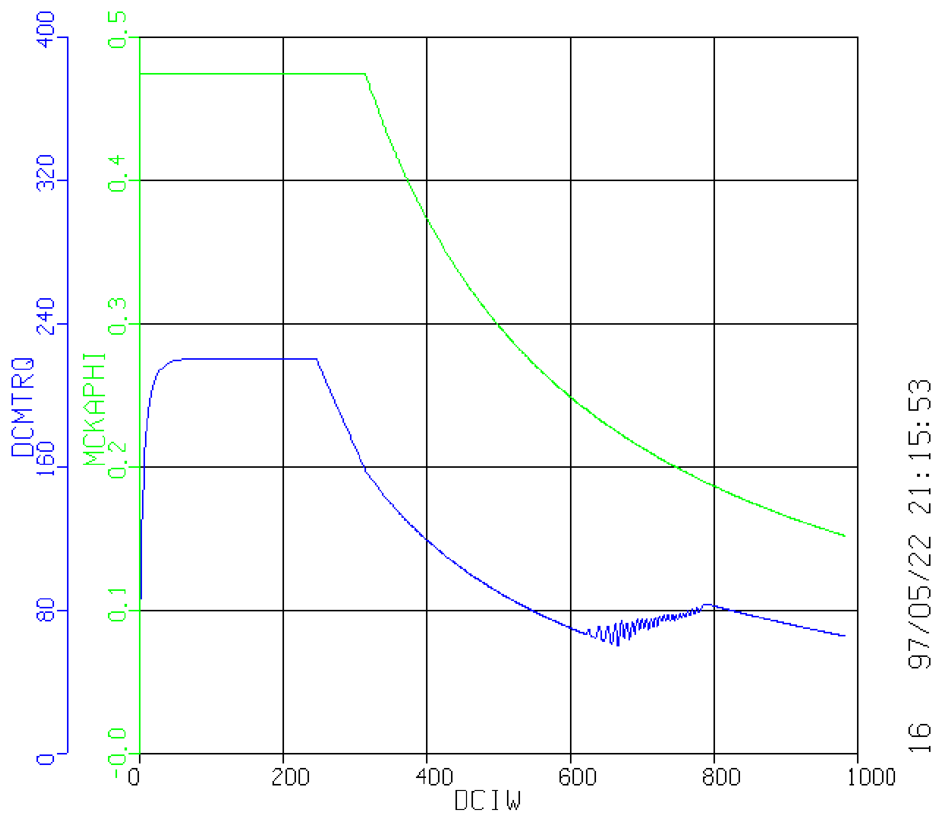

Figure 5.6.33: DC Motor Torque (Nm, solid line) and DC Motor Field (dotted line) verses Time (sec) during Maximum Acceleration of the EP HVPP / DC Traction Motor Design.

Since the batteries are giving as much power as possible, the generator armature current should be analyzed next.

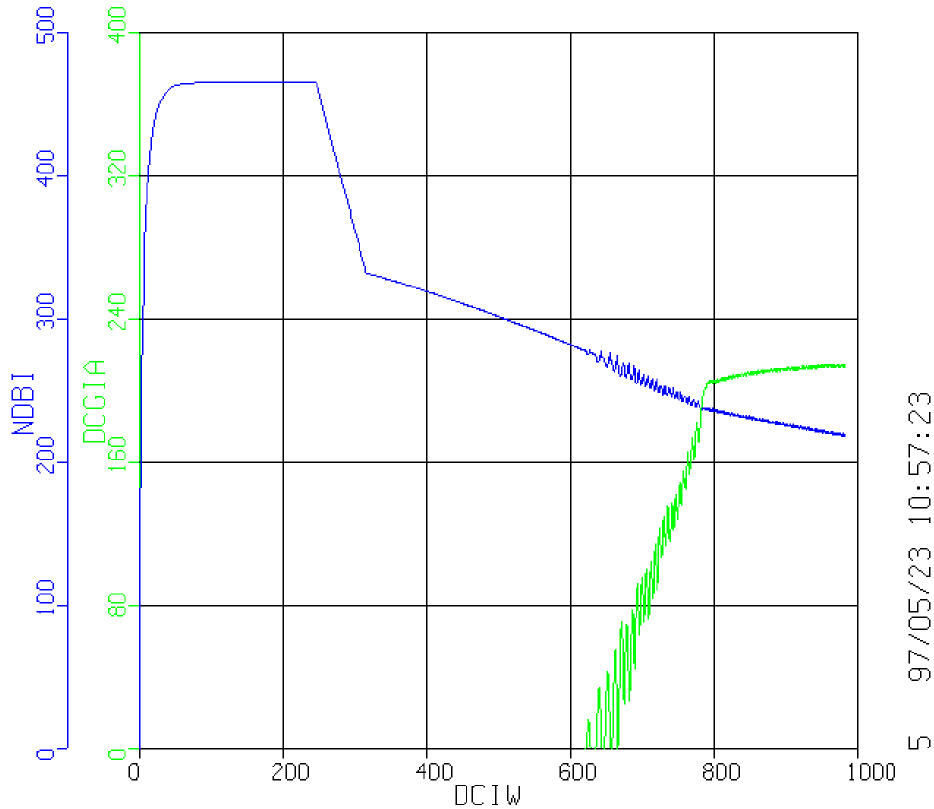

Figure 5.6.34: Battery Bank Current (amps, solid line) and DC Generator Armature Current (amps, dotted line) verses Time (sec) during Maximum Acceleration of the EP HVPP / DC Traction Motor Design.

From looking at figure 5.6.20, it is now obvious that the engine must come up to speed sooner so that the generator can provide current sooner to improve the acceleration of this vehicle. The ice controller was modified to achieve this objective.

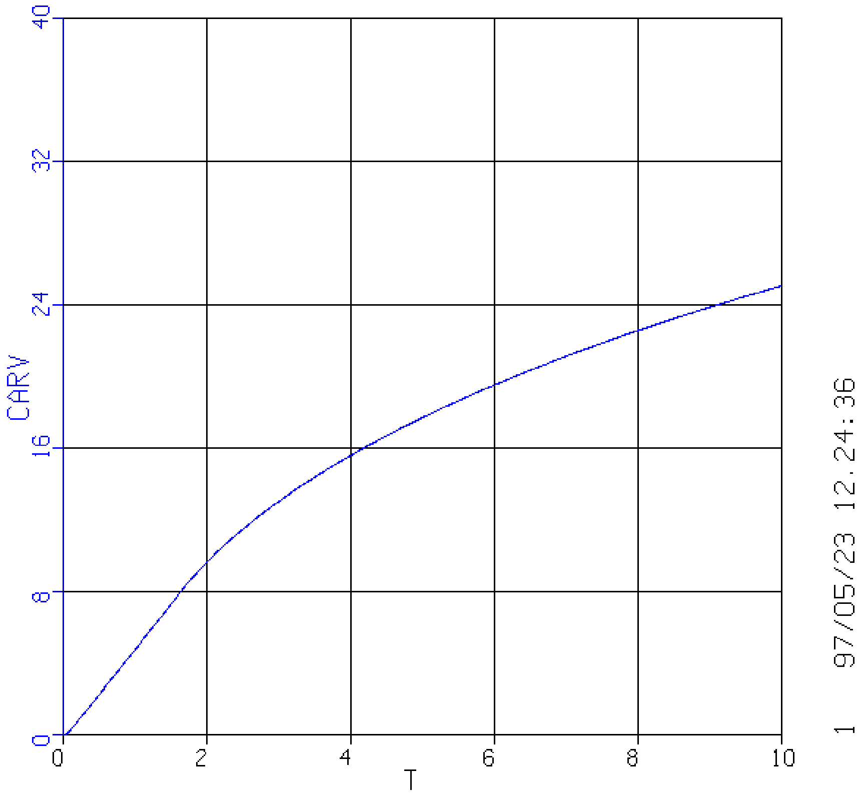

Figure 5.6.35: Vehicle Velocity (m/sec) verses Time (sec) during Maximum Acceleration of the EP HVPP / DC Traction Motor Design with the Improved ICE Control.

The acceleration of the vehicle using the improved ICE control is shown in figure 5.6.21.

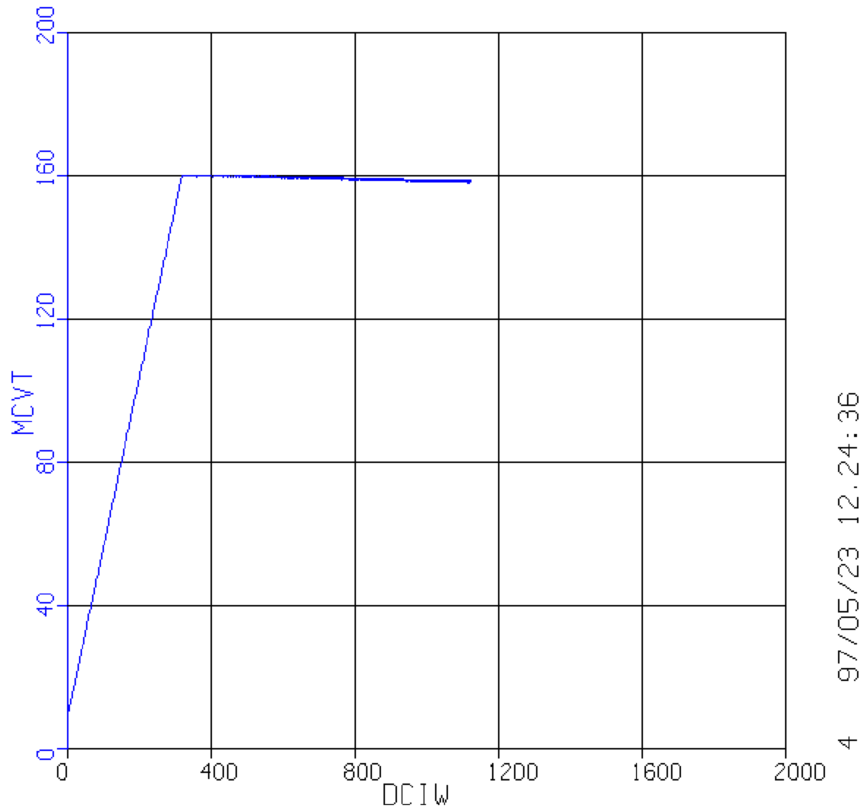

Figure 5.6.36: Motor Controller Voltage verses DC Motor Speed (rad/sec) during Maximum Acceleration of the EP HVPP / DC Traction Motor Design with the Improved ICE Control.

The dc motor controller voltage holds much closer to its set point of 160 volts with the improved ICE controller as seen in figure 5.6.22.

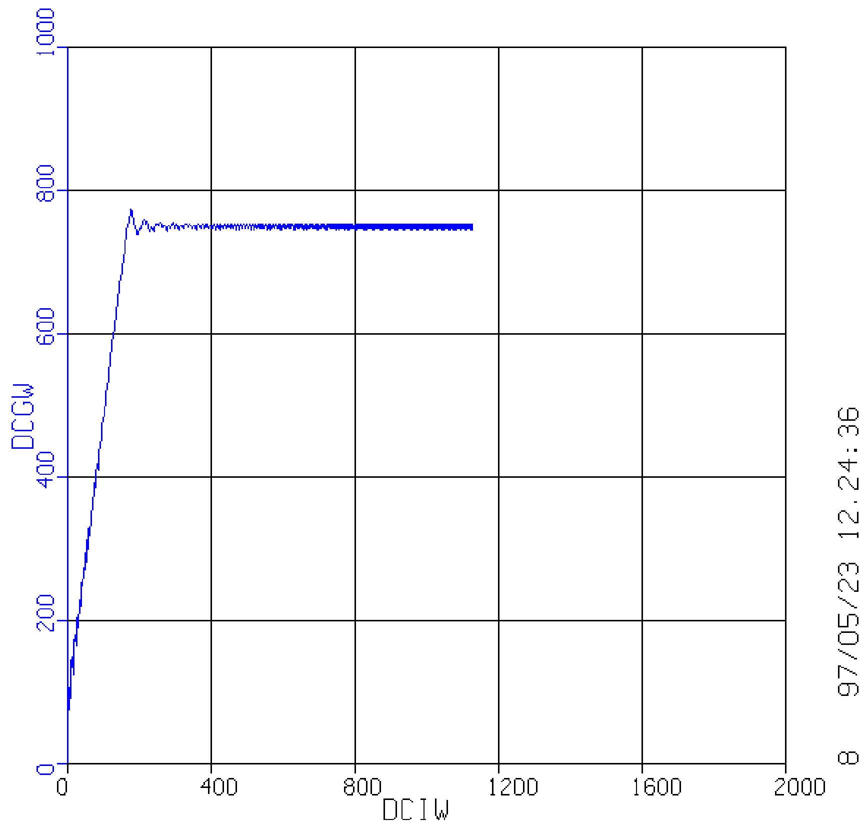

Figure 5.6.37: Engine RPM verses DC Motor Speed (rad/sec) during Maximum Acceleration of the EP HVPP / DC Traction Motor Design with the Improved ICE Control.

The engine speed response to the maximum acceleration transient is much faster now as shown in figure 5.6.23.

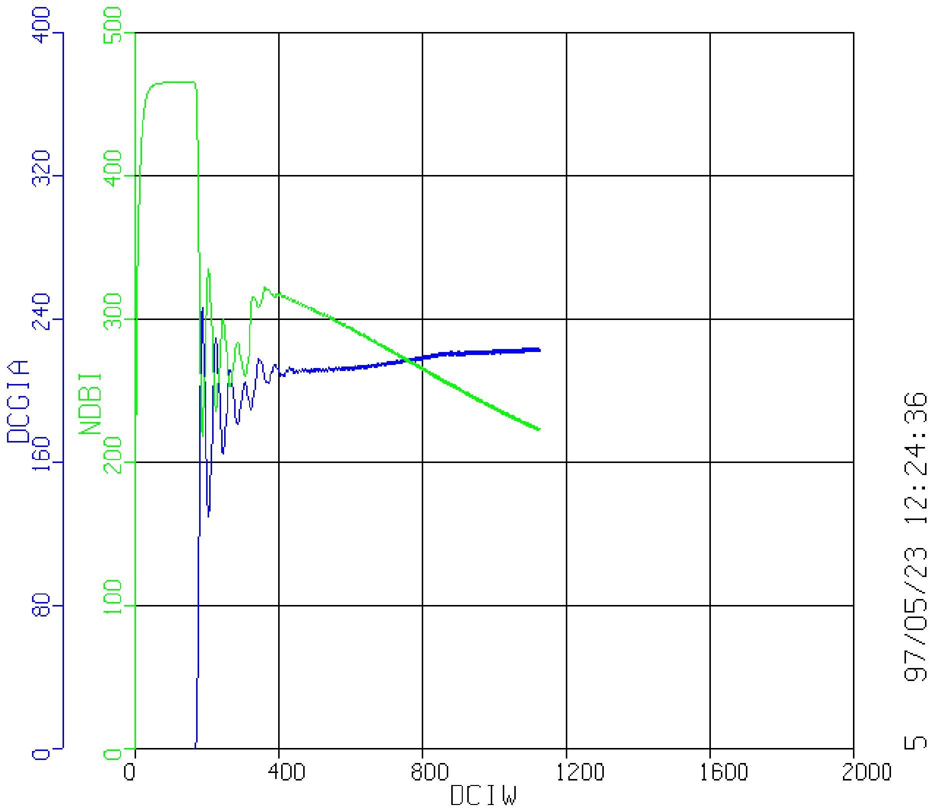

Figure 5.6.38: Generator Armature Current (amps, solid line) and Battery Bank Current (amps, dotted line) verses DC Motor Speed (rad/sec) during Maximum Acceleration of the EP HVPP / DC Traction Motor Design with the Improved ICE Control.

The generator armature current and battery current are shown in figure 5.6.24. It is interesting to note that the generator supplies more current as the batteries ability to deliver current diminishes.

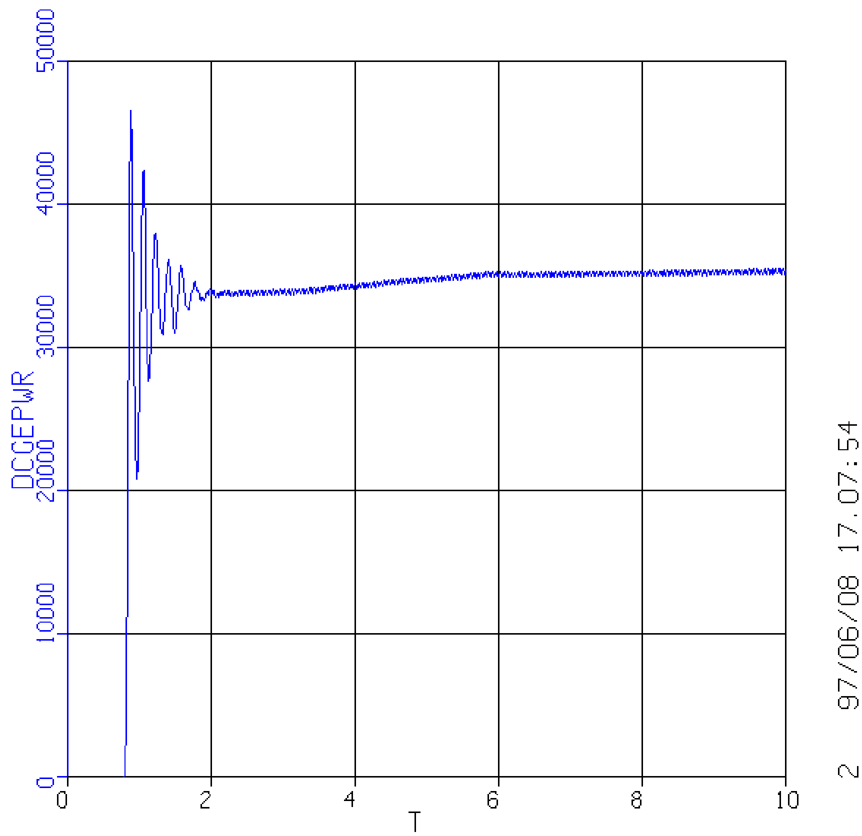

Figure 5.6.39: Generator Output Power (watts) verses Time (sec) during Maximum Acceleration of the EP HVPP / DC Traction Motor Design with the Improved ICE Control.

The power output from the controller is shown in figure 5.6.25.

Considering the power capabilities of this engine and the power capabilities of the generator, the power output could be improved. Slight adjustments were made to the controller to improve the power delivery. Although small, the improved acceleration is notable and is shown in figure 5.6.26.

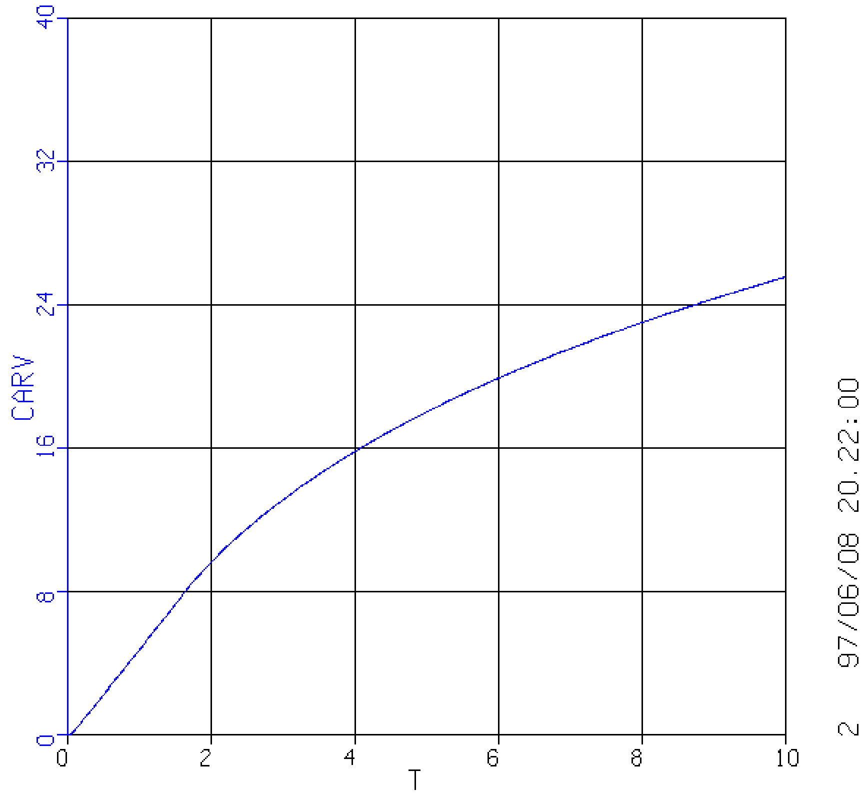

Figure 5.6.40: Vehicle Velocity (m/sec) verses Time (sec) during Maximum Acceleration of the EP HVPP / DC Traction Motor Design with the Improved Generator Control.

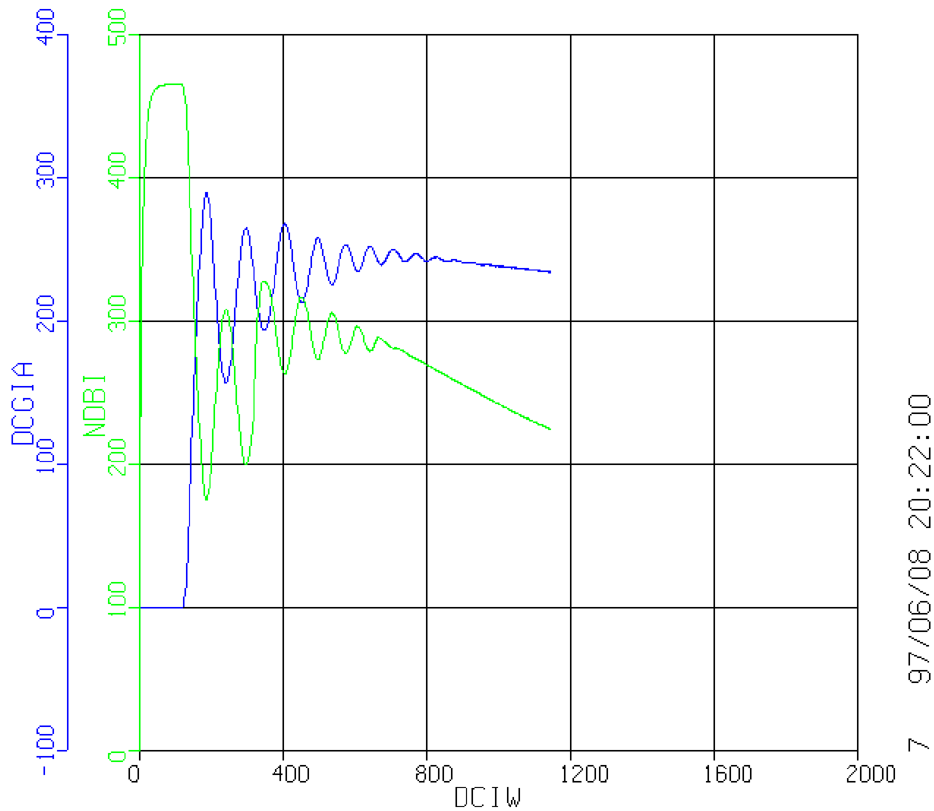

Figure 5.6.41: Generator Armature Current (amps solid line) and Battery Bank Current (amps, dotted line) verses DC Motor Speed (rad/sec) during Maximum Acceleration of the EP HVPP / DC Traction Motor Design with the Improved Generator Control.

The generator armature current and battery bank current are shown in figure 5.6.27, and the generator power output is shown in figure 5.6.28.

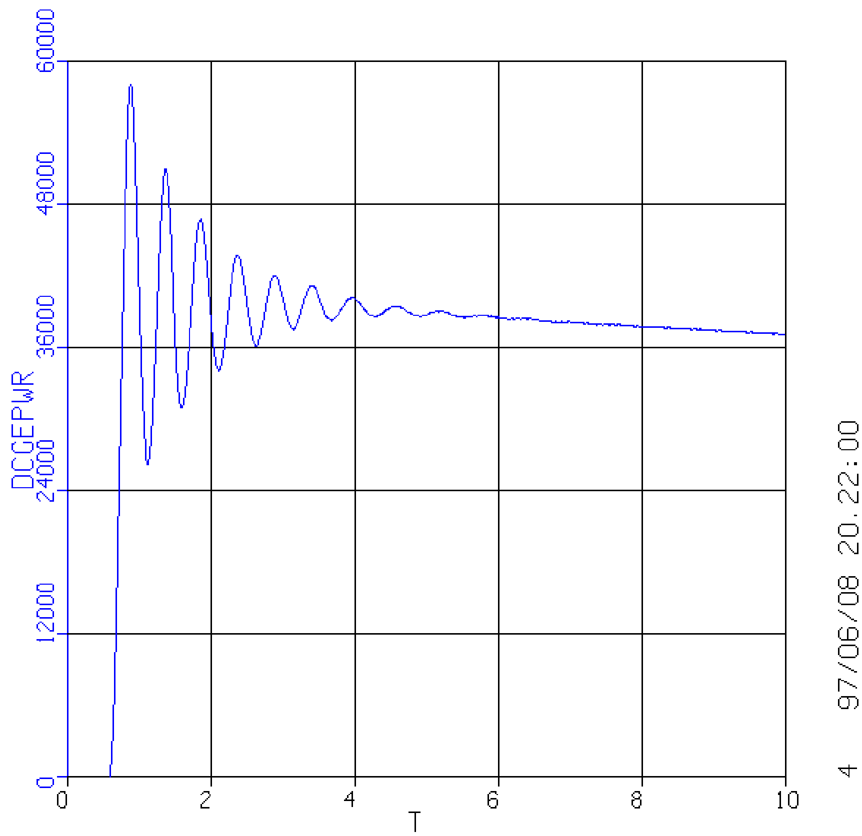

Figure 5.6.42: DC Generator Output Power (watts) verses Time (sec) during Maximum Acceleration of the EP HVPP / DC Traction Motor Design with the Improved Generator Control.

Although the cause of the low power region at the beginning of this section may have seemed immediately obvious when considering the power plant architecture, this troubleshooting scenario illustrates how the models can be used to predict and correct problems before construction. Also, the improvements made to the generator controller could have been taken much further, this scenario of improving predicted performance illustrates how a proposed design can be studied and improved in a more detailed study. This architecture is not unique, but its balance of power is. The models and the modeling methods could be used to investigate many different designs and improve their performance. This endeavor is worthwhile, because this level of modeling gives accurate predictions and realistic predictions of dynamics.

5.6.2.2Using an Induction Motor

The second EP HVPP was similar to the first. It used a 750 cc ICE, a 46 kW separately excited dc generator, two 18 kW nominal IM's, and 28 lead acid deep cycle batteries weighing 520 kg. The dc generator was connected directly to the engine without a clutch. The overall constant gear ratio from the dc traction motor to the wheels was 12.0.

One of the latest attempts to perform a maximum acceleration with this virtual power plant is shown in figure 5.6.29.

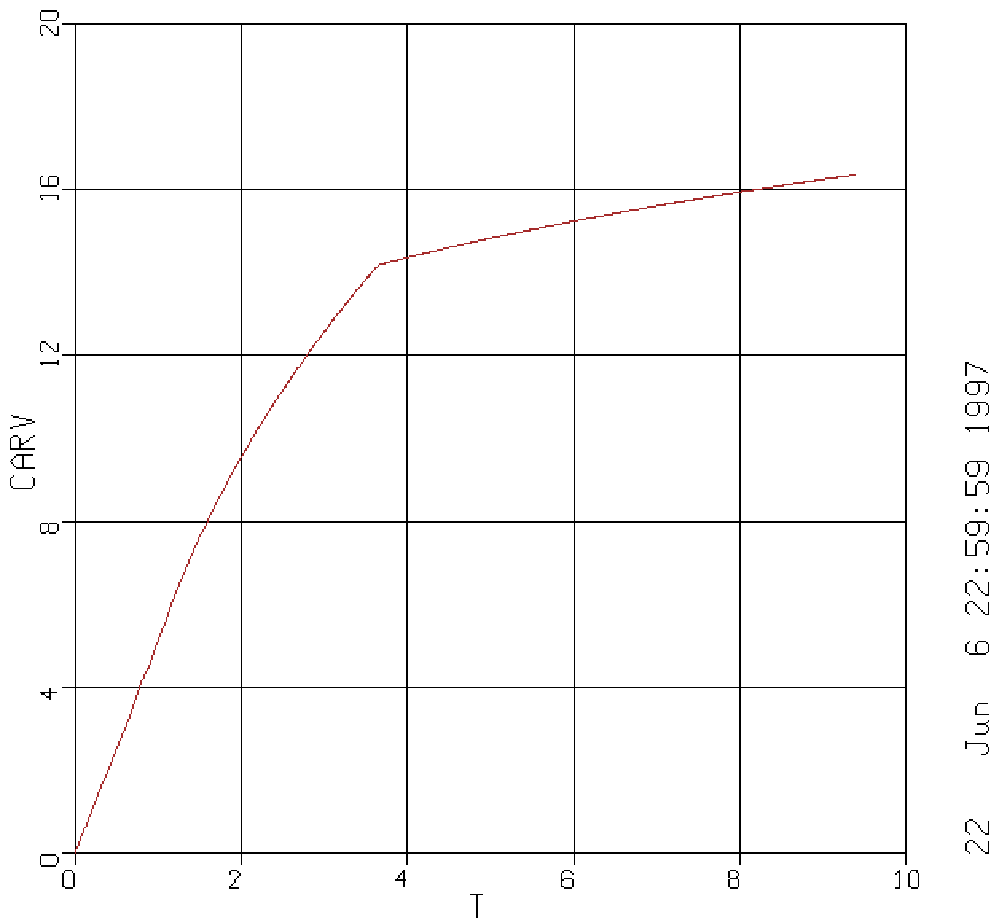

Figure 5.6.43: Vehicle Velocity (m/sec) verses Time (sec) for the EP HVPP / IM Design during Maximum Acceleration.

Even with the help of the dc generator, the battery voltage did not remain high enough to prevent the controlled IM from exceeding the breakdown. The breakdown torque was exceeded while the controller was in the slip control region as shown in figure 5.6.30. The slip would have gone higher, but there was a maximum slip speed verses rotor speed function in the controller that prevented the slip speed from going excessively high during this condition.

The author was still making attempts to correct this problem at the writing of this dissertation. All attempts using the type of control described for the IM powered EV in section 4 have not been able to prevent the controller from exceeding the breakdown torque. But the models have helped to investigate the nature of the problem, and some slight improvements have been made. In cases where the controller prevented the IM from exceeding the breakdown torque, the acceleration of the vehicle was very slow. It may be necessary to use a more sophisticated type of control such as vector control for this plant configuration.

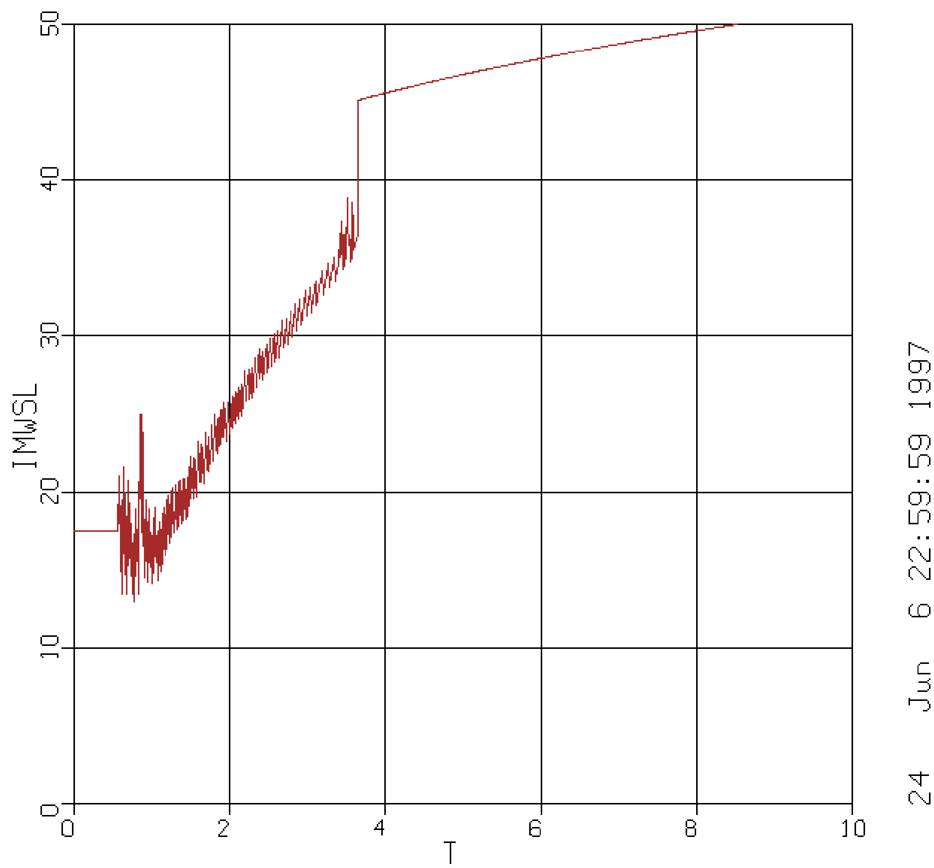

Figure 5.6.44: IM Slip Speed (rad/sec) verses Time (sec) for the EP HVPP / IM Design during maximum acceleration.

5.7Summary

This section illustrated how the design and modeling methodologies could be used to search for critical design parameters, and operational anomalies of, proposed HVPP designs to make virtual design improvements. The design methods provide a sound framework for considering alternative design concepts and architectures for present and future HVPP designs. The modeling methods proved to make accurate predictions, and they displayed realistic dynamics.

The methods were illustrated by applying them to four different HVPP's. Each concept was first applied to the function system diagram. Then, bond graph models were formed from the system diagrams. The bond graphs were used to inspect the causality and dependencies of the overall numerical models for the HVPP's. In each case, the MRD scheme allowed simplifications to the bond graphs where numerical dependencies would have normally resulted. The bond graph models were then used as guides in the formation of the ACSL graphic models. The graphic models were formed from the MRD drive train components, the modules for the detailed models and user defined controllers. The graphic models were simulated and used to briefly illustrate how a designer might use them when investigating ways to improve the performance of new HVPP concepts. More detailed studies will be performed in future works.

Parallel HVPP's were studied, and the modeling methods provided the necessary information and flexibility to improve the predicted performance. Typical series HVPP's are essentially EV's with on board charging systems. The EV's in section 4 can be modified slightly and used to study the performances of these typical series HVPP's. Therefore, to further illustrate the future application of the models, an atypical series HVPP, also called an electrical parallel HVPP, was studied. Coordinating the power supplies in this concept was quite challenging. Adequate coordination of the power supplies could be achieved with the electrical parallel HVPP that used a DC motor. But, the electrical parallel HVPP that used an IM presented challenges in the power supply coordination that were beyond the author's current motor control capabilities. However, this example was valuable, because the models correctly indicated the nature of the problems, and information from the simulations helped determine the direction that the control evolution must take.

In section 4, it was found that regenerative braking was not very practical when using batteries to store the vehicles kinetic energy. Thus, predictions from the models are consistent with current knowledge. In order for batteries to be practical in regenerative braking, they must be able to handle high charging currents. Furthermore, the high voltages during high battery charging rates require excessive operating ranges for the electric machines which results in unreasonable electric machine designs. Regenerative braking is desirable, and devices with much lower power densities that are more capable of delivering and receiving high power during severe transients will be studied in future works.

6SUMMARY

6.1The Interest in Hybrid Vehicle Power Plants

Three major steps that must be completed before a consensus can be reached on which hybrid vehicle power plant concepts should be mass produced were postulated:

Step 1: Establish design and modeling methodologies that give realistic predictions of the performance and realistic characteristics of various HVPP concepts.

Step 2: Use the design and modeling methodologies to identify the most promising HVPP concepts.

Step 3: Construct prototypes of the HVPP concepts identified in Step 2 and thoroughly test them.

Step 4: Manufacture the best concepts from step 3.

Designers need flexible design tools that can be used to make realistic performance predictions, and display realistic dynamics, of proposed designs. Such tools can help eliminate, or at least indicate, many of the difficulties designers may face in the development of prototypes, which will help save time and money.

During the abstract phase of design, designers consider only the functions of the design to make sure they have defined everything the design must "do," that is, what must be provided by the design. This is important, because, if any functions the design must provide are overlooked, the conceptual phase of the design, where designers consider "how" they will achieve the required functions, will fail or, at best, be poor. Therefore, in order for a modeling methodology to have a greater likelihood of success, it should originate from abstract system design considerations of the system being modeled. The author has identified no existing abstract design tools or abstract design philosophies for hybrid vehicle power plants.

Most models currently used in HVPP studies are empirically generated performance maps. Such models cannot show how changes in design parameters will affect the performance of the plant; that is, they are not flexible. Since their development did not originate from abstract design considerations, they may possibly miss important design considerations and not result in the best possible design concepts.

6.2Objectives of this Work

This work sought to make a contribution to step 1 by extending existing design and modeling methodologies that could be used to study a wide variety of HVPP architectures and operational schemes. The abstract portion of the design methodology should establish essential functions and functional relationships for any HVPP. Models developed using the modeling methodology should be capable of identifying critical design parameters of hybrid vehicle power plants and their sub-components. Models developed from this methodology should also serve as flexible design tools. The methodology should allow quick and easy construction and modification of HVPP models with various configurations. The developed models should be detailed enough to indicate sensitivities resulting from various sub-component interfaces. The models should also be useful for determining relationships and sensitivities among the design, operating and performance parameters.

6.3The Design Methodology

A function structure that includes the essential functions required of any HVPP was developed. These essential functions were used to form an abstract tool, a function system diagram, for pre-conceptual abstract analysis of HVPP's. The function structure development and the creation of the function system diagram are unique contributions of this work, because no abstract design tools have yet been introduced or discussed in the literature.

The function system diagram is a high level, or macroscopic, tool that provides a skeletal frame of the basic HVPP concept for the genesis of specific HVPP concepts. It serves as a mental table for the group as they discuss and jointly evaluate trial concepts and tradeoffs. Differences in energy management between various concepts are clearly demonstrated in a standardized manner.

The value of such a tool was experienced in previous design team work. The design team found the function system diagram to be a valuable tool in the following ways:

1) It allows design group members to visually communicate their thoughts to one another within a standardized convention.
2) It visually relates the energy and information transfer between the devices that will be designed to fulfill the functions of the function structure without actually showing concepts that might bias or hinder the creativity of the design team.
3) Provides traceability of requirements to the functions that must be provided by any HVPP design.
4) It shows the functions the design must fulfill without regard to physical limitations and yet reminds the group of basic physical limitations that exist such as the existence of uni-directional energy transmission and transformation devices.
5) Once actual concepts are devised to satisfy the functions, the new system diagram provides a concise, clear, and visual convention for recording the history of concepts that were compared, rejected and refined by the group.

6.4The Modeling Methodology

There are three important aspects to the modeling methodology of this work: approach, level of detail and modularity. Modeling approach is important, because a HVPP is a multi-disciplined design that requires a careful coordination of the contributing disciplines. Designers should adopt a common convention and modeling methodology to minimize the difficulties of working within a multi-disciplined team. Therefore, the generalized modeling approach was applied and communicated using bond graphs. The level of modeling was the most important aspect to the success of the modeling methodology. Component level modeling was chosen, because it is detailed enough to realistically predict performance, but not so detailed that simulations are slowed to impractical speeds. Modularity is important, because designers need to be able to investigate and evaluate alternative design configurations and operating schemes. There are a variety of possible HVPP configurations that need to be evaluated. There is also a variety of components that can be used in a HVPP. Furthermore, there is sometimes a large variety of configurations that can be proposed for one of the power supplies in a HVPP.

6.4.1ICE Modeling

The first modeling of this work was the ICE modeling. The engine models developed from the sub-component models exhibited sensitivities and revealed critical design parameters comparable to real engines and predicted performance with good accuracy. These features are important to making the ICE sub-component models good tools for the construction of HVPP models. Although spark advance was constant verses speed in the developed models (due to the constant flame duration combustion model that was explained above), the modeled engine’s torque prediction was sensitive to this setting. In order to further improve accuracy of the predicted torque, optimal valve timing for both the exhaust and intake valves of the cylinders had to be found. The optimal values found for valve timing were in the same range of values used for real engines. It was determined that the performance of the modeled engines could be improved by balancing the volumes and cross-sectional areas of the intake and exhaust ports and by adjusting the configuration of the overall intake and exhaust systems in the same fashion as with real engines. The models were accurate for fuel consumption predictions when good mixing of fuel and air are achieved by the final design. The models do not however account for bends and roughness of the intake and exhaust channels. They only predict the effects of cross-sectional area and volume changes of these passages.

The simplifying assumptions used in the development of the ICE model modules did not diminish the predictive capabilities of the ICE models. These assumptions also did not diminish the ability of the models to indicate realistic sensitivities to parameter value changes as indicated by the discussion above and as seen by the ICE model performance in sections 3.2 and 4. These finding were important to this work, because without these simplifying assumptions, the models would be slowed to impractical speeds for HVPP performance predictions and would therefore not be practical design tools.

6.4.2 Drive Train Modeling

The drive train modeling was initially motivated by the need to realistically predict the sudden loading of the engine when the clutch was engaged and was motivated to properly account for discontinuities. The drive train modeling scheme called the modular rigid discontinuous (MRD) drive train modeling scheme was devised to answer these important modeling issues. The MRD drive train modeling scheme easily accommodates dependencies and discontinuities that occur in drive train modeling. The dependencies arise when sub-systems with their own inertias are rigidly connected to other sub-systems with their own inertias. The discontinuities arise when systems require a break in the drive train connections as with a clutch and ICE. These strengths of the MRD scheme allow designers to rapidly reconfigure drive trains for testing new architecture concepts without having to reconsider dependencies and discontinuities that can require major rewriting of codes. The key to this method was the passing of generalized momentums and inertias through the drive train and through any devices that cause discontinuities. Speed calculations could be performed at any point in the drive train system. There was direct correspondence between all velocities in the systems when the systems were fully connected, and the scheme allowed the separate systems to operate properly when they were disconnected from one another. Momentum was passed through the disconnection points in proportion to the degree of connection. This scheme works in systems with or without breakable connections (e.g. with or without clutches). Special treatment of standard integration routines had to be made to reset state variables at appropriate times in the simulation.

6.4.3 Electric Machine Modeling

DC Machine models do not require validation, because they are very accurate when compared to experimental results. An IM model that could meet the modeling objectives of component / process level decomposition was developed using the generalized approach and bond graph modeling techniques. The electrical, magnetic, and mechanical processes in the machine were modeled as separate, discrete regions or processes. The model reproduce realistic performance characteristics, and therefore proved to be adequately accurate for the purposes of this work. It showed the proper sensitivity to design parameter changes. However, in a squirrel cage IM design, design parameters cannot be changed easily without affecting many other design parameters, so a careful IM design process was followed when adjusting IM design parameters to ensure that the interrelations of design change effects were properly considered [25]. The IM model requires more computation time than any of the other models in this work, but the speed was found to be tolerable. Ten seconds of dynamic simulation required 3 hours to run on a Digital VAX Alpha computer.

Design parameter values for an existing production IM used in vehicle applications were estimated to validate the IM model as demonstrated in section 3.4 and 4.2. Simulation predictions using the model and the estimated design parameters exhibited characteristics one would expect to measure from a real machine, and the modeled IM exhibited sensitivities to design changes that would be experienced in experimentation as shown in section 3.3. When used in a variable speed application, the IM model also exhibited realistic sensitivities to control and design parameter value changes and gave realistic performance predictions as shown in section 3.3. It proved to be very valuable in the process of developing variable speed IM controls. When IM ratings and vehicle parameter values comparable to a GM impact were used to simulate an EV, the vehicle simulation results predicted the same acceleration performance of the GM Impact.

6.4.4Battery Modeling

The battery model is not a unique development of this work, but it proved to be extremely valuable to the objectives of this work. The most influential interface sensitivities encountered were due to the batteries. Their dynamics influenced the design of the plant more than any other component. The model is accurate and is based on simple first principles. As claimed by the authors who developed the model [28], adequately accurate simulation predictions could be achieved by making small adjustments to the capacitance based on knowledge of a given battery’s energy storage capacity and power density. Since the developers did not test the battery model for the more severe transients that occur in an EV, it was necessary to adjust the functions for nonlinear resistances to achieve an accurate prediction for power density. (More accurate results can be achieved by experimentally identifying the nonlinear parameters for specific batteries of interest).

6.5Application of the Methodologies

The design and modeling methods were illustrated by applying them to three non-hybrid power plants and to four different HVPP’s as summarized in table 6.5.1. Bond graph models were formed from the concept system diagrams that were developed from the general function system diagram’s structure. The bond graphs were used to inspect the causality and dependencies of the overall numerical models for the HVPP’s. In each case, the MRD scheme allowed simplifications to the bond graphs where numerical dependencies would have normally resulted. The bond graph models were then used as guides in the formation of the detailed models using the ACSL graphic model modules. The graphic models were formed from the MRD drive train components, the modules for the detailed models, and user defined controllers. The graphic models were simulated and used to briefly illustrate how a designer might use them when investigating ways to improve the performance of new HVPP concepts.

Modeled Vehicle Power Plants	
Non-Hybrid Vehicle Power Plants	**Conventional Vehicle - Ascot Motorcycle**
	Electric Vehicle - DC Machine Powered
	Electric Vehicle - Induction Machine Powered
Hybrid Vehicle Power Plants	**Parallel Hybrid Vehicle with DC Motor and Batteries**
	Parallel Hybrid Vehicle with Induction Motor and Batteries
	Series Vehicle with DC Motor and Batteries
	Series Vehicle with Induction Motor and Batteries

Table 6.5.1: Overview of Models Built in this Work.

The virtual non-hybrid vehicles formed from the sub-component models that were developed using the modeling methodology indicated that the models give realistic performance predictions, or, at least, that they indicated realistic dynamic behavior as demonstrated in section 4. Therefore, HVPP models formed from the same sub-component models can meet the original objective which was to help designers identify critical design parameters. Furthermore, the models indicated relationships and sensitivities among the design, operating and control parameters. All of the vehicle models were modular, were easy to build, and were easy to reconfigure. Considering these things together, the models were detailed enough to give guidance of ways to improve the performance of the non-hybrid power plant vehicles and the HVPP's as illustrated throughout sections 4 and 5.

Findings using these models were consistent with current knowledge regarding regenerative braking. The models confirmed that regenerative braking is not very practical when using batteries to store the vehicle's kinetic energy. The models confirmed that, in order for batteries to be practical in regenerative braking, they must be able to handle high charging currents. Also, the high battery voltages that exist during high power battery charging require excessive operating ranges for the electric machines, which results in unreasonable electric machine designs. Regenerative braking is desirable. Therefore, devices with much lower power densities, capable of delivering and receiving high power during severe vehicle transients, will be modeled in the future developments of this work.

6.6Summary of Findings

The above findings are reviewed and categorized. There are three general findings regarding the utility of the modeling methodology used in this work. Models developed using the modeling methodologies for the studies in this work

1) were useful in identifying critical design parameters

2) proved to be flexible design tools that could be used to study different HVPP architectures and operational schemes.
3) identified relationships and sensitivities among the design, operating and control parameters
4) were useful in finding ways to improve performance.

There are two important findings regarding the level of detail that was chosen for the modeling in this work. Component level modeling of the vehicle power plant sub-component models in this work

1) yielded accurate performance predictions
2) exhibited realistic dynamics.

The modular-rigid-discontinuous (MRD) drive train modeling scheme was very important in meeting the objectives of this work. For the plants studied in this work, the MRD scheme

1) made it possible to modularize the vehicle power plants
2) automatically accommodated dependencies that arise when sub-systems with their own inertias are rigidly connected and thus simplified the vehicle power plant models
3) properly modeled the relations between systems that connect and disconnect during operation.

The ICE models in this work

1) were easily reconfigured, and were thus modular
2) were accurate even when ICE parameter values were changed and when the ICE models were reconfigured
3) should be useful for investigating new innovations such as variable valve actuation, because valve timing settings were realistic.

The IM modeling

1) is the first IM model developed using bond graphs and the generalized approach
2) decomposed the IM into its electrical, magnetic and mechanical components / processes
3) gave realistic performance predictions and displayed realistic dynamics.

The most sensitive component in the plants studied were the batteries. Therefore, in these studies

1) electric machine control logic affected plant performance more than any other design factor
2) regenerative braking was not very practical due to battery limitations and due to the excessive operating ranges that regenerative braking requires.

7CONCLUSIONS

7.1Specific Conclusions

The conclusions below are drawn from the summary given in section 6. Conclusions are given for the design methodology and then for each major sub-component modeling effort. Further conclusions are made for the modeling through inference of the findings for the vehicle power plant simulations.

7.1.1Abstract Design Methodology

Conclusions regarding the abstract tools developed in section 2 are subjective. However, the arguments are consistent with well established system design methods [6]. The HVPP concept is a phase in mankind's century old design refinement of the automobile. It is the hope of the author that the use, and/or refinement, of these abstract tools will provide a universal holistic base of thought that will lead the community of HVPP designers to a broader range of concepts from which potentially better designs will emerge. The application of abstract design tools to HVPP design is the first contribution of this work.

7.1.2Modeling Methodology

The modeling methodology provides three contributions to field of HVPP design and modeling. First, modeling is done using a common approach, the generalized approach, to help the different disciplines in HVPP design work better together. This was explained in the introduction and was experienced first hand by the author when he explained ICE modeling to electrical engineers in a multi-disciplined design group. The application of this approach is shown in sections 3, 4 and 5. Second, it sought to use (as often as possible) a common level of modeling detail (i.e. decomposition) for the sub-component models. Component level modeling, explained in the introduction, was chosen with the presupposition that it would best meet the objectives by providing the best balance of realistic performance predictions and simulation speed. This presupposition was found to be correct as shown in sections 3 and 4. Third, the modeling methodology achieved modularity at a detailed level and also accommodated dependencies and discontinuities as explained in section 3.1 and as illustrated in sections 4 and 5.

7.1.2.1Drive Train Modeling

The MRD drive train modeling scheme developed in section 3.1 is an important contribution to the development of HVPP modeling tools. It accommodates dependencies and properly accounts for discontinuities that occur in drive train modeling. It will allow designers to rapidly reconfigure drive trains for evaluating alternative architecture concepts without having to reconsider dependencies and discontinuities that can require major rewriting of codes.

7.1.2.2ICE Modeling

The level of ICE modeling and modularity proposed and developed in this work was first used herein. It has also been successfully used in another HVPP model for which the author originally developed this model. To the best knowledge of the author, a more detailed level of modeling has not been previously used in the dynamic simulation of HVPP's which makes the HVPP models presented in this work significant. The best tradeoffs between detail, accuracy, modularity, and current simulation speed capabilities were utilized to develop models that would meet the current objectives. The modeled ICE sub-components will give designers the ability to easily reconfigure their ICE models and the ability to accurately predict performance for any size engine. The ICE models are accurate and detailed enough to give good direction in the design of ICE enhancements such as variable valve actuation. The fuel consumption predicted by the models will be accurate for engines that are capable of near ideal mixing of the fuel and air.

7.1.2.3Electric Machine

The significant contribution of the IM model is that it is the first IM model developed using the generalized approach and bond-graph modeling techniques where the electrical, magnetic, and mechanical processes in the machine were modeled as separate, discrete regions or processes. The model's decomposition and generalized nature make it an ideal tool for a multi-disciplined design team for the reasons explained in section 1. It is accurate and exhibits realistic sensitivities to design parameter changes. Decomposing the machine into electrical, magnetic, and mechanical processes and modeling these separate processes also allows a better understanding of the processes, and better visualization of state variables, in their respective realms at any time in the simulation. This was another important element of the modeling that was set forth in section 1.

7.1.2.4Battery Modeling

The battery model used was obtained from the literature, and the initial aim of the work did not include creation of a battery model. It was necessary to have a good battery model to fulfill the overall objectives of this work as explained in section 3.4. Even though the battery model is an equivalent circuit model, and the explanation of how the objectives would be fulfilled dictated that these types of models should be avoided, this battery model was appropriate for this work considering the current state of battery modeling. It does not model the actual chemical reactions and processes in the battery, but it does give the end user a good indication of the difficulties encountered when using batteries in vehicle power applications. It properly emulates dynamic battery phenomena. This makes it an important tool for this work.

7.1.3 Vehicle Simulations

Based on experiences with the non-hybrid virtual vehicles formed from the sub-component models that were developed using the modeling methodology, HVPP models developed using the proposed methodology will give accurate indications of what can be expected from proposed HVPP concepts. Furthermore, these models should yield accurate performance predictions and will exhibit realistic dynamic responses. Therefore, they can meet the original objective which was to help designers identify critical design parameters, and they will be able to indicate relationships and sensitivities among the design, operating and control parameters. Using the methodology will ensure that they are modular and flexible design tools. The combination of these benefits indicate that models developed using the modeling methodology will help HVPP designers find ways to improve the performance of multi-component dynamic systems.

7.2 Discussions

The models in this work do run slowly, and associates have expressed a high degree of frustration to the author on this point. However, one must consider the purpose of any modeling effort. The objective for the modeling in this work was to develop a methodology that would reveal critical design parameters in any conceivable HVPP. Furthermore, the models should properly indicate sensitivities in component interfaces, and relations between design, performance and control parameters. The modeling methodology is meeting this objective, primarily because the level of modeling detail chosen provided the best balance between speed and accuracy in light of current computational capabilities. And, even though the models are slow, they are not prohibitively slow. The predictive capabilities of models developed using the methodology make them attractive for analyzing and refining designs.

The best thing for this work is to have other disciplines apply the modeling methodology to components within their specific realms of expertise. Recall step 1 in moving toward the mass production of HVPP’s. One person, or even several engineers from one discipline, cannot do justice to fulfilling this step. For this work to be a continuing contribution to HVPP design, HVPP designers from other disciplines must get involved and develop component models in accordance with these methodologies, or even refined versions of these methodologies. As the library of virtual sub-component models builds, and as the design methods improve, the potential of the HVPP community to determine the best configurations will increase.

Electric machine control logic is not too difficult to develop when working with a near constant voltage source. But, any voltage source on an EV, or on a HVPP, is most likely going to experience some significant fluctuations. This makes the development of electric machine control logic much more challenging. The studies in this work indicate that electric machine control logic is an extremely important design factor affecting the performance of the configurations that were studied in this work. Thus, it is highly desirable to involve electric machine control experts in applying and using the methodologies of this work to develop more flexible and robust electric machine controls.

7.3Summary of Conclusions

The findings in this work have led the author to make the following major conclusions. The modular-rigid-discontinuous (MRD) drive train modeling scheme

1) makes it possible to modularize rigidly connected dynamic systems
2) will handle dependencies when sub-systems with their own inertias are rigidly connected
3) simplifies the modeling and study of rigidly connected dynamic systems
4) properly models interactions of dynamic systems connecting and disconnecting.

ICE models developed in the future with the modeling methodology

1) can be easily reconfigured
2) will be accurate even when design parameter values are changed and reconfigured
3) will be useful for investigating new ICE innovations.

The IM model

1) should have value as a cross-disciplined design tool in HVPP modeling
2) will give accurate predictions
3) will display realistic dynamics.

Virtual vehicles formed from the sub-component models that are developed using the modeling methodology

1) will give accurate indications of what can be expected from proposed HVPP concepts
2) will yield accurate performance predictions
3) will exhibit realistic dynamic responses
4) can be used to identify critical design parameters
5) will be modular and flexible design tools that can be used to study a wide variety of HVPP architectures and operational schemes
6) will identify relationships and sensitivities among the design, operating and control parameters
7) can help find ways to improve the performance of multi-component dynamic systems

Conclusions drawn from specific experiences with the batteries in this work indicate that it is necessary to have designers of electric machine controllers contribute controller and power electronic model modules to the model component library using the methodologies.

7.4Future Work and Directions

Power electronics modeling is directly related to electric machine control. Power electronic components were not modeled in this work, but they need to be. They control the interface between the electric storage devices (usually batteries at this point in history) and the electric machines, and they have their own unique dynamics that influence the performance of the plant.

The development of low power density devices that would be used to deliver and store energies in high power transients could greatly improve the performance of HVPP's and EV's. In some power plant configurations, the batteries could be replaced by these devices. If used in EV's, they could handle the high power transients while the batteries operated in ranges of higher efficiency. The design of devices that show the greatest potentials for this purpose are multi-disciplined devices too. If these devices do become practical for EV and HVPP design, they will still most likely have higher energy densities than batteries (kg/kW). Thus, battery designers will continue to consider methods of improving the efficiency, energy densities and power densities of batteries.

Considering the current state of battery modeling and design, the battery modeling used in this work is accurate and acceptable. It gives good insight into dynamic battery phenomena when used in the power plant models. However, it would be best to have models that were based on the actual physical measurements of the battery components. Models that currently do this are finite element based, and they would not be practical for vehicle performance predictions. Thus, HVPP designers can only hope for a faster means of computation in the future, so that finite element models can be used when necessary.
Improving the speed of the models is still a major concern, but it is also important to maintain, and even improve upon, their accuracy and usefulness in the design process. We must be looking to the future when we think about how we want to model. Microprocessor speed has improved exponentially over the last ten years. Projections in speed improvements made by major microprocessor companies one year ago appear to be well on track, and their speed projections for the next 4 years will enable the detailed models of this work to run significantly faster. It is highly likely that the microprocessors used by design engineers ten to twenty years from now will enable designers to use finite-element based models to make vehicle performance predictions and to meet objectives far more extensive than those in this work. When this occurs, the models like the ones in this work, which are considered "so slow," will be considered simple models, and they will be used to identify initial design parameter values. Those who want to anticipate this future should learn how to use finite element methods to model dynamic systems, because

it is inevitable that models will become more detailed and more valuable in design as microprocessor speeds increase.

REFERENCES

[1] J. B. Heywood, *Internal Combustion Engine Fundamentals*. New York, NY: McGraw-Hill, Inc., 1988.

[2] A. F. Burke, "Hybrid/Electric Vehicle Design Options and Evaluations", *Tech. Rep. 920447, SAE*, 1992.

[3] J.R. Bumby, I. Forster, "Optimisation and Control of a Hybrid Electric Car," *IEE Proceedings*, Vol. 134, Pt. D, No. 6, November 1987.

[4] A. F. Burke, "On-Off Engine Operation for Hybrid/Electric Vehicles," *Tech. Rep. 930042, SAE*, 1993.

[5] D.L. Buntin, *Control System Design for a Parallel Hybrid Electric Vehicle,* College Station, TX: Texas A&M University Thesis, Electrical Engineering, 1994.

[6] G. Pahl, W. Beitz, *Engineering Design*, A Systematic Approach, New York, NY: Springer-Verlag, 1988.

[7] D. C. Karnopp, D. L. Margolis, R. C. Rosenberg, *System Dynamics: A Unified Approach*, New York, NY: Wiley-Inter-Science, 1990.

[8] *ACSL Model, ACSL Reference Manual, Version 11*, Concord, MA: MGA Software, 1995.

[9] *ACSL Model, User's Guide, Version 11 for Windows*, Concord, MA: MGA Software, October 1996.

[10] *ACSL Model, Graphic Modeller User's Guide, Version 4 for Windows*, Concord, MA: MGA Software, March 1996.

[11] J. Y. Wong, *Theory of Ground Vehicles*, New York, NY: John Wiley & Sons, Inc., 1978.

[12] Ferdinand P. Beer, E. Russell Johnston, Jr., Vector Mechanics for Engineers, Statics and Dynamics, New York, NY: McGraw-Hill, Inc., 1977.

[13] A. A. Amsden, *KIVA-3: A KIVA Program with Block-Structured Mesh for Complex Geometries*, Los Alamos National Laboratory, Los Alamos, NM, 1993.

[14] S. Widener, *Virtual Indicated Performance of Reciprocating Engines User's Manual*, San Antonio, TX: Southwest Research Institute, 1994.

[15] Frank P. Incropera, *Introduction to Heat Transfer*, New York, NY: John Wiley & Sons, Inc., 1996.

[16] "Cycle World Test: Honda Ascot VT500," *Cycle World*, pp. 50-55, August, 1983.

[17] *Automotive Handbook*, Distributed by SAE, Warrendale, PA., Robert Bosch GmbH, 1993.

[18] Daniel Charles Ross, "Ford Taurus SHO," *Motor Trend*, vol. 41, pp. 48-51, July 1989.

[19] George McPherson, Robert D. Laramore, *An Introduction to Electrical Machines and Transformers*, New York, NY: John Wiley & Sons, Inc., 1990.

[20] Irving M. Gottlieb, *Electric Motors and Control Techniques*, New York, NY: McGraw-Hill, Inc., 1994.

[21] Andrzej M. Trzynadlowski, The Field Orientation Principle in Control of Induction Motors, Boston, MA.: Kluwer Academic Publishers, 1994.

[22] Bob Brant, *Build Your Own Electric Vehicle*, Blue Ridge Summit, PA: Tab Books of McGraw-Hill, Inc., 1994.

[23] P. P. Silvester, Finite Elements for Electrical Engineers, New York, NY: Cambridge University Press, 1996.

[24] F. J. Bueche, *Introduction to Physics for Scientists and Engineers*, New York, NY: McGraw-Hill, 1980.

[25] A. K. Sawhney, *A Course in Electrical Machine Design*, Delhi, India: Dhanpat Rai & Sons, 1996.

[26] Paul C. Krause, Oleg Wasynczuk, Scott D. Sudhoff, *Analysis of Electric Machinery*, New York, NY: IEEE Press, 1995.

[27] S. W. Moore, *The Development of a Computerized Battery Simulator Optimized for Use in the ELPH 2.0 Simulation Environment,* College Station, TX: Texas A&M University Thesis, Electrical Engineering, 1996.

[28] Ziyad M. Salameh, Margaret A. Casacca, William A. Lynch, "A Mathematical Model for Lead-Acid Batteries," *IEEE Transactions on Energy Conversion*, vol. 7, No. 1, March 1992.

[29] Margaret A. Casacca, Ziyad M. Salameh, "Determination of Lead-Acid Battery Capacity Via Mathematical Modeling Techniques," *IEEE Transactions on Energy Conversion*, vol. 7, No. 3, September 1992.

[30] J. M. D. Murphy, F. G. Turnbull, Power Electronic Control of AC Motors, New York, NY: Pergamon Press, 1988.

[31] G. W. Vinal, *Storage Batteries 4^{th} Edition*, New York, NY: John Wiley & Sons, Inc., 1955.

APPENDIX A

Generalized System Analogies				
Generalized Names and Symbols	**Mechanical Systems**	**Electrical Systems**	**Hydraulic Systems**	**Magnetic Systems**
Effort, e	Force, F	Voltage, V	Delta Pressure, dP	Magnetomotive Force, MMF
Displacement, q	Distance, x	Charge, q	Volume, V	Flux, φ
Flow, $f = {}^{dq}/_{dt}$	Velocity, V	Current, i	Volume Flow, ${}^{dV}/_{dt}$	Flux Rate of Change, $\dot{\varphi} = {}^{d\varphi}/_{dt}$
${}^{df}/_{dt}$	Acceleration, $a = {}^{dV}/_{dt}$	${}^{dI}/_{dt}$	Pressure Momentum	———
Power = e*f	Power = F*V	Power = V*i	Power = dP* ${}^{dV}/_{dt}$	Power = M* $\dot{\varphi}$
Inertia, I	Mass, M	Inductance, L	${}^{\rho L}/_{A}$	———
Momentum, Mom=I*f	Momentum = M*V	Flux Linkage, λ	${}^{\rho L}/_{A} * {}^{dV}/_{dt}$	———
Generalized Kinetic Energy, $KE = {}^{1}/_{2}*I*f^{2}$	Kinetic Energy, ${}^{1}/_{2}*M*V^{2}$	${}^{1}/_{2}*M*i^{2}$ *(usually considered magnetic energy)	${}^{1}/_{2} * {}^{\rho L}/_{A} * {}^{dV}/_{dt}{}^{2}$	———
Inertial Effort, $I*{}^{df}/_{dt}$	F = M*a	$L*{}^{di}/_{dt}$	${}^{\rho L}/_{A} * \frac{dV}{dt}$	———
Capacitance, C	$C = {}^{1}/_{k}$ compliance = inverse of stiffness	Capacitance, C	${}^{\rho g}/_{A}$	Reluctance = ${}^{L}/_{\mu A}$
Generalized Potential Energy, $PE = {}^{1}/_{2}*{}^{1}/c*q^{2}$	Potential Energy, ${}^{1}/_{2}*k*x^{2}$	${}^{1}/_{2} * {}^{1}/_{C} * q^{2}$	${}^{1}/_{2} * {}^{\rho g}/_{A} * V^{2}$	${}^{1}/_{2} * {}^{L}/_{\mu A} * \varphi^{2}$
Capacitive Effort 1/C*q	Spring Force = k*x	1/C*q	${}^{\rho g}/_{A} * V$	${}^{L}/_{\mu A} * \varphi$
Dissipater, R	D	R	(Non-Linear)	(Non-Linear)
Power Loss, $R*f^{2}$	$D*V^{2}$	$R*i^{2}$	Power Loss	Eddy Currents Loses
Dissipater Effort, R*f	D*V	R*i	Head Loss	Hysteresis, Flux Leakage

Table A.1: Analogies between Generalized and Typical System Modeling.

Generalized modeling is a conceptual approach to systems modeling. It views state variables, efforts and energies of different systems in a common way. Table A.1 provides an analogy among generalized, mechanical, electrical, hydraulic and magnetic systems. For simplicity, only linear elements are shown. This table is not meant to be an all inclusive list for the systems listed. For example, potential energy in mechanical systems can be stored in ways other than spring compression, and spring displacement can depend on more than one state variable (e.g. x1-x2).

Using the generalized approach, a simple electrical system will be modeled to illustrate the use of bond graphs. This is meant to serve as a basic explanation of bond graphing techniques. For a more detailed explanation, see [Bond Graph Book]. An electrical system was chosen, because bond graphs relate more directly to electrical systems than other system types. Once the bond graph is complete, the process of obtaining the systems' differential equations from it will be shown.

The electrical system that will be bond graphed is shown in figure A.1. There are two fundamental elements used in bond graphs. They are bonds and multi-ports. Multi-ports store or transfer energy. Bonds, which connect multi-ports, represent the power flow between the multi-ports. Each bond is used to represent an effort and a flow. The various multi-port elements are classified as 1-port, 2-port, or 3-port elements. A device having more than its normal number of ports is referred to as a field [Bond Graph Book].

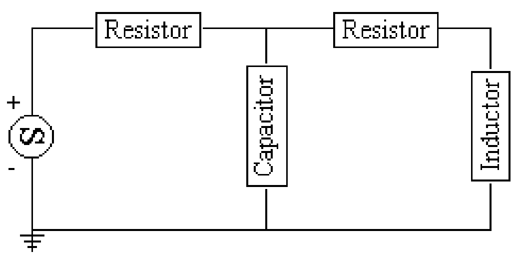

Figure A.1: Simple Electrical System

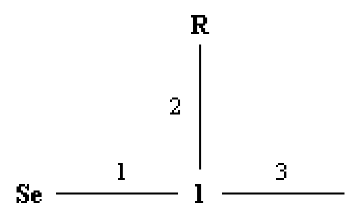

Figure A.2: Step 1 of Figure A.1's Bond Graph

The 1-port devices in figure A.1 are the voltage source, the resistors, the inductor (labeled with an **I** to follow the generalized notation) and the capacitor. To help avoid confusion with the inductor, currents will be modeled with a lower case **i**. There are no 2-ports in this simple system. However, their use will be illustrated in the last example. There are two types of 3-port elements. They are referred to as **1** junctions which represent regions of common flow (currents for the present example), and **0** junctions which represent regions of common efforts (voltages for the present example). Also, **1** junctions can be thought of as locations in the system where efforts sum to zero, and **0** junctions are locations in the system where flows sum to zero. Figure A.2 shows the initial development of the bond graph using these elements.

Starting at the positive side of the voltage source, power flows out of the voltage source and into the resistor. Does the resistor have the same flow (i.e. current) as the voltage source or the same effort? It has the same flow, so the voltage source and the resistor are connected to a **1** junction via bonds. Bond 3 remains to the right of the **1** junction to connect to the next multi-port device in the system. Looking at the circuit again, we see that this flow will divide at the node. A node has a single voltage, or it is a location in the system where the flows sum to zero. There is one flow in, and two flows out. So a **0** junction is placed at the end of bond 3 with two additional power bonds as shown in figure A.3. Consider the flow associated with bond 5. This same flow passes through the next resistor and the inductor. Therefore, this resistor and inductor are connected to a **1** junction with bonds 6 and 7 as shown in figure A.4. The flow of bond 4 will pass through the capacitor and then encounter a node. The flow from the inductor and resistor also flow into this node. Looking carefully, we see that this node is essentially the reference state (zero effort reference) for this system. So, the last step is to add the 1-port capacitor to bond 4. The finished bond graph is shown in figure A.5. Consider the last two steps from a different perspective.

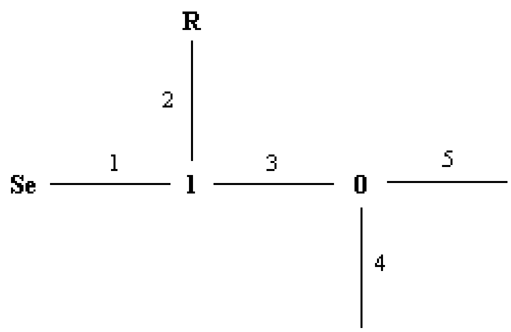

Figure A.3: Step 2 of Figure A.1’s Bond Graph

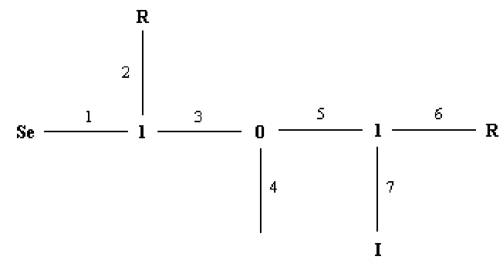

Figure A.4: Step 3 of Figure A.1’s Bond Graph

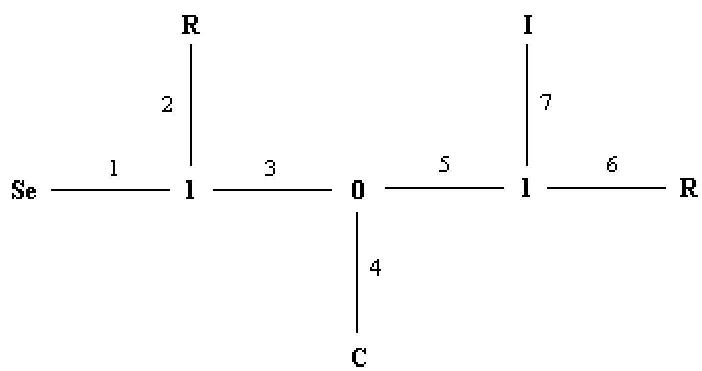

Figure A.5: Step 4 of Figure A.1’s Bond Graph

The voltage drop across the capacitor is the same as the sum of the voltage drops across the inductor and resistor. The bond graph represents this. Bond 5 represents the sum of the voltage drops across the inductor and resistor. This effort sum comes from the **1** junction. Bond 4’s effort represents the voltage of the capacitor. Bond 4 and bond 5 are connected to a zero junction and therefore have the same effort values (i.e. voltage).

There are two remaining steps. Each of the bonds must be assigned a sign convention, and the causality of each bond must be determined. Causality dictates whether a flow responds from effort(s), or an effort responds from flow(s). It is obvious to electrical engineers that the inductor current will be determined by integrating the sum of the voltages in the inductor’s loop and dividing by the inductance.

$$i = \frac{\sum V}{L}$$ **Equation A.1**

However, for the mechanical engineer, who is now using his understanding of generalized modeling, this should also be obvious. An inductor is analogous to a mass, and all engineers know that the sum of the forces (efforts) on a mass equal the mass times the acceleration. Furthermore, they know to determine the velocity of this mass by integrating the acceleration of the mass. Since the effort on the inertial element (i.e. inductor) is used to determine the flow, the causal stroke is placed at the top of bond 7 as shown in figure A.6. Also, since an integration is performed to determine the flow, it is said that the inductor is in integral causality. Integral causality is preferred. For an explanation of derivative causality and why it should be avoided, see [Bond Graph Book]. Another way to think of the desired causality for an inertial element is to remember that effort leads flow. This is true for inductors, masses, etc.

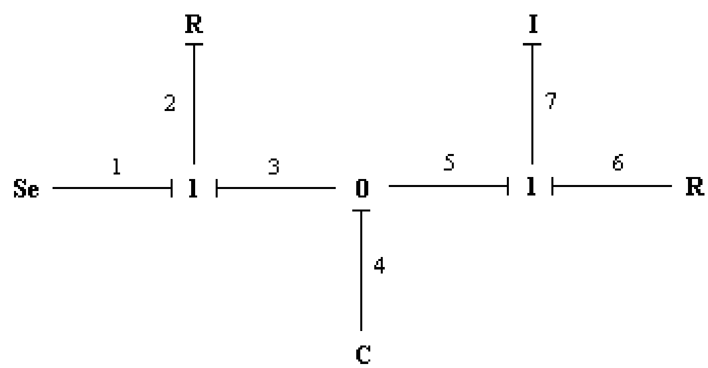

Figure A.6: Step 5 of Figure A.1's Bond Graph

There is one causal stroke per bond. When the causal stroke of the bond is next to a multi-port, the multi-port is receiving an effort from that bond and returning a flow to that bond. When the causal stroke of the bond is not next to a multi-port, the multi-port is receiving a flow from that bond and returning an effort to that bond. Principles used to determine causal stroke placements will become more obvious through the remainder of this example.

The inductor has now been used to determine the common flow of itself and the resistor (i.e. the common flow of their **1** junction). Therefore, we draw the causal strokes for bonds 5 and 6 next to the **1** junction, because only one bond can determines the flow for a 1 junction. Conversely, it is true that only one bond can determine the effort at a **0** junction which will be seen shortly. Bond 6's causal stroke now indicates that its effort is a function of its flow. We know this to be true. The voltage across the resistor is equal to the resistance times the current. Bond 5 indicates that a voltage is coming from the left side of the circuit. Bond 7 indicates that its voltage is equal to the sum of the voltages of bonds 5 and 6.

The current of bond 4 is determined from the sum of the flows of bonds 3 and 5. Bond 4 indicates that a flow is given to the capacitor, and the capacitor returns a force. It is thus said that bond 4 sets the effort for the **0** junction, and thus determines the efforts for bonds 3 and 5. The current into the capacitor is integrated to determine a charge. Thus, the capacitor is in integral causality. Then the charge is divided by the capacitance to determine the voltage of bond 4 (i.e. the voltage drop across the capacitor).

Finally consider the **1** junction connected to the voltage source. Using the causality rule for **1** junctions, and the knowledge that the voltage source is supplying an effort, the causality of the resistor must be such that it determines the flow for this **1** junction.

Sign conventions will now be set before writing the differential equations given by the bond graph. These sign conventions are shown in figure A.7 by half arrows. Half arrows are used to indicate power bonds in bond graphs. (Full arrows on the end of a bond indicate a control signal flow, or negligible power flow).

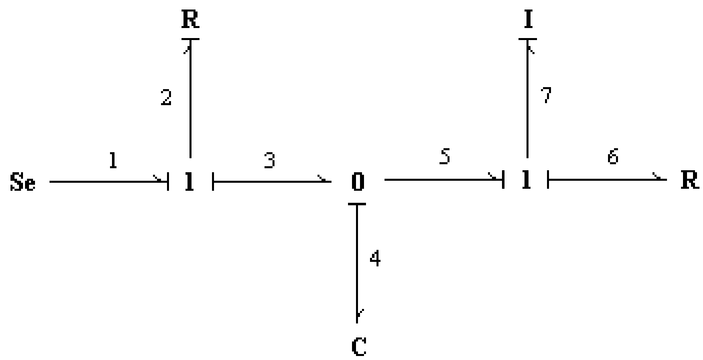

Figure A.7: Last Step of Figure A.1's Bond Graph

Consider all of the flow and effort equations indicated by the bonds and their sign conventions. The equations of table A.2 result. It is interesting to note that the equations of table A.2 could be written directly to a simulation language such as ACSL to simulate this system. Algebraic reduction of the table A.2 equations results in the set of first order differential equations given in equations A.2 and A.3.

Flows	f1 = f2	f2 = e2/R	f3 = f2	f4 = f3 - f5	f5 = f7	f6 = f7	$f7 = \frac{1}{I}\int e7$
Efforts	e1 = Se	e2 = e1 - e3	e3 = e4	$e4 = \frac{1}{C}\int f4$	e5 = e4	e6 = R*f6	e7 = e5 - e6

Table A.2: Bond Equations from Figure A.7.

$$\dot{i} = \frac{1}{L}\left(\frac{q}{C} - RI\right)$$ **Equation A.2**

$$\dot{q} = \frac{Se}{R} - \frac{q}{RC} - i = \frac{Se}{R} - \frac{\dot{i}L}{R}$$ **Equation A.3**

The basic steps of generalized modeling using bond graphs have been shown. Now consider using these steps to model a system comprised of fluid, mechanical, electrical and magnetic components like the one shown in figure A.8. This will illustrate the basic steps of the proposed modeling methodology. This system will also introduce the use of the two 2-port elements: gyrators and transformers. The system drawing has already been pre-labeled with the generalized elements that are present. They are, in order from left to right, an effort source, a resistance, a gyrator (i.e. the coil), a capacitance (the reluctance that depends upon the location of the moveable core segment), an inertia (the combined mass of the moveable core segment, the rod and the piston), a transformer (the conversion of piston force to cylinder pressure), and another capacitance (due to the area of the piston). The bond graph for this system is shown in figure A.9. Development of the bond graph will be explained by following an explanation of the system drawing.

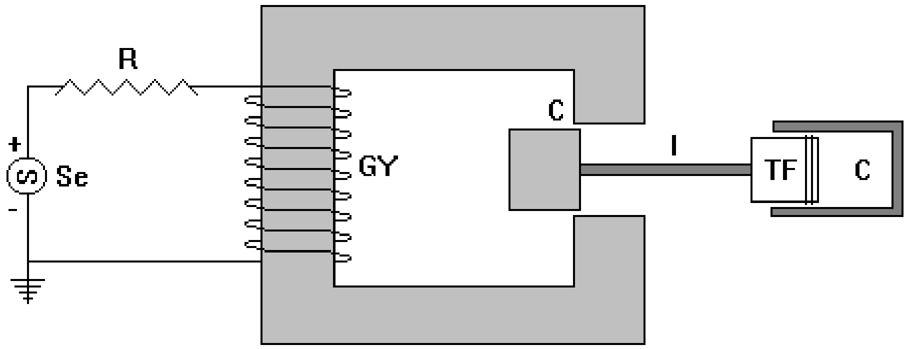

Figure A.8: System Containing Electrical, Magnetic, Mechanical and Hydraulic Elements.

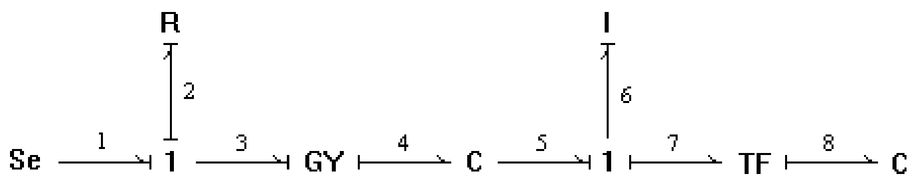

Figure A.9: Bond Graph of the System Shown in Figure A.8.

Moving from left to right through the system drawing the first element considered is the voltage source (an effort source). This effort source shares a common flow with the resistor, so both are connected to a **1** junction. At this point, a causal stroke can be added to bond 1 for the effort source.

The next element encountered is a coil on a permeable core. This is a 2-port element that acts as a gyrator. The action of this gyrator will be explained after all causalities have been set. For now, it is sufficient to know that there are two possible causalities for a gyrator: both causal strokes next to the gyrator symbol, or both causal strokes away from the gyrator symbol. There are also only two possible causalities for a transformer. In each instance, one causal stroke is next to the transformer symbol, and the other is away from the symbol.

The power passing through the gyrator encounters the reluctance (or inverse permeance) which is the inverse of a generalized capacitance. Note that this capacitance has two bonds connected to it. Considering the energy relation for the reluctance, this is not surprising. The generalized potential energy of this element depends on flux and reluctance, but the reluctance is non-linear and depends upon the position of the moveable section. Thus, the stored energy in this system element depends upon two generalized displacement quantities (i.e. it depends upon two state variables), and two bonds are connected to it. Taking the partial derivatives of this energy relation with respect to each state variable yields two effort relations. One will be for the mechanical side, and the other for the magnetic side. Placing this capacitance in integral causality sets the causal strokes for bonds 4 and 5. Using the causality rules for gyrators, and **1** junctions, the causality for bonds 2 and 3 are also set.

The next element encountered is an inertia. Since this has a common flow with the moveable core segment, the capacitance (reluctance) and the inertia (lumped mass) are connected to a **1** junction. The piston also has a common flow with the inertia, but it acts as a transformer into the hydraulic realm. After passing through the transformer, the translational mechanical flow becomes a volume flow into a generalized capacitance (air cylinder). Putting the inertia in integral causality and again following the causal rule for **1** junctions, the remainder of the causalities are set.

For the gyrator causality shown, a voltage applied to the coil causes a time variation of flux in the core. This is the flow variable in the magnetic realm. Thus the coil (a gyrator), converts an effort to a flow. This generalized action is the same in the opposite direction. An effort (the MMF acting on the coil) is converted to a flow (current). If the gyrator had the other possible causality, efforts would result from flows in both directions. These bond equations can be algebraically reduced to give a set of first order differential equations as was done with equations A.2 and A.3.

APPENDIX B

This section provides a simple procedure by which good initial estimates of engine design parameters can be made based on design criteria. Estimates are made based on a parallel HVPP configuration. The first step is to determine the maximum power required from the ICE. Key ICE design parameters will be determined from this value and other parameter values commonly known for an engine of this power rating.

Typical engines are sized to meet peak power needs (accelerations). Since parallel HVPP's are primarily accelerated by an electric motor, the most demanding situation remaining for the ICE is peak cruising. The most demanding peak cruise is dictated by a combination of design criteria given by the design team. One example of possible peak cruising criteria would be as follows:

> Maintain 75 MPH on a 2% uphill grade while supplying all possible auxiliary loads and charging the batteries.

An ICE's power requirements can be determined from road load requirements, auxiliary power requirements, and other related power plant requirements. Road load [1] is calculated using equation B.1

$$P_{rl} = (C_f mg + \tfrac{1}{2} C_D A_f V^2 + ma + mg\sin(\theta)) \cdot V \qquad \textbf{Equation B.1}$$

where C_D is drag coefficient, rolling resistance is C_f, inertia of the car is **m**, the frontal area is $\mathbf{A_f}$, gravity is **g**, and vehicle velocity is **V**. Auxiliary loads include items such as lights, air conditioning, heating, stereo, etc. Specific values will depend upon the actual size of the auxiliary components. A ICE for a parallel HVPP may need to make additional power available during peak cruising to charge the batteries. Thus, the total maximum power required from the engine will be the sum of road load, auxiliary, and charging power required at the desired maximum cruising conditions.

The output power from an engine is determined through the effective conversion rate of chemical fuel/air energy to mechanical energy or brake power. The brake power is calculated using Equation B.2. Air mass is determined as shown by Equation B.3 where ρ is density of the cylinder intake air, V_d is displacement volume of the engine, and η_{th} is volumetric efficiency. Air mass taken into the engine per cycle and Fuel Air ratio (**F/A**) result in a mass of fuel per cycle. Multiplying the heating value (**Qhv)** by the mass of fuel and combustion efficiency (η_f) gives the energy release from the fuel per cycle. Multiplying the last quantity by revolutions per second (**N**) gives the power released by the fuel per cycle. Considering mechanical efficiency (η_m), the thermodynamic heat engine efficiency (η_{th}), and the revolutions per power cycles ($\mathbf{n_r}$) yields the predicted engine power. Four stroke engines would be $\mathbf{n_r}$=2, and two strokes would be $\mathbf{n_r}$=1.

$$P_b = \frac{AirMass \cdot F/A \cdot Qhv \cdot \eta_f \cdot N \cdot \eta_m \eta_{th}}{n_r} \qquad \textbf{Equation B.2}$$

$$AirMass = \rho V_d \eta_v \qquad \textbf{Equation B.3}$$

The four efficiencies above and the intake air density are functions of the engine's operational, design and control parameters. In order to make initial estimates of engine design parameters, it is necessary to estimate these values. Current SI ICE's do not exceed efficiencies of 30%. Smaller engines have efficiencies that are as low as 10%. Because HVPP's use smaller engines, an overall engine efficiency (η_{eng}) of 0.10 (10%) was used in Equation B.4. Intake air density was assumed to be 0.4 of ambient air density.

$$P_b = \frac{\rho V_d (F/A) Q_{hv} N \eta_{eng}}{n_r}$$ **Equation B.4**

Values are now known for P_b, F/A ratio, Q_{hv}, η_{eng} and n_r in Equation B.4. Using the known values of Equation B.4 lumped together as a constant constraint K, displacement can be plotted as a function of speed. A reasonable combination of speed and displacement are then chosen from this plot. One should look at speed and displacement data from engine manufacturers for engines close to the required power.

$$V_d = \frac{K}{N}$$ **Equation B.5**

Displacement per cylinder is determined by dividing the determined displacement by the number of cylinders. Once the volume per cylinder has been determined, a typical bore to stroke ratio for the engine size is used to determine the bore of the cylinders and the stroke. The displacement of a cylinder would be found using Equation B.6. The stroke can be replaced by the quotient of stroke and bore to stroke ratio which results in Equation B.7 which is used to solve for bore. Then, the stroke to bore ratio can be used to find the stroke. Compression ratios for typical parallel HVPP's would be in the range of 8 to 12, and this will define the clearance volume for the cylinders.

$$V_{cyl} = \frac{\pi B_{cyl}{}^2 L}{4}$$ **Equation B.6**

$$V_{cyl} = \frac{\pi B_{cyl}{}^2 \dfrac{B_{cyl}}{B/L}}{4}$$ **Equation B.7**

The next parameters for the cylinders are opening and closing angles for intake and exhaust valves, their diameters and maximum lift heights (considerations for ports in two stroke engines are different). Consider the dimensional limitations of the cylinder head. Using the available cylinder head area, the designer must choose his preferred arrangement and number of intake valves, exhaust valves and spark plugs in the cylinder head. This choice will determine the limits of cylinder valve diameter. Equations B.8 and 5.9 help determine reasonable lift heights for the valves. The maximum possible cross-sectional area for flow is limited to the difference between valve diameter and valve stem diameter.

$$\text{MaxArea} = \frac{\pi D_{vlv}^2}{4} - \frac{\pi D_{vs}^2}{4}$$ **Equation B.8**

where D_{vlv} is the diameter of the valve opening, and D_{vs} is the diameter of the valve stem. Thus, maximum height will be dictated by Equation B.9. Lift above this height would simply result in a shorter time to the maximum possible valve flow area.

$$\text{MaxHeight} = \frac{\text{MaxArea}}{\pi D_{vlv}}$$ **Equation B.9**

Valve timing parameters are extremely important and greatly affect the performance of the ICE. There are many considerations for proper valve timing. Two basic ones are discussed here. The torque of an SI ICE is directly related to the mass of fresh air that enters the cylinders, and the mass of air that enters the cylinders depends upon valve timing. The most important effect in understanding how to optimize valve timing is the delay of cylinder filling and emptying at higher engine speeds. As speed increases, there is less time per crank angle degree for the air (or fuel air mixture) to get into and out of the cylinders. Cylinder filling and emptying is delayed by the increased flow friction. Thus, the intake and exhaust valves are closed at later crank angle degrees than the ends of their respective cycles.

The other major consideration in valve timing is valve actuation time. If the valves could be opened instantaneously, they could be actuated directly at the beginning of their cycles (top and bottom dead center). However, because it takes a number of crank angle degrees for the valves to fully open, it is desirable to open the valves earlier than their cycles dictate. This ensures for example that the intake valve is opened a sufficient height by TDC, and that flow resistance is minimized at the beginning of the intake cycle. At lower speeds this is not very important, but flow restriction of an opening valve makes early intake valve opening extremely desirable at high speed’s. The same analogy is true for the exhaust valve, except it must start opening before bottom dead center at the beginning of the exhaust cycle. By keeping the flow friction minimal, the mass of air brought into the cylinder will be maximized, and this will result in more torque at a given speed.

A few other important parameters must also be estimated for the model. The parameters for the remaining thermal fluid system components of the ICE are intake and exhaust port areas and volumes, intake and exhaust manifold areas and volumes, and maximum area for throttle valves. Optimal engine performance is quite dependent upon these parameters. The spark timing is constant in the model, because the flame duration is set to always take place over the same number of crank angle degrees for all engine speeds. This assumption is reasonable based on the reasons discussed previously. However, it will still be necessary to search for an optimal flame duration and spark angle for the model using simulations.

Ascot Engine Values

Density	FA	Qhv	N (rad/s)	Nr	RPM's
0.46	0.0685	44000000	942.408	2	9000

nv	nf	nm	nth	Overall Efficiency	Vd (liters)
0.8	0.9	0.7	0.3	0.1005	0.534

Num Cyls	Bore to Stroke Ratio	Bore	Stroke	Mean Piston Speed
2	1.15	0.073114515	0.0636	20.934

Approximates Steel Density	Piston Mass	Intakes Valves / Cyl	Exhaust Valves / Cyl
7850	1.0477	1	1

Diameter Intake Valve	Diameter Exhaust Valve	Diameter Valve Stem
0.029	0.029	0.005

Max Height Intake	Max Height Exhaust
0.007	0.007

Values for Engine Used in Hybrid Vehicles

Constraints

Desired Torque	Desired Speed	Total Power Needed
52.0	750.0	39000

Density	FA	Qhv	N (rad/s)	Nr	RPM's
0.46	0.0685	4.40E+07	750	2	7162.5

nv	nf	nm	nth	Overall Efficiency	Effective Efficiency	Vd (liters)
0.65	0.8	0.7	0.8	0.2912	0.1	0.750

Num Cyls	Bore to Stroke Ratio	Rod to Crank Ratio	Bore	Stroke	Mean Piston Speed	Rod Length
2	1.15	3	0.082	0.071	18.660	0.107

Approximates

Steel Density	Piston Mass	Intakes Valves / Cyl	Exhaust Valves / Cyl
7850	0.736	2	2

Diameter Intake Valve	Intake Port Scale Down	Intake Port Volume	Length of Intake Port	Area of Intake Port	Diameter of Intake Port
0.037	0.800	0.000	0.250	0.001	0.039

Diameter Exhaust Valve	Exhaust Port Scale Down	Exhaust Port Volume	Length of Exhaust Port	Area of Exhaust Port	Diameter of Exhaust Port
0.037	0.800	0.000	0.250	0.001	0.039

Max Height Intake	Max Height Exhaust	Diameter Valve Stem
0.009	0.009	0.005

APPENDIX C

This section contains the ACSL graphical blocks and related code for the modular-rigid-discontinuous drive train scheme described in section 3.1.

MRD Power Supply / Load Interface Block

Calculation Block Diagram

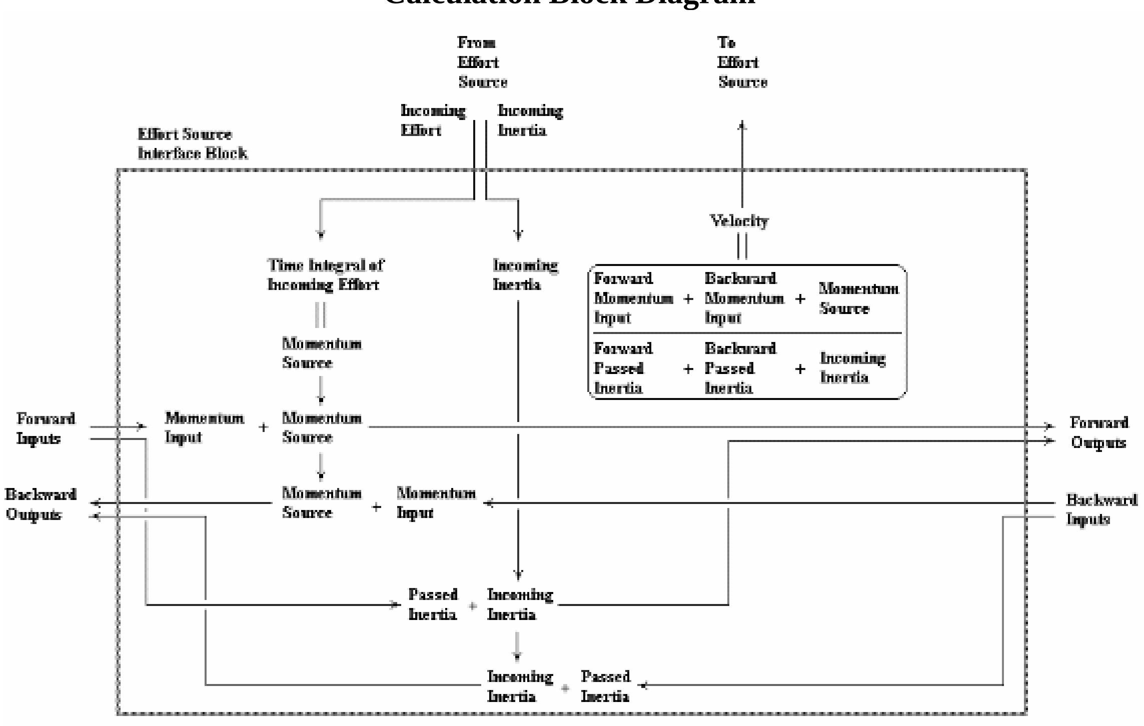

ACSL code: MRDInt.gsl

```
                                   Initial
Initial   ! power supply in the below comments could be replaced by "load"
          ! Exclamation marks mark the beginning of a comment field
          Constant wic = 0.0 ! Initial condition for power supply speed
          Constant I = 0.0354 ! The inertia of the power supply
          MomIC = I*wic ! Calculate the initial momentum of the power supply
          w = 0.0 ! Initialize the speed of the power supply
End ! of Initial

          ps = integ(trq,MomIC)     ! calculate the momentum component for the power supply
                                    ! at every time step
          speed = (pfi + ps + pbi)/(ifi + I + ibi)     ! determine the speed of the power supply
                                                       ! by summing the momentum components and
                                                       ! then dividing by the instantaneous lumped inertia
          pd = I*speed ! calculate the actual momentum of the power supply at every time step.
```

w = speed ! name an extra variable
pwr = trq*w ! calculate power output of the power supply.

pfo = ps + pfi ! add the forward in momentum to the power supply momentum
! to determine the forward out momentum.
ifo = I + ifi ! add the forward in inertia to the power supply inertia
! to determine the forward out inertia.

! The next two lines are the same as the previous two, except they are for the backward passed values.
pbo = ps + pbi
ibo = I + ibi

Shown in Model Application Interfacing an Induction Motor Power Supply

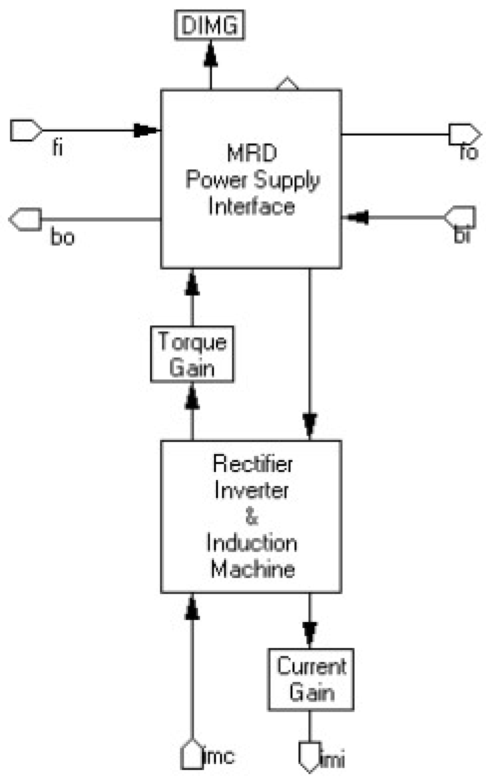

MRD Ratio Block

Calculation Block Diagram

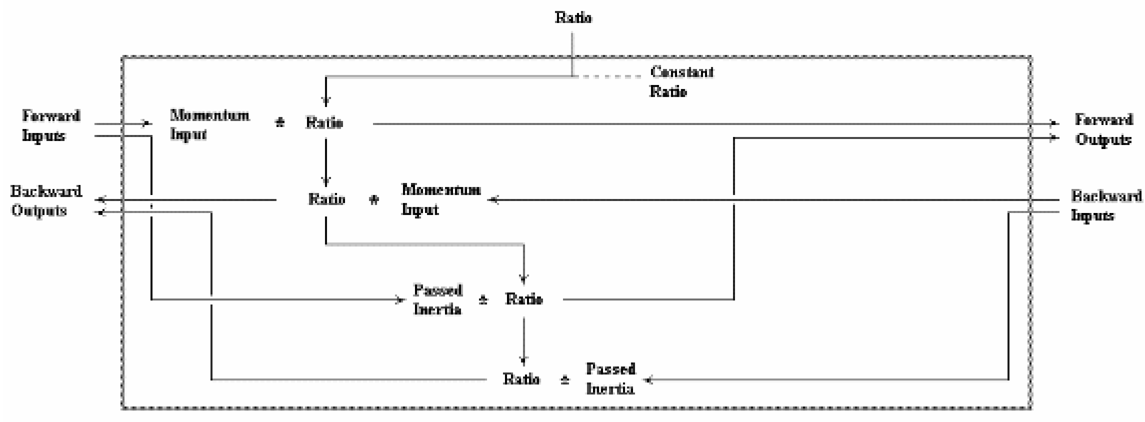

ACSL Code

Variable Ratio Code: VRatio.gsl

```
! ratio is a variable input. momentums and inertias are properly modified by the ratio.
        pfo = pfi*ratio
        ifo = ifi*(ratio)**2
        pbo = pbi/ratio
        ibo = ibi/ratio**2
```

Constant Ratio Code: CRatio.gsl

```
! ratio is a constant. momentums and inertias are properly modified by the ratio.
Initial
        Constant ratio = 4.99
End
        pfo = pfi*ratio
        ifo = ifi*(ratio)**2
        pbo = pbi/ratio
        ibo = ibi/ratio**2
```

Variable Version Shown in Model Application with Gear Ratio Block

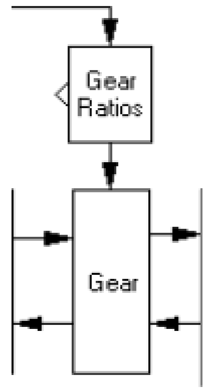

MRD Clutch / Disconnecting Point Block

Calculation Block Diagram

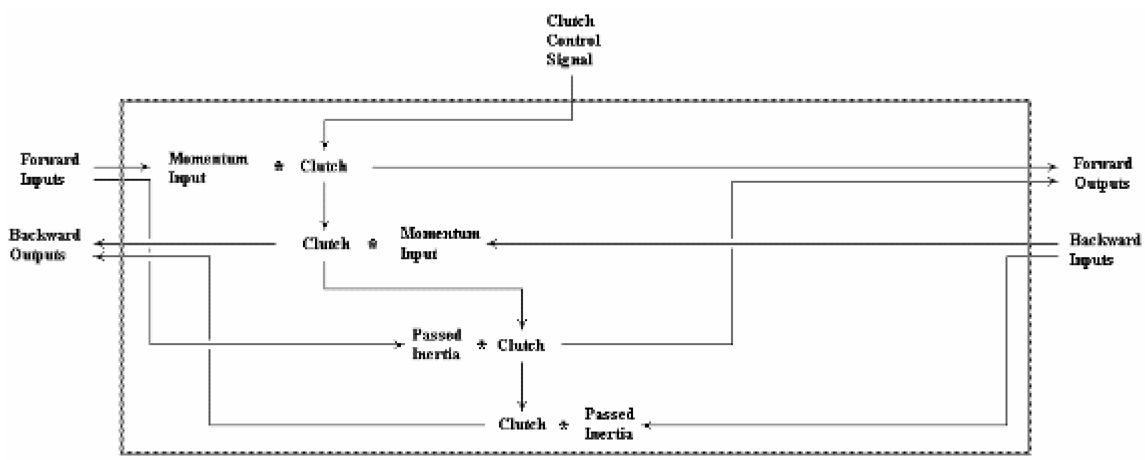

ACSL Code: Clutch.gsl

```
! cl is the input for the degree of clutch connectivity.
        pfo = pfi*cl        ! Calculate forward momentum out, etc.
        ifo = ifi*cl
        pbo = pbi*cl
        ibo = cl*ibi
```

Shown in Application between ICE and Variable Transmission

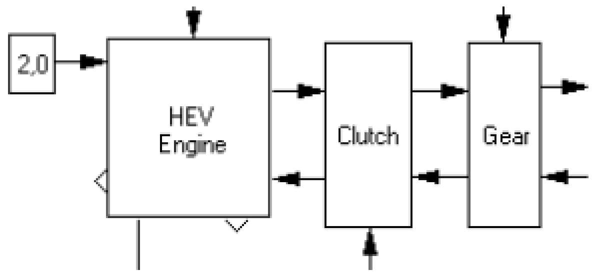

MRD Coupling Block

Calculation Block Diagram

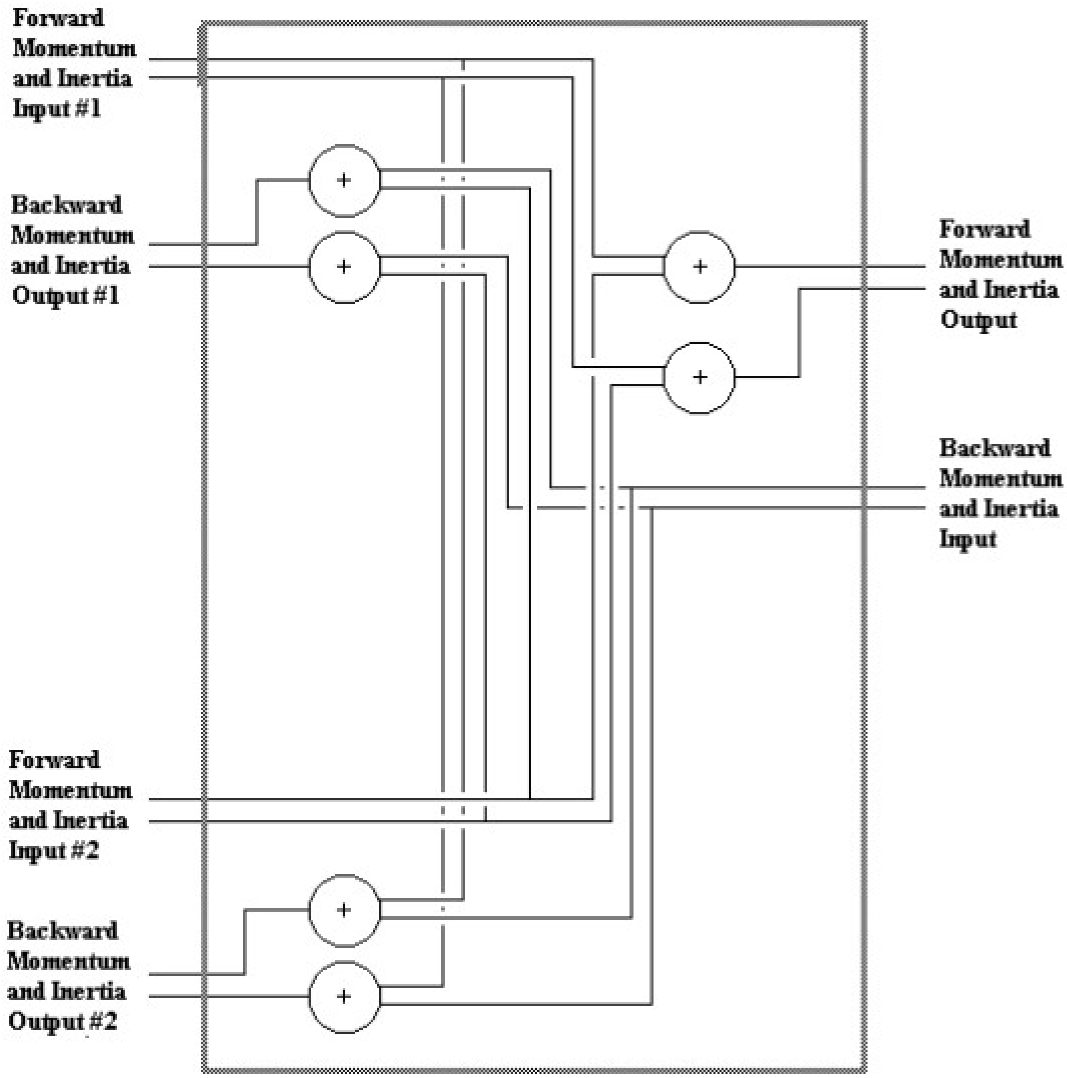

ACSL Code: Coupling.gsl

```
pfo = pf1i + pf2i
ifo = if1i + if2i
pb1o = pbi + pf2i
pb2o = pbi + pf1i
ib1o = ibi + if2i
ib2o = ibi + if1i
```

Shown in Application for Parallel HVPP

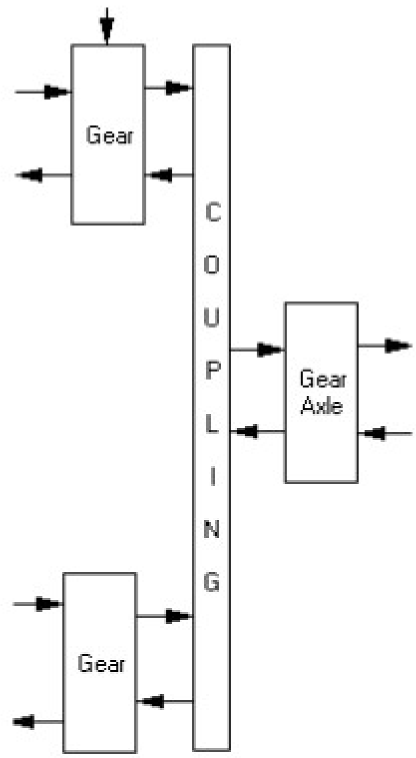

APPENDIX D

The principles shown in Appendix A will be applied to the bond graph in figure D.1. The bonds of figure D.1 are first numbered. To eliminate excessive repetition of the principles being illustrated, only one fluid path of the engine is considered without exhaust and ring leakage. Indications will be made in the equations of where terms for other system portions should be considered. All of the effort and flow equations are obtained straight from the bond graph and are shown in Table D.1. Flow functions for thermal fluid resistances are indicated in functional form. These functions are explained in the body of the thesis. Note that energy loss occurs in the cylinder due to heat transfer, therefore the capacitance of the cylinder is shown as a **CR** for capacitance and resistance (i.e. resistance to heat transfer). The integral equations contain no flow determinations for the thermal fluid system, because fluid flow inertia was assumed negligible. Furthermore, the integral equations contain no mechanical quantity calculations, because mechanical compliances were assumed to be perfectly rigid. However, shaft angle must be determined from integration of shaft velocity, because it is needed as a control signal for the cylinder valves.

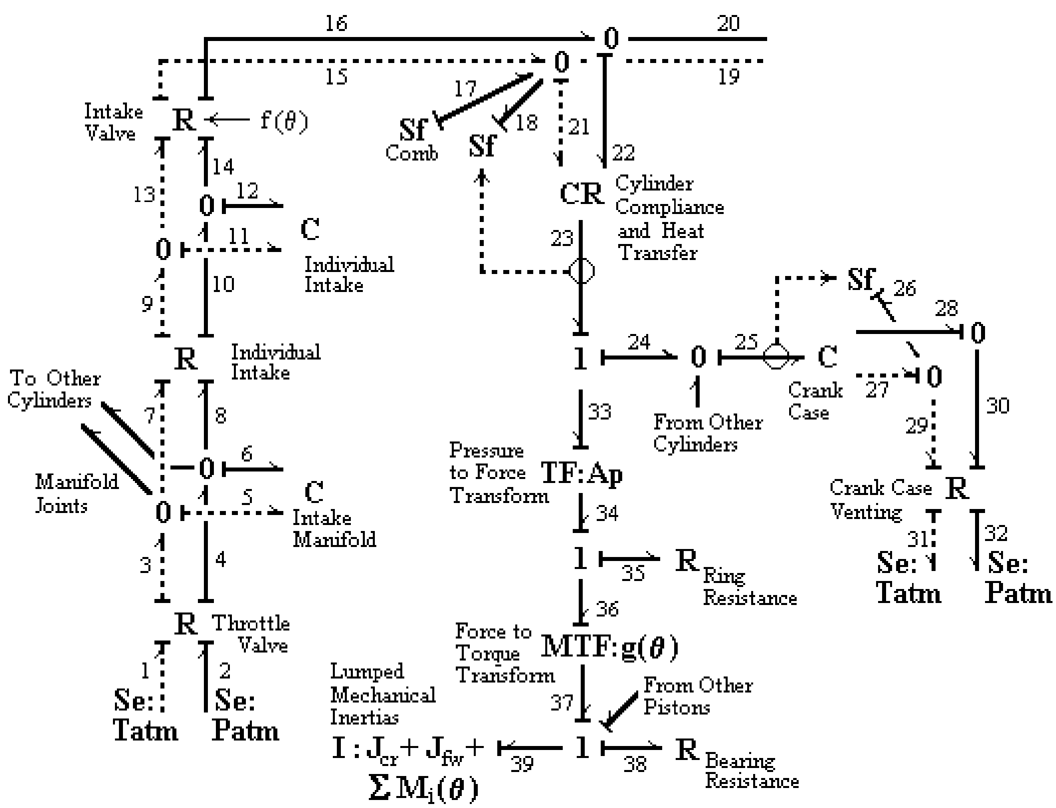

Figure D.1: Reduced ICE Bond Illustration of Equation Development.

System Equations from Bond Graph			
Pseudo Bonds			
Effort Equations		**Flow Equations**	
Temperature Efforts	**Pressure Efforts**	**Energy Flows**	**Mass Flows**
$e_1 = T_{atm}$	$e_2 = P_{atm}$	$f_1 = f_3$	$f_2 = f_4$
$e_3 = e_5$	$e_4 = e_6$	$f_3=F(f_4,Cp(e_1),e_1)$	$f_4=F(e_1,e_2,e_4,\gamma(e_1),A_{th})$
$e_5 = q_5/(Cv_{air}(e_5)*q_6)$	$e_6 = (R*q_5)/(Cv_{air}(e_5)*V_{im})$	$f_5 = f_3 - f_7 -$ (flows to other intake ports)	$f_6 = f_4 - f_8 -$ (flows to other intake ports)
$e_7 = e_5$	$e_8 = e_6$	$f_7 = f_9$	$f_8 = f_{10}$
$e_9 = e_{11}$	$e_{10} = e_{12}$	$f_9=F(f_{10},Cp(e_7),e_7)$	$f_{10}=F(e_7,e_8,e_{10},\gamma(e_7),A_{ip})$
$e_{11} = q_{11}/(Cv_{air}(e_{11})*q_{12})$	$e_{12} = (R*q_{11})/(Cv_{air}(e_{11})*V_{ip})$	$f_{11} = f_9 - f_{13}$	$f_{12} = f_{10} - f_{14}$
$e_{13} = e_{11}$	$e_{14} = e_{12}$	$f_{13} = f_{15}$	$f_{14} = f_{16}$
$e_{15} = e_{21}$	$e_{16} = e_{22}$	$f_{15}=F(f_{16},Cp(e_{13}),e_{13})$	$f_{16}=F(e_{13},e_{16},e_{14},\gamma(e_{13}),A_{iv}(\theta))$
$e_{17} = e_{21}$	$e_{18} = e_{23}*f_{23}$	$f_{17} =$ Combustion	$f_{18} = e_{23} * f_{23}$
$e_{19} = e_{21}$	$e_{20} = e_{22}$	$f_{19} =$ Energy Flow from Exhaust Valve	$f_{20} =$ Mass Flow from Exhaust Valve
$e_{21} = (q_{21} - HT)/(Cv_{air}(e_{21})*q_{22})$	$e_{22} = (R*(q_{21} - HT))/(Cv_{air}(e_{21})*q_{23})$	$f_{21} = f_{15} - f_{19} - f_{18} + f_{17}$	$f_{22} = f_{16} - f_{20}$
$e_{27} = q_{27}/(Cv_{air}(e_{27})*q_{28})$	$e_{28} = (R*q_{27})/(Cv_{air}(e_{28})*q_{25})$		$f_{26} = e_{25} * f_{25}$
$e_{29} = e_{27}$	$e_{30} = e_{28}$	$f_{27} = f_{29}$	$f_{28} = f_{30}$
$e_{31} = T_{atm}$	$e_{32} = P_{atm}$	$f_{29} = f_{31}$	$f_{30} = f_{32}$
		$f_{31}=F(f_{32},Cp(e_{29}),e_{29})$	$f_{32}=F(e_{29},e_{30},e_{32},\gamma(e_{29}),A_{cv}(\theta))$

True Bonds	
Effort Equations	**Flow Equations**
$e_{23} = e_{22}$	$f_{23} = f_{33}$
$e_{24} = e_{25}$	$f_{24} = f_{33}$
$e_{33} = e_{23} - e_{24}$	$f_{25} = f_24 +$ (flows from bottoms of other pistons)
$e_{34} = e_{33} * A_p$ (Piston Area)	$f_{33} = f_{34} * A_p$
$e_{35} = f_{35} * R_r + F_{rc}$ (Viscous and Coulomb Friction)	$f_{34} = f_{36}$
$e_{36} = e_{34} - e_{35}$	$f_{35} = f_{36}$
$e_{37} = e_{36} * g(\theta)$ (Piston to Crank Shaft Conversion)	$f_{36} = f_{37} * g(\theta)$
$e_{38} = f_{38} * R_{br} + T_{br}$ (Viscous and Coulomb Friction)	$f_{37} = f_{39}$
$e_{39} = e_{37} - e_{38}$	$f_{38} = f_{39}$

Table D.1

Integral Equations		
Determined Quantities of Pseudo Bonds		**Determined Flows of True Bonds**
Energy Quantities	**Mass Quantities**	**Rotational Flows**
$q_5 = \int f_5$	$q_6 = \int f_6$	$f_{39} = \int e_{39}$/(Lumped Mechanical Inertias)
$q_{11} = \int f_{11}$	$q_{12} = \int f_{12}$	
$q_{21} = \int f_{21}$	$q_{22} = \int f_{22}$	
$q_{23} = \int f_{23}$		
$q_{25} = \int f_{25}$		
$q_{27} = \int f_{27}$	$q_{28} = \int f_{28}$	

Table D.1 continued

Generalized variables have been used in the equations of table D.1 and distinguished from one another with bond numbers. However, many people use variable names either before or after the equations have been algebraically reduced. The equations of table D.1 can be used directly in a simulation software utility for computer simulation. Most of these utilities automatically arrange the system equations into the necessary order. Some simulation utilities allow graphical entry of the bond graphs into the computer and then determine the system equations straight from the bond graphs.

Algebraic reduction of the equations in table D.1 is a simple matter. Those familiar with the meanings of bond graphs can write the algebraically reduced equations directly by looking at the bond graph. However, the development above helps to enforce the representations of the system equations in the bond graph for those who are new to bond graphs. Once the equations are algebraically reduced, they can be joined into small groups which serve as model modules, or sub-component models. Configuration manipulation is performed by rearranging these modules into new configurations. As this is done the terms, or names of system state variables and design parameters, in the model modules will change to reflect the new configuration connections and design. This supports the criteria for modular models and easy reconfiguration.

APPENDIX E

This appendix contains ACSL code for the ICE graphical block modules.

Code for Four Stroke Cylinder and Piston Block

```
        Constant CylNum = 1
        Constant NumCyls = 2
        Constant Bore = 0.082
        Constant Stroke = 0.071
        Constant RodLength = 0.107
        Constant PistonMass = 0.74
        Constant RingResist = 0.001
        Constant CompRatio = 10.5
        Constant SparkAdvance = 30.0
        Constant WallTemp = 340.0
        Constant DegreesOfFlameDuration = 80.0
        Constant HeatingValue = 44.0e6
        Constant FuelToAirRatio = 0.0685

Initial
        Sort
        CR = Stroke/2.0
        PA = 3.1415927*Bore**2.0/4.0
        DV = PA*Stroke
        CRRat = CR/RodLength
        CRat = CompRatio
        ClearVolume = DV/(CRat-1.0)
        ClearLength = ClearVolume/PA

        Ref = 0.0;              gamma = 1.4
        Patm = 105472.0;        Tatm = 300.0
        PI = 3.1415927;   TV = VIC;           MP = Patm
        VIC = ((CR/CRRat+CR-CR*cos(0.0-720.0&
                /NumCyls*(CylNum-1)/57.29578)-CR/CRRat&
                *sqrt(1-(CRRat*sin(0.0-720.0/NumCyls&
                *(CylNum-1)/57.29578))**2))*PA+ClearVolume)
        MIC = VIC*1.225;        EIC = MIC*Tatm*718.0
        MPmem = Patm;           MVmem = VIC
End ! of initial

        SA = SparkAdvance
        Qhv = HeatingValue
        FA = FuelToAirRatio
        FD = DegreesOfFlameDuration
        WT = WallTemp

        th = CrankAngle*57.29578
        thp = (th-720.0/NumCyls*(CylNum-1))/57.29578
```

```
trans = (CR*sin(thp)+(CR*CRRat*sin(thp)&
        *cos(thp))/sqrt(1-(CRRat*sin(thp))**2))

VolFlow = CrankSpeed*trans*PA
Area = (CR/CRRat+CR-CR*cos(thp)&
        -CR/CRRat*sqrt(1-(CRRat*sin(thp))**2)&
        +ClearLength)*Bore*PI+2*PA
Torque = ((Pressure)*PA&
        -(VolFlow)/PA*RingResist)*trans
PistonRotInertia = trans**2.0*PistonMass

tha = th+720.0/NumCyls*(NumCyls-CylNum+1)-(360.0-SA)
thsprk = mod(tha,720.0)

IF(thsprk.GT.(2.0*FD)) THEN
        xbd = 0.0
ELSE
xbd = CrankSpeed*57.29578/(1+exp(5.0&
                -10.0*thsprk/FD))
END IF

MassUBFlow = mfi-xbd*MassUB
MassUB = INTEG(MassUBFlow,MIC)
MassBFlow = xbd*MassUB+mfo
MassB = INTEG(MassBFlow,0)
Mass = MassUB + MassB
Procedural(yb=MassB,MassUB)
yb=MassB/(MassB+MassUB)
        If(yb.GT.1.0) yb = 1.0
End ! Of Procedural

Volume = INTEG(VolFlow,VIC)
TotEF = Qhv*FA*xbd*MassUB+(efi+efo)&
        -Pressure*VolFlow-HeatTrans
Energy = INTEG(TotEF,EIC)

Cva = 613.29+0.31904*Temperature&
          -8.9293e-5*Temperature**2&
          +8.8328e-9*Temperature**3
Cvp = 782.26+0.3241*Temperature&
          -2.1429e-4*Temperature**2&
          +9.7778e-8*Temperature**3
Cvr = Cva*(1.0-yb)+Cvp*yb

res = Temperature-1.0/Cvr*Energy/Mass
Temperature = IMPLC(res,300.0)
Pressure = 287.0/Cvr*Energy/Volume

Procedural(HeatTrans=Area,Volume,VolFlow,&
        mfi,mfo,Temperature,Pressure,xbd)

If((mfimem.NE.0.0).AND.(mfi.EQ.0.0)) Then
```

```
        Ref = DV*Temperature/((Pressure/1000)*Volume)
        mfimem = mfi
    Else
        Ref = Ref
    End If

    If((abs(mfi)+abs(mfo)).GT.0.0) THEN
        c1 = 6.18; c2 = 0.0
        MPmem = Pressure; MVmem = Volume
        MP = MPmem; MV = MVmem
        gamma = 1.4506-1.6384e-4*Temperature&
            +5.8378e-8*Temperature**2&
            -7.3897e-12*Temperature**3
    Else If(((abs(mfi)+abs(mfo)).LE.0.0).AND.&
      (xbd.LE.0.0).AND.(VolFlow.LT.0.0)) THEN
        c1 = 2.28; c2 = 0.0
        MP = MPmem*(MVmem/Volume)**1.4
    Else If(((abs(mfi)+abs(mfo)).LE.0.0).AND.&
      (xbd.GT.0.0)) Then
        c1 = 2.28; c2 = 3.24e-3
        MP = MPmem*(MVmem/Volume)**1.4
    End If
    HeatTrans = 3.26*(Pressure/1000.0)**(0.8)&
        /Bore**(0.2)/Temperature**(0.55)&
        *(c1*CrankSpeed/6.2832*Stroke*2.0+c2*Ref&
        *(Pressure/1000.0-MP/1000.0))**(0.8)&
        *Area*(Temperature - WT)
    End ! Of Procedural
```

Code for Intake Valve Block

```
Initial
    Constant OpenAngle = -40.0 ! Valve Open Angle in Degrees
    Constant CloseAngle = 230.0 ! Valve Close Angle in Degrees
    Constant LiftProfile = 0.09 ! Valve Lift Profile
    Constant MaxHeight = 0.009 ! Maximum Valve Lift Height
    Constant Diameter = 0.037 ! Valve Diameter
    Constant CylNum = 1 ! Cylinder Number
    Constant NumCyls = 2 ! Number of Cylinders
    Constant Strokes = 4 ! Number of Strokes per Full Engine Cycle

    VO = OpenAngle
    VC = CloseAngle
    VPr = LiftProfile
    VH = MaxHeight
    VD = Diameter
    PI = 3.1415927
    RDRat = 180.0/PI
End ! of Initial

    TempAngle = ShaftAngle*RDRat+Strokes*180.0&
        /NumCyls*(NumCyls-CylNum+1)-(VO)
```

```
ValveAngle = mod(TempAngle,Strokes*180.0)+(VO)

AreaFrac =(1/(1+exp(VPr*(VO)+5-ValveAngle*VPr))&
          +1-1/(1+exp(VPr*(VC)-5&
          -ValveAngle*VPr))-(((VC)-(VO))&
          +sqrt(((VC)-(VO))*((VC)-(VO))))&
          /(2*sqrt(((VC)-(VO))*((VC)-(VO)))))
Area = AreaFrac*VH*PI*VD

If(AreaFrac.GT.1.0e-7) Then
If(Pu.LT.Pd) Then
          Dir = -1.0
          gamma = 1.4506-1.6384e-4*Td&
                    +5.8378e-8*Td**2-7.3897e-12*Td**3
          Cp = 900.39+0.31904*Td&
                    -8.9293e-5*Td**2+8.8328e-9*Td**3
          Puse = Pd
          Tuse = Td
          PRTemp = Pu/Pd
Else
          Dir = 1.0
          gamma = 1.4506-1.6384e-4*Tu&
                    +5.8378e-8*Tu**2-7.3897e-12*Tu**3
          Cp = 900.39+0.31904*Tu&
                    -8.9293e-5*Tu**2+8.8328e-9*Tu**3
          Puse = Pu
          Tuse = Tu
          PRTemp = Pd/Pu
End If

PrCrit = (2/(gamma+1))**(gamma/(gamma-1))

If(PRTemp.LE.PrCrit) Then
          Pr = PrCrit
Else
          Pr = PRTemp
End If

          massflow = Dir*(Area)*Puse/Sqrt(Tuse)&
                    *Sqrt(2*gamma/(287.0*(gamma-1)))&
                    *Sqrt(Pr**(2/gamma)&
                    -Pr**((gamma+1)/gamma))
          energyflow = massflow*Cp*Tuse
Else
          massflow = 0.0;          energyflow = 0.0
End If

mfd = massflow; mfu = -massflow
efd = energyflow; efu = -energyflow
```

Code for Exhaust Valve Block

```
Initial
        Constant OpenAngle = 470.0 ! Valve Open Angle in Degrees
        Constant CloseAngle = 740.0 ! Valve Close Angle in Degrees
        Constant LiftProfile = 0.09 ! Valve Lift Profile
        Constant MaxHeight = 0.009 ! Maximum Valve Lift Height
        Constant Diameter = 0.037 ! Valve Diameter
        Constant CylNum = 1 ! Cylinder Number
        Constant NumCyls = 2 ! Number of Cylinders
        Constant Strokes = 4 ! Number of Strokes per Full Engine Cycle

        PI = 3.1415927
        RDRat = 180.0/PI
        VO = OpenAngle
        VC = CloseAngle
        VPr = LiftProfile
        VH = MaxHeight
        VD = Diameter
End ! of Initial

        TempAngle = ShaftAngle*RDRat+Strokes*180.0&
                /NumCyls*(NumCyls-CylNum+1)-(VO)
        ValveAngle = mod(TempAngle,Strokes*180.0)+(VO)

        AreaFrac =(1/(1+exp(VPr*(VO)+5-ValveAngle*VPr))&
                +1-1/(1+exp(VPr*(VC)-5&
                -ValveAngle*VPr))-(((VC)-(VO))&
                +sqrt(((VC)-(VO))*((VC)-(VO))))&
                /(2*sqrt(((VC)-(VO))*((VC)-(VO)))))
        Area = AreaFrac*VH*PI*VD

        If(AreaFrac.GT.1.0e-7) Then
        If(Pu.LT.Pd) Then
                Dir = -1.0
                gamma = 1.4221-1.8752e-4*Td&
                        +6.9668e-8*Td**2-9.099e-12*Td**3
                Cp = 1072.86+0.3241*Td-2.1429e-4*Td**2&
                        +9.7778e-8*Td**3
                Puse = Pd
                Tuse = Td
                PRTemp = Pu/Pd
        Else
                Dir = 1.0
                gamma = 1.4221-1.8752e-4*Tu&
                        +6.9668e-8*Tu**2-9.099e-12*Tu**3
                Cp = 1072.86+0.3241*Tu-2.1429e-4*Tu**2&
                        +9.7778e-8*Tu**3
                Puse = Pu
                Tuse = Tu
                PRTemp = Pd/Pu
        End If

        PrCrit = (2/(gamma+1))**(gamma/(gamma-1))
```

```
        If(PRTemp.LE.PrCrit) Then
                Pr = PrCrit
        Else
                Pr = PRTemp
        End If

                massflow = Dir*(Area)*Puse/Sqrt(Tuse)&
                        *Sqrt(2*gamma/(287.0*(gamma-1)))&
                        *Sqrt(Pr**(2/gamma)&
                        -Pr**((gamma+1)/gamma))
                energyflow = massflow*Cp*Tuse
        Else
                massflow = 0.0;         energyflow = 0.0
        End If

        mfd = massflow; mfu = -massflow
        efd = energyflow; efu = -energyflow
```

Code for Air Passage Block

```
Initial
        MIC=Volume*1.225
        EIC=Volume*1.225*300.0*718.0
        Constant Volume = 0.0006
End ! of initial

        Pu = Pressure
        Pd = Pressure
        Tu = Temperature
        Td = Temperature
        NetMassFlow = mfu+mfd
        NetEnergyFlow = efu+efd

        Mass = INTEG((NetMassFlow),MIC)
        Energy = INTEG((NetEnergyFlow),EIC)

        res = Temperature -1.0/Cv*Energy/Mass
        Temperature = IMPLC(res,300.0)

        Cv = 613.29+0.31904*Temperature &
                -8.9293e-5*Temperature**2 &
                +8.8328e-9*Temperature**3

        Pressure = 287.0/Cv*Energy/Volume
```

Code for Exhaust Passage Block

```
Initial
        Constant Volume = 0.0005
        MIC=Volume*1.225
        EIC=MIC*300.0*718.0
```

```
End ! of initial
          Pu = Pressure
          Pd = Pressure
          Tu = Temperature
          Td = Temperature
          NetMassFlow = mfu+mfd
          NetEnergyFlow = efu+efd

          Mass = INTEG(NetMassFlow,MIC)
          Energy = INTEG(NetEnergyFlow,EIC)

          res = Temperature - 1.0/Cv*Energy/Mass
          Temperature = IMPLC(res,300.0)

          Cv = 782.26+0.3241*Temperature &
                    -2.1429e-4*Temperature**2 &
                    +9.7778e-8*Temperature**3

          Pressure = 287.0/Cv*Energy/Volume
```

Code for Air Resistance Block

```
Initial
          Constant Area = 0.0012
End ! of Initial

          If(Pu.LT.Pd) Then
                    Dir = -1.0
                    gamma = 1.4506-1.6384e-4*Td&
                              +5.8378e-8*Td**2-7.3897e-12*Td**3
                    Cp = 900.39+0.31904*Td&
                              -8.9293e-5*Td**2+8.8328e-9*Td**3
                    Puse = Pd
                    Tuse = Td
                    PRTemp = Pu/Pd
          Else
                    Dir = 1.0
                    gamma = 1.4506-1.6384e-4*Tu&
                              +5.8378e-8*Tu**2-7.3897e-12*Tu**3
                    Cp = 900.39+0.31904*Tu&
                              -8.9293e-5*Tu**2+8.8328e-9*Tu**3
                    Puse = Pu
                    Tuse = Tu
                    PRTemp = Pd/Pu
          End If

          PrCrit = (2/(gamma+1))**(gamma/(gamma-1))

          If(PRTemp.LE.PrCrit) Then
                    Pr = PrCrit
          Else
                    Pr = PRTemp
```

```
        End If

        massflow = Dir*(Area)*Puse/Sqrt(Tuse)&
                        *Sqrt(2*gamma/(287.0*(gamma-1)))&
                        *Sqrt(Pr**(2/gamma)&
                        -Pr**((gamma+1)/gamma))
        energyflow = massflow*Cp*Tuse

        mfd = massflow; mfu = -massflow
        efd = energyflow; efu = -energyflow
```

Code for Exhaust Resistance Block

```
Initial
        Constant Area = 0.0024
End ! of Initial

        If(Pu.LT.Pd) Then
                Dir = -1.0
                gamma = 1.4221-1.8752e-4*Td&
                        +6.9668e-8*Td**2-9.099e-12*Td**3
                Cp = 1072.86+0.3241*Td-2.1429e-4*Td**2&
                        +9.7778e-8*Td**3
                Puse = Pd
                Tuse = Td
                PRTemp = Pu/Pd
        Else
                Dir = 1.0
                gamma = 1.4221-1.8752e-4*Tu&
                        +6.9668e-8*Tu**2-9.099e-12*Tu**3
                Cp = 1072.86+0.3241*Tu-2.1429e-4*Tu**2&
                        +9.7778e-8*Tu**3
                Puse = Pu
                Tuse = Tu
                PRTemp = Pd/Pu
        End If

        PrCrit = (2/(gamma+1))**(gamma/(gamma-1))

        If(PRTemp.LE.PrCrit) Then
                Pr = PrCrit
        Else
                Pr = PRTemp
        End If

        If(Area.NE.0.0) Then
                massflow = Dir*(Area)*Puse/Sqrt(Tuse)&
                        *Sqrt(2*gamma/(287.0*(gamma-1)))&
                        *Sqrt(Pr**(2/gamma)&
                        -Pr**((gamma+1)/gamma))
                energyflow = massflow*Cp*Tuse
        Else
```

```
    massflow = 0.0;         energyflow = 0.0
End If

mfd = massflow; mfu = -massflow
efd = energyflow; efu = -energyflow
```

Code for Air Throttle Block

```
Constant MaxArea = 0.0024

Area = MaxArea*AreaFraction

If(AreaFraction.GT.1.0e-7) Then
If(Pu.LT.Pd) Then
    Dir = -1.0
    gamma = 1.4506-1.6384e-4*Td&
        +5.8378e-8*Td**2-7.3897e-12*Td**3
    Cp = 900.39+0.31904*Td&
        -8.9293e-5*Td**2+8.8328e-9*Td**3
    Puse = Pd
    Tuse = Td
    PRTemp = Pu/Pd
Else
    Dir = 1.0
    gamma = 1.4506-1.6384e-4*Tu&
        +5.8378e-8*Tu**2-7.3897e-12*Tu**3
    Cp = 900.39+0.31904*Tu&
        -8.9293e-5*Tu**2+8.8328e-9*Tu**3
    Puse = Pu
    Tuse = Tu
    PRTemp = Pd/Pu
End If

PrCrit = (2/(gamma+1))**(gamma/(gamma-1))

If(PRTemp.LE.PrCrit) Then
    Pr = PrCrit
Else
    Pr = PRTemp
End If

    massflow = Dir*(Area)*Puse/Sqrt(Tuse)&
        *Sqrt(2*gamma/(287.0*(gamma-1)))&
        *Sqrt(Pr**(2/gamma)&
        -Pr**((gamma+1)/gamma))
    energyflow = massflow*Cp*Tuse
Else
    massflow = 0.0;         energyflow = 0.0
End If

mfd = massflow; mfu = -massflow
efd = energyflow; efu = -energyflow
```

APPENDIX F

This appendix contains code for the ideal induction machine.

ACSL Code for Ideal Induction Motor Graphical Block

```
INITIAL
        Integer NPPPs, NBs, PPs
        PI=3.1415927
        Constant Poles=2
        Constant Phases=3
        Constant StDia=0.145948
        Constant Length=0.144430
        Constant PhR=0.1161
        Constant BarR=4.92e-5
        Constant MagR=18.869
        Constant TurnsPP=66.0
        Constant wf=0.955
        Constant AirGap=0.000490
        Constant Kgap=1.751
        Parameter(NPPPs = 3)
        Parameter(NBs = 31)
        PPs=Poles/2.0
        GYr=0.5
        GYs=wf*TurnsPP
        Muo = 4*PI*1e-7
        ReluctAir=2.0*AirGap*Kgap/(Muo*PI&
                *(StDia-AirGap)*Length)

        Constant Steep = 80.0
        Dimension tv(3)
        Dimension ba(NBs),spa(NPPPs),&
        sv(NPPPs),sfr(NPPPs),sf(NPPPs),sfICs(NPPPs),&
        si(NPPPs),ressi(NPPPs),siICs(NPPPs),&
        bv(NBs),bi(NBs),bfr(NBs),bm(NBs)

        Do La ia = 1, NPPPs
          spa(ia)=PPs*2*PI/NPPPs*(ia-1)
          sfICs(ia)=0.0
          siICs(ia)=0.0
        La .. Continue
END     ! OF INITIAL

        wsf = ws/PPs
        wsl = wsf-w
        sl = wsl/wsf

        sa=INTEG(w,0)
```

```
Procedural(vp,ws=)
        vp = vb*(1.0-exp(-steep*t))
        ws = 2*PI*((fc-0.001)&
                *(1.0-exp(-steep*t))+0.001)
End ! of Procedural

Procedural(tv=vp,ws)
        tv(1)=vp*cos(ws*t)
        tv(2)=vp*cos(ws*t-2*PI/3)
        tv(3)=vp*cos(ws*t-4*PI/3)
End ! of Procedural

Procedural(ba=sa)
Do L1 i1 = 1, NBs
        ba(i1)=PPs*(sa-2*PI/NBs*(i1-1))
L1 .. Continue
End ! of Procedural

Procedural(ressi=MMFRes,MMFResAng,spa,&
        bm,ba)
Do L2a i2a = 1, NPPPs
  ressi(i2a)=si(i2a)*GYs-MMFDamp&
          -MMFRes*cos(spa(i2a)-MMFResAng)
Do L2b i2b = 1, NBs
          ressi(i2a)=ressi(i2a)&
                +bm(i2b)*cos(spa(i2a)-ba(i2b))
L2b .. Continue
L2a .. Continue
End ! of ressi Procedural

si=IMPVC(ressi,siICs)

Procedural(sv=tv,si)
epwr=0.0
Do L3 i3 = 1, NPPPs
        If(i3.LE.3) sv(i3)=tv(i3)-PPs*si(i3)*PhR
        If(i3.GT.3) sv(i3)=tv(i3-3)-PPs*si(i3)*PhR
        epwr=epwr+tv(i3)*PPs*si(i3)
L3 .. Continue
End ! of Procedural

Procedural(sfr=sv)
Do L4 i4 = 1, NPPPs
        sfr(i4)=PPs*sv(i4)/GYs
L4 .. Continue
End ! of Procedural

sf = INTVC(sfr,sfICs)

Procedural(bv=bfr)
Do L5 i5 = 1, NBs
        bv(i5)=bfr(i5)*GYr
```

```
L5 .. Continue
End ! of bv Procedural

Procedural(bi=bv)
Do L6 i6 = 1, NBs
        bi(i6)=bv(i6)/BarR
L6 .. Continue
End ! of bi Procedural

Procedural(bfr=PPPFluxRes,PPPFluxResAng,ba)
Do L7 i7 = 1, NBs
        bfr(i7)=-wsl*PPPFluxRes&
                *sin(ba(i7)-PPPFluxResAng)
L7 .. Continue
End ! of Procedural

FieldResult(PPPFluxRes,PPPFluxResAng,&
        PPPFluxResX,PPPFluxResY,spa,sf,NPPPs)

MMFResX=ReluctAir*PPPFluxResX
MMFResY=ReluctAir*PPPFluxResY
MMFRes=ReluctAir*PPPFluxRes
MMFResAng=PPPFluxResAng
MMFDamp=MagR*(PPPFluxRes*wsl)/Phases

Procedural(bm=bi)
Do L8 i8 = 1, NBs
        bm(i8)=bi(i8)*GYr
L8 .. Continue
End ! of Procedural

FieldResult(BarMMFRes,BarMMFResAng,&
        BarMMFResX,BarMMFResY,ba,bm,NBs)

!Beta and Torque
Beta2=BarMMFResAng-MMFResAng
SinAng=sin(Beta2)
trq=-MMFRes*BarMMFRes*PPs*SinAng/ReluctAir
mpwr=trq*w

FieldResult(tvr,tvra,tvrx,tvry,spa,tv,NPPPs)
FieldResult(ti,tia,tix,tiy,spa,si,NPPPs)

eapwr=tvr*ti*Poles/3.0
If(EAPwr.GT.0) epwrrat=epwr/eapwr

pf=cos(tvra-tia)
If(epwr.NE.0.0) Then
        eff=mpwr/epwr*100.0
Else
        eff=0.0
End If
```

APPENDIX G

This appendix contains code for the electric machine models and electric machine controller logic.

ACSL Code for Induction Motor Graphical Block

```
INITIAL
        Integer NPPPs, NBs, PPs
        PI=3.1415927

        Constant Poles=2
        Constant Phases=3
        Constant StDia=0.145948
        Constant Length=0.144430
        Constant PhR=0.1161
        Constant BarR=4.92e-5
        Constant slp = 7.01e-7
        Constant rlp = 1.788e-6
        Constant TurnsPP=66.0
        Constant wf=1.2
        Constant AirGap=0.000490
        Constant Kgap=1.751

        Parameter(NPPPs = 3)
        Parameter(NBs = 31)

        PPs=Poles/2.0
        GYr=0.5
        GYs=wf*TurnsPP
        Muo = 4*PI*1e-7
        ReluctAir=2.0*AirGap*Kgap/(Muo*PI&
                *(StDia-AirGap)*Length)

        Dimension tv(3)
        Constant Steep = 40.0

        Dimension ba(NBs),spa(NPPPs),&
        sv(NPPPs),si(NPPPs),sfr(NPPPs),smfr(NPPPs),&
        slfr(NPPPs),slf(NPPPs),slfics(NPPPs),slm(NPPPs),&
        rlfr(NBs),rlf(NBs),rlfics(NBs),rlm(NBs),&
        rmfr(NBs),rfr(NBs)


        Do La ia = 1, NPPPs
          spa(ia)=PPs*2*PI/NPPPs*(ia-1)
          slfics(ia)=0.0
        La .. Continue

        Do Lb ib = 1, NBs
```

```
        rlfics(ib)=0.0
      Lb .. Continue

END   ! OF INITIAL

      wsf = ws/PPs
      wsl = wsf-w
      sl = wsl/(wsf + 0.0001)
      wr = w

      sa=INTEG(w,0)

      Procedural(vp,ws=)
            vp = vb ! vb*(1.0-exp(-steep*t))
            ws = 2*PI*fc       ! 2*PI*((fc-0.001)&
                               ! *(1.0-exp(-steep*t))+0.001)
      End ! of Procedural

      Procedural(tv=vp,ws)
            tv(1)=vp*cos(ws*t)
            tv(2)=vp*cos(ws*t-2*PI/3)
            tv(3)=vp*cos(ws*t-4*PI/3)
      End ! of Procedural

      Procedural(ba=sa)
      Do L1 i1 = 1, NBs
            ba(i1)=PPs*(sa-2*PI/NBs*(i1-1))
      L1 .. Continue
      End ! of Procedural

      Procedural(si=slm)
      Do L2 i2 = 1, NPPPs
            si(i2)=slm(i2)/GYs
      L2 .. Continue
      End ! of si Procedural

      Procedural(sv=tv,si)
      epwr=0.0; ti=0.0
      Do L3 i3 = 1, NPPPs
            If(i3.LE.3) sv(i3)=tv(i3)-PPs*si(i3)*PhR
            If(i3.GT.3) sv(i3)=tv(i3-3)-PPs*si(i3)*PhR
            epwr=epwr+tv(i3)*PPs*si(i3)
      L3 .. Continue
      End ! of Procedural

      Procedural(sfr=sv)
      Do L4 i4 = 1, NPPPs
            sfr(i4)=PPs*sv(i4)/GYs
      L4 .. Continue
      End ! of Procedural

      Procedural(smfr=wsf,f,spa,fa)
```

```
Do L5 i5 = 1, NPPPs
        smfr(i5)=f*sin(spa(i5)-fa)*wsf
L5 .. Continue
End ! of bv Procedural

Procedural(slfr=sfr,smfr)
Do L6 i6 = 1, NPPPs
        slfr(i6)=sfr(i6)-smfr(i6)
L6 .. Continue
End ! of bv Procedural

slf=intvc(slfr,slfics)

Procedural(slm=slf,slp)
Do L7 i7 = 1, NPPPs
        slm(i7)=slf(i7)/slp
L7 .. Continue
End ! of bv Procedural

Procedural(rfr=rlm)
Do L8 i8 = 1, NBs
        rfr(i8)=rlm(i8)/(GYr**2)*BarR
L8 .. Continue
End ! of Procedural

Procedural(rmfr=wsf,f,spa,fa)
Do L9 i9 = 1, NBs
        rmfr(i9)=f*sin(ba(i9)-fa)*wsl
L9 .. Continue
End ! of Procedural

Procedural(rlfr=rfr,rmfr)
Do L10 i10 = 1, NBs
        rlfr(i10)=-rmfr(i10)-rfr(i10)
L10 .. Continue
End ! of Procedural

rlf=intvc(rlfr,rlfics)

Procedural(rlm=rlf,rlp)
Do L11 i11 = 1, NBs
        rlm(i11)=rlf(i11)/rlp
L11 .. Continue
End ! of bv Procedural

FieldResult(slmr,slmra,slmrx,slmry,spa,slm,NPPPs)
FieldResult(rlmr,rlmra,rlmrx,rlmry,ba,rlm,NBs)
rtp(mr,mra=(slmrx+rlmrx),(slmry+rlmry))

f = mr/ReluctAir
fa = mra
```

```
        !Beta and Torque
        beta = rlmra-mra
        SinAng=sin(beta)
        trq = -mr*rlmr*PPs*SinAng/ReluctAir
        mpwr=trq*w

! ***** Power Calculations
        FieldResult(tvr,tvra,tvrx,tvry,spa,tv,NPPPs)
        FieldResult(ti,tia,tix,tiy,spa,si,NPPPs)
        co = sign(ti,trq)
        eapwr=tvr*ti*Poles/3.0
        If(EAPwr.GT.0) epwrrat=epwr/eapwr
        pf=cos(tvra-tia)
        If(epwr.NE.0.0) Then; eff=mpwr/epwr*100.0
        Else; eff=0.0; End If
```

ACSL Code for IM Controller Graphical Block

```
Initial
        Constant Tb = 57.0
        Constant wb = 314.159
        Constant VPeak = 312.0
        Constant OR = 3.5
        Constant MaxSlipW = 5.0
        MaxTrq = Tb*OR

End ! of Initial

        If(abs(tc).LT.MaxTrq) Then
                DesSlipW = tc/MaxTrq*MaxSlipW
        Else If(abs(tc).GE.MaxTrq) Then
                DesSlipW = sign(MaxSlipW,tc/MaxTrq)
        End If

        ws = wr + DesSlipW
        fc = ws/(2*3.1415927)

        If(abs(ws).LT.wb) Then
                vp = ws/wb*VPeak
        Else If(abs(ws).GE.wb) Then
                vp = VPeak
        End If

        pwr = vp*imi
```

ACSL Code for DC Machine Graphical Block

```
INITIAL
        Constant Ra = 0.02
        Constant La = 0.001
```

```
END     ! OF INITIAL

        wr = w
        dli = (vt - KaPhi*w - ti*Ra)
        trq = KaPhi*ti

        mpwr = trq*w
        epwr = ti*vt
        eff = mpwr/(epwr+0.0001)

!       *** Code for Neglecting La ***
!       ti = (vt - KaPhi*w)/Ra
!       resti = ti - (vt - KaPhi*w)/Ra
!       ti = implc(resti,0.0)
```

ACSL Code for DC Machine Controller Graphical Block

```
Initial
        Constant Ra = 0.02
        Constant La = 0.001
        Constant Tb = 220.5
        Constant wbf = 315.0
        Constant wbv = 315.0
        Constant VPeak = 160.0
        Constant MaxPwr = 85000.0
        KaPhiB=(VPeak**2/Ra - MaxPwr)*Ra/(VPeak*wbf)

        Table TFrac, 1,3 /0.0,220.5,1e20,0.0,1.0,1.0/

End ! of Initial

! ***** No Regen *****
        ia = limint(dli,0.0,0.0,1.0e20)/La
        ti = ia

        If(wr.GE.wbf.AND.tc.GT.0.0) Then
                KaPhi=(VPeak**2/Ra - MaxPwr)*Ra/(VPeak*wr)*TFrac(tc)
        Else If(wr.LT.wbf.AND.tc.GT.0.0) Then
                KaPhi=KaPhiB*TFrac(tc)
        Else
                KaPhi = 0.0
        End If

        If(wr.GE.wbv.AND.tc.GT.0.0) Then
                vtd = VPeak
                If(vtd.GE.vb) Then; vt = vb
                Else If(vtd.LT.vb) Then; vt = vtd; End If
        Else If(wr.LT.wbv.AND.tc.GT.0.0) Then
                vtd = (Tb*Ra/KaPhiB+KaPhiB*wr)
                If(vtd.GE.vb) Then; vt = vb
                Else If(vtd.LT.vb) Then; vt = vtd; End If
```

```
Else
        vt = 0.0
End If

bpwr = vt*ia
```

APPENDIX H

The parameter values for this 18 kW nominal power induction machine are presented in a Design Overview table first. The values for Design Overview table come from the tables that follow the Design Overview table.

Design Overview

Design of Squirrel Cage Induction Motor for I

Designer Inputs

Ratings	
Connection Type:	Delta
Power Output (KW):	18
Phase Voltage (rms):	220
Max Supply Frequency (hz):	50
Phases:	3
Efficiency:	90.739%
Power Factor:	0.88
Max Shaft Speed (Synchronous rpm):	3000

Factors Affecting Main Dimensions	
Average Air Gap Flux (Bav):	0.45
Specific Electric Loading Ampere-Conductors/m (ac) (5<ac<45)*10^3 :	31000
Winding Factor:	0.955
Choose L/Tau (pg. 602):	0.63
Choose Slots per Pole per Phase (q'):	6
Choose Average Stator Flux Density (T):	1.5
Choose Average Rotor Flux Density (T):	1.5
Specify Lamination Factor:	0.9

Factors Affecting Specific Stator Dimensions	
Current Density (J < 4.0) (Amp/mm^2):	3.8
Enter "1" Round or "2" for Rectangular:	2
Min Round Conductor Diameter (mm): Or, Rectangular Area (mm^2):	8.988
See Conductor Tables (pg 890)	
Choose Round Diameter (mm): Or Rectangular Area (mm^2):	9.860
Enter Diameter w/ Insulation (mm): Or Rectangular Area w/ Insulation (mm):	10.240
Slot Height (mm)	Slot Width (mm)
0.00	5.00

Factor for Tooth Pulsation Losses (0.5 < f < 1.0):	0.7

Factors Affecting No-Load Current - Go To Magnet Sheet	
Calculated Stator (Slot Width)/(Air Gap) Ratio	10.196
Calculated Rotor (Slot Width)/(Air Gap) Ratio	6.118
Kcs for Carter's Coefficient for Stator (pg 124, figure 4.9):	0.83
Kcs for Carter's Coefficient for Rotor (pg 124, figure 4.9):	0.65
See pg 120 Fig 4.2 for following H's H's Based on Bt60	
Stator Teeth:	530
Stator Core:	1000
Rotor Teeth:	575
Rotor Core:	1000

Overall Performance
and
Stator Circuit Design Specifics

Power Output (KW)	Phase Voltage (rms)	Connection Type
18	220	Delta
Average Air Gap Flux (Bav)	**Ampere-Conductors per Meter (ac) (5000 < ac < 45000)**	**Efficiency**
0.45	31000	91%

	Stator Specifications and Calculations	
Synchronous (rev/sec)	**Poles**	**Output Coefficient (c_o)**
50	2	146.545
Stator Phase Current (amp)	**Chosen L/Tau (pg. 602)**	**Stator Inner Diameter (D) (m)**
34.155	0.63	0.146
Flux per Pole (Webers)	**Inner Circumference of Stator (m)**	**Chosen Slots per Pole per Phase (q')**

Stator Core Design Specifics

Slot Height (mm)	Slot Width (mm)	Tooth Arc (mm)
0.00	5.00	7.74
3.00	5.00	8.26
5.00	9.00	4.61
24.00	9.00	7.93

One Third Height	One Third Width	One Third Arc
11.333	9.000	5.714

Given Current Density (J < 4.0) (Amp/mm^2)	Minimum Conductor Cross-Sectional Area	Calculated Cross-Sectional Conductor Diameter (mm)
3.8	8.988	3.383

See Table 17.6 pg. 890 for Conducter Specifications

Chosen Round Conductor Diameter (mm)	Round Conductor Diameter w/ Insulation (mm)	Conductor Cross-Sectional Area
9.86	10.24	9.860

Rotor Circuit
and
Rotor Core Design Specifics

Slot Height (mm)	Slot Width (mm)	Tooth Arc (mm)
0.00	3.00	11.69
2.00	3.00	11.29
3.00	5.70	8.38
12.00	5.70	6.56
One Third Height	**One Third Width**	**One Third Arc**
9.000	5.700	7.167
Mean Average Flux Density (BmeanAv) (T)	**Max Mean Average Flux Density (T) (1.3 < B < 1.7 for hot rolled)**	**Recalculated Rotor Slot Area >= Previous (mm^2)**
1.032	1.621	51.3
Total Volume of Rotor Core and Shaft (m^3)	**Total Steel Volume of Rotor (m^3)**	**Density of Steel Used in Rotor (Kg/m^3)**
1.494E-03	1.897E-03	7850

End Ring Design

End Ring Current (amps)	Enter End Ring Current Density (4 < J < 7)	Cross-Sectional Area of End Ring (mm^2)
1809.061	6	301.510

Machine Losses

Material Resistivity	End Ring Resistance (ohms)	Rotor End Ring Current (amps)
2.065E-08	5.084E-05	1809.061
	Combined Resistance Losses	
Total Copper Losses (watts)	**Rotor Resistance Referred to Stator (ohms)**	**Total Resistance per Phase as Seen in Stator (ohms)**
774.343	0.149	0.265
	Iron Losses	
	Stator Iron Losses	
Stator Tooth Volume (m^3)	**Entered Stacking Density of Steel Used (Kg/m^3)**	**Mass of Stator Teeth Steel (Kg)**
7.297E-04	7600	5.546
Iron Power Loss in Stator Teeth (watts)		
69.324		
Entered Specific Loss for Bavg in Core (pg. 146) (watts/Kg)	**Volume of Stator Core (m^3)**	**Mass of Stator Core (Kg)**
12.5	3.622E-03	27.530
***** Rotor Core and Teeth Losses are negligable because slip is small and rotor is laminated**		
Factor for Tooth Pulsation Losses (0.5 < f < 1.0)	**Tooth Pulsation Losses (watts)**	**Total Iron Losses (watts)**
0.7	289.418	702.873
Total Losses at Full Load (watts)	**Efficiency (Confirm w/ Criteria)**	**Real Component of No Load Amperes/Phase**
1837.216	90.74%	1.610

Magnetics of the Machine

0.859	0.6122	418.396
	Stator Teeth	
B in Stator Teeth at 60° Electrical (Bt_{60})	**See pg 120 Figure 4.2 for H**	**MMF of Teeth (use height of tooth)**
1.364	530	12.72
	Stator Core	
B average for Stator Core (T)	**See pg 120 Figure 4.2 for H**	**MMF per Pole per Phase in Stator Core (use mean path)**
1.5	1000	121.557
	Rotor Teeth	
B in Rotor Teeth at 60° Electrical (Bt_{60})	**See pg 120 Figure 4.2 for H**	**MMF of Teeth (use height of tooth)**
1.404	575	6.9
	Rotor Core	
B average for Rotor Core (T)	**See pg 120 Figure 4.2 for H**	**MMF per Pole per Phase in Rotor Core (use mean path)**
1.5	1000	42.394
	Magnetizing Current Calculations	
Total Ampere Turns	**Magnetizing Current per Phase (pg 178) (amps)**	**No Load Current Magnitude per Phase (amps)**
601.968	8.156	8.314
Loading Effect (30% < Value < 40%)		

Machine Reactances

Total Slot Leakage Reactance per Phase as Seen at Terminals (ohms):

Overhang Leakage Effects

Value of Ks (Figure 4.58, pg 170)	Calculation of $L_o*\lambda_o$	Overhang Leakage Reactance per Phase (ohms)
0.96	1.585E-06	0.723

Zig Zag Leakage Effects

Width of Stator Tooth Face (m)	Width of Rotor Tooth Face (m)	Stator Slot Pitch (m)
7.736E-03	1.169E-02	1.274E-02
Air Gap Length (m)	**Specific Zig-Zag Permeance**	**Zig-Zag Leakage Reactance per Phase (ohms)**
4.904E-04	1.593E-06	0.1049

Total Machine Leakage Reactances/Impedences

Overall Leakage Reactance per Phase (ohms)	Overall Resistance per Phase (ohms)	Resultant Machine Impedence per Phase (Not Air Gap Flux) (ohms)
1.084	0.265	1.116

APPENDIX I

This appendix contains code for the battery model.

Code for Battery Graphical Block

```
Initial
        Table R1d, 1, 14 /11.2,11.25,11.35,11.5,11.65,11.75,&
                11.9,12,12.25,12.5,13,13.25,13.5,13.78,&
                0.8,0.6,0.4,0.3,0.2,0.15,0.1,0.09,0.07,&
                0.05,0.04,0.05,0.065,0.1/
        Table R1c, 1, 16 /10.8,11.25,11.5,11.75,12,12.25,12.5,&
                12.75,13,13.25,13.5,13.65,13.72,13.75,13.78,13.8,&
                0.25,0.15,0.1,0.08,0.08,0.1,0.15,0.2,0.25,0.5,1,&
                1.5,2,2.5,3,3.5/
        Table Rsd, 1, 14 /11.2,11.25,11.35,11.5,11.65,11.75,&
                11.9,12,12.25,12.5,13,13.25,13.5,13.78,&
                0.8,0.6,0.4,0.3,0.2,0.15,0.1,0.09,0.07,&
                0.05,0.04,0.05,0.065,0.1/
        Table Rsc, 1, 16 /10.8,11.25,11.5,11.75,12,12.25,12.5,&
                12.75,13,13.25,13.5,13.65,13.72,13.75,13.78,13.8,&
                0.25,0.15,0.1,0.08,0.08,0.1,0.15,0.2,0.25,0.5,1,&
                1.5,2,2.5,3,3.5/
        Table Rp,  1, 13 /10.8,12,12.1,12.2,12.4,12.5,12.7,12.8,&
                13,13.1,13.2,13.3,14,95,95,93,91.5,81,72,45,30,&
                12,7,4.75,4,4/

        Constant C3AHrs = 158.0
        Constant C3WHrs = 879.0
        Constant SOC0 = 10.8
        Constant SOC100 = 14.0
        Constant C1 = 1000.0
        Constant k = 4.1
        Cb = (C3AHrs**2.0)/(2.0*C3WHrs)*3600
        qcic = C3AHrs*3600
        vc = C3AHrs*3600/Cb
        vcic = vc
        vb = vc

End ! of Initial

        Rpar = Rp(vc)
        ip = vc/Rpar
        ic = -(ip + ib)

        Cap = Cb*1.0/(1.0+Exp(k*SOC0+5-vc*k))

        If(ib.LE.0.0) Then
                RS = Rsc(vc)/4.0
```

```
Else If(ib.GT.0.0) Then
        RS = Rsd(vc)/4.0
End If

qc = integ(ic,qcic)
resvc = vc - qc/Cap
vc = implc(resvc,vcic)

vs = ib*RS
vb = vc - vs - vc1

vc1 = qc1/c1
ic1 = vc1/R1
qc1 = integ((ib - ic1),0.0)
If(ib.LE.0.0) Then
        R1 = R1c(vc)/4.0
Else If(ib.GT.0.0) Then
        R1 = R1d(vc)/4.0
End If
```

Code for Battery Bank Graphical Block

```
Initial
        Constant NumParPaths = 1 ! The number of parallel paths in the bank
        Constant NumBattsSer = 39 ! The number of batteries in each series path
End ! of Initial

        vo = vi*NumBattsSer     ! Bank Voltage
        co = ci/NumParPaths     ! Current Per Series Path
```

APPENDIX J

This appendix contains code for the driver blocks and logic controllers.

Code for Conventional Driver

```
!***********************************************************
!************* PID Control of Driver's Head **************
Initial
        Constant P = 10000.0
        Constant I = 350.0
        Constant D = 15.0
        Constant NumberOfGears = 5
        Logical NGC
        NGC = .TRUE.

        ShUp = 40000.0; ShDn = 0.0
        dgn = 1; gn = 1; tmem = 0.0

        Table CED, 1, 4 / 0.0, 0.2, 2.0, 5.0,&
                          0.0, 0.0, 1.0, 1.0 /
        Table CGC, 1, 6 / -1.0,0.0,0.4,0.5,1.0,2.0,&
                          1.0,1.0,0.0,0.0,1.0,1.0 /
        NOGs = NumberOfGears
        rpm = 0

End ! of Initial

!***********************************************************
!************* Driver's Mental Drive Cycle in m/s ********

        Table DesVel, 1, 10  &
                /0,5,15,25,35,40,50,60,70,75,&
                 0,0,15,15,0,0,27,27,0,0 /

!***********************************************************
!************* Driver's Torque Command to Power Plant ****

        DV = DesVel(t)
        DeltV = DV - V
        vo = V

        tc   =     P*DeltV &
                + I*integ(DeltV,0) &
                + D*(DeltV-integ(DeltV,0))/0.1
        DA   =  (DV-integ(DV,0))/0.1

        If(NGC.AND.tc.GT.0.0) Then
                th = tc*CGC(clt)
```

```
        Else
                th = 0.0
        End If

        If((tc.LE.0.0.AND.V.GE.0.0)) Then
                bc = tc
        Else;   bc = 0.0;End If

!.OR.&
!           (tc.GT.0.0.AND.V.LE.0.0))

!*******************************************************
!************* Driver's Clutching and Gear Changing ******

        Procedural(tmem=)
        If(rpm.GT.ShUp.AND.NGC.AND.dgn.LT.NOGs) Then
                dgn = dgn + 1;    NGC = .FALSE.
                tmem = t
        Else If(rpm.LT.ShDn.AND.NGC.AND.dgn.GT.1) Then
                dgn = dgn - 1;    NGC = .FALSE.
                tmem = t
        Else If(gn.NE.dgn.AND.Cl.EQ.0.0.AND.(.NOT.NGC)) Then
                gn = dgn;         NGC = .TRUE.
        End If
        End ! of Procedural

        SCHEDULE DICE .XN. DV - 2.0
        SCHEDULE DCAR .XN. DV - 2.0
        SCHEDULE DIMG .XN. DV - 2.0
        SCHEDULE DICE .XP. rpm - ShUp
        SCHEDULE DCAR .XP. rpm - ShUp
        SCHEDULE DIMG .XP. rpm - ShUp
        SCHEDULE DICE .XN. rpm - ShDn
        SCHEDULE DCAR .XN. rpm - ShDn
        SCHEDULE DIMG .XP. rpm - ShUp

        clt = t - tmem
        Cl = CED(DV)*CGC(clt)
```

Code for EV Driver

```
!*******************************************************
!************* PID Control of Driver's Head **************
Initial
        Constant P = 250.0
        Constant I = 350.0
        Constant D = 45.0
        Constant MaxTrq = 220.5
End ! of Initial

!*******************************************************
```

```
!************* Driver's Mental Drive Cycle in m/s ********

! ***** Idle, Accel, Cruise, Decel, Idle
!           Table DesVel, 1, 6  &
!                     /0,5,15,25,35,40,&
!                      0,0,27,27,0,0/

! ***** All Out Acceleration *****
            Table DesVel, 1, 3  &
                     /0 ,0.1 ,2 ,&
                      0 ,100 ,100 /

!**********************************************************
!************* Driver's Torque Command to Power Plant ****

            DV = DesVel(t); DeltV = DV - V; vo = V; dvo = DV

            Dtc = D*(DeltV-integ(Dtc,0))/0.1
            Itc = I*integ(DeltV,0.0)
            tc   =        P*DeltV + Itc + Dtc
            DA = (DV-integ(DA,0))/0.1

            If(tc.GT.0.0.AND.DA.GE.0.0) Then
                     th = tc
            Else;       th = 0.0; End If

            If(tc.LE.0.0.AND.V.GT.0.0.AND.DA.LE.0.0) Then
                     bc = tc
            Else;       bc = 0.0;End If
```

Code for Hybrid Logic

Version 1

```
! Parallel Hybrid Logic Control Scheme with driver clutch control and
! NO Regenerative Braking.
Initial
            Constant MaxICETrq = 63.0
            Constant MaxIMGTrq = 200.0

End ! of Initial

            If(tc.GT.MaxICETrq.AND.tc.LT.(MaxICETrq+MaxIMGTrq)) Then
                     IMGtc = tc - MaxICETrq
            Else If(tc.GT.(MaxICETrq+MaxIMGTrq)) Then
                     IMGtc = MaxIMGTrq
            Else;       IMGtc = 0.0;        End If

            bco = bci
            vo = vi
```

Version 2

```
! Parallel Hybrid Logic Control Scheme with good clutch control and
! NO Regenerative Braking.
Initial
        Constant MaxICETrq = 63.0
        Constant MaxIMGTrq = 200.0
        Constant DisEngRPM = 1100.0
        Constant EngRPM = 1500.0
        Constant TR = 0.267
        Constant GR = 12.0

        Logical Engage, Disengage, Engine
        Engage = .FALSE. ;  Disengage = .TRUE. ; Engine = .FALSE.

        vi = 0.0; tmem2 = -10.0; Cl = 0.0

        Table CEF, 1, 4 / -1.0, 0.0, 0.5, 10.0,&
                          0.0, 0.0, 1.0, 1.0 /

End ! of Initial

        If(tc.GT.0.0.AND.vi.GT.(EngRPM/9.55*TR/GR)) Then
                ICEtc = tc; Engine = .TRUE.
        Else;   ICEtc = 0.0; Engine = .FALSE. ;   End If

        If(tc.GT.MaxICETrq.AND.tc.LT.(MaxICETrq+MaxIMGTrq)) Then
                IMGtc = tc - MaxICETrq
        Else If(tc.GT.(MaxICETrq+MaxIMGTrq)) Then
                IMGtc = MaxIMGTrq
        Else;   IMGtc = 0.0;     End If

        bco = bci
        vo = vi

!************* Automatic Clutching ******

        ClDiff = rpm - DisEngRPM

        SCHEDULE DICE .XN. rpm - (DisEngRPM+5.0)
        SCHEDULE DCAR .XN. rpm - (DisEngRPM+5.0)
        SCHEDULE DIMG .XN. rpm - (DisEngRPM+5.0)

        Cl = CEF(clt2)

        If(rpm.GT.EngRPM.AND.Cl.EQ.0.0.AND.Engine) Then
                Engage = .TRUE.
                Disengage = .FALSE.
                tmem2 = t
        Else If(rpm.LE.DisEngRPM.AND.Cl.EQ.1.0) Then
                Engage = .FALSE.
```

```
    Disengage = .TRUE.
    tmem2 = t
End If

Procedural(clt2=)
If(Engage) Then
    clt2 = t - tmem2
Else If(Disengage) Then
    clt2 = tmem2 - t + 0.5
End If
End ! of Procedural
```

VITA

Thomas Wayne Ives was born September 24, 1961. He received his Bachelor of Science Degree in Mechanical Engineering from The University of Texas at Austin in December 1984. He held his first engineering position in the Naval Nuclear Power Program with Westinghouse Electric Corporation. This position gave him direct contact with the Naval Nuclear program as a civilian. He completed Officer's Naval Nuclear Power School in Orlando, Florida in January 1986. He completed Naval Nuclear Prototype Training at the Idaho National Engineering Laboratory (INEL) in November 1986 receiving the Naval qualification of Engineering Officer of the Watch for operation of the A1W Plant which is a prototype of one of the four U.S.S. Enterprise dual reactor plants. In March of 1987, he received Naval qualification as an Engineering Duty Officer. In July of 1987, he became a qualified Nuclear Plant Engineer. In November of 1987, he passed the Naval Reactors Engineers Exam, and subsequently received the qualification of Shift Test Engineer. As a Shift Test Engineer, he directed a crew of nuclear navy personnel through the daily requirements of a comprehensive test program following the overhaul of the A1W prototype which also involved overseeing reactor plant conditions, operations, and maintenance. In June of 1989, he left Westinghouse to accept a position at the Texas A&M University (TAMU) Nuclear Science Center (NSC). While there, he managed the operations of a 1MW research reactor and commenced his graduate work in Mechanical Engineering. He left his position at the TAMU NSC in July of 1991 to concentrate more fully on his graduate studies. He has worked as a Research Assistant and as a Teaching Assistant for the Mechanical Engineering Department at TAMU, and he has also worked as a Research Assistant for the Electrical Engineering Department. He received his Master of Science degree in Mechanical Engineering from Texas A&M University in May of 1995. His Master of Science research was in the field of robot calibration for which he has two journal publications and one journal publication in review.

He married Nola Sue Nichols in March of 1988. In July of 1993, God blessed them with a son, Gabriel Thomas Ives. In September of 1996, God blessed them with a daughter, Anna Michelle Ives. The Ives family is currently living in Boise, Idaho where Thom is employed by SCP Global Technologies. The Ives family can be reached at 400 Benjamin Lane, Boise Idaho 83704.